Regulation of Lysosome Positioning and Function by Small GTPase Arl8b

A Thesis Submitted to

Jawaharlal Nehru University, New Delhi

For the degree of

Doctor of Philosophy

In the Faculty of Science

By

GAURAV KUMAR

CSIR-Institute of Microbial Technology, Chandigarh

April, 2022

सीएसआईआर - सूक्ष्मजीव प्रौद्योगिकी संस्थान
सैक्टर 39 - ए, चण्डीगढ़ - 160 036 (भारत)
CSIR - INSTITUTE OF MICROBIAL TECHNOLOGY
(A CONSTITUENT ESTABLISHMENT OF CSIR)
Sector 39-A, Chandigarh - 160 036 (INDIA)

सीएसआईआर - इमटैक
CSIR - IMTECH

Certificate

This is to certify that the research work embodied in this thesis entitled "**Regulation of lysosome positioning and function by small GTPase Arl8b**", has been carried out by **Mr. Gaurav Kumar** under the guidance of **Dr. Amit Tuli** at the CSIR-Institute of Microbial Technology (IMTECH), Sector 39-A, Chandigarh, India. This work is original and has not been submitted in part or full for any other degree or diploma to any other University. Wherever contributions of others are involved, every effort is made to indicate this clearly, with due reference to the literature, and acknowledgements of collaborative research and discussions.

Supervised by:

Dr. Amit Tuli

Signature

Submitted by:

Gaurav Kumar

Signature

दूरभाष : 0172-6665201 } Reception
0172-6665202
0172-6665..... (Direct)
फैक्स : 0091-172-2690632 (COA)
Fax : 0091-172-2690585 (Director)
0091-172-2690056 (Purchase)
एस. टी. डी. कोड़ : STD CODE : 172
Web : http://imtech.res.in

Acknowledgements

It was a roller coaster ride!!!

My PhD journey was full of excitement and uncertainty. I've learned a lot in the last 5-6 years, not only about science but also about life in general. However, I was not alone on my voyage, and this great adventure would not have been possible without the incredible individuals I have or have had in my life. As I near the end of my PhD journey, I'd want to express my gratitude to everyone who has been involved, either directly or indirectly.

This adventure began with my first encounter with Dr. Amit Tuli, my supervisor and mentor, during the interview in 2016. This was the beginning of my first engagement with him. I consider myself fortunate to have him as my PhD supervisor. I am eternally grateful to him for exposing me to this fascinating field. He has always been there for me and pushed me to achieve things I thought I'd never be able to do. The knowledge and experience I have received from working with him is precious and cannot be adequately expressed in words. I'll never forget his words "Gaurav, this is your project, you should own it," since it influenced me a lot and always helped me when I got stuck during my experiments. Despite the fact that everyone knows he can be tough and hyper critical at times, I really admire his passion for science and the sort of efforts he puts in to instill a scientific temperament in his students. I'd like to dedicate the following lyrics from Kabir's "doha" to him since, in my opinion, they are the most accurate description of him.

"गुरू कुम्हार शिष कुंभ है, गढ़ि गढ़ि काढ़ै खोट।
अन्तर हाथ सहार दै, बाहर बाहै चोट।।"

"Mentor is the Potter, student is the (unbaked) pot. Gives Shape and cures the flaws with care. Protecting (always) with palm from inside. While pounding the pot from outside."

I would want to offer my heartfelt appreciation to our collaborator and my mentor, Dr. Mahak Sharma, at IISER Mohali. I owe her a debt of gratitude for all of the wise counsel and critiques she has provided throughout my PhD. Her thoughtful recommendations and feedback have made a significant contribution to the quality of the work presented in this thesis. She has made a significant

contribution to my professional development as a researcher. I had a great time discussing many topics with her, including experiments, lab culture, the work of other scientists, movies, series, and so on. I'm humbled by the amount of care and confidence she has for me.

I am grateful to Dr. Ashwani Kumar, Dr. Deepak Sharma and Dr. Saumya Ray Chaudhuri for being a part of my research advisory committee and rigorously evaluating my work throughout various presentations and providing me with valuable suggestions. I also want to thank Dr. Ashish Ganguly for his timely help and suggestions whenever I needed them.

Also, I would like to thanks Dr. Nitin Mohan (IIT Kanpur) for advice on single-particle tracking-related experiments and Drs. Marlieke Jongsma (Utrecht University, the Netherlands), Ilana Berlin (Utrecht University, the Netherlands), and Carlos Guardia (NIEHS, USA) for their helpful suggestions in performing analysis of lysosome distribution. I also acknowledge Prateek Arora (FACS Facility, IISER Mohali) for technical help in flow cytometry, Maria Ericson (Harvard Medical School, USA) for EM imaging, Ross Tomaino (Harvard Medical School, USA) for mass spectrometry analysis.

A cheerful lab environment is vital for a focused mind and productive work, and I would like to thank for this my senior lab members Dr. Subhash Babu Arya, Harmeet Kaur, and Divya Jagga. Dr. Subhash was our lab's first student, and when I initially arrived, he was a hero figure of the lab, and I admired the way he worked and handled multitasking. I can't express how grateful I am to him for teaching me all I know about the research we do in the lab. Harmeet and Divya were like elder sisters to me; they were always there to assist and teach me the important tasks of the lab. To maintain the same culture, I always regarded the lab as my own place and the lab members as my family. I'd like to thank Ujeeta, Sanya, Sheetal, and Bidisha for their assistance with the day-to-day experiment work. I am grateful to my junior lab members, Suraj, Kshitiz, Abhishek, and Priya, for supporting me in maintaining the lab's healthy culture. They were all eager to assist me anytime I needed it. I'll miss our late weekend meal after all of the lab work. I will never forget Mr. Parmod, a special member of our lab who has been our lab support for the last four years, and I hope he continues to do so in the future.

On this voyage, I am fortunate to be a part of one more lab. I would like to thank the members of MS Lab (IISER Mohali) for hosting me from time to time and helping me with my work. I'd like to acknowledge Devashish, Ritturaj, Amit, Neha, Sankalita, Prateek, Kanupriya, Yogita, Shalini, Gagandeep, Aastha, Sahil, Shreshtha and Dhruva in particular.

I am blessed to have Rajesh (Kurbaan Singh), Sumit (Debate man), Harsh (Kaandi chora), Naushad (Chachaaa! Yoon Hi Hai), and Hilal (Question Bank) as best mates. We all enjoyed a plethora of sweet and salty recollections. They were constantly ready for scientific, ethical, or political debates, as well as general chatting. I'm sure I'll miss the meals, the tea time chats, music on demand, cricket, vacations and trips we had together. I hope we stay friends for the rest of our lives and that this S.N.G.H.R.H. never disintegrates.

When you are away from your family, some of your friends become your family, and for this, I would want to express my gratitude to my friends cum family members, Anu Singh, Rajesh, Gunjan, and Sumeeta for their support and understanding. Throughout the previous five years, you all have given me a huge amount of care and compassion. I am thankful to Anu Singh and Rajesh for preventing me from collapsing and losing hope throughout various tough situations of life.

I would like to recognize my batch mates SB16 with whom I started this journey 5 years ago, Sapna, Lucky, Anuradhika, Saloni, Amandeep, Khadim, Gaurav, Rahul, Raghavendra, Happy, Priyanka, Bhupinder, Manish, Jagriti, Pooja, Nancy, Arunima, Manisha, Sanpreet, Nishant, Pradeep, Megha, Neha. Special thanks to Sapna (Dream girl), Rahul and Anuradhika for helping me either with resources or suggestions at one point of time or the other during these five years.

Throughout the roller coaster journey of my PhD, there were times when I was perplexed and unsure of what to do. At these times, the presence of seniors and their experience was much needed. Thus, I want to thank my seniors; Drs. Vineet Kumar, Amanpreet, Shashi Anand, Sarabhjeet Kaur, Vibhuti Rana (and her lovely daughter Mishku "dadi maa"), Bhagya Raj, Poushali Chakraborty. In particular, I'd want to express my gratitude to Vineet Sir and Amanpreet Ma'am (Bharjai) for constantly listening to me and encouraging me through my PhD and personal life's low points. I also appreciate the help from my seniors Drs. Anil Kumar, Ritesh Sevalkar. Prashant Singh, Anil Patidar, Asmita Dhiman, Shekhar, Amardeep, Navin Baid, Drishti Tiwari, Prabhat Ranjan, Nittu, Simarpreet Kaur, Debarghya Ghosh,

Hina Khan. Special thanks to Shekhar sir and Nittu for their support and late night Maggi feast during my early days at IMTECH.

Seeking out and sharing knowledge with others about what one knows is an enjoyable activity that increases one's self-confidence and motivation. I am blessed to have curious juniors like Kshitiz (Lord Walia) , Priya (Mini Subhash), Suraj, Abhishek (Brodaa), Amit Dasila (Partner in crime), Shivani, Shweta, Harshvardhan, Yachna, Shobit (shobhuuu), Charan, Anu, Nandita, Khushboo, Bhanwar, Vandana, Aarushi, Rajendra, Abhinit, Jai, Sahil, Sandeep, Radhey, Sidhu, Gagan (GOGAN), Sourav, Rinku, Sandhya, Roohani, Jainis, Namra, Krishna, Rathina (Lungi). They all are super talented and I wish them all the best for their future.

I acknowledge director of IMTECH, Dr. Sanjeev Khosla and former directors Dr. Anil Koul and Dr. Manoj Raje for providing outstanding laboratory facilities and scientific infrastructure favorable to research. Thanks to Dr. Deepak Sharma, the Hostel Warden, for providing and taking care of the hostel. I'm grateful to Dr. Kartikeyan Subramanian, Dr. Charu Sharma, and Dr. Balvinder Singh for organizing the IMTECH-JNU Ph.D. program and for their assistance whenever it was needed. Ms. Shashi Batra, and Mr. Janki Ji, were really helpful throughout my PhD registration and thesis submission. Because part of my work entailed animal experiments, I'd like to thank Dr. Neeraj Khatri, Dr. Sachin, Mr. Bhupinder Singh, Mr. Sohnelal, Mr. Sandeep, and Mr. Pawan for their assistance during experimentation at the animal facility. I would like to appreciate all the mess staff for providing the delicious food (Specially my salad).I'm also grateful to Deepak Bhatt and Anjali Koundal for the well-maintained confocal microscopy, which was critical to my research.

I am quite thankful for the CSIR (Council of Scientific and Industrial Research) scholarship and the Wellcome Trust DBT India alliance. I would like to give thanks to the whole IMTECH family, the Instrumentation facility, the PTM division, the Bioinformatics center, the Library, the Administration, Store, and Purchase section, and the ESD division for maintaining all of the instrumental facilities in working condition. I would also want to thank the gardeners and sweepers for keeping the campus clean and lovely. It's always a pleasant to see how clean and green our campus is. Thank you to the security staff for making the campus so safe and too much secure.

During the final year of my PhD, I had to visit IISER Mohali often, and I had to stay at my mentor's house on occasion for work. I'd want to thank Dr. Amit Tuli,

Dr. Mahak Sharma, and their daughter Taara for treating me as if I were a part of their family; I was never treated as a guest in their home. Taara's dancing and chatting was quite relaxing throughout the intense period of manuscript writing and revision. She's a "chota pocket bada dhamaka," and trust me, she knows a thing or two about lysosomes and HeLa cells. I'd also want to thank Alma di, Seema di, and Pinky for the great food (so yummy) and coffee, as well as for looking after me throughout my time at IISER.

The term "Old is Gold" best matched to my friends who were not at IMTECH but were always with me in my ups and downs, and it would be unfair if I forgot to include the names of those who stayed behind the scenes during this journey. I'd want to express my profound appreciation to Sunandani, Ankit (manu), Ankita (Golu), Brahmjot (Bj), Pallavi, Satya, , Sidharth (sidhu), Baldeep (bali), and Surabhi for bearing with me through difficult moments.

I can't express how grateful I am for my family's support and encouragement, without which none of this would have been possible. My parents, have always believed in me and supported me when I questioned myself. I'm lucky to have my two brothers by my side. Vinay, my Big Brother, is a continual source of inspiration and hard work; whatever I am today is because of him and his faith in me. I'm envious of how much he cared about our whole family. If you're with me, my brother, I can achieve anything in this world. Thank you so much for all you've done for me. Sahil, he is the best younger brother anybody could have, even though we disagree a lot, but I adore him and want to thank him for all the help he has provided me along this journey. Last but not least, I always cherish the times I spend with our family's newest generation, Samaira and Aryan.

THANK YOU EVERYONE, WE DID IT!!!

"HASDE VASDE RHO"

RABB RAKHA

Table of Contents

Content	Page No.
Acknowledgement	**I-V**
Table of Contents	**VI-VII**
List of Figures	**VIII**
List of Tables	**IX**
Abbreviations	**X-XIII**
Chapter 1: Review of Literature	**1-29**
1. Lysosome and lysosome-related organelles	**1**
2. Lysosome biogenesis	**3**
2.1. Trafficking of lysosomal proteins from the trans-Golgi network	4
2.2. Endosome maturation pathway	5
2.2.1. Early endosome	5
2.2.2. Late endosome, lysosome and the endolysosome	6
2.2.3. Formation and maturation of late endosomes	7
2.2.4. Lysosome reformation	8
3. Lysosome motility and positioning	**9**
3.1. Molecular regulators of lysosome motility	10
3.1.1. Motor proteins	11
3.1.2. Small GTPase and their effectors	11
3.2. Regulation of lysosome positioning	14
3.2.1. Nutrient availability	14
3.2.2. Membrane contact with other organelle	15
3.2.3. Intracellular pH	16
4. Bone remodeling and lysosomes	**16**
4.1. Bone cells	16
4.1.1. Osteoblasts	17
4.1. 2. Osteocytes	17
4.1. 3. Osteoclasts	17
4.2. Bone remodeling cycle	17
4.3. Differentiation and activation of osteoclasts	18
4.4. The role of lysosome in osteoclast biology	23
4.5. Autophagy in osteoclast differentiation and function	26
4.5.1 Autophagy regulates osteoclastogenesis	26
4.5.2. Role of autophagy proteins in bone resorption activity of osteoclasts	27
5. Scope and objectives of the study	**27**
Chapter 2: RUFY3 links Arl8b and JIP4-Dynein complex to regulate lysosome size and positioning	**30-76**
Abstract	**30**
Introduction	**31**
Results	**34**
A) RUFY3 is an Arl8b effector that localizes to lysosomes	34
B) Arl8b recruits RUFY3 on lysosomes	37
C) RUFY3 promotes perinuclear positioning of lysosomes	40

D) RUFY3 is essential and sufficient to drive perinuclear lysosome positioning	43
E) RUFY3 mediated perinuclear lysosome positioning is independent of Rab7	46
F) RUFY3 recruits the JIP4-dynein-dynactin complex to mediate retrograde transport of lysosomes	49
G) Depletion of RUFY3 reduces lysosome size	54
H) RUFY3 regulates nutrient-dependent lysosome repositioning but not autophagic cargo clearance and endocytic trafficking to lysosomes	57
Discussion	61
Materials and Methods	66
Chapter 3: Regulation of osteoclast function by the small GTPase Arl8b	**77-104**
Abstract	**77**
Introduction	**78**
Results	**80**
A) Arl8b regulates lysosome positioning and distribution in osteoclast	80
B) Arl8b regulates bone resorption activity of osteoclasts	82
C) RUFY4 is an osteoclasts specific effector of Arl8b	85
D) RUFY4 binds to Arl8b through its N-terminal RUN domain-containing region	88
E) RUFY4 regulates peripheral lysosome distribution in osteoclasts but is not required for osteoclasts differentiation *in vitro*	91
F) RUFY4 act as a linker between the small GTPase Arl8b and LC3 to mediate fusion of lysosome and ruffle border	93
Discussion	**95**
Materials and Methods	**98**
Summary	**105-106**
References	**107-130**
Appendix	**131-140**
A) List of DNA constructs used in the study presented in chapter 2	
A) List of antibodies used in the study in chapter 2	
B) List of DNA constructs used in the study in chapter 3	
C) Reprint of publications	

List of Figures:

Figure 1: A schematic illustration of the diverse cellular functions performed by lysosomes.

Figure 2: The process of lysosomal biogenesis.

Figure 3: Lysosome distribution in a typical mammalian cell.

Figure 4: Molecular machinery implicated in lysosome motility.

Figure 5: The small GTPase cycle.

Figure 6: Different stages of the bone remodeling process.

Figure 7: The key molecules influencing osteoclast development and activity.

Figure 8: The osteoclast differentiation signaling network.

Figure 9: Bone resorbing osteoclasts.

Figure 10: Arl8b directly binds to variant 1 but not variant 2 of RUFY3.

Figure 11: Arl8b recruits RUFY3 on lysosomes.

Figure 12: Wild-type RUFY3, but not the Arl8b binding-defective mutant, promotes perinuclear lysosome clustering.

Figure 13: RUFY3 is essential and sufficient to drive perinuclear lysosome positioning.

Figure 14: RUFY3 mediated perinuclear lysosome positioning is independent of Rab7.

Figure 15: RUFY3 links Arl8b to the JIP4-dynein complex.

Figure 16: RUFY3 mediates lysosome motility by recruiting dynein motor on lysosomes.

Figure 17: RUFY3 depletion reduces lysosome size.

Figure 18: RUFY3 regulates nutrient-dependent lysosome repositioning.

Figure 19: (a) Three distinct hypothetical scenarios to explain the significance of different lysosomal adaptors that engage the dynein-dynactin complex for retrograde transport.
(b) Model illustrating the opposing motor adaptors recruited by Arl8b.

Figure 20: Arl8b silencing disrupts the lysosomes distribution in osteoclasts.

Figure 21: Arl8b is required for bone resorption by osteoclasts.

Figure 22: RUFY4 is a RANKL-inducible gene and an osteoclast-specific effector of Arl8b.

Figure 23: RUFY4 directly binds to Arl8b via its N-terminal RUN domain–containing region.

Figure 24: RUFY4 regulates peripheral lysosome distribution in osteoclasts but is dispensable for osteoclastogenesis.

Figure 25: RUFY4 promotes the interaction of Arl8b and LC3B.

List of Tables:

Table 1: Different types of lysosome-related organelles.

Table 2: Lysosomal proteins involved in the acidification of the extracellular matrix.

Table 3: List of proteins involved in lysosomal regulation in osteoclasts.

Abbreviations:

3-MA	:	3-Methyladenine
ALG2	:	Asparagine-linked glycosylation protein 2
ALR	:	Autophagic Lysosome Reformation
AMPK	:	AMP-activated Protein Kinase
Arl11	:	ADP-Ribosylation Factor-Like Protein 11
Arl8	:	ADP-Ribosylation Factor-Like Protein 8
Baf A1	:	Bafilomycin A1
BMDM	:	Bone Marrow Derived Macrophages
BNIP3	:	Bcl-2/adenovirus E1B 19kDa Interacting Protein 3
BORC	:	BLOC-One–Related Complex
C-FMS	:	Colony-Stimulating Factor Receptor
DC-STAMP	:	Dendritic Cell-Specific Transmembrane Protein
DHC	:	Dynein Heavy Chain
DIC	:	Dynein Intermediate Chain
DMEM	:	Dulbecco's Modified Eagle Medium
EBSS	:	Earle's Balanced Salt Solution
ECVs	:	Endocytic Carrier Vesicles
EDTA	:	Ethylenediamenetetraacetic acid
EE	:	Early Endosomes
EGTA	:	Ethyleneglycoltetraacetic acid
ELR	:	Endocytic Lysosome Reformation
ER	:	Endoplasmic Reticulum
ERK	:	Extracellular signal-Regulated Kinase
FAM98A	:	FAMily with sequence similarity 98 member A
FBS	:	Fetal Bovine Serum
FKBP	:	FK506 Binding Protein
FRB	:	FKBP-Rapamycin Binding domain
FSD	:	Functional Secretory Domain
FYCO1	:	FYVE-and Coiled coil domain containing 1
GAP	:	GTPase-Activating Protein
GDIs	:	Guanine Dissociation Inhibitors
GEF	:	Guanine Nucleotide Exchange Factor
GFP	:	Green Fluorescent Protein
GSK	:	Glycogen Synthase Kinase
GST	:	Glutathione S-Transferase

GTPases	:	Guanosine Triphosphatases
HIF-1α	:	Hypoxia Inducing Factor-1α
HOPS	:	Homotypic Fusion and Vacuolar Protein Sorting
HSCs	:	Hematopoietic Stem Cells
IB	:	Immunoblot
IF	:	Immunofluorescence
IgG	:	Immunoglobulin G
ILV	:	Intraluminal vesicles
IP	:	Immunoprecipitation
JIP4	:	JNK Interacting Protein 4
JNK	:	c-Jun N-terminal Kinases
LAMP1	:	Lysosomal-Associated Membrane Protein-1
LAMP2	:	Lysosomal-Associated Membrane Protein-2
LAMTOR2	:	Late Endosomal/Lysosomal Adaptor and MAPK and mTOR Activator 2
LAP	:	LC3-Associated Phagocytosis
LDL	:	Low-Density Lipoprotein
LE	:	Late Endosome
LRO	:	Lysosome-Related Organelles
MAPKs	:	Mitogen-Activated Protein Kinases
MCS	:	Membrane Contact Sites
M-CSF	:	Macrophage-Colony Stimulating Factor
MFI	:	Mean Fluorescence Intensity
MMPs	:	Matrix Metalloproteinases
MPR	:	Mannose 6-Phosphate Receptor
MSCs	:	Mesenchymal Stem Cells
MTOC	:	Microtubule-Organizing Center
mTORC1	:	Mammalian Target of rapamycin complex 1
MVB	:	Multivesicular Body
NDEL1	:	Nuclear Distribution protein nudE-like 1
NFATc1	:	Nuclear Factor of Activated T-cells 1
NGS	:	Normal Goat Serum
OCIF	:	Osteoclast Inhibitory Factor
OC-STAMP	:	Osteoclast Cell-Specific Transmembrane Protein
ODF	:	Osteoclast Differentiation Factor
OPG	:	Osteoprotegerin
ORP1L	:	OSBP Related Protein 1

OSCAR	:	Osteoclast-Associated Receptor
PBS	:	Phosphate Buffer Saline
PFA	:	Paraformaldehyde
PI3K	:	Phosphoinositide 3-Kinases
PIntd3P	:	Phosphoinositide-3-Phosphate
PKB	:	Protein Kinase B
PLEKHM1	:	Pleckstrin Homology domain-containing family M member 1
PLEKHM2	:	Pleckstrin homology domain-containing family M member 2
PLR	:	Phagocytic Lysosome Reformation
PNS	:	Post-Nuclear Supernatant
PtdIns(3, 5)P_2	:	Phosphoinositide-3,5-Phosphate
RANK	:	Receptor Activator of Nuclear Factor-Kappa B
RANKL	:	Receptor Activator of Nuclear Factor-Kappa B Ligand
RB	:	Ruffled Border
RILP	:	Rab-Interacting Lysosomal Protein
RIPA	:	Radio Immunoprecipitation Assay
ROI	:	Region of Interest
RUFY1	:	RUN and FYVE domain containing protein 1
RUFY2	:	RUN and FYVE domain containing protein 2
RUFY3	:	RUN and FYVE domain-containing protein 3
RUFY4	:	RUN and FYVE domain containing protein 4
RUN	:	RPIP8, Unc14, NESCA
ShRNA	:	Short Hairpin RNA
SIFs	:	*Salmonella*-Induced Filaments
SIM	:	Structured Illumination Microscopy
SiRNA	:	Small Interfering RNA
SKIP	:	SifA and Kinesin-Interacting Protein
SNAREs	:	Soluble N-ethylmaleimide-Sensitive Factor Attachment Protein receptors
SZ	:	Sealing Zone
TBC1D15	:	TBC1 Domain Family Member 15
TFE3	:	Transcription Factor E3
TFEB	:	Transcription Factor EB
TfR	:	Transferrin Receptor
TGN	:	Trans-Golgi network
TMEM55b	:	Transmembrane Protein 55b
TNF	:	Tumor Necrosis Factor

TOLLIP	:	Toll Interacting Protein
TRAFs	:	TNF Receptor- Associated Factors
TRANCE	:	Tumor necrosis factor-Related Activation-induced Cytokine
TRAP	:	Tartrate-Resistant Acid Phosphatase
TRPML1	:	Transient Receptor Potential Mucolipin 1
VAP-A	:	Vamp-Associated Protein A
WGA	:	Wheat Germ Agglutinin

Chapter 1
Review of Literature

Chapter 1

Review of Literature

The aim of this section is to emphasize on the various functions of lysosomes in mammalian cells. How lysosomes are formed and what factors influence their biogenesis and reformation will be explained. Furthermore, this chapter will present information about the molecular machinery that assists lysosomes to execute diverse functions in different cell types such as osteoclasts and epithelia cells. In particular, the involvement of small GTPases (Guanosine Triphosphates) and their effectors in regulation of lysosome motility and function will be highlighted. Overall, the information included in this chapter will provide information about the research work presented in this thesis.

1. Lysosome and lysosome-related organelles

Lysosomes are membrane-bound organelles that contain over 60 acid hydrolases known to catalyze the breakdown of a wide variety of macromolecules, including proteins, carbohydrates, lipids, and nucleic acids. Lysosomes were discovered in 1950 as a sac-like structures enclosed by a membrane containing acid phosphatase. Christian De Duve coined the term "lysosome" (lytic particles) in 1955 as it was found to contain five distinct hydrolytic enzymes with an acidic pH optimum that work on a variety of substrates (Sabatini & Adesnik, 2013). The membrane of lysosomes possesses a variety of integral membrane proteins, including V-ATPase, transporters, and ion channels, which are responsible for maintaining a high proton content in the lumen of lysosome. Aside from that, they include roughly 200 highly glycosylated proteins, such as lysosomal membrane-associated protein-1 (LAMP1) and lysosomal membrane-associated protein-2 (LAMP2), which protect the lysosome membrane from being damaged by the activity of lysosome hydrolase (Ballabio & Bonifacino, 2020; Luzio et al., 2014; Yang & Wang, 2021).

Lysosomes are present in every human cell except red blood cells. However, lysosomes may vary in number and size in different cell types. For instance, lysosomes in hepatocytes are generally less than 1 micron in diameter, whereas in macrophages may

reach a diameter of several microns. In contrast to the conventional lysosome, which serves as a source of hydrolytic enzymes for the degradation of intracellular and extracellular cargo, various cells contain what is known as lysosome-related organelles (LROs) (Fukuda, 2016). These organelles are similar to the lysosome in terms of their luminal content, but contain additional enzymes or adaptor proteins that are required for unique functions depending on the cell type (**Table 1**) (Bowman et al., 2019; Luzio et al., 2014; Shrestha et al., 2016a).

Table 1: Different types of lysosome-related organelles.

Lysosome-related organelles	**Cell type**	**Functions**
Secretory lysosomes	Osteoclasts	Bone resorption
Lytic granules	Cytotoxic T-cells and Natural-killer cells	Secretion of cytolytic granules
Melanosomes	Melanocytes	Secretion of melanin for pigmentation
Weibel-padel bodies	Endothelial cells	Helps in blood clotting
MHC class II	Dendritic cells	Antigen presentation
Acrosomes	Sperm cells	Secretion of hydrolytic proteins during fertilization with egg

Due to its canonical degradative role, the lysosome is often referred to as the cell's "trash bag" or "degradative compartment." However, several studies conducted over the past two decades have dramatically changed the perception of the lysosome from a simple and static "trash bag" to a sophisticated and dynamic "control room" of the cell that serves as a perfect workspace for various signaling complexes. For example, Mammalian target of rapamycin complex 1 (mTORC1), glycogen synthase kinase (GSK), and AMP-activated protein kinase (AMPK) are some of the well-characterized signaling complexes that function on the lysosome surface in association with various upstream and downstream molecular players where they sense, integrate, and process various extracellular and intracellular signals to ultimately determine the metabolic fate of the cell (anabolism or catabolism), thereby assisting in maintaining cell homeostasis (Appelqvist et al., 2013; Inpanathan & Botelho, 2019; Lim & Zoncu, 2016; Perera & Zoncu, 2016).

The diverse cellular processes in which lysosomes participate encompass autophagy, nutrient sensing and metabolic signaling, plasma membrane repair, immune response, cell migration, cancer metastasis, bone resorption and gene regulation (**Figure 1**) (Dykes et al., 2016; Garg et al., 2011; Inpanathan & Botelho, 2019; Lacombe et al., 2013; Marwaha et al., 2017; Michelet et al., 2018; Saitoh et al., 2017). Owing to the role of lysosomes in so many cellular functions, lysosomal dysfunction has a significant influence on cellular homeostasis. As a result, it should come as no surprise that lysosomal dysfunction is a contributing factor to a wide range of disorders, such as lysosome storage disorder, cancer, cardiovascular diseases, neurodegenerative disorders, and osteoporosis (Appelqvist et al., 2013; McGrath et al., 2021; Van Wesenbeeck et al., 2007; Q. Zhao et al., 2020).

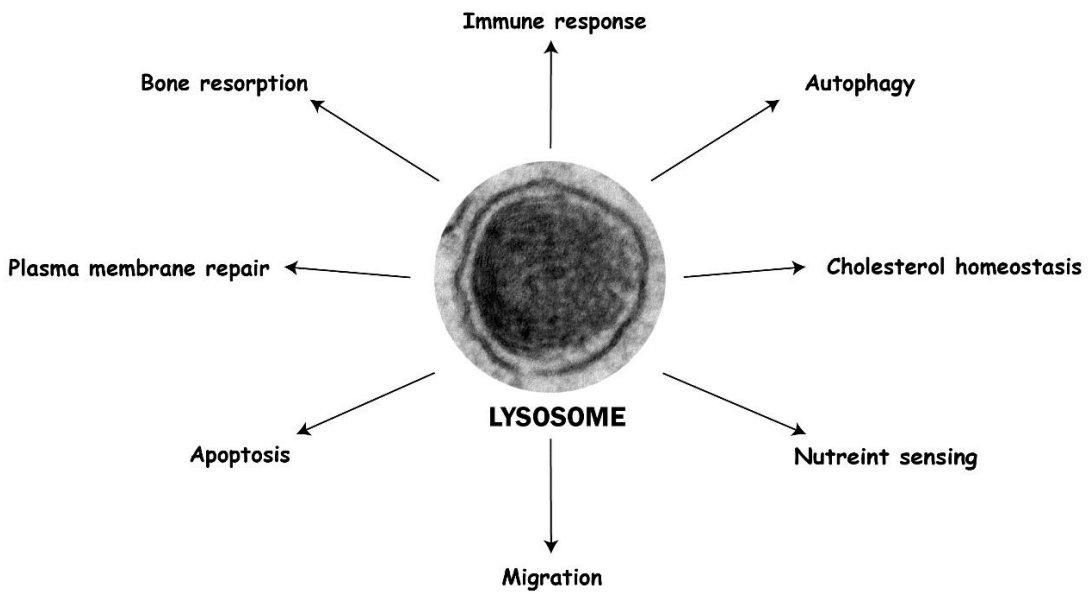

Figure 1: A schematic illustration of the diverse cellular functions performed by lysosomes. Aside from the degradation of internalized material, including intracellular pathogens, various cell type-specific or position-specific roles of lysosomes in maintaining cellular homeostasis have been discovered in recent years, including nutrient sensing, regulation of cell motility, proliferation, and cell death.

2. Lysosome biogenesis

As mentioned in the above section, lysosomes are crucial for a plethora of cellular and physiological processes and are implicated in many human disease conditions. Cells have evolved a mechanism to maintain the lysosome homeostasis under varied stress conditions. Lysosome biogenesis aids in the restoration of the quantity and content of

lysosomes that have been depleted through different processes such as starvation-induced autophagy, plasma membrane repair, and secretion (Dykes et al., 2016; Luzio et al., 2014). Lysosome biogenesis is based on two key cellular processes: trafficking from the trans-Golgi network (TGN) to deliver lysosomal proteins and the endosome maturation pathway as shown in **Figure 2**.

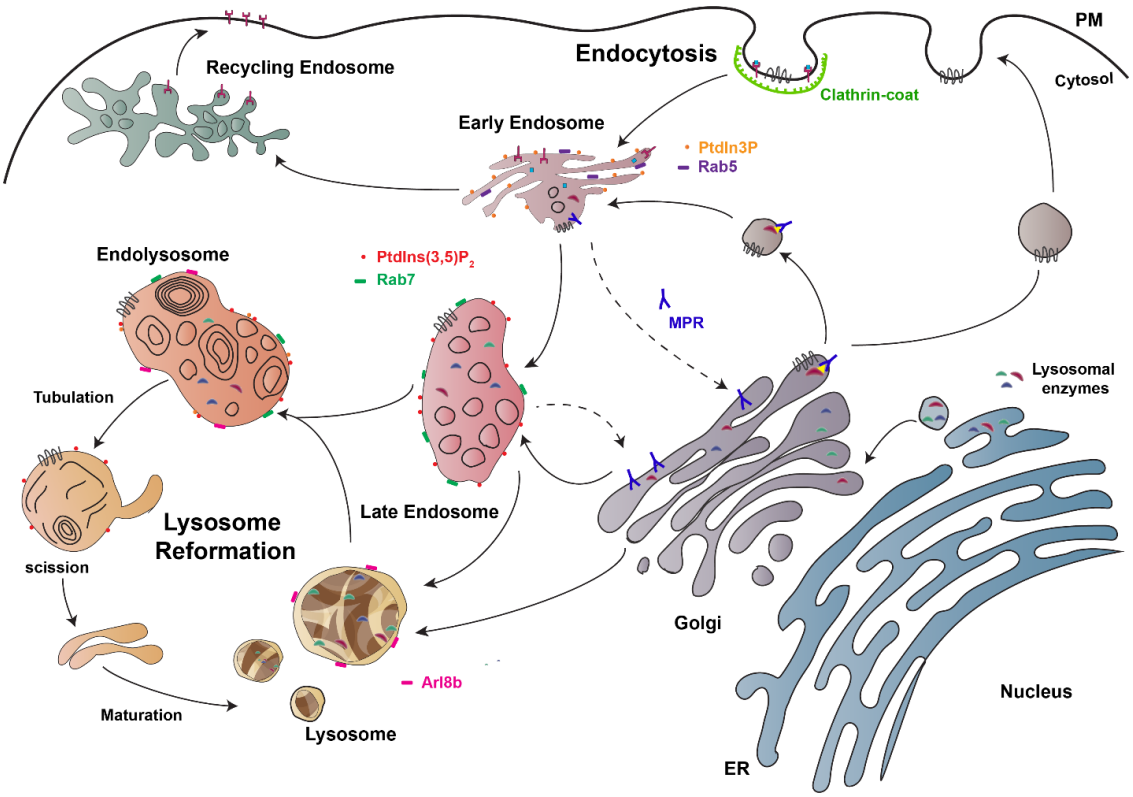

Figure 2: The process of lysosomal biogenesis. Lysosome biogenesis involves two key cellular processes. Trafficking of lysosomal resident proteins from the TGN: Lysosomal hydrolases are produced and modified in the endoplasmic reticulum (ER) by coupling with oligo-saccharides before being delivered to the Golgi apparatus. From the TGN, hydrolases are transferred to early endosomes (EE) with the aid of the mannose 6-phosphate receptor (MPR). The transmembrane proteins of the lysosome are sorted to the early endosome either through the TGN (direct route) or through the plasma membrane and endocytosis (indirect route). The endosome maturation pathway: The endosome maturation route transports lysosomal protein from the EE to the lysosome. EEs mature or are transformed into late endosomes and eventually into lysosomes during this stage of lysosome formation. Figure modified from (Yang & Wang, 2021).

2.1. Trafficking of lysosomal proteins from the Trans Golgi network (TGN)

After acid hydrolases and other degradative enzymes are synthesized in the endoplasmic reticulum (ER), they are delivered to the trans-Golgi network (TGN), where they are modified by the addition of phosphate groups to mannose sugar. The mannose 6-phosphate receptor (MPR) then recognizes these enzymes and they get

packed into a clathrin-coated vesicles. These vesicles subsequently merge with the tubular-vesicular early endosome and MPR got recycled back to the TGN. Some enzymes, however, can use sortilin to navigate an M-6-P independent route to the early endosome (EE) (Braulke & Bonifacino, 2009; Saftig & Klumperman, 2009). In a similar fashion, newly synthesized lysosomal transmembrane proteins can reach the EEs directly or indirectly. The direct route to the EE is through the TGN, while the indirect route involves vesicles first fusing with the plasma membrane, from there they are endocytosed and transported to the EE (Braulke & Bonifacino, 2009; Huotari & Helenius, 2011). Furthermore, several investigations have documented that lysosomal transmembrane proteins (LAMP1 and LAMP2) may go directly from the TGN to the late endosome and subsequently to the lysosomes through non-clathrin mediated vesicles/carriers carrying Vps41 and VAMP7 (Pols et al., 2013; Staudt et al., 2017; Van Der Beek et al., 2019).

2.2. Endosome maturation pathway

The delivery of lysosomal protein from the EEs to the lysosomes occurs through the endosome maturation pathway. In this phase of lysosome biogenesis, early endosomes mature or get converted into late endosomes and further to lysosomes. The maturation process involves the switching of endosome-specific small GTPase proteins and phospholipids.

2.2.1. Early endosome

Early endosome (EE) development marks the beginning of the endosome maturation process. Endocytic vesicles and their homotypic fusion events give rise to EEs. The size, shape, luminal content, and function of EEs are heterogeneous and vary from cell to cell type, but they are often smaller in size and predominantly located in the cell periphery (Huotari & Helenius, 2011). EEs function as sorting stations for diverse cellular components, keeping selected components from the plasma membrane and TGN for subsequent trafficking to the late endosomes (LEs) and lysosomes along the route while recycling others. EEs are complex structures composed of several tubular-vacuolar networks, the membrane and luminal composition of tubular region of endosomes are very distinct from those of vacuolar regions. High luminal pH, low calcium levels, the presence of Rab5 small GTPase, and phosphoinositide-3-phosphate

(PIntd3P) are all distinctive indicators of EEs (Borchers et al., 2021; Naslavsky & Caplan, 2018; Yang & Wang, 2021).

2.2.2. Late endosomes, lysosomes and the endolysosome

Late endosome (LE) compartments are produced primarily near the plasma membrane and subsequently migrate into the perinuclear region in a microtubule-dependent manner during their maturation stage, where they fuse with pre-existing late endosome or lysosome compartments (Huotari & Helenius, 2011). LEs are oval in shape, with sizes ranging from 300 to 1000 nm, and have a pH range of 4.8-6. The lumen and membrane of LEs are primarily composed of two kinds of components: those destined for degradation (receptors and signaling molecules) and those essential for their functioning and structural integrity (membrane proteins such as LAMP and acid hydrolases) (Yang & Wang, 2021). Because LEs have numerous intraluminal vesicles (ILV) in their lumen, they are also called multivesicular bodies (MVB) (Gruenberg and stenmark, 2004; Huotari and Helenius, 2011; Luzio *et al.*, 2014).

Lysosome compartments serve as storage facilities for huge quantities of diverse hydrolases that are ready to be deployed on their substrates. Due to their role as end points for many degradative routes, including endocytic, autophagic, and phagocytic, lysosomes are also referred to as "terminal organelles". Lysosomes are further distinguished by the presence of multilamellar structures in their lumen, which are thought to have evolved as a result of the gradual degradation of luminal lipids (Luzio et al., 2014; Wartosch et al., 2015).

Endolysosome, which are formed by the fusion of acidic late endosomes and hydrolase-containing lysosomes, exhibit properties of both the organelles and are regarded as the true sites of degradation (Bright et al., 2016; Luzio et al., 2014). Due to this, they are also termed "digestive lysosomes." Despite their unique physical properties, it is difficult to distinguish late endosome, lysosome, and endolysosome compartments. One possible explanation for this is that the process of endosome maturation, fusion, and fission is dynamic, continuous, and asynchronous (Yang & Wang, 2021). While some authors used these three terms interchangeably, others often referred to them together as "late endocytic compartments" or "lysosomes".

The presence of the small GTPase Rab7 and phosphoinositide-3,5-phosphate (PtdIns(3, 5)P_2) distinguishes late endocytic compartments from EEs (Yang & Wang,

2021). Arl8b is another essential late endocytic compartment-specific small GTPase (Bagshaw et al., 2006). Moreover, studies have demonstrated that Rab7 and ADP-ribosylation factor-like protein 8b (Arl8b) have relatively different preference for late endosome and lysosome (most likely Rab7–late endosome; Arl8b-terminal lysosome) and, with the aid of their share effector Pleckstrin homology domain-containing family M member 1 (PLEKHM1) and fusion machinery Homotypic fusion and vacuolar protein sorting (HOPS), Soluble N-ethylmaleimide-Sensitive Factor Attachment Protein receptors (SNAREs), these two small GTPase coordinates the fusion of late endosome and lysosome to generate double positive compartments (most likely endolysosome) (Marwaha et al., 2017). Additionally, by recruiting the Rab7-GTPase-activating protein (GAP) TBC1 Domain Family Member 15 (TBC1D15), Arl8b and its effector SifA and kinesin-interacting protein (SKIP) commence the process of Rab7 removal from the limiting membranes of double positive compartments (M. L. Jongsma et al., 2020).

2.2.3. Formation and maturation of late endosomes

The development of late endosomes (LEs) from EEs is initiated by small GTPase-Rab7 recruitment to a particular microdomain of EEs and the establishment of a transitory hybrid compartment. Two distinct mechanisms for the formation of Rab7-positive LEs from these hybrid compartments have been proposed. The first mechanism involves the conversion of Rab5-GTP to Rab5-GDP, and the removal of Rab5 from these hybrid compartments results in the formation of Rab7-positive LEs (Rink et al., 2005). The second mechanism involves the fission of the Rab7-enriched domain of the hybrid organelle, followed by the formation of small endocytic carrier vesicles (ECVs) containing lysosomal components that eventually fuse with pre-existing LEs (Gruenberg et al., 1989). The maturation occurs when newly generated LEs undergo modifications that distinguish them from EEs, provide them with their own identity, and commit them to the degradation branch of the endosome maturation pathway. The following are the major changes that occurs during formation of LEs from EEs.

- *Rab switching*: As previously stated, Rab5 is lost from the limiting membranes of LEs in exchange for Rab7. The presence of Rab7 on LE membranes during maturation causes the recruitment of Rab7-specific effectors from the cytoplasm,

resulting in significant modifications in the characteristics of newly generated LEs. In addition to Rab7, Arl8b and Rab9, are recruited on LE membranes, but Rab11 and Rab4 are removed during the maturation process (Cinti et al., 2017a; Podinovskaia et al., 2021; Rink et al., 2005).

- *Phosphoinositide conversion*: The other significant modification is the transformation of PIntd3P to PtdIns(3,5)P_2. WDR91, a Rab7 effector, inhibits VPS34-mediated synthesis of new PIntd3P on LEs, thereby promoting the synthesis of PtdIns(3,5)P_2 (Ebner & Koch, 2019; Liu et al., 2016; Schink et al., 2016).
- *Morphological changes*: When compared to the tubular-vesicular architecture of EEs, LEs become oval in form with multiple ILVs in the lumen. Also, LEs grow in size during its maturation process (Huotari & Helenius, 2011).
- *Recruitment of HOPS and motor proteins:* LEs gain a new set of fusion machinery (HOPS and SNAREs) on their limiting membrane, which enables them to fuse with LEs, lysosomes, and autophagosome but not with EEs (Marwaha et al., 2017; Spang, 2016). Furthermore, the Rab7 effector-RILP recruits dynein motors and aids in the perinuclear migration of LEs (Jordens et al., 2001).
- *Changes in luminal content*: This results in a low pH, an increased concentration of chloride ions, and significant changes in the concentrations of calcium, sodium and potassium ions (Kane, 2006; Lafourcade et al., 2008).

2.2.4. Lysosome reformation

The last step of the endosome maturation pathway includes the fusion of LEs and lysosomes and the formation of a hybrid organelle called the endolysosome, which is the site of the majority of degradation. Endolysosome creation depletes the cell lysosome pool, and to restore it, the cell initiates a regeneration process called endocytic lysosome reformation (ELR). The process comprises tubulation followed by fission and, in certain instances, budding to generate new lysosomes from endolysosomes (Luzio et al., 2014; Wartosch et al., 2015; Yang & Wang, 2021). Independent studies have shown that the lysosomal calcium channel-TRPML1 and the PtdIns3P 5-kinase-PIKfyve, which synthesize PtdIns(3,5)P2, are indispensable for the lysosome reformation (Bissig et al., 2017; Pryor et al., 2000). As with the ELR pathway, lysosome reformation may take place from the autolysosome via the autophagic lysosome reformation (ALR) pathway or from the phagolysosome through the phagocytic

lysosome reformation (PLR) pathway, depending on the source of the cargo for degradation (Du et al., 2016; Gan et al., 2019).

3. Lysosome motility and positioning

Although lysosomes are found throughout the cytoplasm of the cell, they can be classified into two pools: perinuclear/juxta-nuclear lysosomes, which are less motile, and peripheral lysosomes, which are substantially more motile (**Figure 3**).

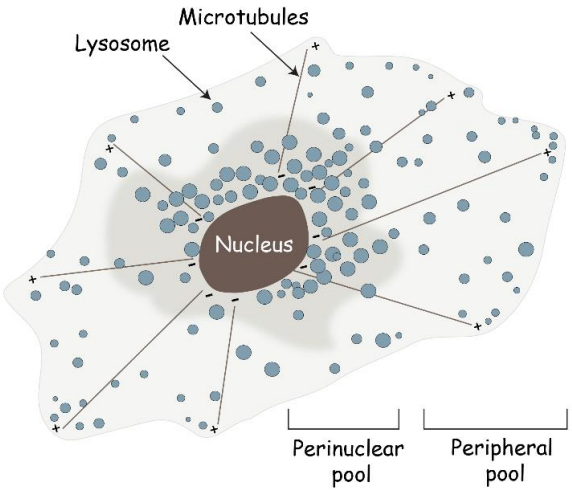

Figure 3: Lysosome distribution in a typical mammalian cell. Within the cell, lysosomes are can be classified into two populations: the perinuclear pool, which is concentrated around the nucleus and relatively immobile, and the peripheral lysosome, which is more dynamic and located near the plasma membrane.

Although this lysosomal subcellular distribution is not static and changes with the presence/absence of nutrients, growth factors, cytosolic pH, exposure to oxidative stress, infection (Cabukusta & Neefjes, 2018; Cinti et al., 2017b; Korolchuk et al., 2011a; Raiborg, 2018). By altering lysosomal distribution, cues such as nutrients and/or growth factors influence lysosome-mediated cellular responses under these physiological conditions. For instance, depletion of nutrients and/or growth factors results in lysosome clustering in the perinuclear region, where the proteolytic compartments may have more propensity to tether and fuse with autophagosome. The degradation of autophagy cargo and the subsequent recycling of breakdown products replenishes nutrient reserves during starvation conditions (Poüs & Codogno, 2011). In contrast, growth factor re-stimulation results in lysosome localization near the plasma membrane that facilitates reactivation of the lysosomal-localized mTORC1 signaling complex, and, consequently, gene expression required for protein synthesis (Rui Jia & Bonifacino, 2019). Recent studies have also highlighted the role of lysosome positioning in promoting ER remodeling from sheets to tubules in the peripheral cellular space (Lu et al., 2020; Spits et al., 2021). Also, the proximity of lysosomes to

focal adhesions near the plasma membrane regulates lysosome-dependent focal adhesion disassembly, as well as promotes growth factor-dependent activation of the mTORC1 signaling complex (Rabanal-Ruiz et al., 2021).

3.1. Molecular regulators of lysosome motility

Lysosomes, like other organelles, use microtubule tracks for their bi-directional movement. In a non-polarized cell, microtubule tracks are radially distributed throughout the cell, with minus-ends towards the MTOC (Microtubule-organizing center) in the perinuclear area and plus-ends scattered throughout the cell periphery. Dynein and kinesin are the two kinds of motor proteins responsible for lysosome movement in the retrograde (minus end-directed) and anterograde (plus end-directed) directions, respectively (Granger et al., 2014; Hirokawa et al., 2009). However, motor proteins do not bind directly to lysosomes or other organelles/vesicles. These interactions are usually mediated by small GTPases (also called as GTP-binding proteins) along with their effectors and some other adaptor proteins as shown in **Figure 4** (Pu et al., 2016).

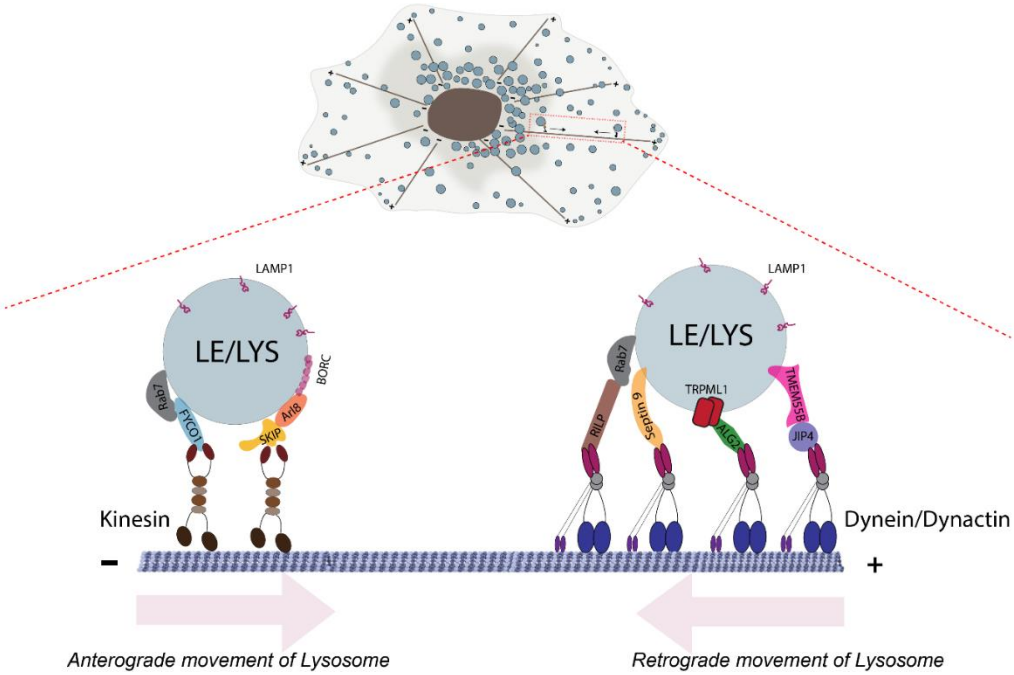

Figure 4: Molecular machinery implicated in lysosome motility. Several adaptors facilitate in the coupling of motor proteins (dynein-dynactin and Kinesin) to lysosomes. The lysosomes anterograde movement is governed by two small GTPases, Rab7 and Arl8b, through their adaptor proteins FYCO1 and SKIP, respectively. In comparison, many pathways for lysosome retrograde transport have been found, including the small GTPase Rab7 and its effector RILP. In addition, TRPML1-ALG2 and TMEM55B-JIP4 are two other retrograde transport pathways that have been shown to be more active in a nutrition-dependent manner. Septin has also been implicated in the retrograde movement of the lysosome via its direct interaction with the dynein-dynactin complex.

3.1.1 Motor proteins

Anterograde transport occurs when lysosomes travel from the minus-end of a microtubule to the plus-end, i.e., from the perinuclear area to the cell periphery. This is facilitated by kinesin motor proteins (Granger et al., 2014). Numerous kinesins are known to be involved in lysosome movement, including kinesin-1 (KIF5A, KIF5B, and KIF5C), kinesin-2 (KIF3), and kinesin-3 (KIF1A and KIF1B), as well as members of the kinesin-13 (KIF2) family, however kinesin-1 is the most well reported in context to lysosome motility. Kinesin-1 is a hetero-tetramer composed of two identical kinesin-1 heavy chains (KIF5A, KIF5B, and KIF5C) responsible for the motility of the motor and two identical kinesin light chains (KLC1, KLC2, KLC3, and KLC4) which mediate the coupling of cargo to the motor (Hirokawa et al., 2009b). Multiple kinesins may exist for a variety of reasons, including functional redundancy, cell type-specific expression, differential regulation, or a propensity for certain microtubule tracks. Considering these instances, it has been shown that kinesin-1 prefers acetylated and GTP-bound microtubule tracks, while slow motors necessary for lengthy processive runs prefer detyrosinated microtubule tracks (Guardia et al., 2016). Kinesin is coupled to the lysosome by small GTPases and their effectors which is discussed in detail in later sections.

In contrast to several kinesin motors, mammalian cells contain a single dynein motor that mediates lysosome movement/transport from the plus-ends to the minus-ends of the microtubules. Dynein is a multimeric protein complex that weighs 1.4 MDa and is composed of two heavy chains, two intermediate chains, two light intermediate chains, and several light chains. Dynactin, a multi-protein complex weighing 1.0 MDa, interacts with dynein to activate the motor and also aids in the binding of the dynein-dynactin complex to the cargo (Olenick & Holzbaur, 2019). Dynein-dynactin coupling to the lysosome is known to be mediated by small GTPase, however, recently some studies have also demonstrated the role of lysosomal transmembrane proteins in dynein recruitment (Ballabio & Bonifacino, 2020).

3.1.2 Small GTPase and their effectors

Small GTPases or GTP-binding proteins work as molecular switches that shuttle between GDP-bound inactive (cytosolic) and GTP-bound active (membrane-bound) states to regulate various cellular functions. As mentioned earlier, motor proteins are

recruited to the organelle membranes by association with their adaptors, generally effectors of Rab and ADP-ribosylation factor (Arf)-like (Arl) small GTP-binding (G) proteins. It initiates with the activation and recruitment of small GTPases and their effectors/cargo-adaptors on the organelle membrane. A small GTPase undergoes a GDP-GTP/inactive-active cycle monitored by GTPase Activating Protein (GAPs), Guanine Nucleotide Exchange Factor (GEFs) and Guanine Dissociation Inhibitors (GDIs). GTP-bound small GTPase facilitates membrane recruitment of its molecular effectors, which then perform downstream processes (**Figure 5**) (Reiner & Lundquist, 2016). Some of these effectors are responsible for the coupling of the organelle with the distinct motor proteins and thus responsible for their net directional movement (Bonifacino & Neefjes, 2017) .

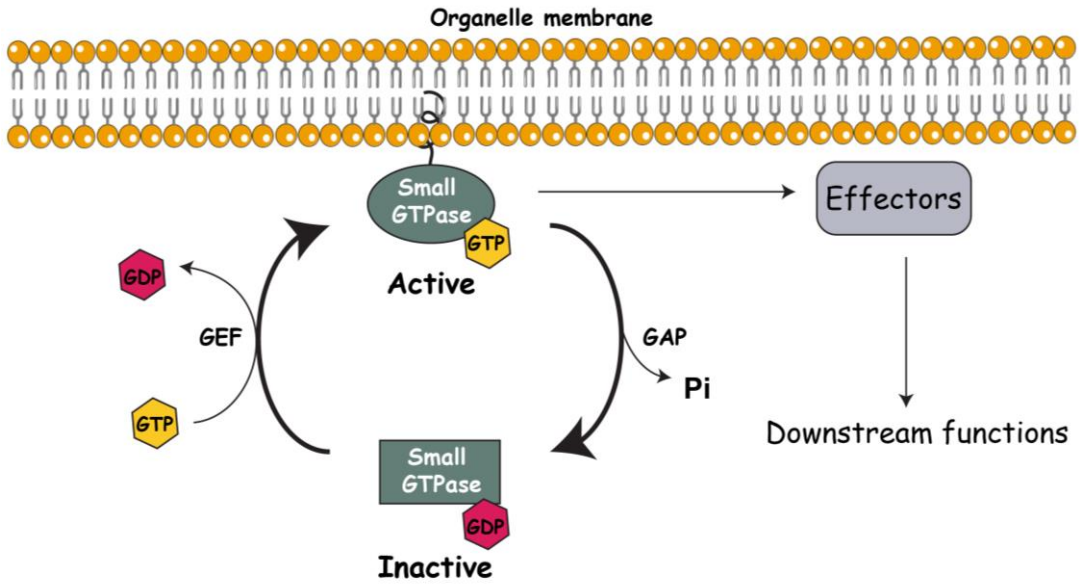

Figure 5: The small GTPase cycle. Small GTPases proteins have inter-convertible states, GDP-bound inactive and GTP-bound active. An upstream signal initiates the dissociation of GDP from the inactive form, followed by the GTP association. GTP binding causes a conformational change in the effector binding region of the GTPase, resulting in the recruitment of specific effectors. This association of GTPase and effector protein results in effector-specific downstream functions. The GDP/GTP exchange is a slow, rate-limiting step and is stimulated by Guanine Nucleotide Exchange Factors (GEFs). Furthermore, GTPases are intrinsically able to hydrolyze GTP to GDP. Since this conversion is slow, GTPase Activating Protein (GAPs) catalyzes the reaction by interacting with the GTPase. In this manner, a small GTPase cycle between inactive and active forms and functions as critical molecular switches in an array of biological processes.

Rab7-RILP represents a well-characterized small G protein-effector complex on lysosomes that recruits the motor dynein-dynactin complex to promote retrograde

motility of lysosomes (Jordens et al., 2001). GTP-bound form of Rab7 also interacts with FYCO1 to recruit kinesin-1 to lysosomes for motility towards the plasma membrane (Raiborg et al., 2015). A key player, now well known for regulating the lysosomal spatial location, is the small G protein Arl8. In mammalian cells, Arl8 has two paralogs, Arl8a and Arl8b, which are 91% similar at the protein level and have an overlapping role in regulating lysosomal distribution (Bagshaw et al., 2006; Hofmann & Munro, 2006). Arl8b, the well-characterized paralog, is recruited to the lysosome surface by its putative GEF, the BORC (BLOC-One–Related Complex) (Pu et al., 2015), which then engages its downstream effector PLEKHM2 (Pleckstrin homology domain-containing family M member 2) also known as SKIP(SifA and Kinesin Interacting Protein) to the lysosome surface, where it recruits kinesin-1 to mediate anterograde movement of lysosome (Udia et al., 2011). Arl8 paralogs also regulate KIF1A-dependent lysosome movement to the cell periphery (Guardia et al., 2016).

Arl8b-mediated lysosome positioning has been shown to regulate lysosome interaction with processes occurring near the cell periphery, including growth factor-mediated activation of mTORC1, lysosome exocytosis, lysosome-mediated ER remodeling, focal adhesion disassembly, and cancer cell metastasis, to name a few (Dykes et al., 2016; Korolchuk et al., 2011a; Lu et al., 2020; Michelet et al., 2018; Rabanal-Ruiz et al., 2021; Rui Jia & Bonifacino, 2019; Saric et al., 2015). Further, the Arl8b-SKIP complex has been shown to promote tubulation of lysosomes in activated macrophages and the formation of tubular LAMP1-positive compartments (also known as *Salmonella*-induced filaments or SIFs) in *Salmonella*-infected cells (Sindhwani et al., 2017; Tuli & Sharma, 2019). Recent work has also shown that Arl8b-mediated lysosomal transport to the cell periphery is required for the exit of β-coronaviruses from lysosomes, where the viruses reside before egress (Ghosh et al., 2020).

In addition to small G proteins and their effectors, a few studies have also shown the role of lysosome membrane protein complexes in recruiting the dynein-dynactin motor, for example, MCOLN1 (TRPML1)-Alg2 and TMEM55B-JIP4 complex. These two starvation-induced mechanisms mediate dynein-dependent transport and clustering of lysosomes in the perinuclear region (Li et al., 2016; Wang et al., 2015; Willett et al., 2017). Recently, Septin 9 (SEPT9), one of the Septin GTP-binding proteins, has been shown to localize to lysosomes and promote dynein-dependent retrograde transport of lysosomes (Kesisova et al., 2021).

3.2. Regulation of lysosome positioning

The functions of lysosomes are governed by their position in the cell, and different pools of lysosomes are implemented into different types of functions. Moreover, various internal and external cues are known to have a role in maintaining the spatial distribution of lysosomes. Lysosomes sense these cues and alter their positioning and motility to meet cellular needs. The sections that follow provide insight into some of these intracellular and extracellular cues that regulate lysosome positioning in the cell.

3.2.1. Nutrient availability

As stated earlier, depletion of nutrients and/or growth factors results in lysosome clustering in the perinuclear region, where the proteolytic compartments may have more propensity to tether and fuse with the autophagosome. This starvation-induced perinuclear clustering is a highly complex process and tightly regulated by a variety of mechanisms. The net perinuclear movement of lysosomes is accomplished by increasing the perinuclear movement and suppressing the peripheral movement of the lysosomes (Ballabio & Bonifacino, 2020).

To enhance lysosome perinuclear clustering in response to starvation, transcription factor EB (TFEB) / transcription factor E3 (TFE3) promotes the expression of transient receptor potential mucolipin 1 (TRPML1) and transmembrane protein 55b (TMEM55b), as well as several other lysosomal and autophagy-related genes. Both proteins are located on the lysosome membrane but act independently in distinct protein complexes to accomplish the same task, increasing the lysosome's perinuclear positioning. Increased expression of TRPML1 (a calcium channel on the lysosome membrane) leads to increased cytosolic calcium levels, which activates the calcium sensor Asparagine-linked glycosylation protein 2 (ALG2), that acts as a linker between TRPML1 and minus-end directed motor dynein, hence promoting retrograde movement of lysosome (Li et al., 2016). Further, TRPML1 may also play a role in promoting autophagosome-lysosome fusion. On the other hand, TMEM55b, a transmembrane protein, recruits JNK Interacting Protein 4 (JIP4) that mediates coupling of the lysosome to the dynein-dynactin complex and eventually directs the juxta-nuclear clustering of the lysosomes (Willett et al., 2017).

Inhibition of the anterograde process can also equally contribute to the enhanced lysosome perinuclear clustering. One mechanism of action involves disruption of the

BORC-ARL8b-Kinesin-dependent peripheral lysosome trafficking. It has been demonstrated that late endosomal/lysosomal adaptor and MAPK and mTOR activator 2 (LAMTOR2), a component of the lysosomal protein complex Ragulator (which is recognised for its involvement in recruiting mTORC1 to the lysosome), adversely regulates the interaction of BORC-ARL8b with kinesin (Filipek et al., 2017; Pu et al., 2017). LAMTOR2 interacts with the lyspersin subunit of the BORC complex in a nutrient-dependent manner as amino acid starvation has been shown to enhance this interaction, which leads to uncoupling of lysosomes and anterograde motor kinesin (Filipek et al., 2017; Pu et al., 2017). Additionally, the absence of nutrients, especially amino acids, further blocks the VPS34-dependent PIntd3P synthesis on lysosome membranes, that renders recruitment of the FYVE and coiled-coil domain autophagy adaptor 1 (FYCO1) on lysosome surface, thereby inhibiting the Kinesin-1 loading and plus-end directed movement of lysosomes, resulting in an increased number of lysosomes in the juxta nuclear region of the cell (Hong et al., 2017).

3.2.2. Membrane contacts with other organelles

MCS (Membrane contact sites) are the unique interface between two organelles. As previously stated, lysosomes are classified into two separate pools: those that are less motile in the perinuclear region and those that are more motile in the periphery region of the cell (Scorrano et al., 2019). MCS contribute significantly in the maintenance of the perinuclear cloud of lysosomes through multiple MCS between the lysosome and organelles, including ER and the Golgi (Neefjes et al., 2017). Jongsma et al. demonstrated the involvement of ER resident protein RNF26, an ubiquitin ligase, in establishing MCS with different endosome vesicles by interaction with their unique adaptors, such as Toll Interacting Protein (TOLLIP) for LEs (M. L. M. Jongsma et al., 2016). The second MCS between the ER and the lysosomes is formed, particularly in cells with low cholesterol levels; in this instance, the ER-localized Vamp-associated protein A (VAP-A) protein interacts with oxysterol-binding protein-related protein 1L (ORP1L) on lysosomes, inhibiting their retrograde movement (Wijdeven et al., 2016). Upon nutrient deprivation, lysosomes are also known to form MCS with the Golgi in the perinuclear region, with the help of the lysosomal protein folliculin and the small GTPase Rab34, which is found on the Golgi membranes (Yip et al., 2016). Additionally, lysosomes form MCS with other organelles such as the peroxisome and

mitochondria to mediate cholesterol transport and mitochondrial fission, respectively (Chu et al., 2015; Scorrano et al., 2019; Wong et al., 2018).

3.2.3. Intracellular pH

Numerous investigations have shown that variations in the cytosolic pH affect the lysosome positioning. When the cytosol's pH is acidic, the majority of lysosomes migrate to the periphery, whereas under alkaline conditions perinuclear clustering is enhanced (Heuser, 1989; Korolchuk et al., 2011a). In addition to this, lysosome positioning is also correlated with their intraluminal pH. In particular, one study has shown that lysosomes positioned in the perinuclear area of the cells are relatively more acidic than the peripheral pool of lysosomes (Bright et al., 2016; Johnson et al., 2016). However, a subsequent study has shown that peripheral and perinuclear pools of lysosomes have a similar pH (Ponsford et al., 2020).

4. Bone remodeling and lysosomes

Bone is a dense, rigid, and calcified tissue that makes up the skeleton of the majority of vertebrae. While bone has a reputation for being a stable, hard, and static tissue that supports and protects vital organs, it is actually a highly specialized and constantly changing tissue in our body (Teitelbaum, 2000). Bone remodeling, the process of replacing old or damaged bone with new bone in response to different stimuli, is a regulated and coordinated mechanism that is necessary for our body's bone and mineral homeostasis. Various components and signaling pathways govern bone remodeling, and the stimulus to activate the remodeling process can be systemic (in response to hypocalcemia) or localized (in response to mechanical stress). The remodeling process is highly controlled and requires cooperation and communication among distinct bone cells. Coordination impairment might contribute to the development of conditions like osteoporosis or osteopetrosis (Crockett et al., 2011).

4.1. Bone cells

Bone is primarily composed of three unique cell types: osteocytes, osteoblasts, and osteoclasts (**Figure 6**). In order to maintain bone homeostasis, these different cell types play distinct yet interdependent functions and are discussed next.

4.1.1. Osteoblasts

Osteoblasts are specialized fibroblast-like cells that develop from mesenchymal stem cells and share a common lineage with chondrocytes and adipocytes. Osteoblasts play a crucial role in bone remodeling and are primarily responsible for synthesizing and secreting components such as type I collagen that form the organic matrix of bone. In addition to this, osteoblasts also facilitate the mineralization of organic matrix. When active, osteoblasts attain a cuboidal shape and are found on the surface of bone formation sites, whereas in their dormant state, osteoblasts establish a lining along the surface of the bone. After fulfilling their remodeling job, osteoblasts may take one of three paths: some become bone lining cells, some undergo apoptosis, and others get entrapped in freshly produced bone and to become osteocytes (H. Zhao, 2012).

4.1.2. Osteocytes

Osteocytes are osteoblast that have reached the end of their development and get entrapped in the bone matrix. Osteocytes are the most common type of bone cell, accounting for more than 90% of all bone cells. Lengthy dendritic processes of the osteocytes, as well as their extensive distribution in the bone matrix, allow them to interact with other cells with ease, and as a result, they function as mechanosensors in the bone. Furthermore, studies have shown the importance of osteocytes in the process of bone mineralization (Mohamed, 2008).

4.1.3. Osteoclasts

Osteoclasts are multinucleated cells derived from the macrophage/ monocyte lineage. These one-of-a-kind giant cells are formed by fusing mononucleated precursor cells in the presence of key cytokines RANKL (Receptor Activator of Nuclear Factor-Kappa B Ligand) and M-CSF (Macrophage-Colony Stimulating Factor). Osteoclasts, also known as bone-eating cells, help in the bone remodeling process and mineral homeostasis by resorbing old and damaged bone (Teitelbaum, 2000). How osteoclasts resorb the bones and the key factors involved in this process is described below.

4.2. Bone remodeling cycle

The bone remodeling cycle is divided into five distinct but overlapping stages: activation, resorption, reversal, formation, and termination (Kenkre & Bassett, 2018) as shown in **Figure 6.** The formation and recruitment of osteoclasts at the site of bone resorption initiates the remodeling cycle, which is followed by the breakdown of the bone matrix by

acid and lysosomal proteases. A stage known as reversal is initiated after resorption has taken place, and consists mostly of preparatory procedures for the deposition of new bone matrix. Throughout this step of preparation, a non-collagenous matrix "cemented line" is deposited over the freshly resorbed region, enabling osteoblast adhesion during the subsequent stage of the cycle. In the formation stage of cycle, osteoblasts generate new bone matrix by secreting type-I collagen and further regulate bone mineralization. After fulfilling their purpose, osteoblast cells undergo apoptosis and/or turn into osteocytes, or layer around the bone surface to become bone lining cells, completing the bone remodeling cycle. Following the termination stage, the bone reverts to a resting condition until the next remodeling cycle begins (Crockett et al., 2011; Fink Eriksen, 2010; Kenkre & Bassett, 2018; Walsh, 2015).

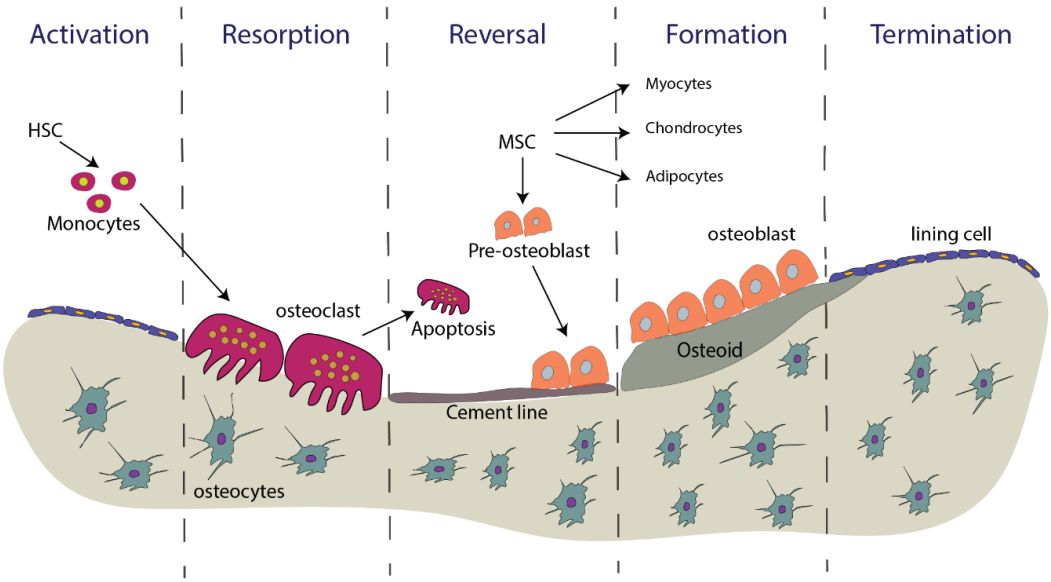

Figure 6: Different stages of the bone remodeling cycle. The steps of activation, resorption, reversal, formation, and termination are shown in this schematic of the bone remodeling cycle. Hematopoietic stem cells (HSCs) and mesenchymal stem cells (MSCs) are two types of stem cells.

4.3. Differentiation and activation of osteoclasts

Osteoclastogenesis is the process by which multinucleated large osteoclasts differentiate from mononucleated monocytes. It is a multi-step process that requires sequential and coordinated action of a plethora of signaling molecules and transcription factors (Miyamoto, 2011; Ohmae et al., 2017; Takayanagi et al., 2002) as shown in **Figure 7**. Osteoclastogenesis also involves other bone cells (osteoblasts and osteocytes), which provide necessary stimuli for osteoclast formation and differentiation (N. K. Lee, 2010; Teitelbaum, 2007).

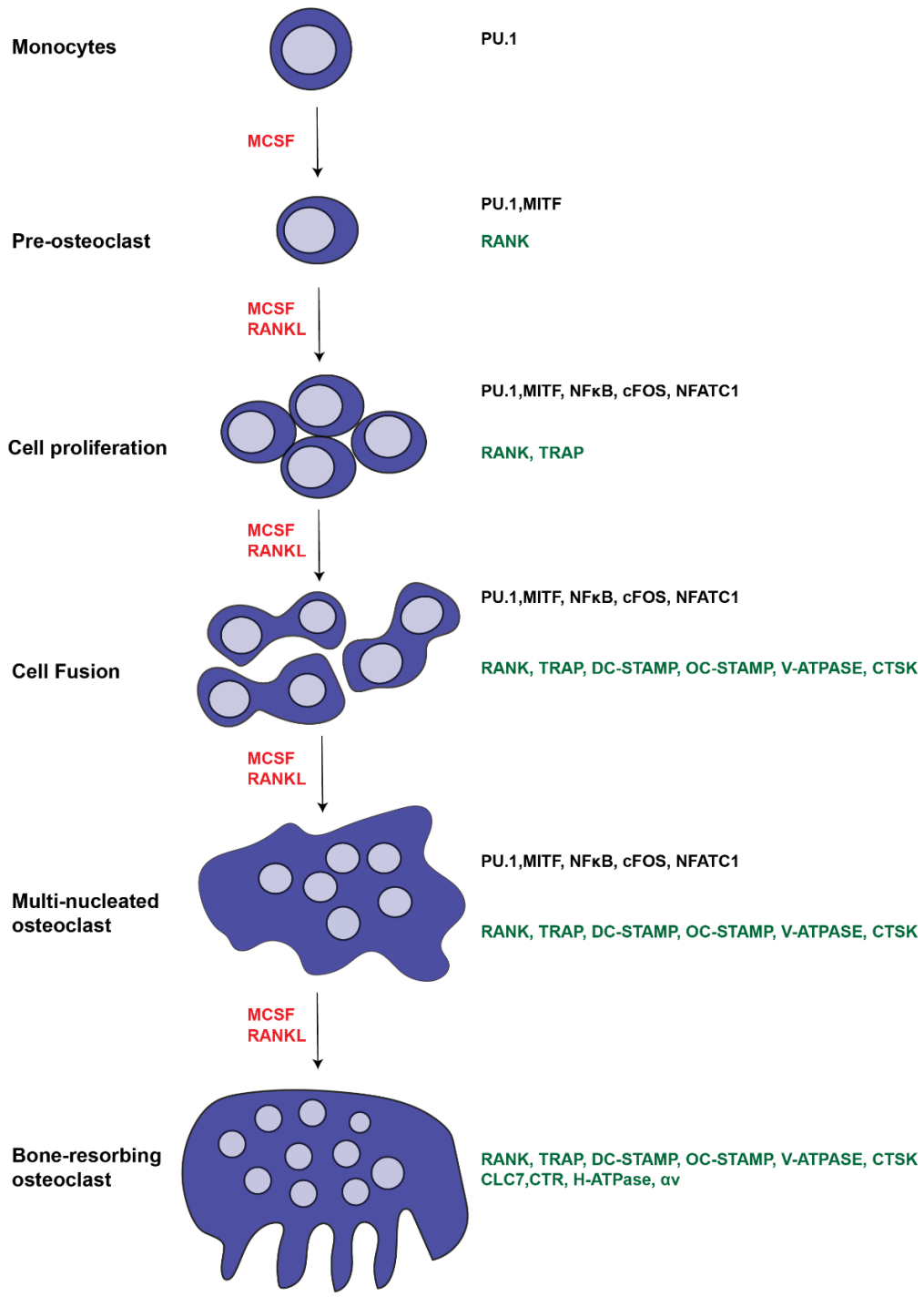

Figure 7: The key molecules influencing osteoclast development and activity. M-CSF and PU.1 govern the development of hematopoietic stem cells into osteoclast precursors, which undergo cell-cell fusion to generate multinucleated cells. RANKL/RANK signaling activates subsequent mediators, resulting in the production of mature osteoclasts that resorb bones.

M-CSF and RANKL are primary signaling molecules required for osteoclasts differentiation. These two cytokines are implicated in almost every aspect of osteoclastogenesis and osteoclasts activity. Both M-CSF and RANKL are generated by a variety of cells, including osteoblasts. The M-CSF secreted by osteoblasts or

osteocytes binds to its cognate receptor colony-stimulating factor receptor (C-FMS) on the surface of monocytes, and thereby initiates osteoclastogenesis (J. M. Kim et al., 2020). As a monocyte survival and growth factor, M-CSF increases monocyte population to achieve the ideal cell density necessary for cell-cell fusion. Additionally, M-CSF increases the expression of receptor activator of nuclear factor-kappa B (RANK) on the surface of monocytes making monocytes more committed to osteoclast development (Marino et al., 2014).

Receptor activator of nuclear factor-kappa B ligand (RANKL) is a type II membrane protein that also goes by the names osteoclast differentiation factor (ODF) and tumor necrosis factor-related activation-induced cytokine (TRANCE). It is a member of the tumor necrosis factor (TNF) superfamily. RANKL protein can be present in two forms, a membrane-anchored protein and a secreted protein. Upon binding of RANKL to RANK on osteoclast precursor cells, a signaling cascade is initiated that induces activation of a variety of pro-osteoclastogenic molecules and transcription factors (Feng, 2005; N. K. Lee, 2017), ultimately resulting in the formation of multinucleated osteoclasts (**Figure 8)**.

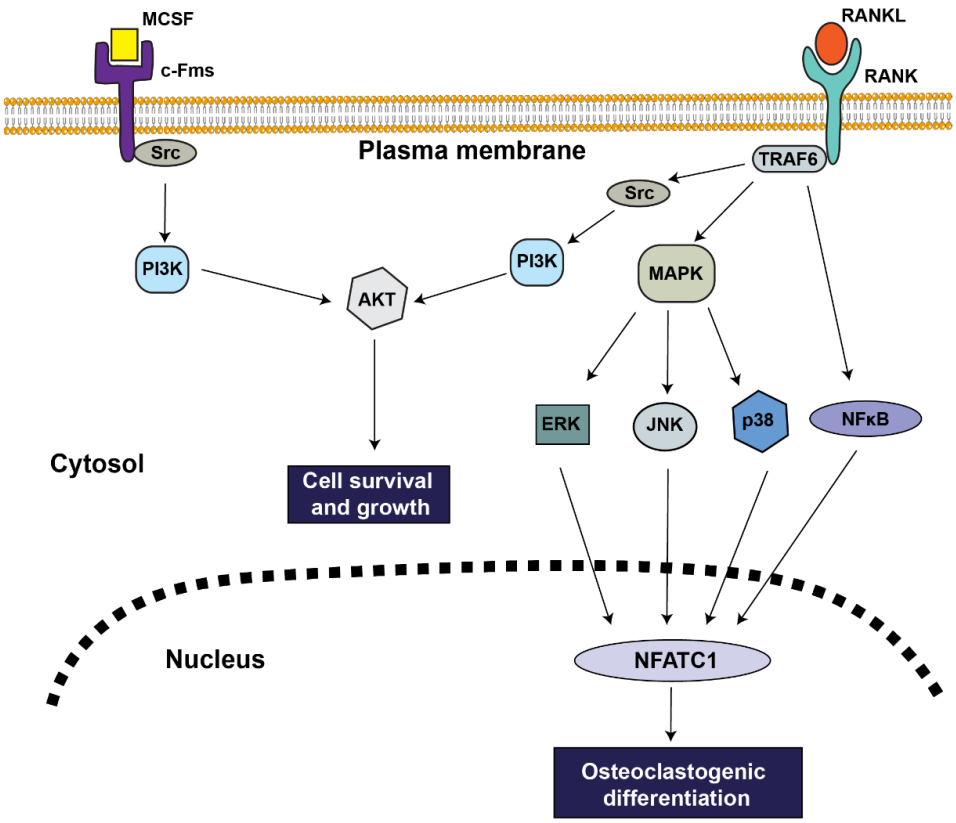

Figure 8: The osteoclast differentiation signaling network. Binding of RANKL to its cognate receptor RANK triggers a number of intracellular signaling pathways via TRAF-6, including Src, NF-κB, ERK, JNK, p38, and NFATc1.

Indeed, many of these factors are indispensable for osteoclast differentiation and activity. TNF receptor- associated factors (TRAFs) adaptor proteins are recruited to the conserved TRAF domains located within the C-terminal cytoplasmic tail of RANK as a result of RANKL binding, which results in the trimerization of RANK. Studies have shown that, of all the TRAF family members, TRAF6 is a key adapter protein in the RANKL-RANK signaling cascade for osteoclast development and function, as the phenotype of TRAF6-lacking mice is strikingly comparable to the skeletal phenotypes of RANK-lacking mice (Lomaga et al., 1999). The recruitment and activation of TRAF6 leads to the activation of Nuclear Factor Kappa-light-chain-enhancer of activated B cells (NF-κB), Mitogen-Activated Protein Kinases (MAPKs) and Protein Kinase B (PKB/AKT). TRAF6 binding to RANK activates Extracellular signal-regulated kinase (ERK), c-Jun N-terminal kinases (JNK), and p38 in osteoclast precursors, via activating MEK1/2, MKK7, and MKK6 respectively. Activated ERK, JNK, and p38 subsequently stimulate their downstream targets, resulting in the activation of pro-osteoclastogenic transcription factors. RANKL stimulation also activates the key pro-survival PI3K/AKT pathway with the assistance of TRAF6 and Src, (Boyce & Xing, 2008; Feng, 2005; N. K. Lee, 2017).

In addition to its role in the survival of osteoclast precursor cells, PI3K has been implicated in actin filament formation through its interaction with gelsolin (Biswas et al., 2004). Nuclear factor of activated T-cells 1 (NFATc1) is the major transcription factor that is involved in the regulation of osteoclast differentiation and activation. As NFATc1 becomes more activated, it translocates to the nucleus, where it stimulates and enhances the expression of osteoclast specific genes such as tartrate-resistant acid phosphatase (TRAP), osteoclast-associated receptor (OSCAR), and cathepsin K. NFATc1 promotes osteoclast cell-cell fusion through transcriptional activation of the vacuolar ATPase V0 domain (Atp6v0d2) d2 variant and the dendritic cell-specific transmembrane protein (DC-STAMP). The ability of NFATc1 overexpression to induce osteoclastogenesis in the absence of RANKL suggests the crucial role of this master regulator in these cells (Feng, 2005; J. H. Kim & Kim, 2016; Takayanagi et al., 2002). Calcium/calmodulin signaling also is implicated in NFATc1 activation, although RANK does not activate calcium signaling in osteoclast precursors. Therefore, RANKL partly activates NFATc1, and costimulatory and RANKL signaling cooperate to induce NFATc1 (N. K. Lee, 2017). In addition to promoting osteoclastogenesis,

osteoblasts also synthesize some factors that negatively regulate the osteoclast maturation and activation process. One such factor is osteoprotegerin (OPG). OPG, also called osteoclast inhibitory factor (OCIF), competitively binds to RANKL and blocks the RANK-RANKL interaction, thereby inhibiting osteoclast differentiation and activation (Boyce & Xing, 2008). Additionally, osteoclasts are known to synthesize and secrete soluble substances that interact with their corresponding receptors on osteoblasts, promoting or inhibiting osteoblast development (J. M. Kim et al., 2020).

The differentiated multinucleated osteoclasts undergo modifications in their cellular compartments to become fully active for bone resorption. The cytoskeleton is reorganized, and three different membrane domains (sealing zone (SZ), ruffled border (RB), and functional secretory domain (FSD)) are established in the cell, resulting in polarization of the osteoclast on the bone surface (Aeschlimann & Evans, 2004; Mulari et al., 2003). Bone resorption by osteoclasts is enabled by these three distinct domains, each with its own function. The reorganization of the actin cytoskeleton in osteoclasts results in the formation of a sealing zone that facilitates cell adhesion to the bone surface and also denotes the area for bone resorption. The sealing zone is composed primarily of numerous small actin ring structures called podosomes (Takito et al., 2018). Following the creation of the sealing zone and osteoclast attachment to the bone surface, the RB is established in the SZ and the FSD is formed on the opposite side of the RB **Figure 9** (Väänänen et al., 2000).

A ruffled border is a specific finger-like structure generated by the fusion of lysosomes (acidic vesicles) with the plasma membrane that is found in the sealing zone of the cell membrane. Proton pumps and other membrane channels are found in abundance along the ruffle border, and contribute to acidification of the cavity between the bones and the ruffle border, which is referred to as the resorption lacuna (Ross, 2009). Because of the acidic environment in the lacuna, the inorganic layer of hydroxyapatite from the bone is dislodged, and the continual fusing of lysosomes to the ruffle border supplies an abundant number of proteases, such as cathepsin K, that breakdown the organic matrix of bone. In the following step, the degraded material from the resorption lacuna is endocytosed and expelled via the functional secretory domain of the osteoclasts (Crockett et al., 2011; Rucci & Teti, 2016).

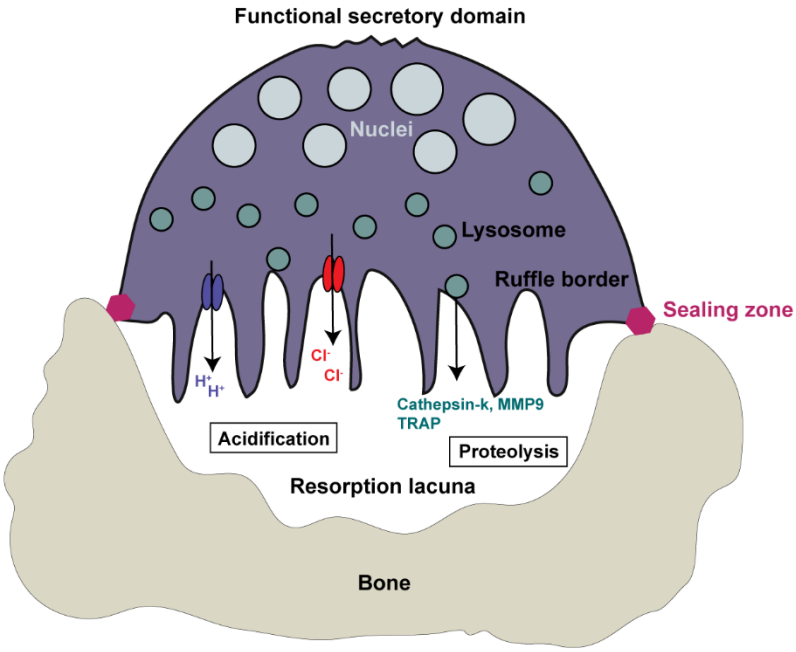

Figure 9: Bone resorbing osteoclasts. When osteoclasts adhere to bone, they become polarize and remodel their cytoskeleton. The sealing zone is characterized by a peripheral ring of adhering structures that surrounds the ruffled border, a specialized region formed of membrane extensions aimed toward the bone. After being taken up by transcytosis, the degraded bone matrix products are transferred to the functional secretory domain.

In addition to bone resorption, the presence of specific proteases and a low pH in the resorption lacuna is required for the activation of osteocalcin, a non-collagenous bone-derived hormone that has been found to alter glucose metabolism, testosterone synthesis, and muscle mass (Komori, 2020). Therefore, lysosomes play an important role in physiological processes mediated by osteoclasts. Furthermore, mutations in genes encoding lysosomal proteins have been related to a variety of human osteoporosis types, demonstrating the relevance of lysosomes in the osteoclast-mediated processes that occur in the body (Lacombe et al., 2013).

4.4. The role of lysosome in osteoclast biology

There are four primary kinds of lysosomal or lysosome-related proteins that are required for osteoclast differentiation and resorption activity. The first group comprises proteins involved in maintaining the low pH of the resorption lacuna (**Table 2**) (Luxenburg et al., 2007; Matsumoto et al., 2018; Visentin et al., 2000). while the second group encompasses enzymes involved in the breakdown of the bone matrix in the resorption lacuna such as Cathepsin-K and MMPs (Matrix metalloproteinases MMPs) (Lacombe et al., 2013).

Table 2: Lysosomal proteins involved in the acidification of the extracellular matrix

Protein name	Function
ATP6V0D2	ATPase H+ Transporting V0 Subunit D2
ATP6V1C1	ATPase H+ Transporting V0 Subunit C1
OSTM1	ClC-7 β subunit
ClC-7	Chloride channel
ATP6a3	V-ATPase accessory subunit
AC45	V-ATPase accessory subunit

The third group includes proteins that are involved in lysosome trafficking, fusion, and ruffle border development, whereas the fourth group contains proteins involved in regulating lysosome biogenesis in osteoclasts. Due to the crucial role that lysosomes play in osteoclast function, the activity of these organelles must be strictly controlled in osteoclasts. This is accomplished by the collaboration of several proteins and processes (**Table 3**). The bulk of these proteins, interestingly, are involved in the transport and mobility of lysosomes (Coxon & Taylor, 2008; G. Stenbeck, 2004; Gudrun Stenbeck & Coxon, 2014).

Table 3: List of proteins involved in lysosomal regulation in osteoclasts.

Protein name	Function in osteoclast
Rab7	Lysosome trafficking and ruffle border formation
Rab3d	Lysosome trafficking
TCTEX-1	Regulates lysosome trafficking via Rab3d
Rab27	Regulates lysosome trafficking and actin ring formation
Synaptotagmin VII	Regulates the secretion of lysosomes
TPCN2	Regulates the secretion of lysosomes
SNX10	Sorting nexin, endosomes trafficking
ATG5	Regulates the secretion of lysosomes
PLEKHM1	Lysosome transport
NDEL1	Lysosome transport to ruffle border via Rab7 and PLEKHM1
TFEB	Transcriptional regulation of lysosomal biogenesis
PKCβ	Transcriptional regulation of lysosomal biogenesis
TRPML1	Regulates NFATC1 activation via calcium release

The members of the Rab family of small GTPases and their downstream effectors, which are well-known for their role in the regulation of endosomal trafficking in various cell types, have also been demonstrated to play a critical role in osteoclast bone resorption activity. Rab7, a small GTPase found on late endosomes and lysosomes, has been extensively studied in osteoclasts, and there is compelling evidence that it is involved in lysosome trafficking and, as a result, bone resorption activity (Roy & Roux, 2020). In active osteoclasts, Rab7 localizes on the ruffle border, and silencing of Rab7 in these cells has been demonstrated to inhibit the creation of acting rings and the ruffle border, as well as significantly reduce the bone resorption activity of these cells. Rab7 requires other adapter and motor proteins in order to ensure proper transport of lysosomes in the sealing zone and the creation of the ruffle border. In this regard, PLEKHM1 is one of the effectors that, through its interaction with family with sequence similarity 98 member A (FAM98A) and Nuclear Distribution protein nudE-like 1 (NDEL1), links Rab7 positive lysosomes to the dynein motor complex (Fujiwara et al., 2016; Ye et al., 2011). Moreover, studies have shown that osteoclasts from PLEKHM1-Knock-out (KO) mice, as well as osteoclasts from human patients with PLEKHM1 loss-of-function mutations, had lower resorption activity as a consequence of the absence of a ruffled border in these cells (Van Wesenbeeck et al., 2007).

Rab3d was identified as the primary osteoclastic Rab3 isoform, and mice deficient of Rab3d had increased bone mass and reduced osteoclast activity when compared to control mice. Furthermore, while osteoclasts lacking Rab3d exhibit typical F-actin rings and podosomes, they show a significant defect in the formation of ruffle borders. Rab3d and its effector Tctex-1, which is a component of the cytoplasmic dynein motor, are involved in secretory vesicle trafficking toward the ruffled border (Pavlos et al., 2011).

The expression of Rab27a is also increased during the development of osteoclasts. Studies found that the secretory lysosome trafficking in osteoclasts was disrupted in Rab27a-deficient mice, and that bone resorption was impaired. These findings suggest that Rab27a is important in secretory lysosome trafficking in osteoclasts. Additionally, reducing Rab27a expression resulted in a significant reduction in osteoclastogenesis, indicating that Rab27a may also be involved in osteoclast development (Tsukuba et al., 2017).

RAB13 expression is substantially increased in osteoclasts during differentiation, although it is not associated with osteoclasts' bone resorption activity. Rab13 deregulation has no effect on osteoclast differentiation, and Rab13 localization is confined to vesicular structures in proximity to the TGN in mature osteoclasts, indicating a role of Rab13 in osteoclast secretory activities (Roy & Roux, 2020). Other Rab family small GTPases, including Rab5c, Rab11b, Rab9, Rab38, and Rab44, have also been found to contribute to osteoclast differentiation or activation. However, further studies are required to determine their precise mechanistic role (Roy & Roux, 2020).

4.5. Autophagy in osteoclast differentiation and function

Autophagy is a conserved survival mechanism in eukaryotic cells that involves the degradation of unwanted cell components (damaged organelles and protein aggregates) in order to create nutrients and energy for the cells and hence promote cell viability (Levine & Kroemer, 2019). This fundamental catabolic process serves as a quality control mechanism in eukaryotic cells and aids in maintaining cellular homeostasis. Initially, the formation of an "autophagosome," a unique double-membraned intermediate organelle that engulfs specific cytoplasmic components such as non-functioning proteins and organelles, marks the beginning of the process of autophagy. Subsequently, by fusing with the lysosome, the autophagosome evolves into an autolysosome, which develops the ability to degrade the ingested material via a variety of hydrolases and proteases (Nakamura & Yoshimori, 2017; Yang & Wang, 2021). In most cases, the autophagy process is governed by a set of nearly 40 autophagy-related (ATG) proteins that have been shown to be extremely conserved in nature (Reggiori & Ungermann, 2017). Various studies in the last few years have shown the importance of core ATG proteins in processes similar to, but distinct from, conventional autophagy, such as LC3-mediated phagocytosis (LAP) and ATG gene-dependent exocytosis and secretion of intracellular cargo (Heckmann & Green, 2019; H. K. Lee et al., 2010).

4.5.1. Autophagy regulates osteoclastogenesis

Osteoclasts, which grow on the surface and core of the bone, are subjected to low oxygen levels in their immediate surroundings. Studies have demonstrated that hypoxia promotes osteoclast development and function by increasing autophagy flux through

activation of hypoxia inducing factor-1α (HIF-1α). Additionally, HIF-1α upregulates the expression of Bcl-2/adenovirus E1B 19kDa interacting protein 3 (BNIP3), which in turn enhances the expression of autophagy and osteoclast-related genes, resulting in increased osteoclastogenesis (Tan et al., 2021; Y. Zhao et al., 2012). In addition to induce the expression of several important genes for regulation of osteoclastogenesis under hypoxic environments, HIF-1 also regulates miRNAs that are implicated in the regulation of autophagy in these cells. Moreover, treatment of osteoclasts with autophagy inhibitors such as Bafilomycin A1 (Baf A1) , Chloroquine and 3-methyladenine (3-MA) inhibits osteoclastogenesis (Xiu et al., 2014; Y. Zhao et al., 2012; Zhu et al., 2016). This suggests that there is a clear link between conventional autophagy and osteoclast formation.

4.5.2. Role of autophagy proteins in bone resorption activity of osteoclast

To release the components that promote bone resorption, osteoclasts must fuse their lysosomes with the ruffle border, as previously explained. Interestingly, mice lacking ATG5, ATG4b, and ATG7 showed non-resorbing osteoclasts owing to faulty lysosome fusing to the ruffle border and cathepsin-K secretion (Deselm et al., 2011). Furthermore, it has been shown that LC3II is present on the ruffle border and that its recruitment is essential for ruffle border development and bone resorption. Cells lacking LC3 conversion machinery, as expected, failed to establish the ruffle boundary and undertake bone resorption. (Gelman & Elazar, 2011; Ohmae et al., 2017; Tran et al., 2016).

PLEKHM1 and Rab7 are two well-known autophagy-related proteins. They contribute to the last phase of autophagy by recruiting the HOPS complex and other components necessary for lysosome-autophagosome fusion. Interestingly, both of these proteins are required for osteoclast activity, since osteoclasts lacking Rab7 or PLEKHM1 fail to create ruffle borders (Fujiwara et al., 2016; Gudrun Stenbeck & Coxon, 2014).

5. Scope and Objective of the study

Lysosomes participate in a variety of physiological functions, including autophagy, nutrient sensing and signaling, plasma membrane repair, immunological response, cell migration, cancer metastasis, bone resorption, and gene control (Ballabio & Bonifacino, 2020; Inpanathan & Botelho, 2019; Lawrence & Zoncu, 2019; Matte & Pasqualim, 2016; Oyarzún et al., 2019; Tsukuba et al., 2017). Since lysosomes are involved in

many cellular activities, lysosomal dysfunction has a profound impact on cellular homeostasis. As a consequence, it should come as no surprise that lysosomal dysfunction contributes to a broad spectrum of ailments, including lysosome storage disorder, cancer, cardiovascular disease, neurological disorders, and osteoporosis (Fennelly & Amaravadi, 2017; McGrath et al., 2021; Oyarzún et al., 2019; Shrestha et al., 2016b; Q. Zhao et al., 2020).

In order to conduct a wide variety of functions, the motility and spatial positioning of lysosomes is very essential. Nevertheless, a range of intracellular and external signals (such as nutrient availability, pathogens, intracellular pH, oxidative stress, and membrane contact sites) are known to have a role in lysosome spatial distribution. Lysosomes sense these stimuli and alter their positioning and motility to fulfil the needs of the cell (Bonifacino & Neefjes, 2017; Dykes et al., 2016; Johnson et al., 2016; Korolchuk et al., 2011b; Laopanupong et al., 2021; Saric et al., 2015; Takemasu et al., 2019; Tuli et al., 2013; Willett et al., 2017). Like other organelles, lysosomes move along microtubule tracks. Microtubule tracks are distributed radially throughout a non-polarized cell, with minus-ends heading towards the MTOC (Microtubule-organizing center) in the perinuclear/juxta-nuclear region and plus-ends scattered across the cell periphery. Dynein and kinesin motor proteins govern retrograde (minus end-directed) and anterograde (plus end-directed) lysosome movement respectively (Granger et al., 2014; Hunt & Stephens, 2011). However, small GTPases and their effectors, as well as other adaptor proteins, promote the linking of motor proteins with lysosomes (Donaldson & Jackson, 2011; Homma et al., 2021; Kjos et al., 2018).

Arl8b, a small G protein, plays a vital role in modulating lysosomal positioning and subcellular functions (Khatter et al., 2015). Overexpression of Arl8b has been shown to increase the number of lysosomes that move bi-directionally along microtubule tracks (Hofmann & Munro, 2006). Subsequent studies revealed that Arl8b and its effector SKIP/PLEKHM2 bind to and recruit the kinesin-1 motor, hence causing anterograde lysosome migration. However, it has not been established if Arl8b can promote long-distance retrograde lysosome trafficking (Keren-Kaplan & Bonifacino, 2021; Pu et al., 2015; Rosa-Ferreira & Munro, 2011). In chapter 2, we have mechanistically explored the role of Arl8b in retrograde movement of lysosomes.

Lysosome positioning mediated by Arl8b and its effectors regulates a broad range of cellular processes in a wide variety of cell types, including plasma membrane repair,

nutrient sensing and response, natural killer cell–mediated cytotoxicity, antigen presentation, cell migration, tubular lysosome formation in macrophages, lysosome exocytosis, lysosome-mediated ER remodelling, focal adhesion disassembly, and cancer cell metastasis (Ghosh et al., 2020; Michelet et al., 2018; Mrakovic et al., 2012; Saitoh et al., 2017; Saric et al., 2015; Tuli et al., 2013).

In addition to this, lysosomes play a critical function in bone remodeling and skeletal homeostasis (Lacombe et al., 2013). The tuned action of osteoclasts and osteoblasts, the two types of bone cells, is required for maintaining the balance in bone resorption and bone formation (Kenkre & Bassett, 2018). In order to resorb bone, osteoclasts need an acidic environment in the region where they reside on the bone and release acid hydrolases to degrade collagen. Interestingly, lysosomes are able to meet all requirements. Several independent investigations have shown that proteins involved endosome trafficking and membrane fusion are necessary for osteoclast ruffle border development and bone resorption activity (Coxon & Taylor, 2008; Roy & Roux, 2020; H. Zhao, 2012a). Furthermore, the importance of lysosomes for osteoclasts has long been established, as shown by the fact that mutations in genes involved in lysosome synthesis and trafficking impede bone resorption activity and result in disorders like osteopetrosis (Lacombe et al., 2013). One such gene is *PLEKHM1*, a mutation in the *PLEKHM1* gene known to cause osteopetrosis in rats and humans (Fujiwara et al., 2016; Van Wesenbeeck et al., 2007). Notably, we previously showed that the Rab7 effector-PLEKHM1 interacts with Arl8b and serves as a linker, facilitating lysosome clustering and fusion with late endosomes and autophagosomes in epithelial cells (Marwaha *et al.*, 2017).

Despite the well-known role of Arl8b in lysosome positing and motility, as well as in membrane fusion, it has not yet been established whether or not Arl8b plays a role in bone remodelling and skeletal homeostasis. In chapter 3, we demonstrate the role of Arl8b in bone resorption activity of osteoclasts.

Chapter 2

RUFY3 links Arl8b and JIP4-Dynein complex to regulate lysosome size and positioning

Chapter 2

RUFY3 links Arl8b and JIP4-Dynein complex to regulate lysosome size and positioning

Abstract

The bidirectional movement of lysosomes on microtubule tracks regulates their whole-cell spatial distribution. Arl8b, a small GTP-binding (G) protein, promotes lysosome anterograde trafficking mediated by kinesin-1. Herein, we report an Arl8b effector, RUFY3, which regulates the retrograde transport of lysosomes. We show that RUFY3 interacts with the JIP4-dynein-dynactin complex and facilitates Arl8b association with the retrograde motor complex. Accordingly, RUFY3 knockdown disrupts the positioning of Arl8b-positive endosomes and reduces Arl8b colocalization with Rab7-marked late endosomal compartments. Moreover, we find that RUFY3 regulates nutrient-dependent lysosome distribution, although autophagosome-lysosome fusion and autophagic cargo degradation is not impaired upon RUFY3 depletion. Interestingly, lysosome size is significantly reduced in RUFY3 depleted cells, which could be rescued by inhibition of the lysosome reformation regulatory factor PIKFYVE. These findings suggest a model in which the "perinuclear cloud" arrangement of lysosomes regulates both the positioning and size of these proteolytic compartments.

The work presented in this chapter was carried out in collaboration with the laboratory of Dr. Mahak Sharma at IISER-Mohali, and was recently published in the Nature Communications 13, 1540 (2022). https://doi.org/10.1038/s41467-022-29077 y.

Introduction

Lysosomes are heterogeneous membrane-bound organelles containing more than 60 acid hydrolases that mediate the degradation of various biological macromolecules, including proteins, carbohydrates, lipids, and nucleic acids (Ballabio & Bonifacino, 2020). Recent studies suggest that lysosomes are sites for storing inactive hydrolases, and the fusion of lysosomes with the cargo-containing acidic late endosomes forms a hybrid compartment-endolysosomes where most of the cargo degradation takes place (Bissig et al., 2017; Bright et al., 2016; Huotari & Helenius, 2011). As late endosomes, lysosomes, and endolysosomes share many commonly analyzed membrane proteins (such as LAMP1), we collectively refer to these compartments as lysosomes. Lysosomes range in numbers of 50-1000 in cultured cells and are primarily present as a relatively immobile pool in the perinuclear region of the cell (sometimes referred to as the perinuclear cloud). A minor population of lysosomes escapes from the perinuclear cloud and undergoes long-range bidirectional transport on the microtubule tracks (Cabukusta & Neefjes, 2018; M. L. M. Jongsma et al., 2016).

Lysosomal subcellular distribution is not static and changes with the presence/absence of nutrients, growth factors, change in cytosolic pH, exposure to oxidative stress, infection etc.(Bonifacino & Neefjes, 2017; Dykes et al., 2016; Korolchuk et al., 2011a; Laopanupong et al., 2021; Saric et al., 2015; Takemasu et al., 2019; Willett et al., 2017). More importantly, cues such as nutrients and/or growth factors influence lysosome-mediated cellular responses under these physiological conditions by altering lysosomal distribution. For instance, depletion of nutrients and/or growth factors results in lysosome clustering in the perinuclear region, where the proteolytic compartments may have more propensity to tether and fuse with autophagosomes (Kimura et al., 2008; Korolchuk et al., 2011a). The degradation of autophagic cargo and subsequent recycling of breakdown products replenishes nutrient reserves under starvation conditions. In contrast, growth factor re-stimulation results in lysosome localization near the plasma membrane that facilitates reactivation of lysosomal-localized mTORC1 signaling complex, and consequently, gene expression required for protein synthesis (Rui Jia & Bonifacino, 2019). Recent studies have also highlighted the role of lysosome positioning in promoting ER remodeling from sheets to tubules in the peripheral

cellular space Also, the proximity of lysosomes to focal adhesions near the plasma membrane regulates lysosome-dependent focal adhesion disassembly and promotes growth factor-dependent activation of the mTORC1 signaling complex (Rabanal-Ruiz et al., 2021; Schiefermeier et al., 2014).

Several factors, including the continuous long-range motility on the microtubule tracks, association with the actin cytoskeleton and tethering to the ER network, regulate the spatial distribution of lysosomes at the whole-cell scale. The microtubule-based motor proteins, cytoplasmic dynein in complex with dynactin and multiple kinesin family members, promote retrograde (towards microtubule minus-end) and anterograde (towards microtubule plus-end) lysosome motility, respectively (Bonifacino & Neefjes, 2017; Hunt & Stephens, 2011). Motor proteins are recruited on the organelle membranes by association with their adaptors, generally effectors of Rab and Arf-like (Arl) small GTP-binding (G) proteins (Donaldson & Jackson, 2011; Homma et al., 2021; Kjos et al., 2018). Rab7-RILP represents a well-characterized small G protein-effector complex that recruits the motor dynein-dynactin complex to promote retrograde motility of the late endocytic compartments (Johansson et al., 2007; Jordens et al., 2001). Rab7 also interacts with FYCO1 (FYVE-and coiled coil domain containing 1) to recruit kinesin-1 for anterograde motility of late endocytic compartments towards the plasma membrane (Pankiv et al., 2010).

A key player, now well known for regulating the lysosomal spatial distribution, is the small G protein Arl8 (Khatter, Sindhwani, et al., 2015). Arl8 has two paralogs in mammalian cells, Arl8a and Arl8b, which are ~91% identical at the protein level and have an overlapping role in regulating lysosomal distribution. Arl8b, the better-characterized paralog, recruits its downstream effector, PLEKHM2 (also known as SKIP for SifA and Kinesin Interacting Protein) on lysosomes, which in turn recruits kinesin-1 to mediate anterograde motility of lysosomes (Hofmann & Munro, 2006; Udia et al., 2011). Interestingly, PLEKHM1, an effector of the late endosomal small G protein Rab7, competes with SKIP/PLEKHM2 for Arl8b-binding and repositions lysosomes towards the perinuclear region. The Arl8b-PLEKHM1 complex also promotes clustering and fusion of autophagosomes/late endosomes with lysosomes by recruiting the multisubunit tethering factor HOPS complex (Marwaha et al., 2017b).

Arl8 paralogs also regulate KIF1A-dependent lysosome movement to the cell periphery (Guardia et al., 2016).

Arl8b-mediated lysosome positioning has been shown to regulate lysosome interaction with processes occurring near the cell periphery, including growth factor-mediated activation of mTORC1, lysosome exocytosis, lysosome-mediated ER remodeling, focal adhesion disassembly, to name a few (Jia et al., 2017; Lu et al., 2020; Michelet et al., 2018; Pu et al., 2015, 2017; Rui Jia & Bonifacino, 2019; Schiefermeier et al., 2014). Further, the Arl8b-SKIP complex has been shown to promote tubulation of lysosomes in activated macrophages and the formation of tubular LAMP1-positive compartment (also known as *Salmonella*-induced filaments or SIFs) in *Salmonella*-infected cells ((Mrakovic et al., 2012; Sindhwani et al., 2017b; Tuli & Sharma, 2019). Recent work has also shown that Arl8b-mediated lysosomal transport to the cell periphery is required for the exit of β-coronaviruses from lysosomes, where the viruses reside before egress (Ghosh et al., 2020).

In addition to small G proteins and their effectors, few studies have shown the role of lysosome membrane proteins complexes in recruiting the dynein-dynactin motor, for example, MCOLN1 (TRPML1)-Alg2 and TMEM55B-JIP4 complex (Li et al., 2016; Willett et al., 2017). These two starvation-induced mechanisms mediate dynein-dependent transport and clustering of lysosomes in the perinuclear region. Recently, Septin9 (SEPT9), one of the Septin GTP-binding proteins, has been shown to localize to lysosomes and promote dynein-dependent retrograde transport of lysosomes (Kesisova et al., 2021).

Here, we report that RUN and FYVE domain-containing protein 3 (RUFY3) binds to Arl8b and recruits the JIP4-dynein-dynactin complex on Arl8b-positive lysosomes. Unlike PLEKHM1 and SKIP/PLEKHM2 (the two shared interaction partners of Arl8b and Rab7), RUFY3 did not interact with Rab7. Accordingly, upon RUFY3 depletion, there was a striking redistribution of Arl8b to the cell periphery, while Rab7 distribution was less affected. Previous studies have shown that Arl8b regulates nutrient-dependent lysosome positioning and autophagosome-lysosome fusion. RUFY3 depletion disrupted the repositioning of lysosomes to the perinuclear region in nutrient-starved cells, although the autophagic flux was not altered in these cells. Notably, endocytic cargo BODIPY-BSA cleavage was modestly reduced in RUFY3 knockdown,

suggesting that lysosomes are less degradative in these cells. Along with reducing the perinuclear immobile pool of lysosomes, surprisingly, RUFY3 silencing also led to a reduction of lysosomes size, which was rescued upon inhibition of lysosome reformation. Our study reveals RUFY3 as a novel dynein adaptor that regulates the positioning of Arl8b-positive lysosomes and also impacts lysosome size, likely by regulating reformation kinetics from these compartments.

Results

A) RUFY3 is an Arl8b effector that localizes to lysosomes

In the search for novel Arl8b binding partners, we performed a yeast two-hybrid assay with Arl8b as bait and human brain tissue cDNA library as prey that led to the identification of RUFY3 (NM_001037442.4; NP_001032519.1; transcript variant 1; 620 amino acids in length; longest isoform) as an interaction partner of Arl8b (**Figure 10a**). Transcript variant 1 (hereafter referred to as RUFY3) is the longest transcript synthesized from the RUFY3 gene, which encodes for six alternatively spliced variants. Variant 2 of RUFY3 (NM_014961.5, NP_055776.1; 469 amino acids in length) is the only RUFY3 isoform that is functionally characterized and regulate polarity and axon growth in neurons and migration and invasion of cancer cells (Char & Pierre, 2020; Kitagishi & Matsuda, 2013; G. Wang et al., 2015; Wei et al., 2014; Xie et al., 2017).

Using yeast two-hybrid and co-immunoprecipitation approaches, we confirmed that RUFY3 interacted with the WT (wild-type) and Q75L (constitutively GTP-bound) forms of Arl8b, but not with the T34N (constitutively GDP-bound) form (**Figures 10b** and **10c**). Consistent with this, RUFY3 interaction with GST(Glutathione S-transferase)-tagged-Arl8b (as bait) was reduced in the presence of excess GDP as compared to GTP, suggesting that RUFY3 behaves as an effector for the small G protein (**Figure 10d**). We also observed the interaction of Arl8b and RUFY3 under endogenous conditions by direct immunoprecipitation of Arl8b from HEK293T cell lysates (**Figure 10e**).

Notably, RUFY3 variant 2 did not show an interaction with Arl8b (**Figure 10f**). Variant 1 (620 amino acids long) and variant 2 (469 amino acids long) of RUFY3 are identical in sequence for the first 445 amino acids. The difference between the two variants lies

in a stretch of residues from 446-620, present in variant 1 but not variant 2 (**Figure 10g**). Indeed, domain deletion analysis revealed that RUFY3 mutant lacking residues 446-561 (hereafter referred to as RUFY3 (Δ446-561)), containing the FYVE-like domain) failed to bind to Arl8b in a yeast two-hybrid assay.

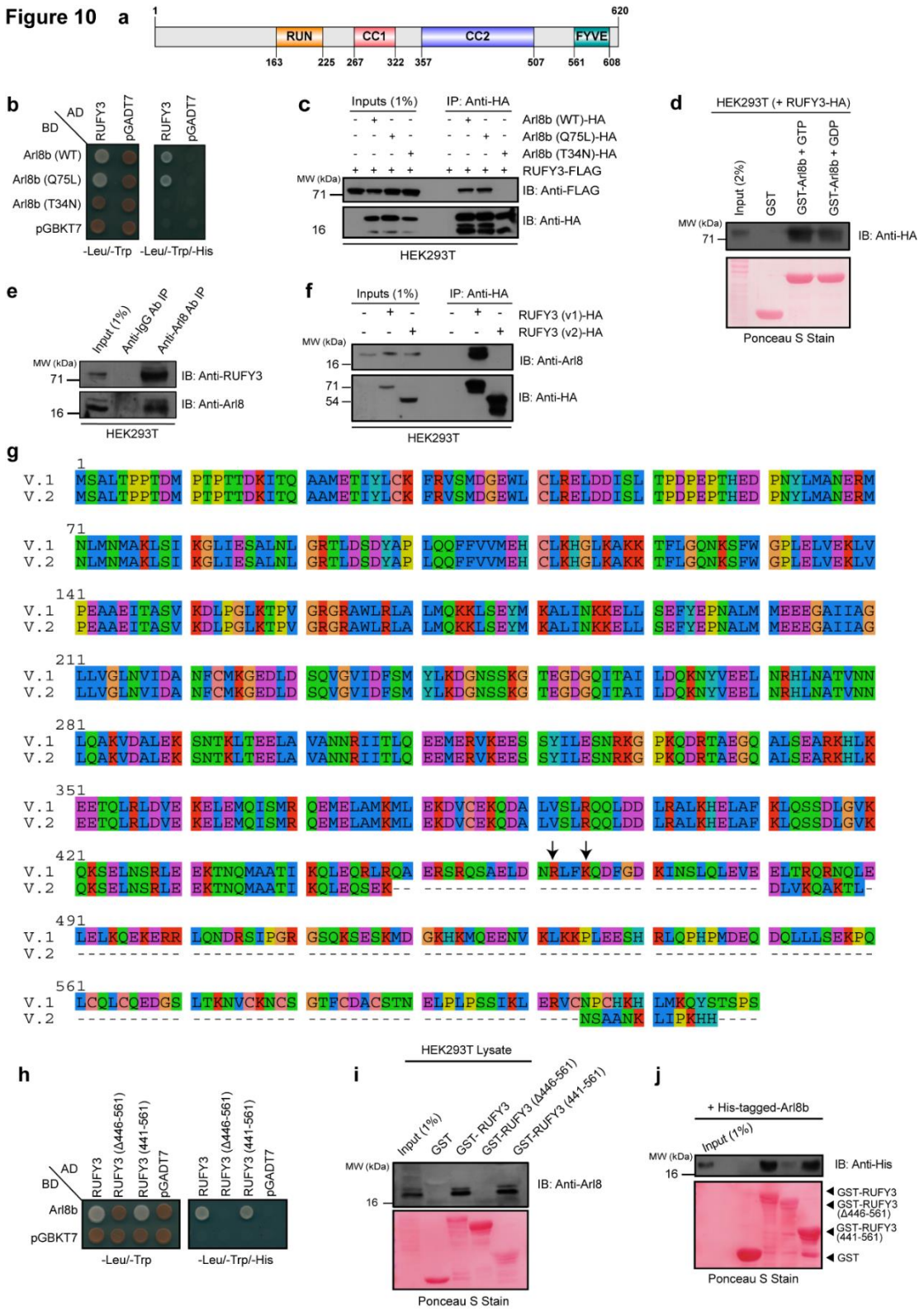

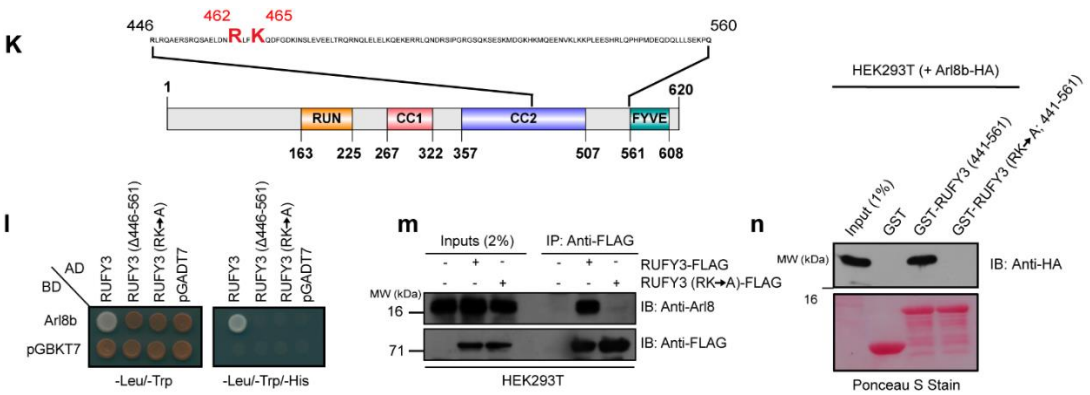

Figure 10: Arl8b directly binds to Variant 1 but not variant 2 of RUFY3. **(a)** Domain architecture of RUFY3 showing an N-terminal RUN domain, two CC (coiled-coil) domain and a C-terminal FYVE-like domain. **(b)** Yeast two-hybrid assay. Cotransformants were spotted on -Leu/-Trp and -Leu/-Trp/-His media to confirm viability and interactions, respectively. **(c)** Lysates of HEK293T cells expressing indicated proteins were immunoprecipitated (IP) with anti-HA antibodies-conjugated-agarose beads and immunoblotted (IB) with the indicated antibodies. **(d)** GST-pulldown assay. Recombinant GST and GST-Arl8b (bound to GDP or GTP) proteins were immobilized on glutathione-conjugated-agarose beads and incubated with HEK293T cell lysate expressing RUFY3-HA. The precipitates were IB with anti-HA antibodies and GST-tagged proteins were visualized using Ponceau S staining. **(e)** Endogenous IP was performed by incubating the HEK293T cell lysates with mouse anti-Arl8 antibody-conjugated-resin or mouse IgG-conjugated-resin, and IB with indicated antibodies. **(f)** The lysates of HEK293T cells expressing indicated plasmids were IP with anti-HA antibodies-conjugated-agarose beads and the precipitates were IB with the indicated antibodies. **(g)** Schematic showing protein sequence alignment of RUFY3 variant 1 with variant 2. The arrowheads mark basic/positively charged residues (R462 and K465) present in RUFY3 variant 1 that are crucial for binding with Arl8b. **(h)** Yeast two-hybrid assay. Cotransformants were spotted on -Leu/-Trp and -Leu/-Trp/-His media to confirm viability and interactions, respectively. **(i)** HEK293T cell lysates were incubated with recombinant GST or indicated GST-RUFY3 fusion proteins bound to glutathione resin. Precipitates were analyzed by Western blotting with anti-Arl8 antibodies. GST-tagged proteins were visualized using Ponceau S staining. **(j)** Indicated GST-tagged RUFY3 proteins immobilized on glutathione resin were incubated with purified His-Arl8b. The precipitates were IB with anti-His antibody and Ponceau S staining was done to visualize purified proteins. **(k)** Schematic representation of Arl8b-binding region of RUFY3 indicating the amino acid residues (R462 and K465) important for binding to Arl8b. **(l)** Yeast two-hybrid assay. Cotransformants were spotted on -Leu/-Trp and -Leu/-Trp/-His media to confirm viability and interactions, respectively. **(m)** Lysates of HEK293T cells expressing indicated proteins was IP with anti-FLAG antibodies-conjugated-agarose beads, and IB with the indicated antibodies. **(n)** Recombinant GST or indicated GST-RUFY3 fusion proteins bound to glutathione resin were incubated with lysates from HEK293T cells expressing Arl8b-HA. The precipitates were immunoblotted with anti-HA antibodies and GST-tagged proteins were visualized using Ponceau S staining.

More importantly, the RUFY3 fragment encompassing 441-561 residues (hereafter referred to as RUFY3 (441-561)) was sufficient for interaction with Arl8b (**Figure 10h**). This was corroborated using GST-pulldown assay wherein Arl8b was interacting

with GST-tagged-RUFY3 (WT) and -RUFY3 (441-561) but not a deletion mutant lacking these residues (**Figure 10i**). To test whether the RUFY3 fragment containing 441-561 residues directly binds to Arl8b, we incubated recombinant His-Arl8b with GST or GST-tagged-RUFY3 (WT), -RUFY3 (Δ446-561) and RUFY3 (441-561). As shown in **Figure 10j**, we found that Arl8b directly binds to the RUFY3 encompassing the 441-561 fragment.

Next, to further narrow down amino acid residues within the RUFY3 (441-561) fragment that affect binding with Arl8b, we first mutated the positively charged residues in this fragment to alanine. This selection was based on our prior study that revealed binding of effectors PLEKHM1 and SKIP/PLEKHM2 to Arl8b requires arginine residues in their RUN domain. From this screening, we found that R462/K465 residues in the RUFY3 (441-561) fragment was crucial for interaction with Arl8b, as mutating these residues to alanine (RK→A) abrogated binding to Arl8b (**Figures 10k-n**).

B) Arl8b recruits RUFY3 on lysosomes

We next analyzed RUFY3 localization by transfecting epitope-tagged-RUFY3 construct in HeLa cells, as none of the available anti-RUFY3 antibodies recognized the protein under endogenous conditions. RUFY3-HA-tagged construct, when expressed in HeLa cells, showed a cytosolic distribution with few punctate structures (in <20% cells with weak to moderate level of expression) visible in the perinuclear region, which could be due to limiting expression of endogenous Arl8b (see inset, **Figures 11a** and **11b**). To better visualize RUFY3 membrane localization that was masked by the cytosolic signal, we permeabilized the cells with a mild detergent before fixation (see inset, **Figure 11c**). Further, to elucidate the identity of the RUFY3-positive compartments, we co-stained these cells with well-characterized endosomal and lysosomal markers. Several RUFY3 punctae were strongly colocalized with the late endosomal/lysosomal markers, LAMP1 and CD63, while little to none colocalization was observed with the early (Rab5) and recycling endosomal markers (Transferrin Receptor-TfR and Rab11) (**Figures 11d-h**; quantification is shown in **Figures 11i** and **11j**). To corroborate whether RUFY3 localizes to lysosomes under endogenous conditions, we used the recently described LYSO-IP method that relies on immuno-purification of subcellular compartments containing the lysosomal transmembrane protein TMEM192 (Abu-Remaileh et al., 2017). We confirmed that the lysosomal fractions obtained using the LYSO-IP method was not contaminated with other membranes by probing for various organelle markers

(**Figures 11k**). RUFY3, similar to LAMP1 and Arl8b, was present in the lysosomal fractions under endogenous conditions, confirming the localization observed with the RUFY3-tagged construct (**Figures 11l** and **11n**).

Figure 11

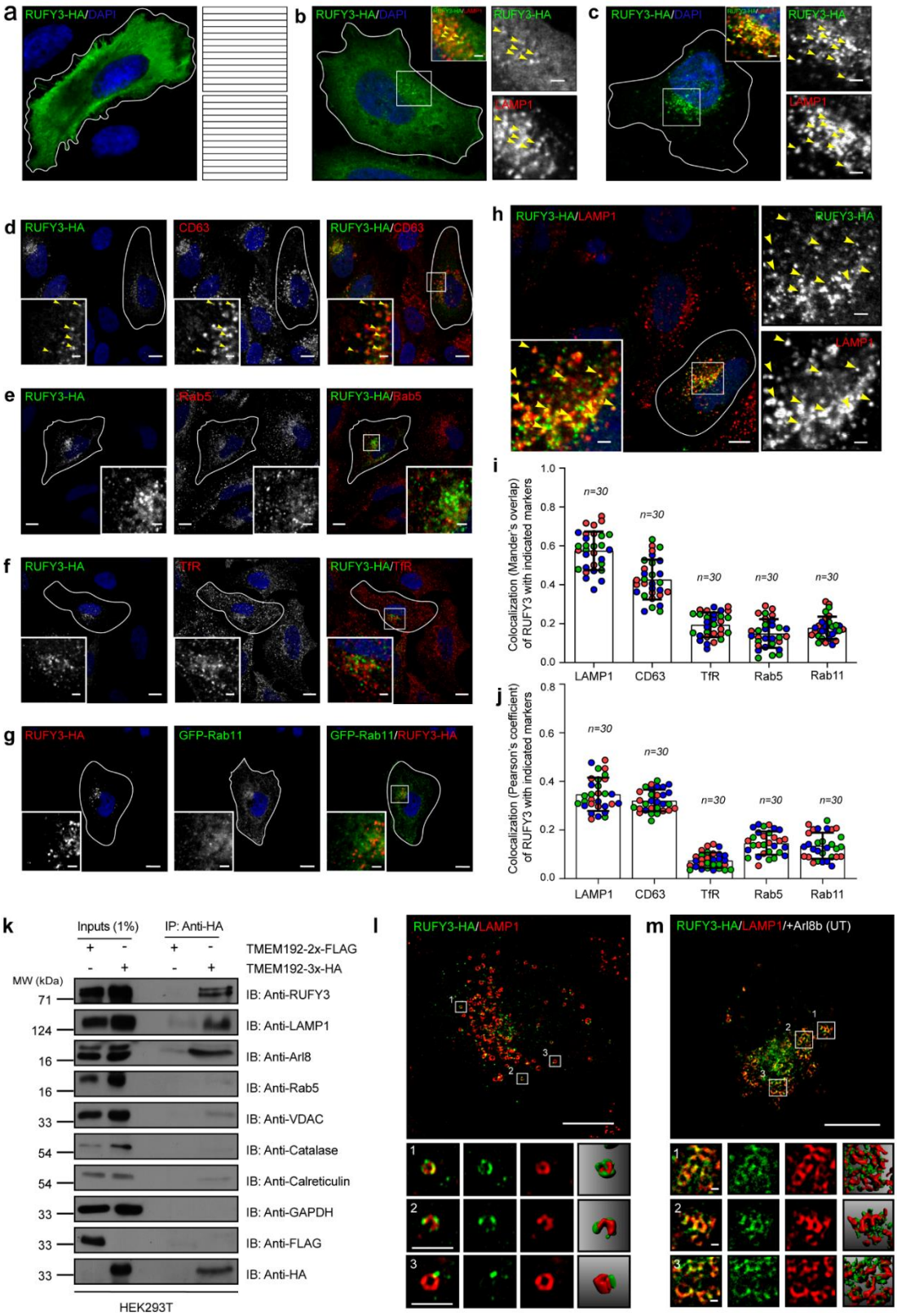

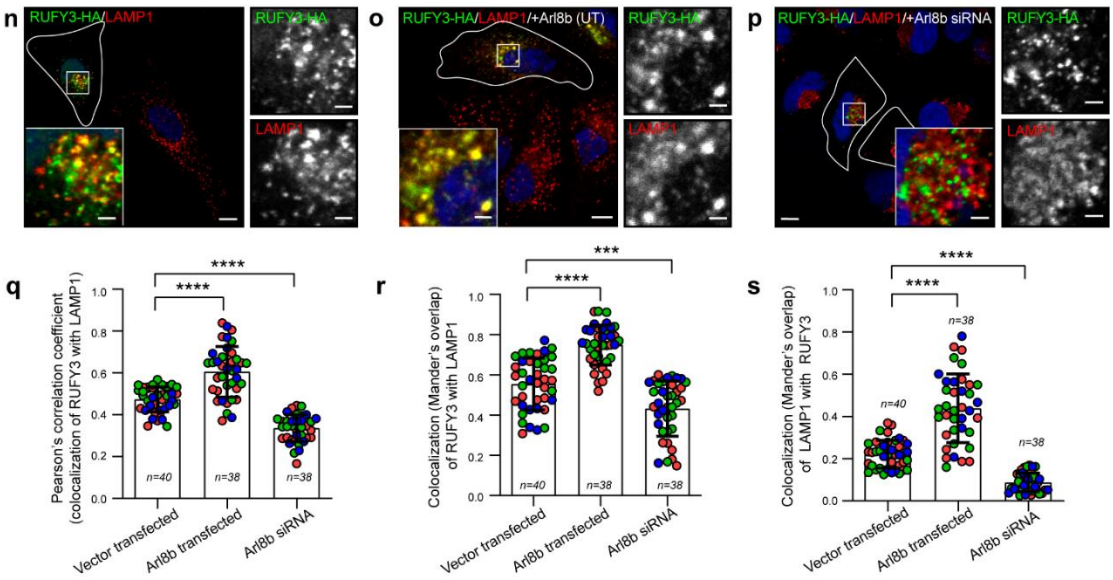

Figure 11: RUFY3 localizes to lysosomes. (a-c) Representative confocal micrographs of HeLa cells transfected with RUFY3-HA plasmid showing varying level of RUFY3 expression. Post fixation, cells were stained for lysosomes and RUFY3 using anti-LAMP1 and anti-HA antibodies, respectively. The transfected cells are outlined and in the insets, a magnified region of the boxed area is shown, depicting the localization of RUFY3 on LAMP1-positive compartments as indicated by yellow arrowheads. Note, in (c), cells were briefly permeabilized with 0.05% saponin for 5 min on ice in order to remove cytosol pool of RUFY3 followed by fixation step. Scale Bars: 10 µm (main); 2 µm (inset). **(d-h)** Representative confocal micrographs of HeLa cells transfected with RUFY3-HA expressing construct and stained for different endocytic markers. A magnified region of the boxed area is shown in the insets depicting colocalized pixels of RUFY3-HA with different marker proteins. Scale Bars: 10 µm (main); 2 µm (inset). **(i-j)** Colocalization of RUFY3-HA with indicated markers was measured using Mander's overlap and pearson's coefficient. Values plotted are mean ± S.D. from three independent experiments. Experiments are color-coded, and the total number of cells analyzed is indicated on the graph. **(k)** Lysates were prepared from HEK293T cells expressing TMEM192-2x-FLAG (control) or TMEM192-3x-HA and subjected to LYSO-IP. The precipitates were IB with indicated antibodies. **(l-m)** Representative SIM image of a HeLa cell transfected with RUFY3-HA or co-transfected with Arl8b (untagged) and stained with indicated antibodies. Insets in (l) show magnification of selected vesicles, highlighting the presence of RUFY3 on the LAMP1-positive vesicles. The fourth column of insets shows an isosurface view of vesicles generated using Imaris software. The insets in (m) depict enhanced colocalization of RUFY3 on lysosomes in the presence of Arl8b. **(n-p)** Representative confocal micrographs of HeLa cells transfected with RUFY3-HA (n), co-transfected with RUFY3-HA and Arl8b untagged (UT) (o) and Arl8b siRNA treated and transfected with RUFY3-HA (p), and stained for lysosomes using an anti-LAMP1 antibody. RUFY3 localization to LAMP1-positive compartments is shown in insets. **(q-s)** Colocalization of RUFY3-HA with LAMP1-positive compartments for experiments presented in (n-p) was quantified using PCC (q) and Mander's overlap (r and s). Values plotted are mean ± S.D. from three independent experiments. Experiments are color-coded, and the total number of cells analyzed is indicated on the graph (****$p<0.0001$; ***$p<0.001$; Student's *t-test*). Scale Bars: 10 µm (main); 2 µm (inset).

One of the primary roles of small G proteins of Rab, Arf and Arl families is to recruit their effectors to target membranes; we next tested whether Arl8b plays a similar role in RUFY3 recruitment lysosomes. Indeed, RUFY3 lysosomal localization was significantly enhanced in cells co-expressing Arl8b (see inset, **Figures 11n** and **11p**; quantification is shown in **Figures 11q-s**). This increased recruitment of RUFY3 upon co-expression of Arl8b was evident from structured illumination microscopy (SIM) images of individual LAMP1-positive vesicles (compare insets of **Figures 11l** and **11m)** showing RUFY3 localization on LAMP1-positive compartments). We noted that RUFY3 localized only to a subset of LAMP1-positive compartments, even in the presence of overexpressed Arl8b (**Figure 11s**, Manders overlap of LAMP1 colocalization with RUFY3). Finally, RUFY3 recruitment to lysosomes was significantly reduced in Arl8b-depleted cells, indicating that RUFY3 behaves as an Arl8b effector (**Figure 11p**; quantification shown in **Figures 11q-s**). Notably, some RUFY3 punctate structures were still present in Arl8b siRNA-treated cells, but these punctae did not colocalize with LAMP1 (see inset, **Figure 11p**). Whether the RUFY3 punctae in Arl8b-depleted cells represent protein aggregates or membrane-bound compartments is unclear.

C) RUFY3 promotes perinuclear positioning of lysosomes

Interestingly, lysosomes were strongly clustered in the perinuclear region upon RUFY3 transfection in HeLa cells (compare untransfected and transfected cells in **Figure 12a**). To corroborate this observation, we quantified lysosomal distribution by two methods – a) measuring the cumulative integrated LAMP1 intensity in the perinuclear region (0-5 μm) and the peripheral region (>15 μm) (**Figure 12d**), and – b) measuring the distance of lysosomes relative to the maximum distance from the center of the nucleus to the cell periphery (Guardia et al., 2016; M. L. Jongsma et al., 2020; M. L. M. Jongsma et al., 2016) (**Figure 12f**) in cells transfected with either vector control or different RUFY3 constructs. As shown in **Figure 12e** and **Figure 12g**, the distribution of lysosomes in RUFY3 (WT) transfected cells was significantly shifted to the perinuclear region and away from the periphery. Importantly, RUFY3 mutant proteins defective in binding to Arl8b (i.e. RUFY3 (Δ446-561) and RUFY3 (RK→A)) did not localize to the LAMP1 compartment or alter lysosome positioning, suggesting that association

with Arl8b is required for RUFY3 lysosomal localization (**Figures 12a-c**; quantification is shown in **Figure 12e** and **Figure 12g**).From several previous studies, it is known that Arl8b is enriched on peripheral lysosomes, and its overexpression drives accumulation of lysosomes near the plasma membrane (see inset, **Figure 12h**) (Garg et al., 2011; Hofmann & Munro, 2006; Khatter, Raina, et al., 2015; Khatter, Sindhwani, et al., 2015). This is attributed to Arl8b interaction with a RUN domain-containing protein, SKIP/PLEKHM2, that binds and recruits kinesin-1 motor to drive the anterograde motility of late endosome/lysosome (LE/Lys) on microtubule tracks (Keren-Kaplan & Bonifacino, 2021; Udia et al., 2011). Interestingly, co-expression of RUFY3 caused a striking shift in Arl8b distribution to the perinuclear region wherein both proteins colocalized on these perinuclear compartments (see inset, **Figure 12i**; Pearson's and Mander's colocalization coefficients are shown in **Figures 12l** and **12m**). Consistent with our analysis of the residues of RUFY3 required for Arl8b binding, no significant colocalization or a change in Arl8b distribution was observed in cells expressing RUFY3 (Δ446-561) and RUFY3 (RK→A) mutants (**Figures 12j** and **12k**; Pearson's and Mander's colocalization coefficients are shown in **Figures 12l** and **12m**). Thus, our data suggest that RUFY3 is an Arl8b effector that promotes the perinuclear positioning of lysosomes.

Figure 12

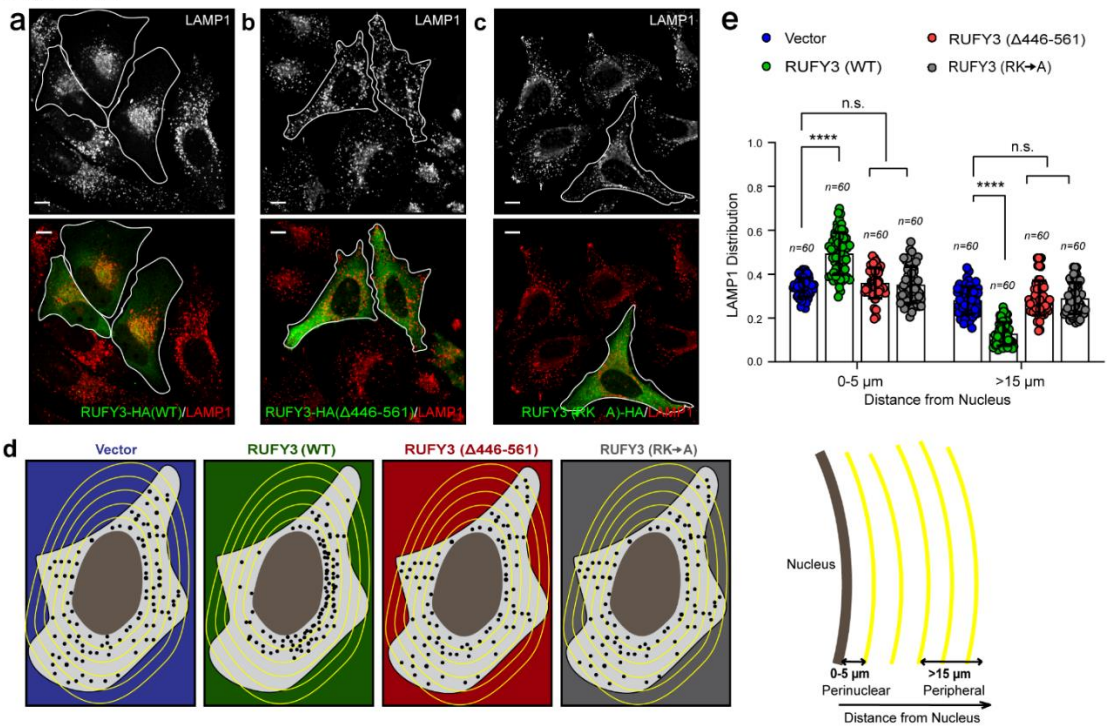

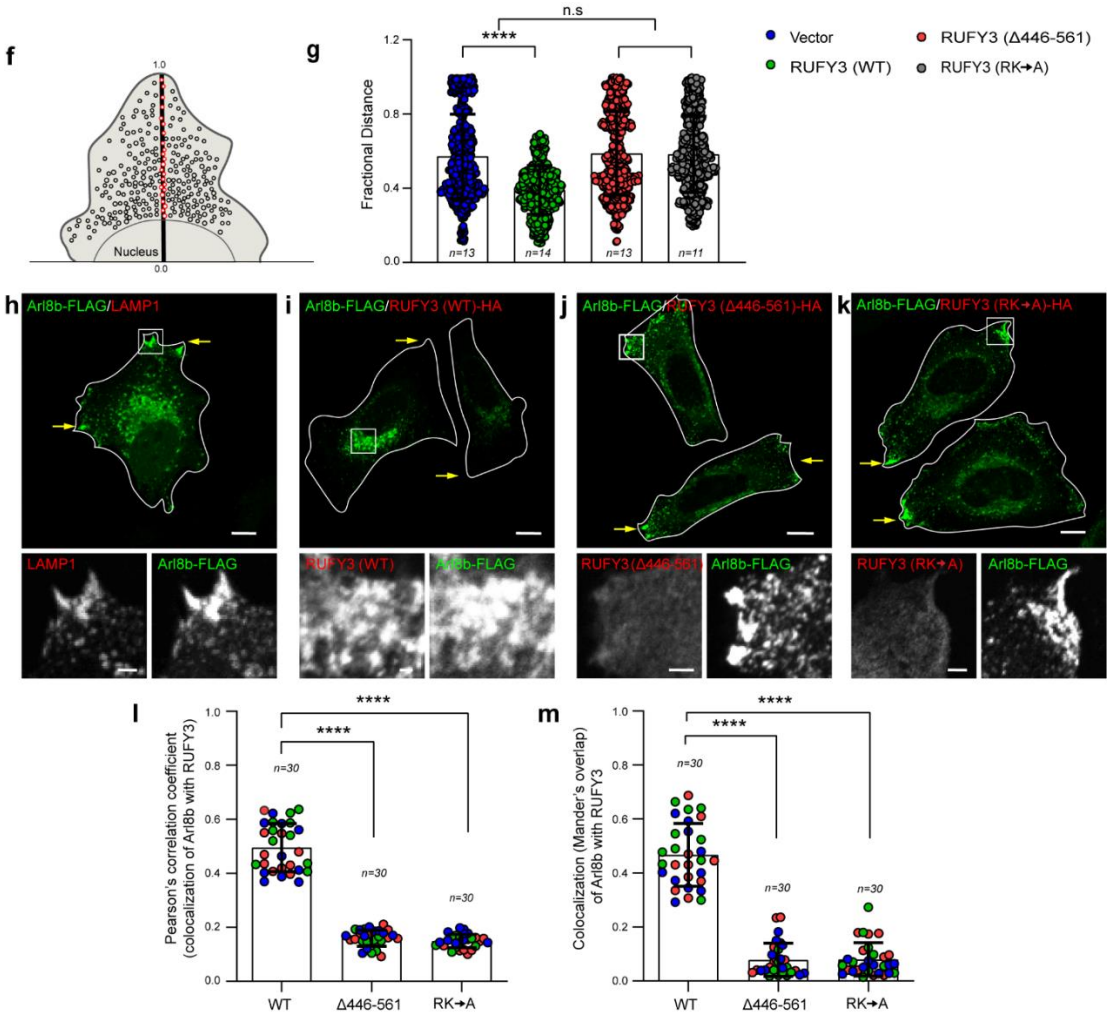

Figure 12: Wild-type RUFY3, but not the Arl8b binding-defective mutant, promotes perinuclear lysosome clustering. **(a-c)** Representative confocal micrographs of HeLa cells expressing RUFY3-HA (WT) (a), RUFY3 (Δ446-561)-HA (b) and RUFY3 (RK→A)-HA (c) and stained for lysosomes using an anti-LAMP1 antibody. Transfected cells are marked with a boundary. **(d)** A schematic depicting the quantification method employed for analyzing the distribution of LAMP1-positive compartments in a cell. **(e)** The distribution of LAMP1-positive compartments in HeLa cell transfected with indicated plasmids. **(f)** Schematic illustrating the methodology for calculating fraction distance of lysosomes from center of the nucleus. **(g)** The graph represents quantification of fraction distance of lysosomes for experiments performed in a-c. Values plotted are mean ± S.D. and the total number of cells analyzed is indicated on the graph (****p<0.0001; n.s., not significant; two-tailed Student's *t*-test). **(h-k)** Representative confocal micrographs of HeLa cells transfected with Arl8b-FLAG alone (f) or co-transfected with indicated RUFY3 expressing plasmids (g-i) and stained with indicated antibodies. The cell boundary is marked with a line and yellow arrows mark the peripheral localization of Arl8b-positive vesicles. **(l-m)** Colocalization analysis of Arl8b with indicated RUFY3 proteins was assessed by calculating Pearson's correlation coefficient (j) and Mander's overlap (k). Values plotted are mean ± S.D. from three independent experiments. Experiments are color-coded, and each dot represents the individual data points from each experiment. The total number of cells analyzed is indicated on the graph (****p<0.0001; two-tailed Student's *t-test*). Scale Bars: 10 µm (main); 2 µm (inset).

D) RUFY3 is essential and sufficient to drive perinuclear lysosome positioning

We used two independent strategies to corroborate whether RUFY3 is essential and sufficient to drive LE/Lys perinuclear positioning. Using the RNA interference approach (siRNA and shRNA), we depleted RUFY3 in HeLa cells and analyzed lysosome distribution. The efficiency of RUFY3 silencing was found to be >90%, as confirmed by Western blotting (**Figures 13a** and **13b**). To monitor lysosomal distribution, besides LAMP1, we also employed Lysotracker and SiR-Lysosome probes that mark acidic and degradative (specific for lysosomal protease cathepsin D) compartments, respectively. Consistent with our results that RUFY3 expression promotes perinuclear clustering of lysosomes, RUFY3 depletion had the opposite effect, i.e. lysosomes were now localized to the cell periphery (for LAMP1 distribution, see **Figures 13c-f** and **Figure 13k;** for Lysotracker distribution, see **Figures 13g-h**; for SiR-Lysosome distribution, see **Figures 13i-j**). Notably, in these experiments, only a subset of the lysosomes was relocated to the periphery upon RUFY3 depletion, and a modestly reduced perinuclear pool of lysosomes was still present in RUFY3-depleted cells. The peripheral lysosomal distribution was rescued in cells expressing siRNA-resistant RUFY3 construct, indicating that the phenotype was specifically due to RUFY3 depletion and not due to the off-target effect of siRNA oligos (**Figures 13e-k**).

Notably, we also found that RUFY3-depleted cells had a ~1.3-fold increase in their surface area than control siRNA or shRNA treated cells (**Figures 13l** and **13m**). Interestingly, cell spreading is reduced upon Myrlysin gene knockout, where lysosomes are clustered in the perinuclear region ((Pu et al., 2015). In contrast, the surface area of cells is increased upon dynein depletion, where lysosomes, similar to RUFY3 depletion (Rishal et al., 2012), are localized to the cell periphery. These observations suggest that lysosome distribution might regulate cell spreading, but the mechanistic basis of how this is achieved remains unclear.

RUFY3 depletion in other cell types, including ARPE-19 (retinal pigment epithelial cells), U2OS (osteosarcoma cells), and A549 (lung adenocarcinoma cells), showed a similar distribution of lysosomes towards the cell periphery (**Figures 13n-p**).

Next, we used the knockout-sideways approach to test whether the presence of RUFY3 on the organelle membrane was sufficient to drive their positioning to the perinuclear region.

Figure 13

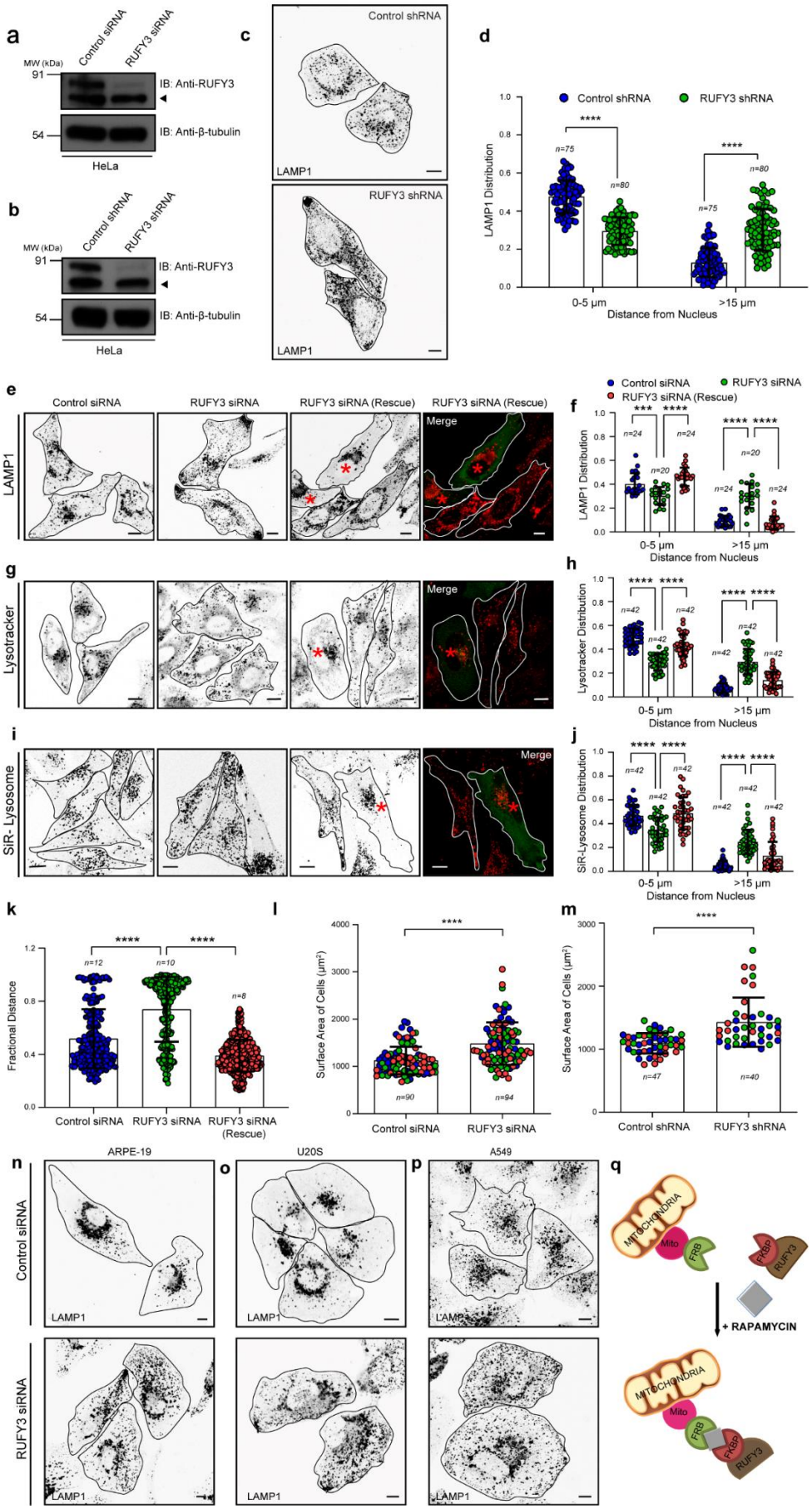
a
Control siRNA
RUFY3 siRNA
MW (kDa)
91
54
IB: Anti-RUFY3
IB: Anti-β-tubulin
HeLa
b
Control shRNA
RUFY3 shRNA
c
LAMP1
d
LAMP1 Distribution
Distance from Nucleus
0-5 µm
>15 µm
e
RUFY3 siRNA (Rescue)
Merge
f
g
Lysotracker
h
Lysotracker Distribution
i
SiR- Lysosome
j
SiR-Lysosome Distribution
k
Fractional Distance
l
Surface Area of Cells (µm²)
m
n
ARPE-19
o
U20S
p
A549
q
MITOCHONDRIA
Mito
FRB
FKBP
RUFY3
+ RAPAMYCIN

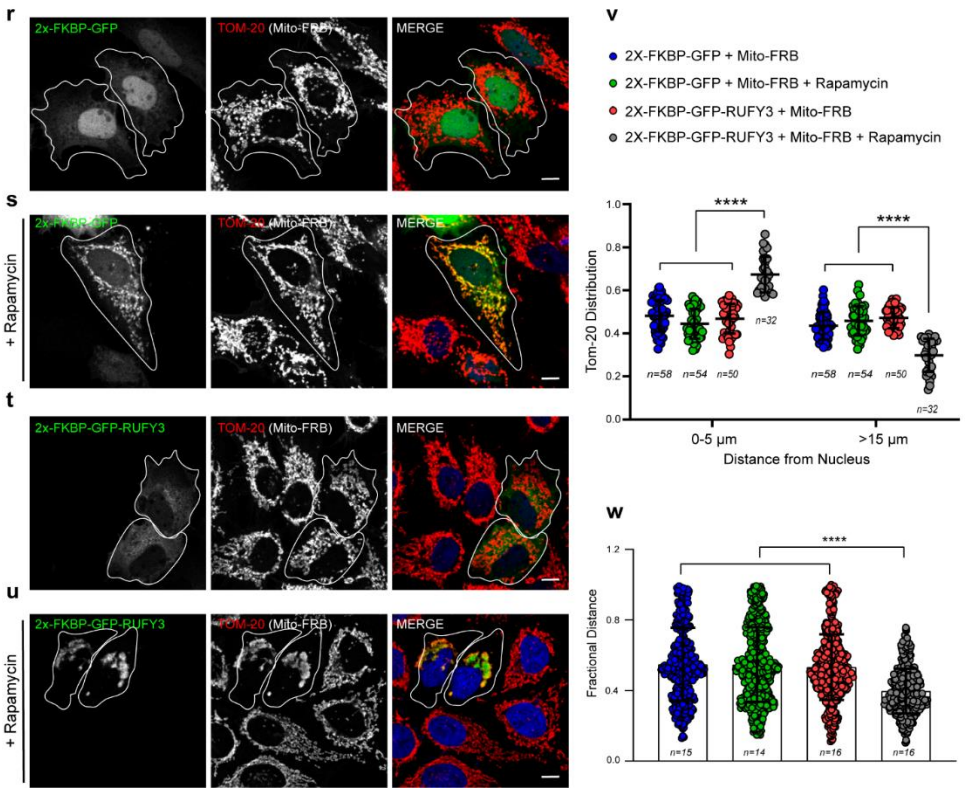

Figure 13: RUFY3 is essential and sufficient to drive perinuclear lysosome positioning. (a-b) Immunoblot showing RUFY3 knockdown efficiency in control and RUFY3 depleted HeLa cells using siRNA and shRNA treatment. The arrowhead corresponds to a non-specific signal detected by the anti-RUFY3 antibody. **(c)** Representative confocal micrographs (represented as grayscale inverted) showing lysosome distribution in HeLa cells expressing control shRNA or RUFY3 shRNA. The lysosomes were stained using an anti-LAMP1 antibody. Scale Bar: 10 µm. **(d)** The distribution of LAMP1-positive lysosomes was quantified from the experiments presented in (c). **(e-j)** Confocal micrographs showing lysosome distribution in HeLa cells treated with indicated siRNAs. The lysosomes were stained using an anti-LAMP1 antibody (**e**), Lysotracker probe (**g**) or SiR-Lysosome probe (i). Cells expressing RUFY3 siRNA-rescue construct is marked by asterisks and image panels are shown in an inverted grayscale. The distribution of lysosomes was quantified from these experiments and shown in b, d and f. Values plotted are mean ± S.D. from three independent experiments. The total number of cells analyzed is indicated on the graph (****p<0.0001; ****p*<0.001; two-tailed Student's *t*-test). **(k)** The graph represents quantification of fraction distance of lysosomes for experiments performed in Figure 3e. **(l-m)** Quantification of the surface area of HeLa cells transfected with either control siRNA or RUFY3 siRNA (l) and control shRNA or RUFY3 shRNA (m). Values plotted are mean ± S.D. from three independent experiments. Experiments are color-coded and the total number of cells analyzed is indicated on the graph (****p<0.0001; Student's *t-test*). **(n-p)** Representative confocal microscopy images (represented as grayscale inverted) of control and RUFY3-silenced ARPE-19 (F), U20S (g), A549 (h) cells stained with an anti-LAMP1 antibody. Scale Bars: 10 µm. **(q)** Schematic representation of the rapamycin-inducible FRB/FKBP protein-protein interaction. **(r-u)** Confocal micrographs of untreated- and rapamycin treated-HeLa cells expressing Mito-FRB with 2x-FKBP-GFP or 2x-FKBP-GFP-RUFY3. To visualize mitochondria, cells were stained using an anti-TOM-20 antibody and transfected cells are marked with a white boundary. **(v)** Distribution of mitochondria based on the Tom-20 signal was quantified from the experiments shown in (**r-u**). Values plotted are mean ± S.D. from three independent experiments. The total number of cells analyzed is indicated on the graph (****p<0.0001; two-tailed Student's *t*-test). Scale Bars: 10 µm. **(w)** The graph represents quantification of fraction distance of mitochondria for experiments performed in Figure 3h. Values plotted are mean ± S.D. from three independent experiments. The total number of cells analyzed is indicated on the graph (****p<0.0001; ***p<0.001; two-tailed Student's *t*-test).

To this end, we used the FRB-FKBP rapamycin-induced heterodimerization system to mislocalize RUFY3 to mitochondria (where it is not present under endogenous conditions) and analyzed mitochondria distribution (**Figure 13q**). As expected, we found mitochondrial localization of FKBP-GFP (vector transfected) and FKBP-GFP-RUFY3 fusion protein in the presence of rapamycin and not in untreated cells (**Figures 13r-u**). Notably, in the presence of rapamycin, RUFY3-transfected cells showed a dramatic clustering of mitochondria in the perinuclear region. In contrast, vector-transfected cells showed typical mitochondrial distributions (compare **Figure 13s** and **Figure 13u**). Quantification of mitochondrial intensity distribution showed increased perinuclear index in cells expressing FKBP-GFP-RUFY3 in the presence of rapamycin (**Figure 13v and Figure 13w**). Taken together, we conclude that RUFY3 localization to the organelle membrane is sufficient to drive their distribution to the perinuclear region.

E) RUFY3 mediated perinuclear lysosome positioning is independent of Rab7

We were intrigued by the observations that only a subset of LAMP1/Lysotracker/SiR-Lysosome-positive vesicles responded to RUFY3 depletion and relocated towards the cell periphery. The two small G proteins, Rab7 and Arl8b and their downstream effectors primarily localize to and regulate the distribution of late endocytic compartments (M. L. Jongsma et al., 2020; Marwaha et al., 2017a). We, therefore, sought to investigate whether RUFY3 is a specific or a shared adaptor of both Arl8b and Rab7. To this end, we first determined whether RUFY3 interacts with Rab7. In a yeast two-hybrid assay, RUFY3 did not bind to Rab7 but showed interaction with Arl8b (**Figure 14a**). RILP, a well-characterized Rab7 effector, was used as a positive control and expectedly showed interaction with Rab7. Supporting this result, we observed co-immunoprecipitation of Arl8b, but not of Rab7, with RUFY3 (**Figure 14b**). Thus, unlike PLEKHM1 and SKIP/PLEKHM2 (the two shared interaction partners of Arl8b and Rab7) (M. L. Jongsma et al., 2020; Marwaha et al., 2017a), RUFY3 did not interact with Rab7. We next investigated whether Rab7 regulates RUFY3 membrane localization using two approaches. First, in cells expressing artificial fusion constructs of Rab7 and Arl8b with a mitochondrial targeting sequence, we analyzed whether RUFY3 is recruited to mitochondria. Consistent with our earlier results that RUFY3 interact with Arl8b, RUFY3 was recruited to mitochondria in the presence of Mito-Arl8b but not Mito-Rab7 (**Figures 14c** and **14d**; quantification shown in **Figure 14e**).

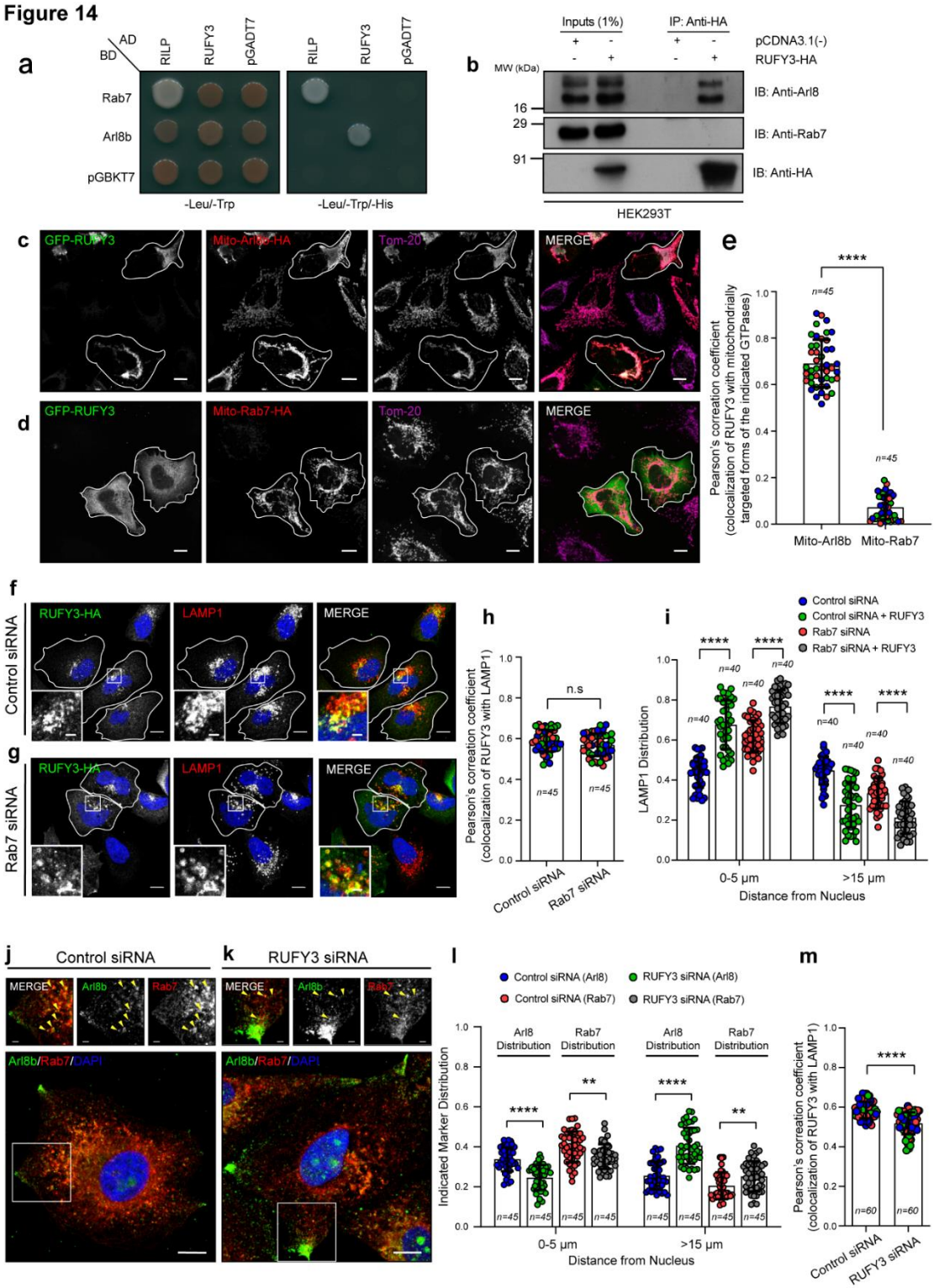

Figure 14: RUFY3 mediated perinuclear lysosome positioning is independent of Rab7. **(a)** Yeast-two hybrid assay. The co-transformants were spotted on -Leu/-Trp and -Leu/-Trp/-His media to confirm viability and interactions, respectively. **(b)** Lysates of HEK293T cells expressing RUFY3-HA was IP with anti-HA antibodies-conjugated-agarose beads and the precipitates were IB with the indicated antibodies. **(c-d)** Confocal micrographs of HeLa cells co-transfected with GFP-RUFY3 and mitochondria localization tagged-Arl8b (Mito-Arl8b-HA) or -Rab7 (Mito-Rab7-HA) and stained with indicated antibodies. Transfected cells are marked with a boundary. **(e)** Colocalization analysis of GFP-RUFY3 with Mito-Arl8b-HA and Mito-Rab7-HA proteins was

assessed by calculating Pearson's correlation coefficient for the experiments shown in c and d. Values plotted are mean ± S.D. from three independent experiments. Experiments are color-coded, and each dot represents the individual data points from each experiment. The total number of cells analyzed is indicated on the graph (****p<0.0001; two-tailed Student's t-test). **(f-i)** Confocal micrographs of HeLa cells treated with control siRNA (f) or Rab7 siRNA (g) and transfected with RUFY3-HA. The cells were stained for lysosomes and RUFY3 using anti-LAMP1 and anti-HA antibodies, respectively. Transfected cells are marked with a boundary. In the insets, a magnified region of the boxed area is shown indicating localization of RUFY3 on lysosomes. Quantification of colocalization analysis of RUFY3 with LAMP1 and distribution of lysosomes from these experiments are shown in h and i, respectively. Values plotted are mean ± S.D. from three independent experiments. The total number of cells analyzed is indicated on the graph (****p<0.0001; n.s., not significant; two-tailed Student's t-test). **(j-m)** Confocal micrographs of HeLa cells treated with control siRNA (j) or RUFY3 siRNA (k) and stained for endogenous Arl8 and Rab7. In the insets, distribution of Arl8 and Rab7 is shown along with yellow arrowheads marking colocalized pixels. Distribution of Arl8- and Rab7-positive endosomes and their colocalization from these experiments are shown in l and m, respectively. Values plotted are mean ± S.D. from three independent experiments. The total number of cells analyzed is indicated on the graph (****p<0.0001; **p=0.0014 (for 0-5 µm); **p=0.0026 (for >15 µm); two-tailed Student's t-test). Scale Bars: 10 µm (main); 2 µm (inset).

Second, we analyzed whether RUFY3 localizes to and alters lysosomal distribution in Rab7-depleted cells. As shown in **Figures 14f-h**, RUFY3 continued to colocalize with LAMP1 in Rab7-depleted cells, indicating that RUFY3 membrane localization is independent of Rab7. Consistent with RUFY3 localization, RUFY3-dependent lysosome perinuclear clustering was observed in Rab7-depleted cells (**Figure 14i**). Finally, we tested the impact of RUFY3 depletion on the positioning of endogenous Rab7 and Arl8b compartments in the same cell. Quantification of intensity profile distribution of both Rab7 and Arl8b revealed striking peripheral relocalization of Arl8b compartments, while Rab7 distribution showed a modest but significant increase in the cell periphery (**Figures 14j-k**; quantification is shown in **Figure 14l**). This altered Rab7 distribution upon RUFY3 depletion is not surprising, as Rab7 and Arl8b colocalize together on a subset of late endocytic compartments (thought to be endolysosomes formed by fusion of late endosomes and lysosomes) (M. L. Jongsma et al., 2020; Marwaha et al., 2017b). Still, RUFY3 depletion affected the spatial organization of the two G proteins, as evident by a modest reduction in Rab7 and Arl8b colocalization (**Figure 14m**). Taken together, these findings indicate that RUFY3 is a specific Arl8b effector that regulates the distribution of lysosomes marked by Arl8b.

F) RUFY3 recruits the JIP4-dynein-dynactin complex to mediate retrograde transport of lysosomes

To investigate the RUFY3 mode of action, we performed a GST-pulldown assay with GST-RUFY3 as a bait protein to identify potential interaction partners. Interestingly, in the GST-RUFY3 eluate, we found peptides corresponding to cytoplasmic dynein heavy chain (DYNC1H1/DHC); dynactin 1/p150glued (DCTN1), a subunit of dynactin complex that mediates dynein activation, and peptides of JIP4/SPAG9 scaffolding protein that interact with dynein/dynactin and link dynein to the organelle membranes. We confirmed RUFY3 and JIP4 interaction by incubating recombinant GST-RUFY3 protein with semi-purified FLAG-tagged-JIP4 isolated from mammalian cells. As shown in **Figures 15a-b**, JIP4 was bound to purified GST-RUFY3 but not GST, implying JIP4 interacts with RUFY3. We also confirmed that JIP4 and RUFY3 form a complex under endogenous conditions by immunoprecipitation of both RUFY3 and JIP4 and probing for the corresponding partner. Dynein and dynactin subunits were also co-immunoprecipitated in the RUFY3-JIP4 complex (**Figures 15c-f**). To test whether RUFY3 recruits JIP4 to Arl8b-positive lysosomes, we analyzed JIP4 localization in cells either expressing Arl8b alone or co-expressing both Arl8b and RUFY3. We found enhanced colocalization of Arl8b and JIP4 in the presence of RUFY3 (**Figures 15g-i**). In agreement with these immunofluorescence observations, immunoprecipitation data confirmed that JIP4 interaction with Arl8b was dependent upon RUFY3 expression levels (**Figures 15j-m**).

We next tested whether dynein and JIP4 are required for the RUFY3-mediated perinuclear clustering of lysosomes. RUFY3 overexpression failed to cause perinuclear clustering of lysosomes in JIP4- or dynein-depleted cells, suggesting that the JIP4-dynein motor complex is required for RUFY3-mediated perinuclear lysosome positioning (**Figures 15n-o** and quantification is shown in **Figure 15p**). Notably, JIP4 and dynein depletion had a more profound effect than RUFY3 on lysosome distribution, with ~45% of Lysotracker-positive vesicles now localized to the cell periphery upon JIP4 and dynein depletion, as compared to ~25% in RUFY3-depleted cells (**Figures 15q-u**). Indeed, these results agree with the overall hypothesis that RUFY3 is a dynein adaptor for a subset of lysosomes (mostly Arl8b-positive) and points to the existence

of other lysosomal adaptors, such as TMEM55B, which binds to JIP4-dynein-dynactin complex and mediates retrograde lysosome motility (Willett et al., 2017). These conclusion led to a hypothesis that RUFY3 recruits the dynein motor on lysosomes and thereby mediates dynein-dependent lysosomal perinuclear positioning.

Figure 15

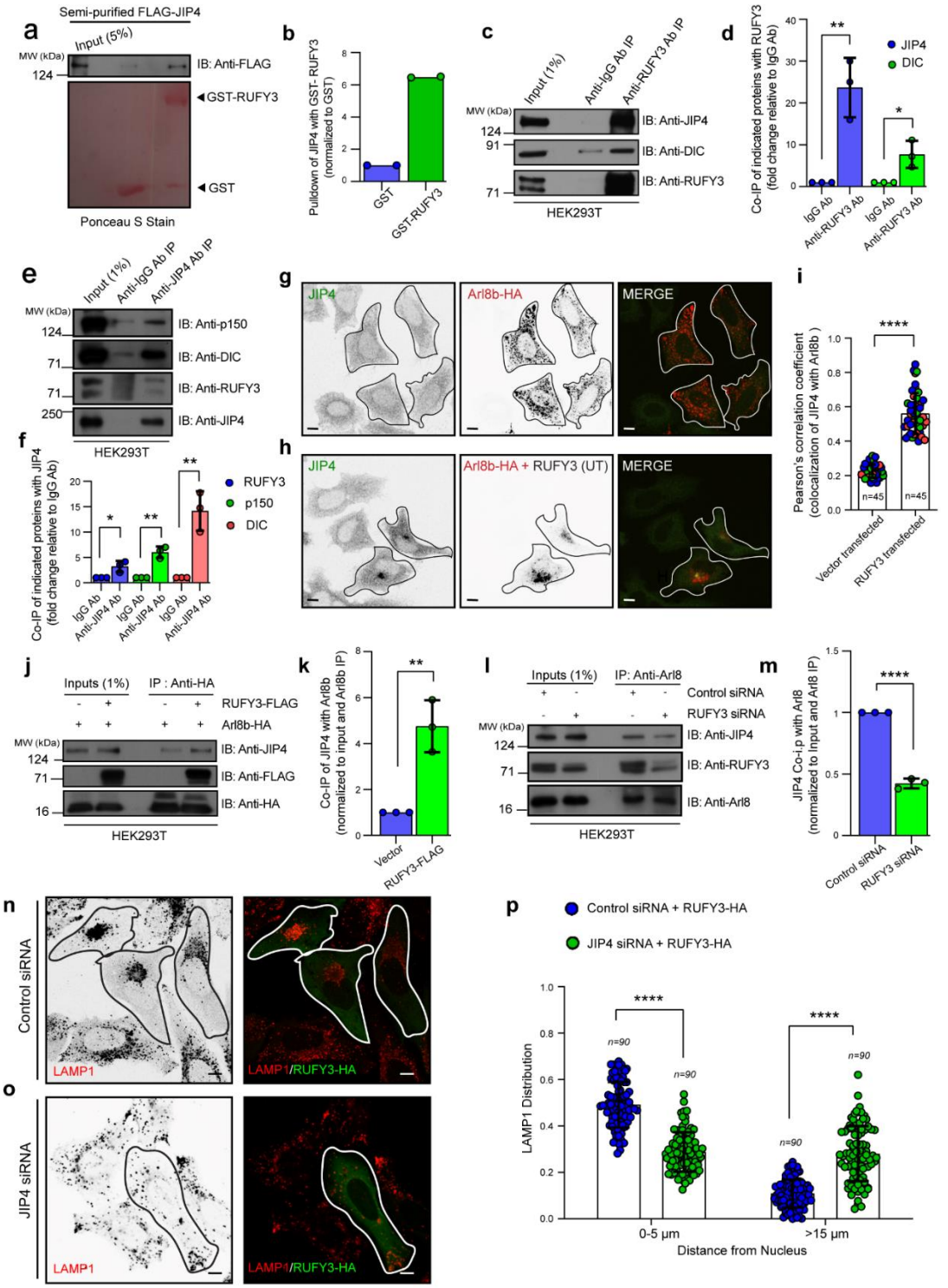

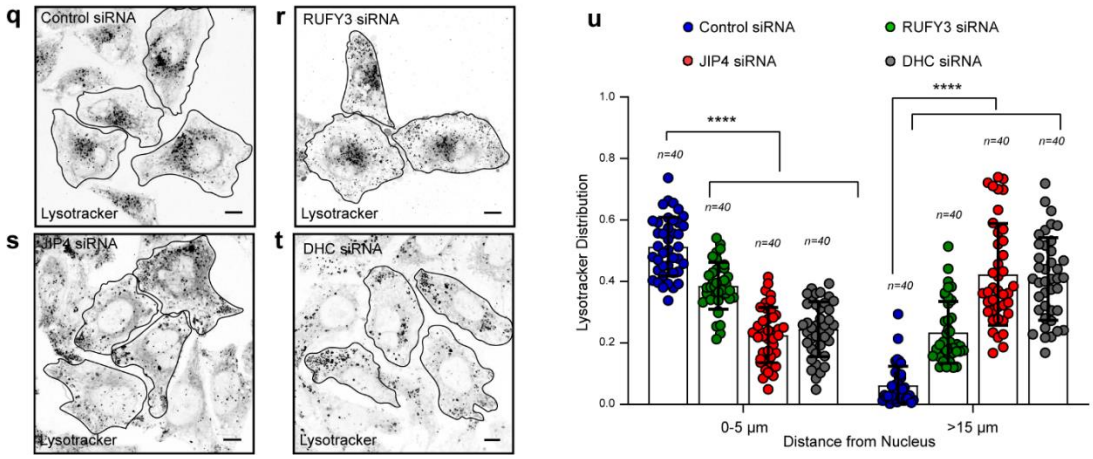

Figure 15: **RUFY3 links Arl8b to the JIP4-dynein complex**. **(a-b)** GST-pulldown assay of semi-purified FLAG-tagged-JIP4 with GST and GST-RUFY3 and immunoblotted (IB) with anti-FLAG antibody. Quantification from two independent experiments is shown in (B). **(c-f)** Lysates of HEK293T cells were subjected to endogenous IP as labeled and the precipitates were IB with indicated antibodies. Quantification of the blots is shown in (d-f). Values plotted are mean ± S.D. from three independent experiments (**p<0.01; *p<0.05; two-tailed Student's *t-test*). **(g-i)** Representative confocal micrographs of HeLa cells transfected with Arl8b-HA (g) or co-transfected with RUFY3 (UT) (h) and stained with indicated antibodies. Transfected cells are outlined and some panels are shown in an inverted grayscale. Colocalization of JIP4 with Arl8b was measured by Pearson's correlation coefficient (i). Values plotted are mean ± S.D. from three independent experiments. Experiments are color-coded, and each dot represents the individual data points from each experiment. The total number of cells analyzed is indicated on the graph (****p<0.0001; two-tailed Student's *t-test*). **(j-k)** HEK293T cell lysates expressing Arl8b-HA or co-expressing Arl8b-HA and RUFY3-FLAG were subjected to IP using anti-HA antibodies-conjugated-agarose beads and the precipitates were IB with the indicated antibodies. Quantification of the blot is shown in (k) and values plotted are mean ± S.D. from three independent experiments (**p<0.01; two-tailed Student's *t-test*). **(l-m)** HEK293T cells were treated with indicated siRNAs and subjected to endogenous IP using an anti-Arl8 antibody. The precipitates were IB with indicated antibodies. Quantification of the blot is shown in (m) and values plotted are mean ± S.D. from three independent experiments (****p<0.0001; two-tailed Student's *t-test*). **(n-o)** Representative confocal images of HeLa cells treated with indicated siRNAs and transfected with RUFY3-HA. The cells were stained for lysosomes and RUFY3 using anti-LAMP1 and anti-HA antibodies, respectively. Transfected cells are outlined, and some panels are shown in an inverted grayscale. **(p)** Distribution of lysosomes was quantified from the images shown in (n-o). **(q-u)** Representative confocal microscopy images of HeLa cells transfected with indicated siRNAs and stained for lysosomes using Lysotracker. Scale Bars: 10 µm. The quantification is shown in (u). Values plotted are mean ± S.D. from three independent experiments. The total number of cells analyzed is indicated on the graph (****p<0.0001; two-tailed Student's *t-test*).

Indeed, the motility behavior of lysosomes (labeled with Lysotracker) analyzed by tracking individual lysosomes showed that similar to dynein depletion, RUFY3 depletion significantly increased the total mobile fraction and the average speed of individual lysosomes (**Figures 16a-c**; quantification is shown in **Figures 16d-e**).

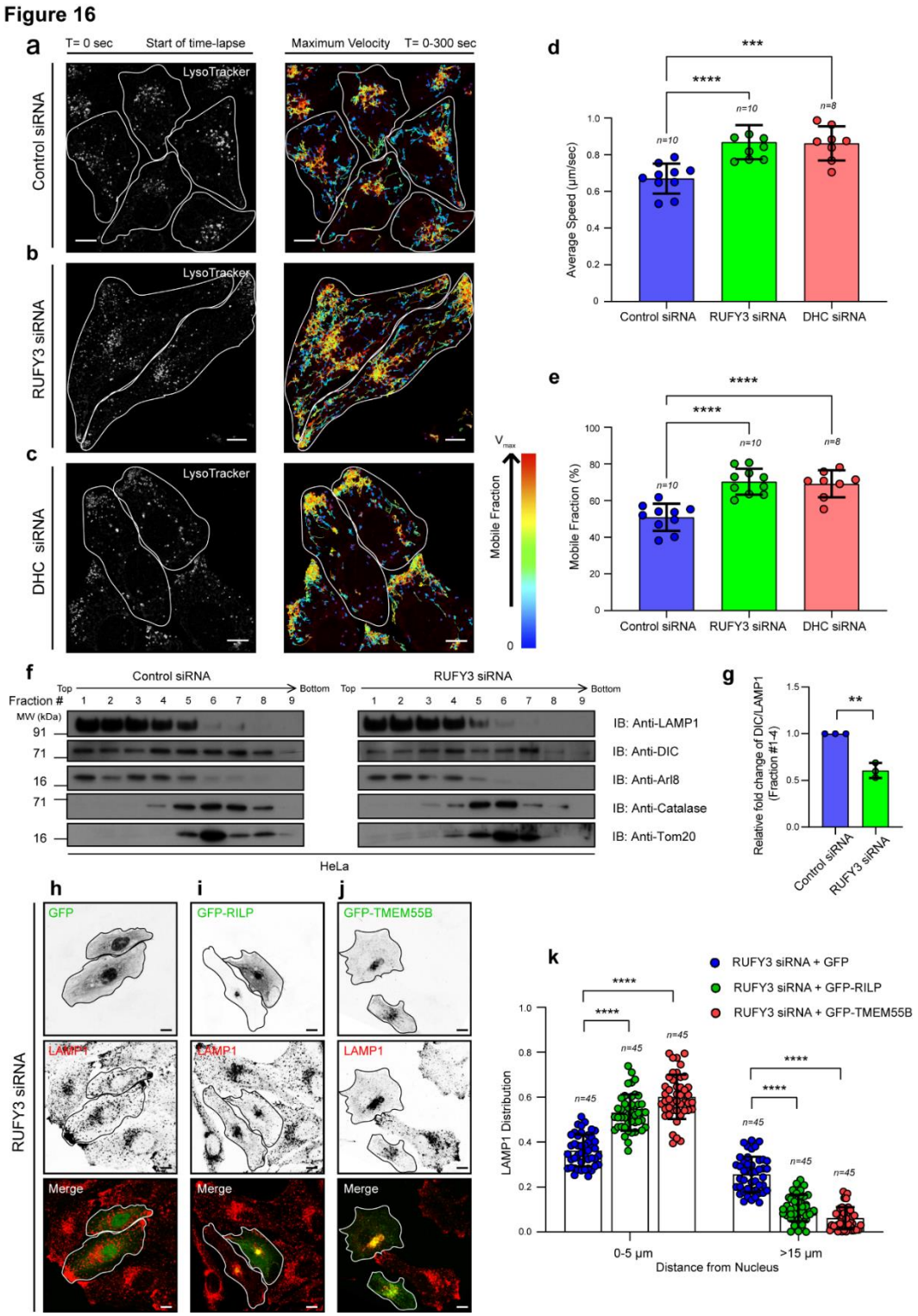

Figure 16: RUFY3 mediates lysosome motility by recruiting dynein motor on lysosomes. (a-c) HeLa cells treated with control siRNA (a), RUFY3 siRNA (b) or DHC siRNA (c) were

incubated with Lysotracker to label lysosomes. Left panels: representative confocal images of live HeLa cells captured at the start of time-lapse imaging (T=0 sec). Right panels: single-particle tracking analysis of Lysotracker-labeled lysosomes for T=300 sec with color-coding to show maximum velocity (blue, immobile; red, max mobility). Scale Bars: 10 µm; see Supplementary Movies 1-3. **(d-e)** The graph represents maximum average speed (d) and a mobile fraction (e) of Lysotracker-labeled lysosomes calculated from two independent live-cell imaging experiments as described in a-c. Values plotted are mean ± S.D., and the total number of cells analyzed is shown on the graph (****p<0.0001; ***p<0.001; two-tailed Student's *t*-test). **(f-g)** Lysosomes enrichment was performed using Opti-prep density ultracentrifugation on post-nuclear homogenate prepared from HeLa cells treated with control siRNA or RUFY3 siRNA. Different fractions were resolved and immunoblotted (IB) with indicated antibodies. The graph represents relative fold change in DIC levels normalized to LAMP1 levels (for fractions #1-4 combined) from control and RUFY3 siRNA treated cells. Values plotted are mean ± S.D. from three independent experiments (**p=0.0011; two-tailed Student's *t*-test). **(h-j)** Representative confocal micrographs of RUFY3-siRNA treated HeLa cells transfected with GFP (h), GFP-RILP (i) or GFP-TMEM55B (**j**) and stained for lysosomes using an anti-LAMP1 antibody. Transfected cells are outlined, and some panels are shown in an inverted grayscale. Scale Bars: 10 µm. **(k)** The distribution of lysosomes based on the LAMP1 signal was quantified from the experiments shown in h-j. Values plotted are mean ± S.D. from three independent experiments. The total number of cells analyzed is indicated on the graph (****p<0.0001; two-tailed Student's *t*-test).

Thus, our data suggest that upon RUFY3 and/or dynein depletion, there is an increase in the proportion of mobile lysosomes. To directly analyze whether RUFY3 regulates dynein subunit levels on lysosomes, we used density gradient ultracentrifugation to enrich lysosomes from control and RUFY3-depleted cells. Indeed, upon RUFY3 depletion, dynein intermediate chain (DIC) levels were reduced in the lysosomal fractions compared to the control cells (**Figures 16f-g**).

We noted that DIC levels in other fractions were also reduced in RUFY3 depleted homogenates, suggesting that RUFY3 might regulate dynein levels on other compartments as well. Finally, based on our hypothesis, we predicted that the expression of other dynein adaptors that localize to LAMP1 compartments should reinstate dynein-dependent lysosome positioning in RUFY3-depleted cells. Indeed, RILP and TMEM55B, both of which interact with and recruit dynein-dynactin on the LAMP1 compartment (Jordens et al., 2001; Willett et al., 2017), repositioned lysosomes to the perinuclear region in RUFY3-depleted cells (compare untransfected with transfected cells, **Figures 16h-j**; quantification is shown in **Figure 16k**). Taken together, these findings show that RUFY3 is an Arl8b effector that recruits dynein on lysosomes to maintain the typical stable pool of immobile lysosomes localized in the perinuclear region of the cell.

G) Depletion of RUFY3 reduces lysosome size

Previous studies have shown that the perinuclear and the peripheral pools of lysosomes have few differential characteristics and functions. The peripheral pool of lysosomes is more poised for crosstalk and fusion with the plasma membrane and serum-dependent-mTORC1 activation (Korolchuk et al., 2011a; Pu et al., 2017; Rui Jia & Bonifacino, 2019). In contrast, the perinuclear lysosomal subpopulation is more suited for interaction with perinuclear late endosomes/autophagosomes and, subsequently, cargo degradation. Moreover, in at least one study, it has been reported that the peripheral pool of lysosomes is less acidic and less accessible to biosynthetic cargo (such as cathepsins). However, a subsequent report has shown that peripheral and perinuclear lysosomes have a similar pH (~4.4). Since RUFY3 depletion results in an increased lysosomal pool near the plasma membrane, we wanted to determine whether lysosome characteristics including, their pH, size and number, are altered in these cells. We used fluorescent dyes Lysotracker and Lysosensor Yellow/blue DND-160, which have different characteristics but share the property of fluorescing in acidic compartments (Ma et al., 2017). Intensity variations in Lysotracker staining report on the size and number of acidic compartments but cannot report variations in pH within the acidic range (Guha et al., 2014). Lysosensor dyes are pH sensitive used for ratiometric measurement of intraorganellar pH of acidic organelles (Diwu et al., 1999). Surprisingly, while we did not observe any significant changes in lysosome pH in RUFY3-depleted cells (5.63±0.19), as compared to control cells (5.49±0.18) (**Figures 17a** and **17b**), there was a two-fold reduction in Lysotracker intensity in RUFY3-depleted cells, as compared to control (**Figure 17c** and **17d**). The decrease in Lysotracker intensity was rescued in cells expressing RUFY3 siRNA-resistant construct, indicating that this phenotype is specifically due to RUFY3 depletion (**Figure 17e**; quantification is shown in **Figure 17f**). These findings suggested that lysosome size is affected by RUFY3 depletion.

To directly assess lysosome size, we analyzed the ultrastructure of LE/Lys by transmission electron microscopy imaging on thin sections of control and RUFY3-depleted cells. As compared to control, lysosomes appeared to be smaller, denser and more numerous upon RUFY3 depletion (see insets, **Figures 17g** and **17h**).

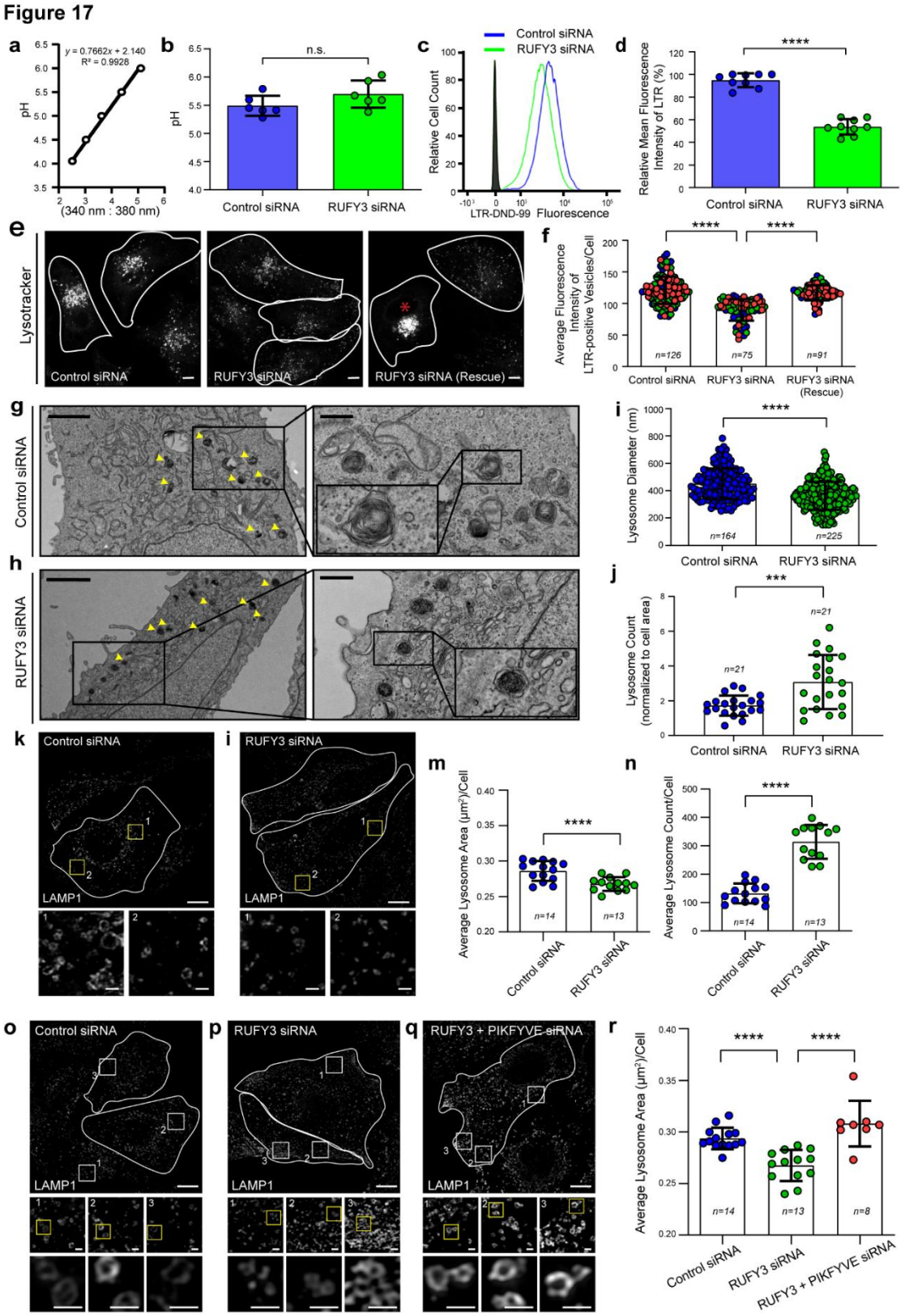

Figure 17: RUFY3 depletion reduces lysosome size. (a) pH calibration curve based on ratiometric fluorescence intensity measurements of Lysosensor Yellow/Blue DND-160. **(b)** Graph showing average pH-value of lysosomes measured from HeLa cells treated with indicated siRNAs. Values plotted are mean ± S.D. from six independent experiments (n.s., not significant; two-tailed Student's *t*-test). **(c-d)** Representative histogram showing mean

fluorescence intensity (MFI) of Lysotracker Red DND-99 (LTR) uptake (1 h) in control siRNA- and RUFY3 siRNA-treated HeLa cells (c), and the graph in d represents relative percentage of MFI for LTR uptake from three independent experiments (****p<0.0001; two-tailed Student's t-test). **(e-f)** Representative micrographs of live HeLa cells treated with indicated siRNAs and labeled with LTR. The asterisk indicates cell transfected with GFP-RUFY3-siRNA-resistant plasmid. Scale Bars: 10 µm. The quantification of average fluorescence intensity of LTR-positive vesicles is shown in f. Values plotted are mean ± S.D. from three independent experiments. Experiments are color-coded and the total number of cells analyzed is indicated on the graph (****p<0.0001; two-tailed Student's t-test). **(g-j)** Representative TEM images of HeLa cells treated with indicated siRNAs. Higher magnifications of lysosomes (dense and multi-lamellar structures, indicated by yellow arrowheads) are shown in the right panels. Scale Bars: 2 µm (main); 0.5 µm (inset). Lysosomes size (i) and numbers (j) were quantified using TEM images. Note: in i, n represents number of lysosomes analyzed for size measurement. **(k-n)** Representative SIM images of HeLa cells treated with indicated siRNAs and stained with anti-LAMP1 antibodies. Insets represent magnified view of boxed areas highlighting differences in lysosome size. The average area (m) and count (n) of LAMP1-positive vesicles per cell was measured in HeLa cells upon treatment with indicated siRNAs. **(o-r)** Representative SIM images of HeLa cells treated with indicated siRNAs and stained with anti-LAMP1 antibody. In the insets, zoomed views of selected ROIs are shown, and quantification of the average area of lysosomes is plotted (r). Values plotted are mean ± S.D. and the total number of cells analyzed are indicated on the graph (****p<0.0001; ***p=0.0006; two-tailed Student's t-test). Scale Bars: 10 µm (main); 1 µm (inset).

The diameter of lysosomes was reduced by ~20% in RUFY3-depleted cells compared to control, which would translate into a ~50% reduction in lysosome volume (**Figure 17i**). We noted a ~1.8-fold increase in lysosome (multi-lamellar structures) numbers in RUFY3-depleted cells compared to control cells (**Figure 17j**). We corroborated these observations by measuring the average area and number of LAMP1-positive compartments from super-resolution imaging of control and RUFY3 knockdown cells. As shown in **Figures 17k-n**, there was a significant reduction in the average area of lysosomes and a corresponding increase in lysosomes number in RUFY3-depleted cells. The mechanism of how RUFY3 regulates lysosome size remains unclear at this time. One of the processes that could result in decreased lysosome size and increased numbers is the membrane fission of these late endocytic compartments. The enzyme PIKFYVE that forms PtdIns(3, 5)P_2 from PtdIns(3)P has been previously shown to regulate lysosome size by promoting tubulation and fission (Araujo et al., 2020; Bissig et al., 2017; Choy et al., 2018). We investigated whether PIKFYVE depletion would restore normal lysosomal size in RUFY3-depleted cells. Indeed, cells co-depleted of RUFY3 and PIKFYVE showed a normal size distribution of lysosomes (see inset in

Figures 17o-q; quantification is shown in **Figure 17r**). Thus, RUFY3 not only maintains a perinuclear lysosomal pool but also regulates lysosome size. It will be interesting to determine whether the RUFY3-JIP4-dynein complex regulates both lysosome positioning and lysosome reformation.

H) RUFY3 regulates nutrient-dependent lysosome repositioning but not autophagic cargo clearance and endocytic trafficking to lysosomes

Previous reports have shown that Arl8b and its upstream regulator-BORC complex regulate nutrient-dependent lysosome positioning to the cell periphery (Pu et al., 2015, 2017). Based on our findings that RUFY3 functions as a dynein adaptor on lysosomes, we expected that RUFY3-depleted cells would fail to show repositioning of lysosomes to the perinuclear region in nutrient-starved cells. Indeed, lysosomes continued to localize at the cell periphery in RUFY3-depleted cells that were subjected to either complete starvation (EBSS-media lacking both serum factors and amino acids) or serum starvation (DMEM-FBS) or only amino acid (DMEM-AA) (**Figures 18a-d**). This was in contrast to the control siRNA treated cells, where as expected, lysosomes were accumulated in the perinuclear region and generally absent from the periphery in all three conditions of starvation (**Figures 18a-d**; quantification is shown in **Figure 18e**).

Lysosome clustering to the perinuclear region in nutrient-deprived cells has been shown to result in the enhanced propensity of fusion with mature autophagosomes, which is important for replenishing the macromolecular building blocks in the starved cells (Kimura et al., 2008). The fusion of autophagosomes and lysosomes and the degradation of autophagic cargo have classically been measured by the amount of autophagosomal protein LC3B remaining in the cells with/without starvation (Klionsky et al., 2021). To address the RUFY3 role in autophagic cargo degradation, we assessed the amount of lipidated LC3 (LC3B-II) levels in fed and starved cells treated with control or RUFY3 siRNA. As shown in **Figure 18f**, while the initial levels of LC3B-II were modestly less in the fed state upon RUFY3 depletion, upon EBSS (Earle's Balanced Salt Solution) treatment, both control and RUFY3-depleted cells showed a similar increase in LC3B-II levels. Also, LC3B-II levels were rescued to a similar extent in control and RUFY3-depleted cells treated with Bafilomycin A1 (BafA1), an inhibitor of lysosomal acidification and, therefore, degradation (**Figure 18g**). These results suggest that RUFY3 does not regulate autophagosome-lysosome fusion. To corroborate the autophagy flux analysis, we also measured the colocalization between

LC3 and LAMP1 in serum-starved-control and -RUFY3-depleted cells treated with BafA1 to ensure the maximal frequency of autolysosomes is observed in these experiments. While there was a modest decrease in the LC3/LAMP1 colocalization in RUFY3-depleted cells, the difference in average Pearson correlation coefficient values from control was minor and not significant (**Figures 18h-i**; quantification is shown in **Figure 18j**). We noted that several peripheral lysosomes in RUFY3-depleted cells were also colocalized with LC3, suggesting that autolysosome formation is also occurring outside the perinuclear region (see inset in **Figure 18i**). Thus, while lysosome repositioning to the perinuclear subcellular location was strikingly reduced upon RUFY3 depletion, no significant changes in autophagosome-lysosome fusion and LC3 flux were observed in RUFY3-depleted cells. Our findings agree with previous work showing that peripheral lysosomes can also undergo fusion with autophagosomes (Jia et al., 2017).

We also assessed whether RUFY3 regulates the delivery of endocytic cargo to lysosomes. To this end, we pulsed control and RUFY3-depleted cells with BODIPY-LDL followed by chase for different time points and determined colocalization with Lysotracker compartments. In addition, we also tested colocalization of endocytosed dextran with Lysotracker compartments in control and RUFY3-depleted cells. As shown in **Figures 18k-n** and **Figures 18o-q**, there was no significant change in colocalization of LDL or dextran with Lysotracker upon RUFY3 depletion (quantification shown in **Figures 18n** and **18r**), suggesting that RUFY3 does not regulate delivery and fusion of endocytic or autophagic cargo vesicles to lysosomes. Interestingly, there was a modest decrease (~25%) in lysosome-mediated cargo degradation upon RUFY3 depletion, as assessed by BODIPY FL-BSA fluorescence intensity that is de-quenched upon proteolytic cleavage in lysosomes (**Figures 18s-u**). These results suggest that although cargo delivery to late endocytic compartments is not affected, RUFY3 depletion likely impacts lysosomal cargo degradation. The impaired degradative ability could be due to reduced lysosome size, as shown in a previous study where lysosomal cargo degradation was less in cells with decreased lysosome size (Meneses-Salas et al., 2020). Furthermore, as Rab7 and Arl8b colocalization is modestly reduced in RUFY3-depleted cells (**Figure 14m**), endolysosome formation (generally regarded as the degradative compartments) might be reduced upon RUFY3 knockdown.

Figure 18

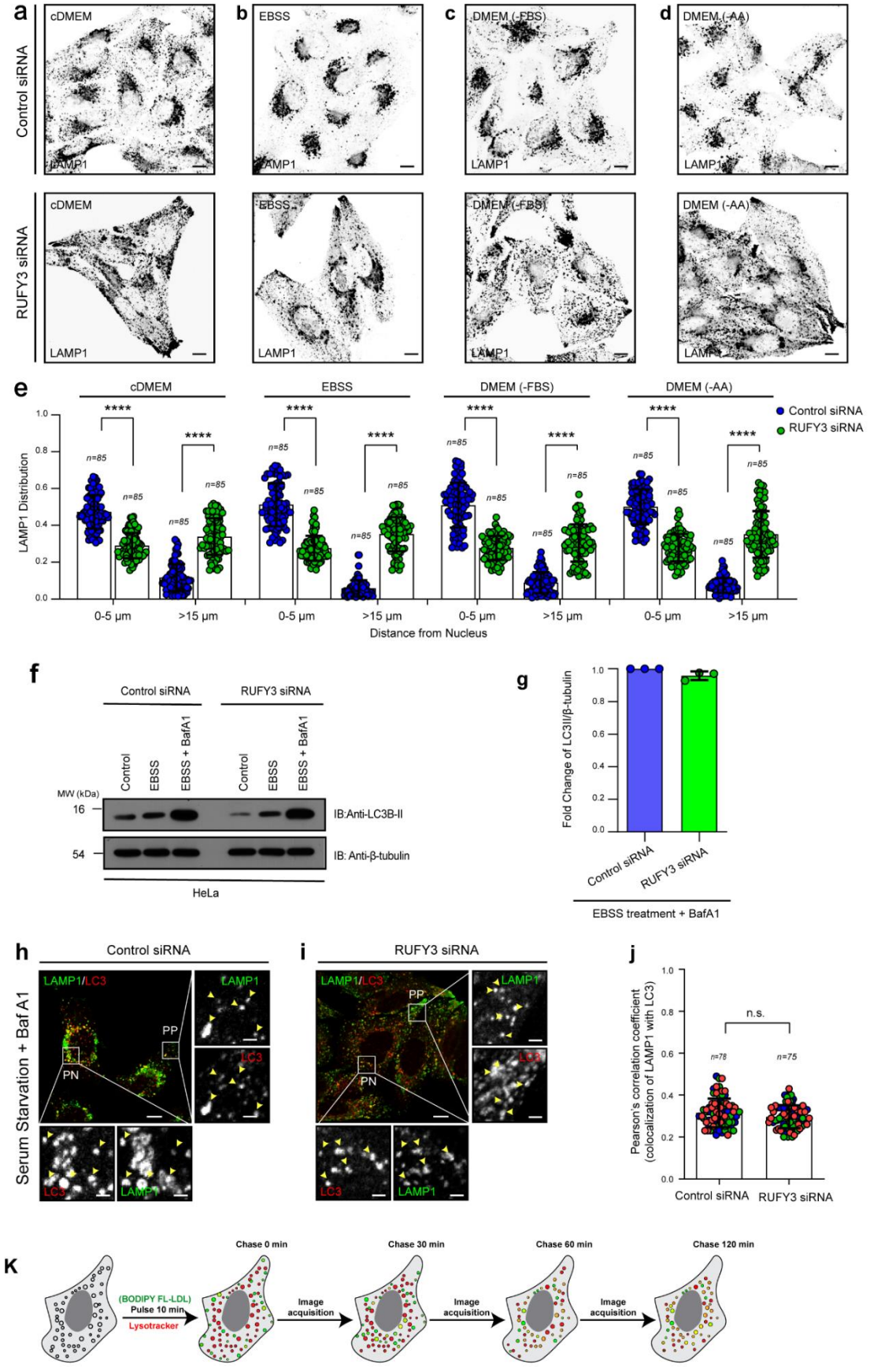
a
b
c
d
cDMEM
EBSS
DMEM (-FBS)
DMEM (-AA)
Control siRNA
RUFY3 siRNA
LAMP1
e
LAMP1 Distribution
Control siRNA
RUFY3 siRNA
0-5 µm
>15 µm
Distance from Nucleus
f
Control siRNA
RUFY3 siRNA
Control
EBSS
EBSS + BafA1
MW (kDa)
16
54
IB:Anti-LC3B-II
IB: Anti-β-tubulin
HeLa
g
Fold Change of LC3II/β-tubulin
Control siRNA
RUFY3 siRNA
EBSS treatment + BafA1
h
i
j
Serum Starvation + Baf A1
LAMP1/LC3
PP
PN
n.s.
Pearson's correlation coefficient (colocalization of LAMP1 with LC3)
K
(BODIPY FL-LDL)
Pulse 10 min
Lysotracker
Image acquisition
Chase 0 min
Chase 30 min
Chase 60 min
Chase 120 min

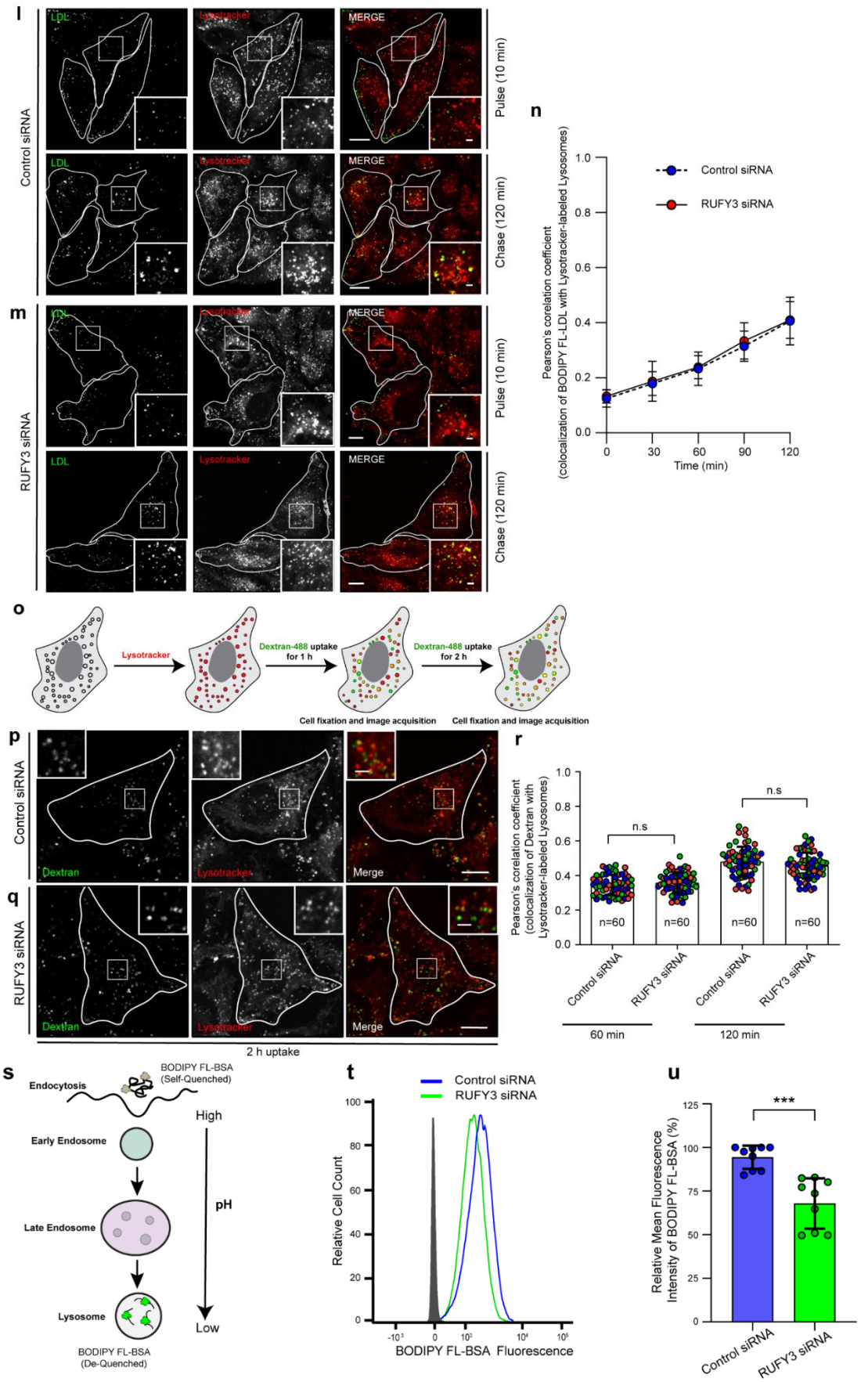

Figure 18: RUFY3 regulates nutrient-dependent lysosome repositioning. (a-e) Representative confocal micrographs (shown as grayscale inverted) of HeLa cells treated with

control siRNA or RUFY3 siRNA and incubated in indicated media for 4 h. Post-treatment, cells were fixed and stained using an anti-LAMP1 antibody. The distribution of lysosomes based on the LAMP1 signal from these experiments is shown in e and values plotted are mean ± S.D. from three independent experiments, and the total number of cells analyzed is indicated on the graph (****p<0.0001; two-tailed Student's t-test). **(f-g)** HeLa cells transfected with indicated siRNAs were grown in complete media or subjected to 2 h starvation using EBSS media in the absence or presence of Bafilomycin A1 (BafA1). Lysates from these cell types were IB with the indicated antibodies. Protein densitometric analysis of LC3B-II levels normalized to β-tubulin is shown in **g**. (**h-i)** Representative confocal images of control (h) and RUFY3-depleted (i) HeLa cells incubated in media lacking serum for 1 h in the presence of BafA1. Post-treatment, cells were fixed and stained for LAMP1 and LC3. In the insets, selected peripheral (PP) and perinuclear (PN) regions of the cell are magnified to show colocalized pixels of LC3 with LAMP1 (denoted by yellow arrowheads). **(j)** Colocalization of LAMP1 with LC3 for the experiments performed in **h** and **i** was analyzed by measuring Pearson's correlation coefficient. Values plotted are mean ± S.D. from three independent experiments. Experiments are color-coded, and the total number of cells analyzed is on the graph (n.s., not significant; two-tailed Student's t-test). **(k)** Schematic represents the methodology used to the trafficking of LDL to lysosomes. **(l-n)** Representative confocal micrographs of BODIPY FL-LDL trafficking to Lysotracker-labeled lysosomes in control and RUFY3-silenced HeLa cells for the indicated time periods. Insets show a magnified view of boxed areas highlighting delivery of BODIPY FL-LDL to Lysotracker-labeled lysosomes. Scale Bars: 10 µm (main); 2 µm (inset). Pearson's correlation coefficient was quantified for the images and values plotted are mean ± S.D. from three independent experiments. **(o)** Schematic represents the methodology used to study the dextran delivery to lysosomes. **(p-r)** Representative confocal micrographs of dextran delivery to Lysotracker-labeled lysosomes in control and RUFY3-silenced HeLa cells for the indicated time periods. Insets show a magnified view of boxed areas highlighting delivery of pulsed dextran to Lysotracker-labeled lysosomes. Scale Bars: 10 µm (main); 2 µm (inset). Pearson's correlation coefficient was quantified for the images and values plotted are mean ± S.D. from three independent experiments. Experiments are color-coded and the total number of cells analyzed is indicated on the graph (n.s., not significant; Student's *t-test*). **(s)** Schematic representation of the BODIPY FL-BSA uptake and de-quenching in lysosomes. **(t-u)** Representative histogram showing - of de-quenched BODIPY FL-BSA after 2 h of incubation in control siRNA- and RUFY3 siRNA-treated HeLa cells as analyzed by flow cytometry (t), and the bar graph in u represents relative percentage of MFI signal for de-quenched BODIPY FL-BSA after 2 h of incubation in HeLa cells treated with control- or RUFY3-siRNA calculated from three independent experiments (***p<0.001; two-tailed Student's t-test). Scale Bars: 10 µm (main); 2 µm (inset).

Discussion

The small G protein Arl8b is a crucial player regulating lysosomal positioning and functions in the subcellular space (Khatter, Sindhwani, et al., 2015). Arl8b overexpression was shown to increase the proportion of lysosomes undergoing bi-directional long-range movement on the microtubule tracks. Subsequent studies revealed that Arl8b binds to effector protein SKIP/PLEKHM2, which in turn binds and

recruits kinesin-1 motor to promote anterograde motility of lysosomes (Keren-Kaplan & Bonifacino, 2021; Pu et al., 2015; Rosa-Ferreira & Munro, 2011; Tuli et al., 2013). However, it was not known whether Arl8b could mediate the long-range retrograde movement of lysosomes. In this study, we have identified RUFY3 as an Arl8b effector that recruits the JIP4-dynein-dynactin complex to mediate the retrograde motility of lysosomes. Notably, while this work was under review, a preprint study reported similar findings on the role of RUFY3 as an Arl8b effector that promotes dynein-dependent retrograde motility of lysosomes (Tal Keren-Kaplan et al., RUFY3 and RUFY4 are ARL8 effectors that couple lysosomes to dynein-dynactin, 25 May 2021, PREPRINT (Version 1) available at Research Square [https://doi.org/10.21203/rs.3.rs-469512/v1]).

Among the six transcript variants of RUFY3 annotated on NCBI, only variant 2 (469 amino acids long) is functionally characterized and shown to regulate axon guidance in neurons and migration of cancer cells, processes that depend on actin cytoskeletal dynamics. This study presents evidence that the longest transcript variant of RUFY3, variant 1 (620 amino acids long), localizes to lysosomes and regulates lysosome positioning. Variant 1 binds to Arl8b via a sequence in its C-terminal region (amino acids 441-561), which is not present in other variants, except for variant 4. Thus, the localization and function of RUFY3 variants may differ based on certain sequence features. As effectors such as PLEKHM1 and SKIP/PLEKHM2 bind to Arl8b via their RUN domains (Marwaha *et al.*, 2017), it was surprising that the RUN domain of RUFY3 was not required for binding to Arl8b. Future work is needed to elucidate what determines the binding of some, but not all, RUN domains to Arl8b.

RUFY3 joins the league of other late endosomal/lysosomal proteins, including RILP, TRPML1, TMEM55B and SEPT9, which interact with dynein-dynactin retrograde motor either directly or via binding to dynein adaptors JIP3 or JIP4 ((Jordens et al., 2001; Kesisova et al., 2021; Li et al., 2016; Willett et al., 2017). This list raises a question as to why several dynein adaptors are required for lysosomal motility (**Figure 19a**). One explanation could be that multiple adaptors are needed to engage a sufficient number of dynein motors to win the tug-of-war against kinesin, which generates force equivalent to eight dynein-dynactin complexes (Soppina et al., 2009) (**Figure 19a (I)**). A second explanation could be that different adaptors are required under different

physiological conditions; for instance, one or more lysosomal dynein adaptors might be required specifically under conditions such as starvation or oxidative stress where lysosomes are clustered in the perinuclear region (**Figure 19a (II)**). Indeed, the expression of lysosomal adaptor TMEM55B is controlled by transcription factors TFEB, TFE3, and SREBF2, activated upon starvation and stress due to cholesterol accumulation in the lysosomal lumen (Willett et al., 2017). Additionally, phosphorylation of TMEM55B by ERK/MAPK regulates lysosome positioning (Takemasu et al., 2019). Interestingly, a recent study has shown the involvement of specific dynein adaptors at different stages of organelle maturation, providing yet another rationale for the existence of multiple dynein adaptors (Cason et al., 2021).

A third reason could be that while markers like LAMP1 are common, different dynein adaptors are essentially required for the motility of distinct compartments (**Figure 19a (III)**). Indeed, recent studies have suggested that there are LAMP1-positive compartments that are non-degradative, and differences in pH and cathepsin activity have been documented between perinuclear and peripheral LAMP1 compartments enriched for Rab7 and Arl8b, respectively (Cheng et al., 2018; Johnson et al., 2016). Interestingly, a recent study proposed a Rab7-to-Arl8b switch mechanism akin to the Rab5-to-Rab7 switch paradigm for the maturation of late endosomes/endolysosomes (M. L. Jongsma et al., 2020). Our data suggest that while RILP (Rab-interacting lysosomal protein) is the dynein adaptor for Rab7 compartments, RUFY3 is the adaptor for compartments enriched for the small G protein Arl8b. The two dynein adaptors, RILP and RUFY3, might regulate the positioning of the late endocytic compartments and the maturation/identity of these membranes and the fate of cargo traffic to and from these compartments. For instance, RILP-mediated Rab7 positioning regulates cargo retrieval from late endosomes, while RUFY3 might promote the close association of Rab7 and Arl8b endosomes and the formation of Rab7-Arl8b hybrid endolysosomal compartments. Eventually, Rab7 to Arl8b switch is mediated by recruitment of Rab7 GAP TBC1D5 by SKIP, converting a Rab7 and Arl8b hybrid perinuclear compartment to an Arl8b-only peripheral compartment. An exciting question for future studies remains whether Arl8b binding to RUFY3 regulates its association with the SKIP-Kinesin-1 complex and what physiological cues and molecular players determine the

switch from SKIP-mediated anterograde motility to RUFY3-dependent retrograde motility of lysosomes (**Figure 19b**).

While RUFY3 was required for the organization of the lysosome population at the whole-cell scale, surprisingly, its depletion also affected the characteristics of individual lysosomes, namely lysosome size. We found that average lysosome volume was reduced by a significant value of almost 50% upon RUFY3 depletion. As noted in earlier studies (Choy et al., 2018; Yordanov et al., 2019), a reduction in lysosome size was accompanied by an increase in lysosome number upon RUFY3 depletion. Thus, a significant proportion of lysosomes in RUFY3 knockdown were smaller, numerous and localized in the peripheral subcellular space. The average velocity of individual lysosomes was increased upon RUFY3 depletion, possibly because the lysosome size was reduced and/or kinesin-mediated forces were dominant on lysosomes (**Figure 19b**).

Is there a common explanation that underlies RUFY3 role in regulating the positioning and size of lysosomes? We speculate that in cells depleted of RUFY3, lysosomes escape more frequently from the perinuclear cloud and move in an Arl8b-SKIP-Kinesin-1 complex-dependent manner on the microtubule highway. Additional experimental evidence is required to establish whether kinesin-1-dependent tubulation and fission events, ultimately leading to lysosome reformation, are also enhanced in RUFY3 depletion. An intriguing question is the true identity of the smaller LAMP1-positive vesicles in RUFY3 depleted cells, i.e. whether these are newly formed terminal lysosomes or vesicles retrieving cargo from late endosomes for recycling to Golgi and plasma membrane? Indeed, previous studies have shown the role of Rab7-retromer and JIP4-kinesin-1 complex in mediating tubulation and cargo retrieval from late endosomes (Marchesin et al., 2015; Rojas et al., 2008; Sapmaz et al., 2019). From this study, we speculate that the RUFY3 role is more likely to be downstream of the late endosomal sorting step and in maintaining the balance between terminal storage lysosomes and endolysosomes.

Future studies will establish whether the correlation between lysosome positioning and size reflects different biogenesis stages of this enigmatic organelle with newly formed immature lysosomes located in the cell periphery. In contrast, mature lysosomes reside in the perinuclear pool poised for fusion with incoming cargo vesicles.

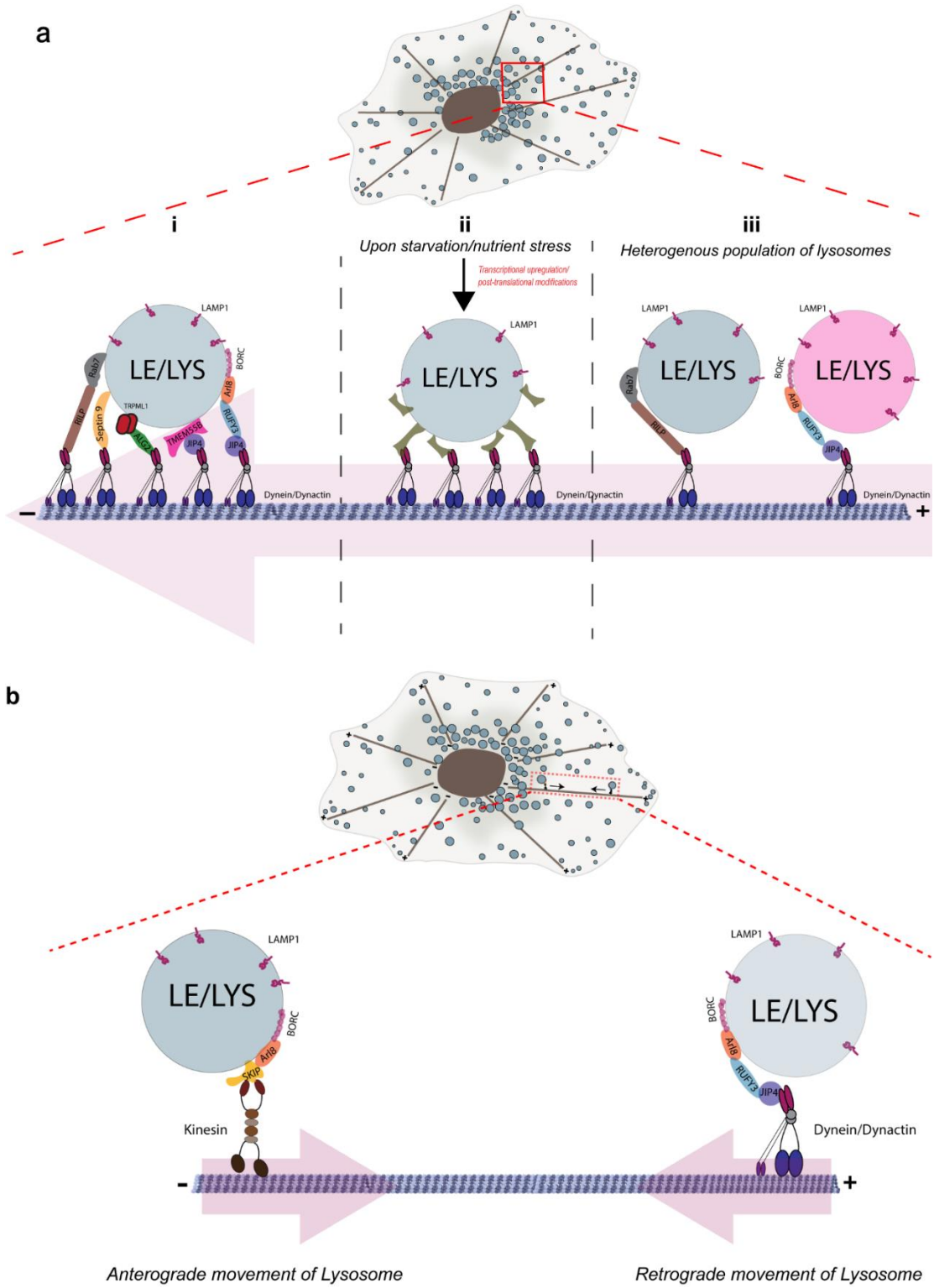

Figure 19: (a) A schematic of three distinct hypothetical scenarios to explain the significance of different lysosomal adaptors that engage the dynein-dynactin complex for retrograde transport. (I) Multiple adaptors may work in concert to recruit enough dynein motors to balance the opposite driving forces exerted by a single kinesin motor. **(II)** Different adaptors may be required under distinct physiological conditions. For instance, during nutrient starvation, expression and/or recruitment of a particular adaptor might increase onto lysosomes. Increased spatial density of lysosomes and autophagosomes in the perinuclear region could

enhance their fusion. **(III)** Different dynein adaptors are required for retrograde transport of distinct populations of lysosomes that may differ in their membrane composition. **(b) Model illustrating the opposing motor adaptors recruited by Arl8b.** Arl8b relieves autoinhibition of SKIP that in turn recruits and activates Kinesin-1 motor to promote anterograde motility of lysosomes. As revealed in this study, Arl8b recruits RUFY3 on lysosome that in turn interacts with JIP4-dynein-dynactin complex to mediate retrograde movement of lysosomes.

Materials and Methods

Cell culture and treatments

HeLa, HEK293T, U2OS and A549 cells (from ATCC) were maintained in DMEM media (Gibco) supplemented with 10% FBS (Gibco) at 37°C with 5% CO_2 in a humidified cell culture chamber. For imaging and flow cytometry experiments described below, phenol red-free DMEM media (Gibco) was used. For culturing ARPE-19 cells (from ATCC), DMEM/F-12 media (Gibco) supplemented with 10% FBS was used. Serum starvation was performed by incubating cells in DMEM with 2 mM L-glutamine for 1 h. Combining amino-acid and serum starvation was performed by incubating cells in EBSS for 4 h. Amino-acid starvation was performed by incubating cells in amino-acid-free DMEM (US Biologicals) supplemented with 10% dialyzed-FBS (Gibco) for 4 h. Each cell type was regularly screened for the absence of mycoplasma contamination by using the MycoAlert Mycoplasma Detection Kit (Lonza) and was cultured for no more than 15 passages.

For gene silencing, siRNA oligos or SMARTpool were purchased from Dharmacon and prepared according to the manufacturer's instructions. Following siRNA oligos were used in this study: control siRNA, 5’-TGGTTTACATGTCGACTAA-3’; RUFY3 siRNA, 5’-GATGCCTGTTCAACAAATGAA-3’; Arl8b siRNA, 5’-AGGT AACGTCACAATAAAGAT-3’; Rab7a siRNA, 5’- CTAGATAGCTGGAGAGATG-3’; JIP4 siRNA, 5’-GAGCATGTCTTTACAGATC-3’; DHC siRNA, 5’-GAGAGGA GGTTATGTTTAA-3’; PIKFYVE siRNA, ON-TARGET plus SMART pool (L-005 058-00-0005). For shRNA mediated gene silencing, control shRNA (SHC016) and RUFY3 shRNA (TRCN0000127915) were purchased from Sigma-Aldrich. Transient transfection of siRNAs was performed with DharmaFECT 1 (Dharmacon) according to the manufacturer’s instructions.

For shRNA-mediated gene silencing, lentiviral transduction was performed as described previously (Garg et al., 2011). Briefly, for lentiviral transduction, HeLa cells were plated at 100,000/well in 6-well plates (Corning) in 8 µg/mL Polybrene (Sigma-Aldrich) and transduced by addition of 100 µL viral supernatant. 24 h later, puromycin (Sigma-Aldrich) was added at 3 µg/mL to select transductants and experiments performed on Days 5-21 following transduction.

Mammalian expression constructs

All the DNA constructs used in this study are listed in appendix table 1.

Antibodies and chemicals

All the antibodies used in this study are listed in appendix table 2. Alexa-Fluor-conjugated-Dextran, Lysotracker dyes, Lysosensor dyes, BODIPY FL LDL, Phalloidin, and DAPI, were purchased from Molecular Probes (Invitrogen). SiR-Lysosome Kit was purchased from Cytoskeleton, Inc. Self-Quenched BODIPY FL conjugate of BSA was purchased from BioVision. Polybrene, Puromycin, EBSS, Rapamycin and Bafilomycin A1 were purchased from Sigma-Aldrich.

Transfection, immunofluorescence and live-cell imaging

Cells grown on glass coverslips (VWR) were transfected with desired constructs using X-treme GENE-HP DNA transfection reagent (Roche) for 16-18 h. Cells were fixed in 4% PFA in PHEM buffer (60 mM PIPES, 10 mM EGTA, 25 mM HEPES and 2 mM $MgCl_2$ and final pH 6.8) for 10 min at room temperature (RT). Post-fixation, cells were incubated with blocking solution (0.2% saponin + 5% normal goat serum (NGS) in PHEM buffer) at RT for 30 min, followed by three washes with 1XPBS. Following the blocking step, cells were incubated with primary antibodies in staining solution (PHEM buffer + 0.2% saponin + 1% NGS) for 1 h at RT, washed three times with 1XPBS and then incubated for 30 min at RT with Alexa-fluorophore-conjugated secondary antibodies in staining solution. Coverslips were mounted using Fluoromount G (Southern Biotech), and confocal images were acquired using Carl Zeiss 710 Confocal Laser Scanning Microscope with a Plan Apochromat 63×/1.4 NA oil immersion objective and high-resolution microscopy monochrome cooled camera AxioCamMRm Rev. 3 FireWire (D) (1.4 megapixels, pixel size 6.45 µm × 6.45 µm). ZEN 2012 v. 8.0.1.273 (ZEISS) software was used for image acquisition. All images were captured

to ensure that little or no pixel saturation was observed. The representative confocal images presented in figures were processed and adjusted for brightness and contrast using Fiji software (Schindelin et al., 2012) or Adobe Photoshop CS.

To minimize the fluorescent signal from the cytosolic pool of overexpressed protein, the cells were permeabilized for 5 min on ice with 0.05% saponin in PHEM buffer before fixation step as described (Hong et al., 2017; Joseph et al., 2002; Pedersen et al., 2020).

To label lysosomes with Lysotracker or SiR-Lysosome probes, uptake was done as per the manufacturer's instructions. Briefly, cells were incubated in phenol red-free complete DMEM media (Gibco) containing SiR-Lysosome (1 µM) or Lysotracker Deep Red (100 nM) for 1 h at 37°C in a cell culture incubator. Cells were washed three times with 1X PBS to remove excess probe followed by fixation with 4% PFA (Paraformaldehyde) in PHEM buffer as described above.

For live-cell imaging experiments, cells were seeded on glass-bottom tissue culture treated cell imaging dish (Eppendorf). For vesicle tracking experiments, cells were incubated in phenol red-free complete DMEM media containing Lysotracker (LTR DND-99; 100 nM) for 10 min at 37°C in a cell culture incubator. Live-cell imaging was performed using Zeiss LSM 710 confocal microscope equipped with an environmental chamber set at 37°C and 5% CO_2.

Structured illumination microscopy (SIM)

For SIM imaging, cells were processed, fixed and stained as described previously. SIM images were captured with Zeiss ELYRA 7 (Lattice SIM Technology) using either Plan Apo 40×/1.40 oil or Plan Apo 63×/1.40 oil objective and sCMOS camera (PCO Edge). A lattice pattern structured samples and 15 phases shifted raw images were acquired for every Z plane with a slice size of 110 nm. The complete system control, imaging and processing of raw image files to final super-resolution images were done using the SIM module of the Zen Black v. 3.0 SR (Zeiss) software (Carl Zeiss MicroImaging).

Image analysis and quantification

Analysis of lysosome distribution: To quantify the distribution of lysosomes based on LAMP1/Lysotracker/SiR-Lysosome signal intensity, Fiji software was used. A boundary was drawn along the periphery of each selected cell using the “freehand”

selection tool. With the "clear outside" function of Fiji software, removed LAMP1 signals from nearby cells. Next, an ROI was drawn around the nucleus (using DAPI fluorescence signal), and LAMP1 signal intensity was measured for that section. The same ROI was then incremented by 5 µm till the cell periphery, and LAMP1 intensity was measured for each incremented ROI. Finally, LAMP1 intensity was calculated for perinuclear (0-5 µm; by subtracting the intensity of 1st ROI from 2nd) and periphery (>15 µm; by subtracting the intensity of 4th ROI from total cell intensity) region of cell as shown in **Figure 12d**. LAMP1 distribution was plotted by dividing each section's intensity (perinuclear and periphery) with whole-cell LAMP1 intensity. The same methodology was employed for quantifying mitochondria distribution (based on TOM-20 signal intensity) from images presented in **Figures 12r-u**.

The analysis of lysosome distribution was also performed by measuring the fractional distance of lysosomes from the cell center using the "plot profile" tool of Fiji software as described previously (Guardia et al., 2016; M. L. M. Jongsma et al., 2016). Briefly, in a confocal micrograph, a line was drawn from the center of the nucleus to the periphery of the cell. Next, using the "plot profile" tool, all the lysosomal marker fluorescent intensities and their corresponding distance values along the line were extracted. After determining the signal threshold, background pixels and their corresponding distances were excluded from the analysis. All the remaining distances (corresponding to the lysosomes pixels only) were converted to fractional distance by dividing all the values by the total distance of the line as shown in **Figure 12f**. The same methodology was employed for quantifying mitochondria distribution (based on TOM-20 signal intensity) from images presented in **Figures 12r-u**.

Analysis of LAMP1 and Lysotracker-positive vesicles: To measure the area and number of LAMP1-positive vesicles from SIM images, Z stacks of each micrograph was converted to 8-bit "Max Intensity Projection" using Fiji software. Using the "Analyze Particle" tool with the "Otsu" threshold was used for calculating the area and number. For TEM micrographs, the diameter of individual lysosomes was measured manually by drawing a straight line across the lysosome using the "Line" tool in Fiji software. For analyzing Lysotracker intensity from confocal micrographs, Fiji software was used.

Surface area analysis: The surface area of cells was quantified manually by drawing the periphery of the cell (using Phalloidin staining) using the "freehand" and "Measure Function" tools in Fiji software.

Colocalization analysis: For all the colocalization analysis, the JACoP plugin of Fiji software was used to determine Pearson's correlation coefficient and Mander's overlap.

Single-particle tracking

To perform a single-particle tracking analysis of lysosomes, cells were incubated with Lysotracker 100 nM (LTR DND-99) for 10 min at 37°C in phenol red-free complete DMEM media. Time-lapse confocal imaging was done as discussed above. To measure mobile fraction and the average speed of lysosomes from time-lapsed images, the "TrackMate" plugin (Tinevez et al., 2017) of Fiji software was used with the following parameters:

- Vesicle diameter, 1 µm

- Detector, DoG

- Initial thresholding, none

- Tracker, Simple LAP tracker

- Linking max distance, 2 µm

- Gap-closing max distance, 2 µm

- Gap-closing max frame gap, 2

- Filters, none

Data were exported to Microsoft Excel spreadsheet (2013) for further analysis.

Cell lysates, co-immunoprecipitation and immunoblotting

For preparing lysates, cells were lysed in ice-cold RIPA lysis buffer (10 mM Tris-Cl (pH 8.0), 1 mM EDTA, 0.5 mM EGTA, 1% Triton X-100, 0.1% SDS, 0.1% sodium deoxycholate, 140 mM NaCl supplemented with phosphostop (Roche) and protease inhibitor cocktail (Sigma-Aldrich)). The samples were incubated on ice for 2 min followed by vortexing for 30 sec, and this cycle was repeated a minimum of five times and subjected to centrifugation at 16,627×g for 10 min 4°C. The clear supernatants were collected, and protein amounts were quantified using the BCA kit (Sigma-Aldrich).

To perform co-immunoprecipitation, cells were lysed in ice-cold TAP lysis buffer (20 mM Tris pH 8.0, 150 mM NaCl, 0.5% NP-40, 1 mM $MgCl_2$, 1 mM Na_3VO_4, 1 mM

NaF, 1 mM PMSF and protease inhibitor cocktail). The lysates were incubated with indicated antibody conjugated-agarose beads at 4°C rotation for 3 h, followed by four washes with TAP wash buffer (20 mM Tris pH 8.0, 150 mM NaCl, 0.1% NP-40, 1 mM $MgCl_2$, 1 mM Na_3VO_4, 1 mM NaF and 1 mM PMSF). The samples were loaded on SDS-PAGE for further analysis.

For immunoblotting, protein samples separated on SDS-PAGE were transferred onto PVDF membranes (Bio-Rad). Membranes were blocked overnight at 4°C in blocking solution (10% skim milk in 0.05% PBS-Tween 20). Indicated primary and secondary antibodies were prepared in 0.05% PBS-Tween 20. The membranes were washed for 10 min thrice with 0.05% PBS-Tween20 or 0.3% PBS-Tween 20 after 2 h incubation with primary antibody and 1 h incubation with secondary antibody. The blots were developed using a chemiluminescence-based method (Thermo Scientific) using X-ray films (Carestream). To perform densitometry analysis of immunoblots, Fiji software was used as described (Kumar et al., 2018).

Recombinant protein purification, GST-pulldown assay and Mass spectrometry analysis

All the recombinant proteins used in this study were expressed and purified in the *E. coli* BL21 strain (Invitrogen). A single transformed colony was inoculated in Luria–Bertani broth containing plasmid vector antibiotic and incubated at 37°C in a shaking incubator for setting-up primary cultures. Following 8-12 h of culturing, 1% of primary inoculum was used to set up secondary cultures and subjected to incubation at 37°C with shaking until absorbance of 0.6 at 600 nm was reached. For induction of protein expression, 0.3 mM IPTG (Sigma-Aldrich) was added to the cultures, followed by incubation for 16 h at 16°C with shaking. Post-induction period, bacterial cultures were centrifuged at 3542×g for 10 min, washed once with 1XPBS, and resuspended in lysis buffer (20 mM Tris and 150 mM NaCl, pH 7.4) containing protease inhibitor tablet (Roche) and 1 mM PMSF (Sigma-Aldrich). Bacterial cells were lysed by sonication, followed by centrifugation at 15,557×g for 30 min at 4°C. The clear supernatants were incubated with glutathione resin (Gbiosciences) to allow binding of GST-tagged proteins or His60 Ni Superflow resin (Takara) for binding of His-tagged proteins on rotation for 1-2 h at 4°C The beads were washed a minimum of six times with wash buffer (20 mM Tris, 300 mM NaCl, pH 7.4) to remove impurities.

For semi-purified preparation of FLAG-tagged-JIP4 from mammalian cells, HEK293T cells transfected with FLAG-JIP4 expressing construct were lysed in NP-40 buffer (30 mM HEPES pH 7.4, 50 mM Potassium acetate, 2 mM Magnesium acetate, 1 mM EGTA, 10% Glycerol, 5 mM DTT, 0.1% NP-40, 1 mM PMSF, protease inhibitor cocktail) by performing three rounds of the freeze-thaw cycle. To carry out this step, cells were incubated on dry ice for 10 min and then transferred to ice-cold water for 10 min. The cell lysate was centrifuged at 20,000×g for 20 min at 4˚C, and the cleared lysate was incubated with anti-FLAG antibody-conjugated-agarose beads (Biolegend) for 3 h at 4˚C on rotation. Beads were washed three times with lysis buffer by incubating for 5 min at 4˚C on rotation. FLAG-JIP4 was eluted from the beads using a FLAG-peptide (Sigma-Aldrich) at a final concentration of 340 µM in lysis buffer.

For GST-pulldown assay using mammalian cells as a source of lysates, cells were lysed in ice-cold TAP lysis buffer (20 mM Tris (pH 8.0), 150 mM NaCl, 0.5% NP-40, 1 mM $MgCl_2$, 1 mM Na_3VO_4, 1 mM NaF, 1 mM PMSF, and protease inhibitor cocktail), followed by incubation in ice for 10 min and centrifuged at 16,627×g for 10 min. Lysates were collected and incubated with GST or GST-tagged proteins bound to glutathione resin at 4°C for 3-4 h with rotation. Following incubation, beads were washed a minimum of six times with TAP lysis buffer, and elution was done by boiling the samples in Laemmli buffer and subjected to SDS-PAGE for further analysis.

For GST-pulldown experiments using purified proteins, recombinant His-Arl8b, GST and GST-tagged proteins were quantified using BCA protein assay kit (Sigma-Aldrich). 5 µg of GST (as a control) and GST-tagged proteins were bound to glutathione beads for 3 h at 4˚C on rotation. The beads were blocked with 5% BSA for 2 h at 4˚C on rotation to prevent non-specific binding. The beads were washed with TAP lysis buffer (20 mM Tris (pH 8.0), 150 mM NaCl, 0.5% NP-40, 1 mM $MgCl_2$, 1 mM Na_3VO_4, 1 mM NaF, 1 mM PMSF, and protease inhibitor cocktail) minimum three times and incubated with 5 µg of His-Arl8b at 4°C for 1h with rotation. After binding, the beads were washed five times with TAP lysis buffer followed by elution in 4x Laemmli buffer and SDS-PAGE for further analysis. A similar protocol was followed for performing binding assay between semi-purified preparations of FLAG-JIP4 with GST and GST-RUFY3 proteins except for the use of NP-40 buffer in place of TAP lysis buffer.

To search for potential interacting partners of RUFY3, GST-pulldown assay followed by identification of proteins using mass spectrometry was done as described previously (Garg et al. 2011; Marwaha et al. 2017). Briefly, recombinant GST-RUFY3 and GST-only (as a control) proteins were used as bait proteins and incubated with lysates prepared from HEK293T cells as described above. The coomassie stained protein bands that were specifically present in the GST-RUFY3 sample lane (Sample A: ~250-280 kDa band; Sample B: ~200-250 kDa; Sample C: ~80 kDa and Sample D: ~16 kDa band) were cut out and submitted to Taplin Mass Spectrometry Facility (Harvard Medical School, Boston, USA) for protein identification. As a control, the whole GST-only sample lane was cut out to identify proteins that might be binding to GST protein only. RAW data are available via ProteomeXchange consortium with identifier PXD027010.

Yeast two-hybrid assay

Matchmaker Gold Yeast Two-Hybrid System (Clontech) was used as per the manufacturer's instructions for carrying out yeast two-hybrid screening. Briefly, human Arl8b cDNA cloned in GAL4-BD vector (pGBKT7) was used as bait. The bait plasmid transformed Y2HGold yeast strain was mated with Y187 strain transformed with human brain cDNA library. Small scale yeast two-hybrid assay was carried out as described previously (Sharma et al., 2021). Briefly, plasmids encoding GAL4-AD and GAL4-BD fusion encoding constructs were co-transformed in *Saccharomyces cerevisiae* Y2HGold strain (Clontech), streaked on plates lacking leucine and tryptophan (-Leu/-Trp) and allowed to grow at 30°C for three days. The co-transformants were replated on a non-selective medium (-Leu/-Trp) and selective medium (-Leu/-Trp/-His) to assess interaction. All the drop-out yeast media was purchased from Takara.

Lysosome immunoisolation

To immunopurify lysosomes, the “LysoIP” method was used with some modifications (Abu-Remaileh et al., 2017). HEK293T cells stably expressing TMEM192-FLAG (control) or TMEM192-HA were collected and resuspended in ice-cold KPBS (136 mM KCl, 10 mM KH_2PO_4, adjusted to pH 7.25 with KOH) buffer and homogenized using dounce homogenizer (~20 strokes). The homogenized cells were gently collected and centrifuged for 2 min at 1000×g. The supernatant obtained was incubated with anti-HA antibodies-conjugated-agarose beads (Sigma-Aldrich) at 4°C for 15 min. Beads were

gently washed thrice with KPBS, and bound lysosomes were eluted in Laemmli buffer and subjected to SDS-PAGE for further analysis.

Subcellular fractionation

To perform lysosome enrichment, subcellular fractionation was carried using the "Lysosome Enrichment Kit" (Thermo Scientific). Briefly, the cell pellet was resuspended in PBS and homogenized with a dounce homogenizer on ice (~20 strokes). To confirm cell lysis, microscopic examination of homogenate was done by adding 0.5% trypan blue dye. The homogenate was subjected to centrifugation at 500×g for 10 min at 4°C, and post-nuclear supernatant (PNS) was diluted in OptiPrep gradient media (Sigma-Aldrich) to a final concentration of 15% OptiPrep. The sample was then carefully overlayered on the top of a discontinuous density gradient (17%, 20%, 23%, 27%, 30%). The gradient was subjected to ultracentrifugation at 145,000×g in an SW60 Ti swinging bucket rotor (Beckman Coulter) for 4 h at 4°C. After the spin, eight fractions of 400 µl each were collected from top to bottom**.** The fractions were spun again at 18,000×g for 20 min in a SW41 Ti rotor at 4°C, and the resulting pellet was suspended in 4X SDS-sample buffer, boiled for 10 min and analyzed by SDS-PAGE and immunoblotting.

Measurement of lysosome pH

To measure the lysosome's pH, Lysosensor Yellow/Blue DND-160 was used as described previously (Ma et al., 2017). Briefly, cells were trypsinized and incubated with 2 µM Lysosensor Yellow/Blue DND-160 (Invitrogen) for 3 min at 37°C in phenol red-free complete DMEM media. Cells were rinsed twice with 1XPBS to remove excess dye and incubated for 10 min in isotonic pH calibration buffers (143 mM KCl, 5 mM Glucose, 1 mM $MgCl_2$, 1 mM $CaCl_2$, 20 mM MES, 10 µM Nigericin and 5 µM Monensin) ranging from 4 to 6. Next, ~10,000 cells/well were distributed into a black 96-well plate (Thermo Scientific), and fluorescence reading was recorded at 37°C using a 96-well plate multi-mode fluorescence reader (Tecan Infinite M-PLEX). Samples were excited at 340 nm and 380 nm wavelengths to detect emitted light at 440 nm and 540 nm, respectively. The pH calibration curve was generated by plotting the fluorescence intensity ratio of 340 nm to 380 nm against the respective pH value of buffers.

Flow cytometry

To quantify Lysotracker uptake, cells were incubated in phenol red-free complete DMEM media (Gibco) containing 100 nM Lysotracker Red (LTR-DND-99; Invitrogen) for 1 h at 37°C. Post-incubation period, media was removed, and cells were trypsinized, washed and resuspended in ice-cold 1XPBS and analyzed by flow cytometry. To measure the proteolytic activity of lysosome, cells were incubated in phenol red-free complete DMEM media (Gibco) containing 20 µg/mL BODIPY FL-BSA (BioVision) for 2 h at 37°C. Post-incubation period, media was removed, and cells were trypsinized, washed and resuspended in ice-cold 1XPBS and analyzed by flow cytometry. Sample acquisition was done with BD FACS Aria Fusion Cytometer using BD FACS Diva software version 8.0.1 (BD Biosciences). Data analysis was done using BD FlowJo version 10.0.1.

Dextran trafficking assay

Dextran delivery to lysosomes was performed as described with some minor modifications (Marwaha et al. 2017). Briefly, to label lysosome, control and RUFY3-silenced HeLa cells were incubated with Lysotracker Deep Red (100 nM) containing phenol red-free complete DMEM media for 10 min at 37°C. Cells were further incubated with dextran (Alexa-Fluor 488-conjugated-dextran; green) for 1 h and 2 h at 37°C. At the end of the incubation period, cells were washed with 1X PBS followed by fixation and mounting as described earlier. The coverslips were imaged immediately by confocal microscopy. The colocalization of dextran with Lysotracker-labeled lysosomes was assessed using the JACoP plugin of Fiji software.

LDL trafficking assay

For LDL trafficking assay, control and RUFY3-silenced HeLa cells seeded on live-cell imaging dishes were starved for 8 h in DMEM media containing 5% charcoal-stripped FBS (Gibco) (starvation media). The cells were then pulsed with BODIPY-FL LDL (7.5 µg/mL; Invitrogen) made in starvation media for 10 min. The cells were washed with 1XPBS and chased in phenol red-free complete media containing Lysotracker Red DND-99 (100 nM) to label lysosomes. Time-lapse confocal imaging was done at 0 min, 30 min, 60 min, and 120 min of the chase. The colocalization between LDL and Lysotracker at different time periods was measured using the JACoP plugin of Fiji software.

Autophagy flux assay

Autophagic flux was determined by checking for the rescue of LC3B-II degradation by treating HeLa cells with V-ATPase inhibitor Bafilomycin A1 (100 nM; Sigma-Aldrich) steady-state or with serum starvation in EBSS for 2 h. After treatment, cells were lysed using ice-cold RIPA buffer supplemented with protease inhibitor. An equal amount of lysates were loaded on SDS-PAGE, transferred to PVDF membrane and probed for LC3B-II and β-tubulin. Densitometry analysis of LC3B-II band intensity normalized to β-tubulin intensity was done using Fiji software.

Transmission electron microscopy (TEM)

Sample processing and TEM was performed at the Harvard Medical School EM Facility (Boston, USA). Briefly, HeLa cells transfected with control siRNA or RUFY3 siRNA were fixed in routine fixative (2.5% glutaraldehyde/1.25% paraformaldehyde in 0.1 M sodium cacodylate buffer, pH 7.4) for 1 h at RT and washed in 0.1 M sodium cacodylate buffer (pH 7.4). The cells were then postfixed for 30 min in 1% osmium tetroxide/1.5% potassium ferrocyanide, washed with water three times, and incubated in 1% aqueous uranyl acetate for 30 min, followed by two washes in water and subsequent dehydration in grades of alcohol (5 min each: 50, 70, 95, 2×100%). Cells were removed from the dish in propylene oxide, pelleted at 1741×g for 3 min, and infiltrated overnight in a 1:1 mixture of propylene oxide and TAAB Epon (Marivac Canada). The samples were subsequently embedded in TAAB Epon and polymerized at 60°C for 48 h. The ultrathin sections were cut on a Reichert Ultracut-S microtome, picked up onto copper grids stained with lead citrate, and examined in a JEOL 1200EX transmission electron microscope having an AMT 2k charge-coupled device camera.

Statistics and reproducibility

Graphs represent mean ± S.D. and p values were calculated using two-tailed Student's t-test (GraphPad Prism 8.0). Differences between groups were considered statistically significant for p values <0.05. All experimental data shown in this report, including immunofluorescence micrographs, were analyzed from at least three independent experiments or at least 8 cells.

Chapter 3

Regulation of osteoclast function by the small GTPase Arl8b

Chapter 3

Regulation of osteoclast function by the small GTPase Arl8b

Abstract

Recent studies have established Arl8b-mediated positioning of lysosomes and lysosome-related organelles as a crucial factor regulating amino acid sensing, cell migration and metastasis, NK cell-mediated cytotoxicity, and antigen presentation. Arl8b mediates lysosomal transport to the cell periphery by recruiting its effector, SKIP, which in turn recruits the motor protein kinesin-1 to lysosomes. Arl8b also binds to the Rab7 effector-PLEKHM1, and this interaction repositions Arl8b-positive lysosomes to the perinuclear region of the cell and promotes autophagosomes-lysosome fusion. Interestingly, frameshift mutations in PLEKHM1 result in osteopetrosis, where the bone-resorbing functions of osteoclasts are impaired. Osteoclasts resorb bone by secreting their lysosomal contents within the confines of a sealing zone between themselves and the bone surface. Here, we have explored the role of Arl8b in bone remodeling and identified a novel effector of Arl8b that is specifically expressed in osteoclasts. We found that Arl8b showed a striking localization beneath the actin rings and ruffled borders in osteoclasts, and significantly impaired lysosome secretion in Arl8b-deficient osteoclasts. Furthermore, unlike wild-type osteoclasts, lysosomes in Arl8b-deficient osteoclasts did not localize beneath actin rings or in the ruffled borders. Furthermore, we identified a novel Arl8b effector, RUN and FYVE domain-containing protein family member 4 (RUFY4), which is specifically expressed in osteoclasts upon RANKL-stimulation and localizes to peripheral lysosomes in the osteoclasts. Interestingly, we found that RUFY4 interacts with LC3 and acts as a linker between the LC3-marked ruffle border and Arl8b-positive lysosomes, further promoting the fusion of lysosomes to the ruffle border, an important process necessary for lysosome secretion and bone resorption. Upon RUFY4 silencing in osteoclasts, the peripheral positioning of lysosomes in the vicinity of actin rings was reduced, resulting in a substantial decrease in TRAP activity and the resorption ability of osteoclasts. Taken together, our findings establish the role of the Arl8b-RUFY4 complex as a crucial component of osteoclast-mediated bone remodeling.

Introduction

Bone is a dense, rigid, and calcified tissue that makes up the bulk of the vertebral skeleton. While bone is often thought of as a stable, hard, and static structure that supports and protects essential organs, it is really a highly specialized and continually changing tissue in our bodies (Teitelbaum, 2000, 2007). Bone remodeling, defined as the process of replacing old or damaged bone with new bone in response to various stimuli, is a coordinated interplay required for overall bone and mineral homeostasis. The coordinated work of osteoclasts and osteoblasts, two kinds of bone cells, is essential to maintain the balance between bone resorption and bone formation. Impaired coordination may lead to the development of conditions such as osteoporosis or osteopetrosis (Crockett *et al.*, 2011).

Osteoclasts are multinucleated cells that, when attached to bone, form a highly convoluted and unique structure from their plasma membrane known as the ruffle border, which is indispensable for the bone resorption activity of osteoclasts. However, the ruffle border varies from the plasma membrane owing to the presence of proteins that are normally found on lysosomal membranes rather than plasma membranes, such as the chloride channel CLC-7 and proton pump V-ATPase subunits (Lacombe, Karsenty and Ferron, 2013; Matsumoto *et al.*, 2018). Notably, these proteins are essential for the maintenance of an optimum acidic pH in the lumen of lysosomes, which is required for the activity of several hydrolases present in lysosomes (Ballabio and Bonifacino, 2020). Likewise, in order to resorb bone, osteoclasts also need an acidic environment and active proteases in the resorption lacuna. Moreover, several studies have shown that the trafficking of lysosomes towards the sealing zone followed by fusion with the ruffle border is essential for the secretion of proteases and thus bone resorption (Coxon and Taylor, 2008; Sun, 2009).

In functionally-active osteoclasts, Rab7, a small GTPase found on late endosomes and lysosomes, is localized on the ruffle border, and silencing of Rab7 in these cells has been demonstrated to inhibit the formation of acting rings and the ruffle border, as well as significantly reduce their bone resorption activity (Zhao *et al.*, 2001; Zhao, Ettala and Väänänen, 2002; Roy and Roux, 2020). Subsequent studies have shown that

PLEKHM1, a known effector of Rab7, couples Rab7 positive lysosomes to the microtubules through its interaction with FAM98A and NDEL1 (Ye *et al.*, 2011; Fujiwara *et al.*, 2016). Moreover, studies have shown that osteoclasts from PLEKHM1-KO mice, as well as osteoclasts from individuals with PLEKHM1 loss-of-function mutations, have lower resorption activity, due to the absence of a ruffled border in these cells (Van Wesenbeeck, Odgren, *et al.*, 2007).

Interestingly, various studies have revealed the role of autophagy-related proteins in the differentiation and activation of osteoclasts. In particular, mice deficient of ATG5, ATG4b, and ATG7 genes were shown to have non-resorbing osteoclasts due to impaired in lysosome fusion to the ruffle border and therefore secretion of cathepsin K (Gelman and Elazar, 2011). Moreover, it has been shown that LC3B-II is localized on the ruffle border and that its recruitment is essential for the formation of the ruffle border and bone resorption. Expectedly, cells lacking LC3 lipidated machinery were unable to form the ruffle border and perform bone resorption. (Deselm *et al.*, no date; Chung *et al.*, 2012; Ohmae *et al.*, 2017). However, how LC3II reaches the ruffle border is still an interesting question to answer. Furthermore, despite the fact that several vesicular trafficking proteins have a role in osteoclast biology, there is not much known about the pathways by which the lysosome traffics to the ruffle border. In addition, the molecular machinery that facilitates for lysosomes to fuse with the ruffle border is not well known.

In our previous work, we have shown that Rab7 effector PLEKHM1 also interacts with a lysosome specific small G-protein, Arl8b, and functions as a linker to facilitate fusion of lysosomes with autophagosomes and late endosomes (Marwaha *et al.*, 2017). Arl8b also links kinesin-1 to the lysosome either directly or through its effector protein, SKIP/PLEKHM2, and thereby governs their anterograde movement in cells (Udia, Ferreira, and Munro, 2011). Furthermore, Arl8b-mediated lysosome positioning has been shown to regulate lysosome engagement with processes occurring at the cell periphery, such as growth factor-mediated activation of mTORC1, lysosome exocytosis, lysosome-mediated ER remodeling, focal adhesion disassembly, natural killer cell–mediated cytotoxicity, and antigen presentation. (Mcmichael, Cheney and Lee, 2010; Garg et al., 2011; Korolchuk et al., 2011a; Tuli et al., 2013; Guardia et al.,

2016; Michelet et al., 2018; Rui Jia and Bonifacino, 2019; Lu et al., 2020). Despite the role of Arl8b in lysosome motility as well as in membrane fusion, it has not yet been established whether Arl8b and its effectors have any role in bone remodeling and skeletal homeostasis.

Herein, we report the function of Arl8b in osteoclast biology and bone remodeling. When examined in osteoclasts, Arl8b was shown to be prominently localized to the lysosomes present near the actin rings. Moreover, in contrast to control osteoclasts, lysosomes in Arl8b-deficient osteoclasts failed to localize near the actin rings, indicating a defect in the mobility and positioning of lysosomes. Accordingly, lysosome secretion was found to be severely impaired in Arl8b-deficient osteoclasts. Interestingly, we found a new Arl8b effector, RUN and FYVE domain containing protein 4 (RUFY4), which, like SKIP and PLEKHM1, interacts with Arl8b through its RUN domain. However, unlike SKIP and RUFY4, it is specifically expressed in osteoclasts upon RANKL stimulation. According to our findings, RUFY4 depletion had no effect on osteoclast differentiation or osteoclastogenesis. Notably, RUFY4 was localized to the peripheral lysosome of osteoclasts near the actin ring. Upon RUFY4 silencing in osteoclasts, the peripheral positioning of lysosomes near actin rings was significantly reduced, resulting in a considerable reduction in TRAP activity and osteoclast resorption ability. Moreover, we found that RUFY4 interacts with LC3 and functions as a linker between the LC3-marked ruffle border and Arl8b positive lysosomes, promoting lysosome fusion to the ruffle border, a critical process for lysosome secretion and bone resorption. The findings of this study together established the involvement of the Arl8b-RUFY4 complex in bone remodeling.

Results

A) Arl8b regulates lysosome positioning and distribution in osteoclasts

Arl8b, among the other Arl GTPases, is the best studied so far and is known to be present specifically on the lysosomes (Hofmann, 2006; Garg et al., 2011; Kaniuk et al., 2011; Udia, Ferreira and Munro, 2011; Tuli et al., 2013). Arl8b-mediated lysosome positioning regulates various cellular processes in different cell types (Pu et al., 2015; Hofmann and Munro 2006; Saric et al., 2015; Marwaha et al., 2017).

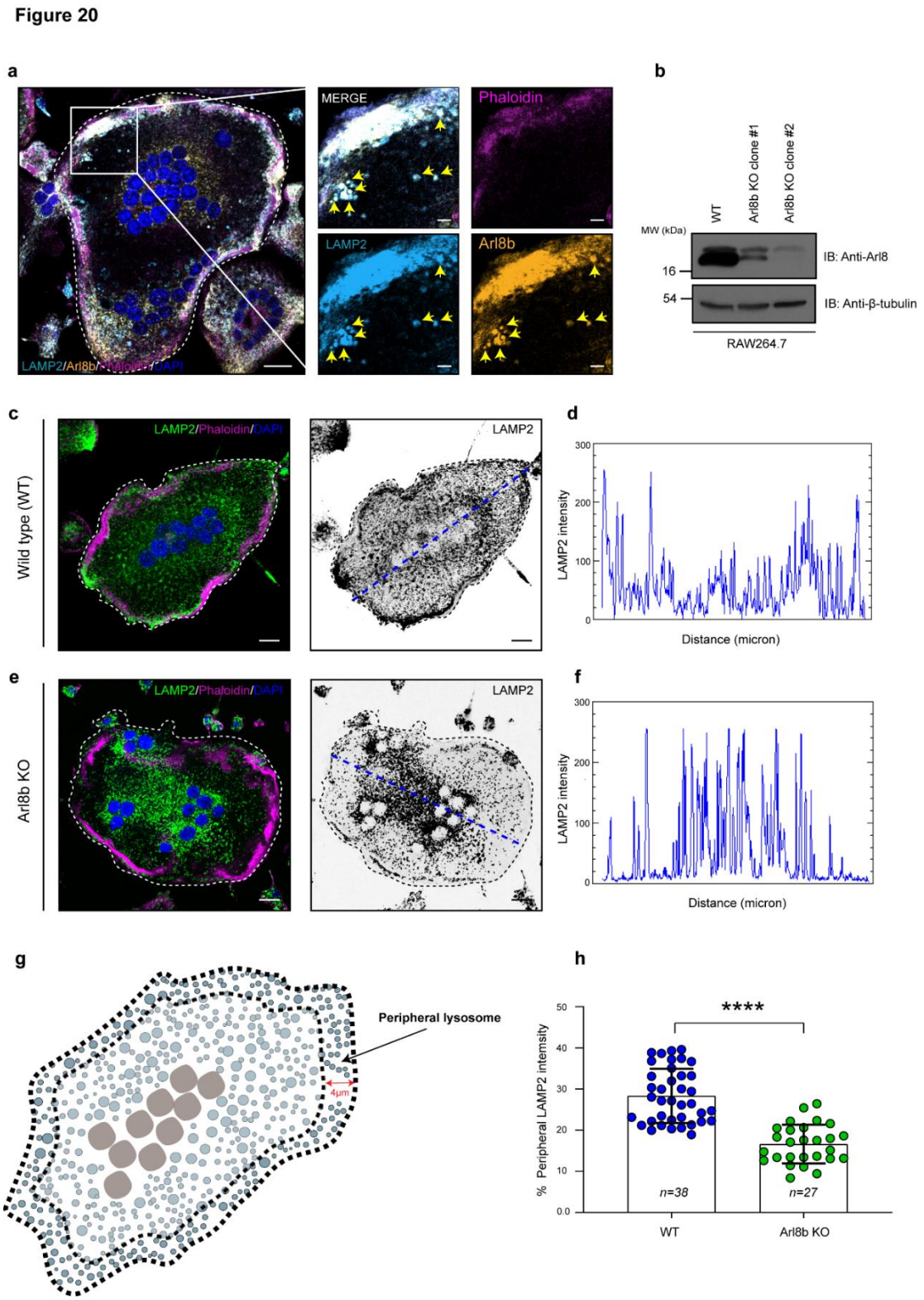

Figure 20: Arl8b silencing disrupts the lysosomes distribution in osteoclasts.

(a) Representative confocal micrographs showing immunostaining of Arl8b and Lamp2 in osteoclasts cultured on glass coverslips. DAPI staining was used to visualize nuclei, and actin was stained using phalloidin. The cell boundary is marked with a white line and yellow arrowheads in the insets, indicating the co-localized pixels of Arl8b and Lamp2. Scale Bars: 10

µm (main); 5 µm (inset). **(b)** Immunoblot of wild-type (WT) and two clones of Arl8b knockout (KO) RAW264.7 cells demonstrating Arl8b knockout efficiency. The blot was also probed for β-tubulin to confirm an equal amount of protein loading. **(c-f)** Confocal micrographs showing immunostaining of LAMP2 in wild-type (WT) and Arl8b knockout (KO) osteoclasts cultured on glass coverslips. LAMP2 signals are also shown in inverted gray scale for better visualization. The graphs in d and f depict the intensity profile of the LAMP2 vesicles under the blue color line drawn in each image. **(g)** A schematic depicting the quantification method employed for analyzing the proportion of LAMP2-positive lysosomes inside a 4 µm wide shell taken from the cell's periphery in osteoclasts. **(h)** Quantification of the fraction of peripheral lysosomes in WT and Arl8b KO cells from the experiments shown in c and d. The values plotted are the mean ± S.D. from two independent experiments. The total number of cells analyzed is indicated on the graph (****$p<0.0001$; two-tailed Student's t-test). Scale bars: 10 µm (main); 2 µm (inset).

However, there are no reports so far about the localization and function of Arl8b in osteoclasts. Therefore, in order to evaluate the localization of Arl8b in osteoclasts, differentiated mature osteoclasts were stained with anti-Arl8b and anti-LAMP2 antibodies. Arl8b was found on peripheral lysosomes, and as expected colocalized intimately with LAMP2-marked lysosomes (see insets in **Figure 20a**). Next, to assess the role of Arl8b in lysosome positioning in osteoclasts, we knocked out Arl8b from RAW264.7 cells using CRISPR/Cas9 tool and validated the KO in two chosen clones (1 and 2) using Western blot **(Figure 20b**). Based on the efficiency of KO, we employed Arl8b KO clone # 2 for further experiments. To analyse lysosome distribution, the wild-type (WT) and Arl8b KO cells were differentiated into osteoclasts and immunostained for lysosomes (using an anti-LAMP2 antibody), and phalloidin was used to label the actin ring. The Arl8b deletion resulted in a significant change in the distribution of LAMP2-positive lysosomes in osteoclasts, with substantially fewer lysosomes located near the actin ring as compared to WT osteoclasts (**Figures 20c-f**). This impact of Arl8b KO on lysosome distribution in osteoclasts was also quantified in multiple cells by calculating the proportion of LAMP2-positive lysosomes inside a 4 µm wide shell taken from the cell periphery (**Figures 20G and 20H**). These results clearly suggest that Arl8b is essential for the peripheral positioning of the lysosome in osteoclasts.

B) Arl8b regulates bone resorption activity of osteoclasts

To resorb bone, lysosomes in the osteoclasts fuse with the ruffle border (RB) and secrete their luminal content, which includes several proteases such as cathepsin K and Tartrate-resistant acid phosphatase (TRAP). Cathepsin K is an osteoclast-specific

cysteine protease that has been demonstrated to be essential in bone resorption by degrading bone matrix proteins such as collagen (Dai et al., 2020). The acidic environment, together with the action of these enzymes, eventually results in the creation of cavities in the bone known as resorption lacunae (RL) or bone pits (**Figure 21a**). After confirming the role of Arl8b in lysosome positioning in osteoclasts and knowing the importance of the lysosome for ruffle border formation and bone resorption activity of these cells, we decided to investigate the role of Arl8b in osteoclastic bone resorption activity using a variety of methods as illustrated in the **figure 21b**. We cultured osteoclasts on three distinct surfaces to test their bone resorption activity: plastic, Osteo assay surface, and dentine discs. The supernatant (media) from cultured cells was utilized to evaluate the amounts of secreted enzymes cathepsin K and TRAP, as well as degraded collagen products such as CTx-1 (in the case of dentines surface only), which indicate the bone resorption activity of osteoclasts either directly or indirectly (Sørensen et al., 2007; Ye et al., 2011). TRAP staining, immunostaining, and Western blotting were performed on cultures grown on glass or plastic surfaces. Osteo assay surface (calcium-phosphate coated plates) and dentine discs were used to culture osteoclast to measure resorbed area and pit volumes generated by the secretory action of these cells (**Figure 21b**).

To assess the role of Arl8b in osteoclast differentiation, TRAP staining was performed on WT and Arl8b KO cells (**Figure 21c**). The multinucleated TRAP-positive osteoclasts were quantified, and it did not show any significant difference in the number of these cells (**Figure 21d**). After ruling out the involvement of Arl8b in osteoclast differentiation, we assessed the TRAP activity in the culture supernatant of these cells, and interestingly, we found that Arl8b KO osteoclasts had ~30% less activity than control (WT) osteoclasts (**Figure 21e**). As mentioned above, cathepsin K is an important player in the resorption activity of osteoclasts. Therefore, we analyzed the levels of cathepsin K in whole cell lysates and culture supernatants by western blotting. Similar to TRAP activity, cathepsin K levels in the culture supernatants of Arl8b KO osteoclasts were considerably lower as compared to control (WT) osteoclasts. (**Figure 21f**). To further confirm the effect of Arl8b depletion on bone resorption activity, both WT and Arl8b KO osteoclasts were cultured on bone-like surfaces; Osteo assay surface plates and dentine discs. Osteoclasts cultured on the Osteo assay surface plates were removed and area resorbed was quantified.

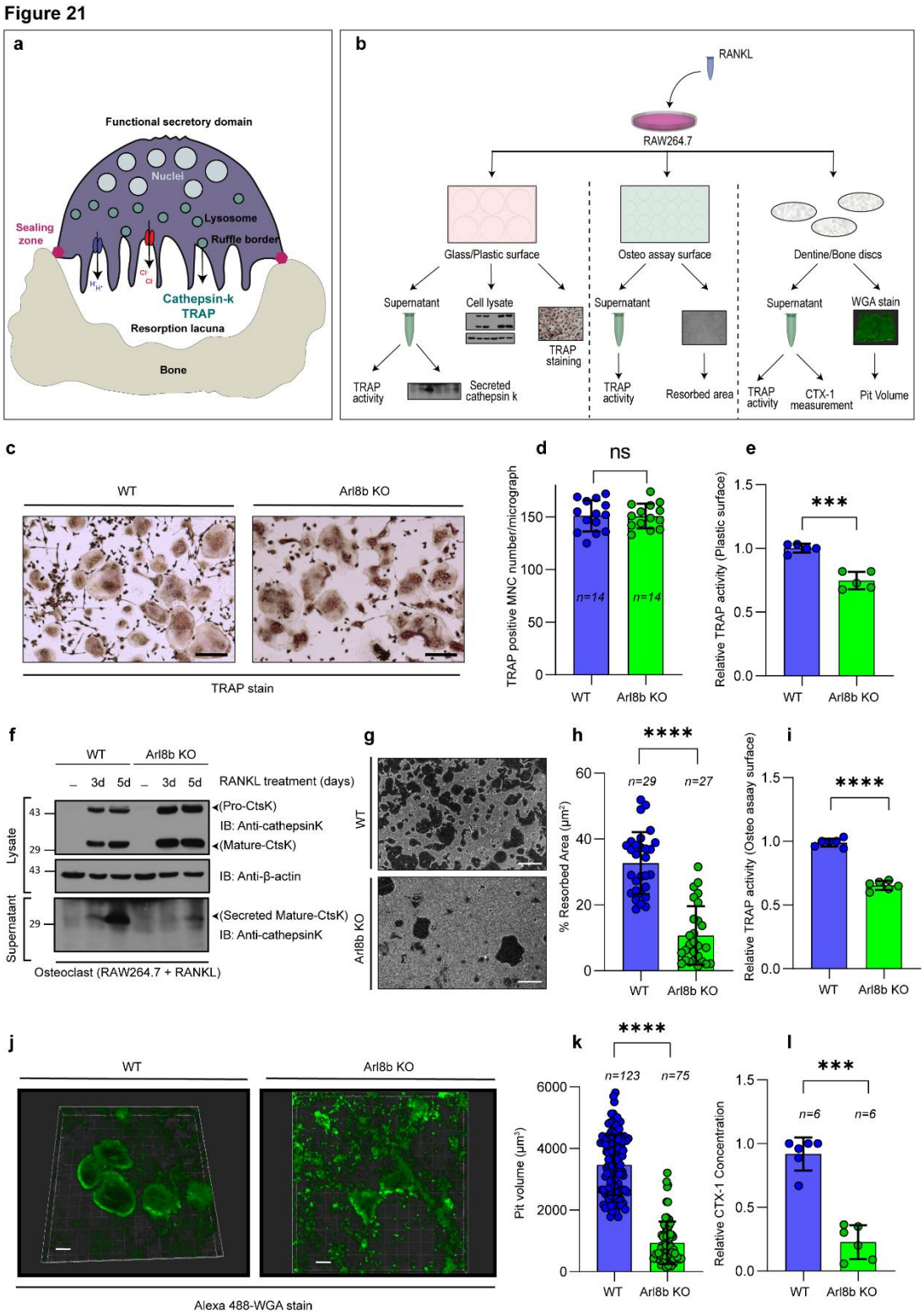

Figure 21: Arl8b is required for bone resorption activity by osteoclasts.

(a) Illustration of a typical active bone resorbing osteoclast**.** Upon adhesion to bone, osteoclasts become polarized, forming a unique structure, termed the ruffled border (RB), and composed of plasma membrane protrusions directed at the target-bone surface. Lysosomes fuse with the RB and secrete protons and proteases, leading to the formation of cavities in the bone. **(b)** A graphical representation of the methodology used in this study to assess the effects of various treatments on bone resorption activity of osteoclasts. **(c-e)** On a 24-well plate, WT and Arl8b

KO osteoclasts were cultured, fixed, and stained for TRAP; Scale bar: 500 µm. The number of TRAP positive multinucleated cells (> 3 nuclei) was quantified (d), and the culture supernatant from these cells was also collected to measure TRAP activity (e). **(f)** The culture supernatant and lysates from WT and Arl8b KO cells cultured on plastic surfaces was subjected to western blot analysis for the presence of cathepsin K. **(g-i)** WT and Arl8b KO osteoclasts was grown on 24-well Osteo Assay plates. To quantify the resorbed area, cells were removed from the surface, followed by the imaging of the wells. The representative processed micrographs are shown (black = resorbed area) in g; Scale bar: 200 µm. The percentage of resorbed area over the total area of the micrograph is plotted in h. The TRAP activity measured from the culture supernatant of Osteo Assay experiments is shown in i. **(j-k)** Representative images of resorbed pits formed by WT and Arl8b KO osteoclasts cultured on dentine disc. The resorption pits were labeled with Alexafluor 488-conjugated wheat germ agglutinin (WGA) after removing the cells from the dentine surface. The pit volume of the resorbed dentine was measured by Imaris software and quantification is shown in k. Scale bar: 10 µm. **(l)** Concentration of CTx-1 in cell culture supernatant of WT- and Arl8b KO-osteoclast was determined and plotted. Values plotted are the mean ± S.D. from two independent experiments. The total number of micrographs (for c and g), pits (for k) and dentine (for l) analyzed is indicated on the graph (****p<0.0001; ***p<0.001; ns, not significant; two-tailed Student's *t*-test).

Area resorbed by Arl8b KO osteoclasts was approximately 50% smaller as compared to WT cells (**Figures 21g-i**). Consistent with this, the volume of pits excavated by Arl8b KO osteoclasts was ~2.5-3 fold smaller than WT cells (**Figures 21j and 21k**). This inhibition of resorption activity in Arl8b KO osteoclasts was supported by the reduced level of CTx-1, a bone resorption marker, (Deselm et al., 2011; Watts, 1999), in the culture supernatant of osteoclasts (**Figure 21l**), suggesting that Arl8b-mediated lysosome positioning is important for bone resorption activity.

C) RUFY4 is an osteoclast specific effector of Arl8b

Next, we employed a GST-Pull down coupled mass spectrometry approach to identify Arl8b osteoclast-specific effectors that may be involved in the bone resorption activity of osteoclasts. To this end, osteoclasts differentiated from RAW264.7 macrophages were lysed and incubated with GST and GST-Arl8b as a bait protein followed by mass spectrometry. Interestingly, in GST-Arl8b eluate we found peptides corresponding to RUN and FYVE domain containing proteins. The RUFY (RUN and FYVE domain containing) protein family consists of four members, all of which share a similar domain organization: an N-terminal RUN domain, a C-terminal FYVE domain, and one or more coiled-coil (CC) domains (**Figure 22a**) (Char & Pierre, 2020; Kitagishi & Matsuda, 2013). To validate our mass spectrometry results, we performed a yeast two-hybrid assay of Arl8b with all RUFY family members (**Figure 22b**). Interestingly,

among all the RUFY family members, only RUFY3 and RUFY4 showed interaction with Arl8b. The interaction of epitope-tagged RUFY4 with Arl8b was further confirmed using a co-immunoprecipitation assay by expressing epitope-tagged RUFY4 and Arl8b in HEK293T cells (**Figure 22c**). In addition to this, our recent work has shown that RUFY3 is an effector of Arl8b and further links Arl8b and the JIP4-Dynein complex to regulate lysosome size and positioning (Kumar et al., 2022).

Next, we examined the mRNA levels of all the RUFY family members in untreated and RANKL-treated RAW264.7 cells using qRT-PCR. Surprisingly, we found that the mRNA levels of *Rufy4* were increased significantly in RANKL-treated RAW264.7 cells as compared to untreated cells, whereas there was no significant difference in the mRNA level of other RUFY family members (*Rufy1*, *Rufy2*, and *Rufy3*) upon RANKL treatment (**Figure 22d**). Consistent with this, when BMDMs (bone marrow-derived macrophages) were treated with RANKL, the levels of *Rufy4* mRNA were significantly increased. We also observed similar RANKL-inducible expression of RUFY4 at the protein level in RAW264.7 cells (**Figures 22e** and **22f**).

Using yeast two-hybrid and co-immunoprecipitation approaches, we confirmed that RUFY4 interacted with the WT (wild-type) and Q75L (constitutively GTP-bound) forms of Arl8b, but not with the T34N (constitutively GDP-bound) form (**Figures 22g** and **22h**). Consistent with this, RUFY4 interaction with GST-tagged-Arl8b (as bait) was reduced in the presence of excess GDP as compared to GTP, suggesting that RUFY4 behaves as an effector for the small G protein (**Figure 22i**). To further corroborate these findings, we examined the intracellular localization of epitope tagged RUFY4 in HeLa cells. FLAG-tagged RUFY4 showed cytosolic and punctate distribution in the perinuclear region of the cells, where it colocalized with LAMP1-marked lysosomes. Following that, when RUFY4-FLAG was co-expressed with various forms of Arl8b; WT, Q75L, and T34N, RUFY4-FLAG became more punctate, membrane bound and less cytosolic, as expected in the presence of WT and Q75L forms of Arl8b. However, in the presence of the T34N form of Arl8b, both proteins remained mainly cytosolic, with only a few small punctate of RUFY4 in the cells (**Figures 22j-m**). We also observed the interaction of Arl8b and RUFY4 under endogenous conditions by direct immunoprecipitation of Arl8b from cell lysates of osteoclasts. These results show that RUFY4 is an osteoclast specific effector of Arl8b (**Figures 22n**).

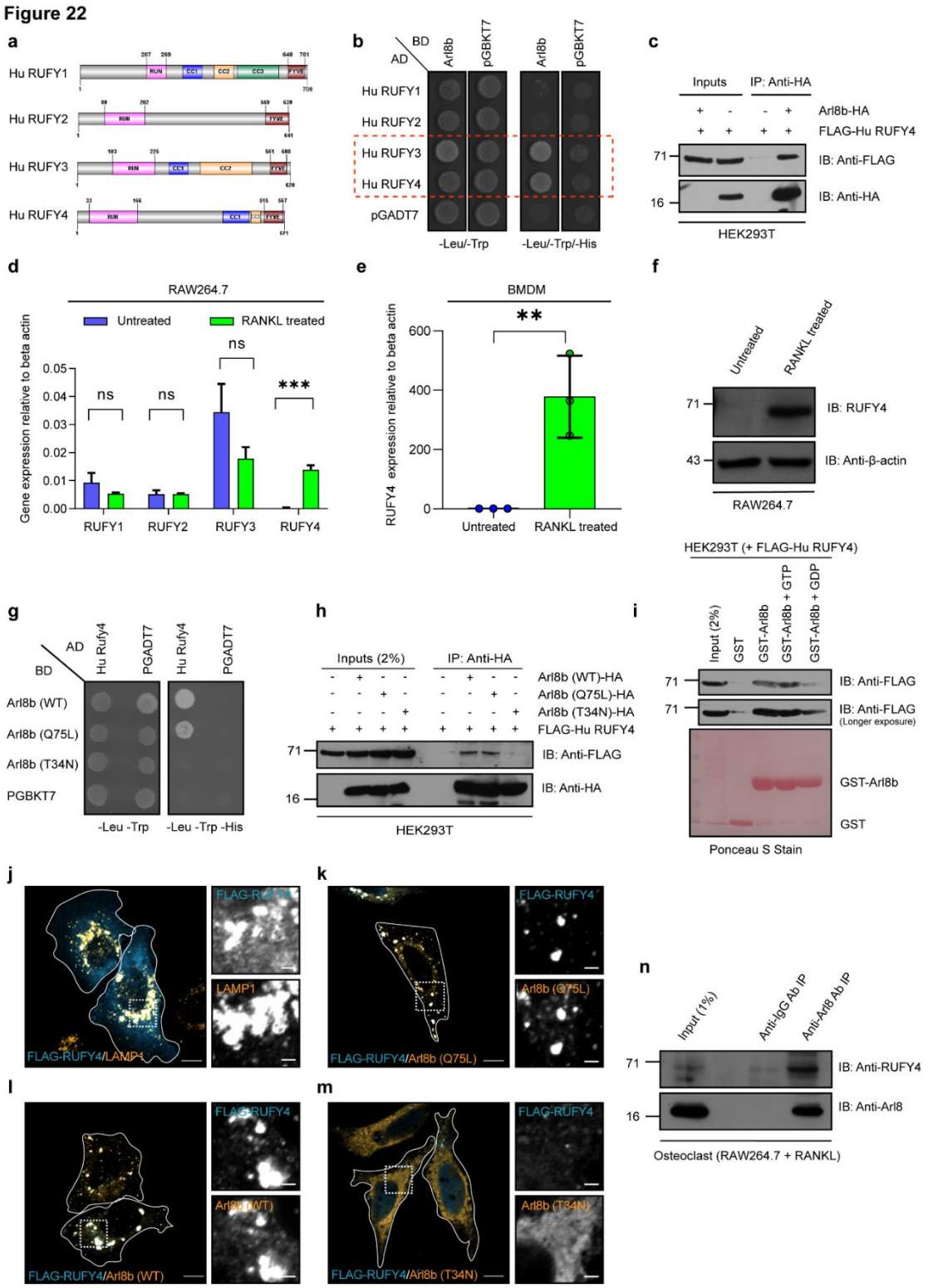

Figure 22: RUFY4 is a RANKL-inducible gene and an osteoclast-specific effector of Arl8b.

(a) Domain architecture of RUFY family members RUFY1, RUFY2, RUFY3, and RUFY4. **(b)** Yeast two-hybrid assay. Co-transformants were spotted on -Leu-Trp and -Leu-Trp-His media to confirm viability and interactions, respectively. AD, GAL4 activation domain; BD, GAL4-DNA binding domain **(c)** RUFY4-FLAG was co-transfected with Arl8b-HA into

HEK293T cells; lysates were immunoprecipitated (IP) with anti-HA antibody resin and immunoblotted (IB) with the indicated antibodies. **(d)** qRT-PCR analyses of the mRNA levels of *Rufy1, Rufy2, Rufy3, and Rufy4* in untreated and RANKL-treated RAW264.7 cells. **(e)** qRT-PCR analyses of *Rufy4* mRNA levels in control and RANKL-stimulated BMDM cell. The values plotted are the mean ± S.D. from three independent experiments (**p<0.01; two-tailed Student's *t*-test). **(f)** Western blot analysis of protein levels for RANKL-inducible RUFY4 in untreated and RANKL-treated RAW264.7 cells; β-actin was used as a loading control. **(g)** Yeast two-hybrid assay. Co-transformants were spotted on –Leu/-Trp and –Leu/-Trp/-His media to confirm viability and interactions, respectively. **(h)** RUFY4-FLAG was co-transfected into HEK293T cells with various forms of Arl8b-HA; lysates were IP with anti-HA antibody resin, and precipitates were IB with the indicated antibodies. **(i)** GST and GST-Arl8b proteins were immobilized on glutathione (GSH) resin and incubated in presence of excess GTP and GDP with HEK293T cell lysates expressing RUFY4-FLAG. The precipitates were immunoblotted with anti-FLAG antibodies. Ponceau S staining was done to visualize purified protein. **(j-m)** Representative confocal micrographs of HeLa cells transfected with RUFY4-FLAG alone or co-transfected with different forms of Arl8b, respectively, and stained with LAMP1 and the indicated epitope-tag antibodies. Bars, 10 µm. **(n)** Endogenous IP was performed by incubating the osteoclast cell lysates with mouse anti-Arl8 antibody-conjugated-resin or mouse IgG-conjugated-resin and IB with indicated antibodies. Scale Bars: 10 µm (main); 2 µm (inset).

D) RUFY4 binds to Arl8b through its N-terminal RUN domain-containing region

Next, we wanted to identify which region of RUFY4 is responsible for binding to Arl8b. To this end, we used different domain deleted mutants of RUFY4; WT (1-571 amino acids), RUN only (1-166 amino acids, containing the RUN domain only) and ΔRUN (167-571 amino acids, lacking the RUN domain) (**Figure 23a**). We then examined their interactions with Arl8b using co-IP and yeast two-hybrid assay and found that RUFY4 (WT) and RUFY4 (RUN only) interacted with Arl8b, whereas RUFY4 (ΔRUN) did not show interaction with RUFY4 (**Figures 23b** and **23c**). This was corroborated using the GST-pulldown assay, which demonstrated that Arl8b interacted with GST-tagged-RUFY4 (RUN domain only), but Arl11, another small G protein from the Arl family used as a negative control in this experiment, did not exhibit any interaction (**Figure 23d**). To test whether RUFY4 (RUN domain only) directly binds to Arl8b, we incubated recombinant His-tagged Arl8b and Rab7 with GST or GST-tagged-RUFY4 (RUN domain only). As demonstrated in **Figure 23e**, RUFY4 (RUN domain only) directly interacts with Arl8b, but not with Rab7, which was used as a negative control in this experiment.

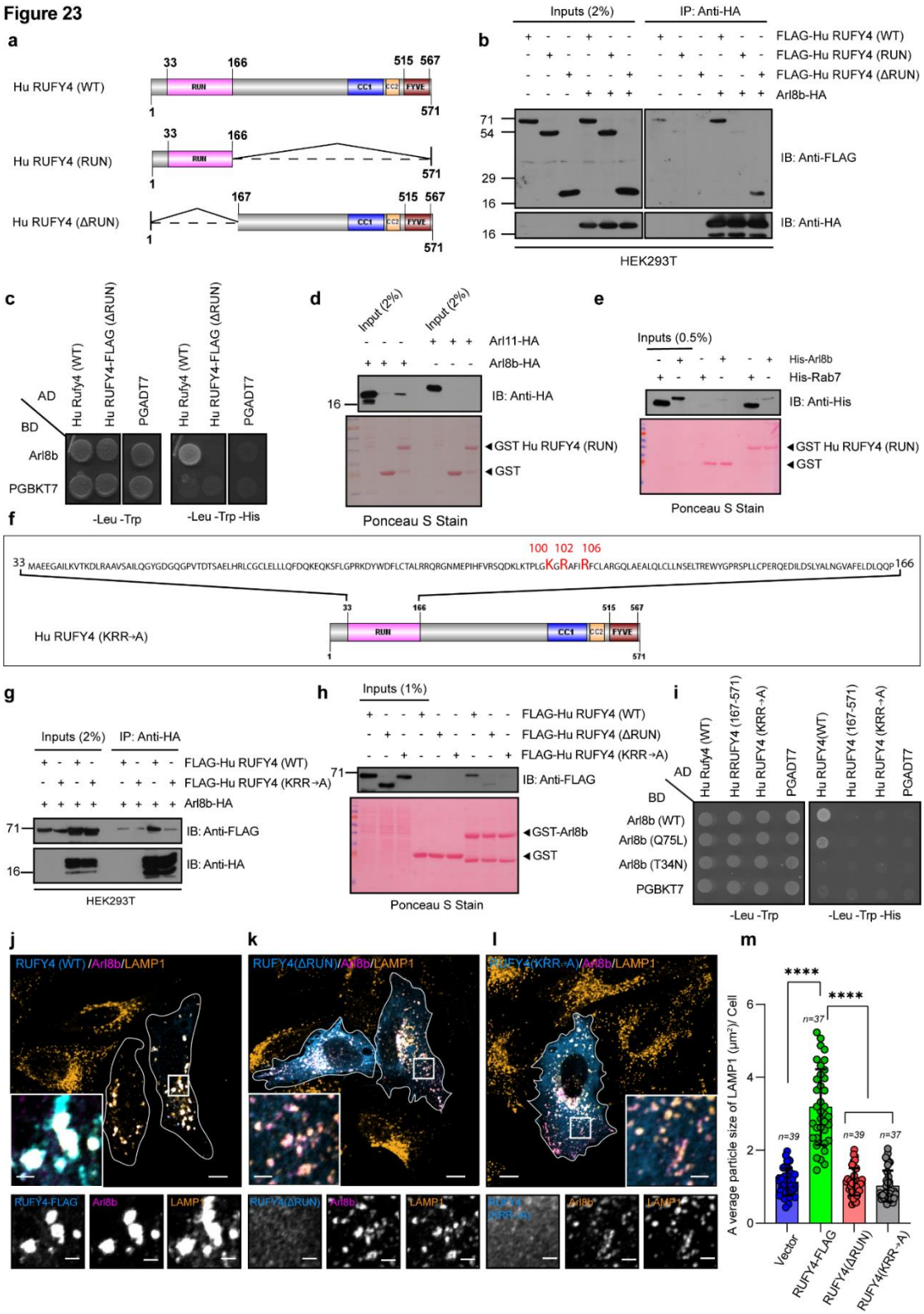

Figure 23: RUFY4 directly binds to Arl8b via its N-terminal RUN domain–containing region

(a) Schematic representation of human RUFY4 (WT) and domain deletion mutant. **(b)** Arl8b-HA was co-transfected with FLAG-RUFY4 (WT), FLAG- RUFY4 (167-571 amino acid, ΔRUN) or FLAG- RUFY4 (1-166 amino acid, RUN domain only) in HEK293T cells. The lysates were immune-precipitated (IP) using anti-HA antibody resin and immunoblotted using

the indicated antibodies. **(c)** Yeast two-hybrid assay. Co-transformants were spotted on -Leu-Trp and -Leu-Trp-His media to confirm viability and interactions, respectively. AD, GAL4 activation domain; BD, GAL4-DNA binding domain. (**d-e)** GST and GST- RUFY4 (RUN) proteins were immobilized on glutathione (GSH) resin and incubated either with HEK293T cell lysates expressing indicating plasmids or with purified His-Arl8b or His-Rab7**.** The precipitates were immunoblotted with anti-HA (d) and anti-His (e) antibodies. Ponceau S staining was done to visualize purified protein. **(f)** A schematic representation of RUFY4's Arl8b-binding region, highlighting the amino acid residues (K100, K102, and R106) required for binding to Arl8b. **(g)** Arl8b-HA was co-transfected with RUFY4-FLAG (WT) or ΔRUN or KRR→A mutant in HEK293T cells. The lysates were IP using anti–HA antibody resin and immunoblotted using the indicated antibodies. **(h)** GST and GST-Arl8b proteins were immobilized on glutathione (GSH) resin and incubated with HEK293T cell lysates expressing FLAG-RUFY4 (WT) or -Arl8b-binding–defective mutants of RUFY4. The precipitates were immunoblotted with anti-FLAG antibodies. Ponceau S staining was done to visualize purified protein. **(i)** Yeast two-hybrid assay. Co-transformants were spotted on -Leu/-Trp and on-Leu/-Trp/-His media to confirm viability and interactions, respectively. **(j-l)** Confocal micrographs of HeLa cells expressing RUFY4-FLAG (WT) (j), RUFY4 (ΔRUN)-FLAG (j) and RUFY4 (KRR→A)-FLAG (l) with Arl8b-GFP, stained with anti-LAMP1 and anti-FLAG antibodies**.** Transfected cells are marked with a boundary. **(m)** The particle size of LAMP1-marked compartments was assessed from the experiments shown in j-l. The values plotted are the mean ± S.D. from three independent experiments. The total number of cells analyzed is indicated on the graph (****p<0.0001; two-tailed Student's *t*-test). Scale bars: 10 µm (main); 2 µm (inset).

In our prior work, we established the critical involvement of basic residues within the RUN domain in the interaction of PLEHKM1 and SKIP with Arl8b (Marwaha et al., 2017). Similarly, to further narrow down the amino acid residues in the RUFY4 (RUN domain) fragment that are crucial for binding to Arl8b, we performed sequence alignment of RUN domains of PLEHKM1, SKIP, and RUFY4 proteins. We found three conserved basic residues at positions K (100), R (102), and R (106) in the RUN domain of RUFY4 (**Figure 23f**). We created triple point mutant (K100A/R102A/R106A; "KRR→A") by replacing basic residues of RUFY4 with alanine and determined interaction with Arl8b using Co-IP (**Figure 23g**), GST pull-down (**Figure 23h**), as well as with a yeast two-hybrid assays (**Figure 23i**). We observed that RUFY4 (KRR→A) failed to interact with Arl8b in all different assays (**Figures 23g-i**), which shows that these three basic residues (K100A/R102A/R106A) in the RUN domain of RUFY4 are responsible for binding to Arl8b. Subsequently, when the epitope-tagged-Arl8b-binding–defective mutants of RUFY4 were co-expressed in Hela cells with Arl8b (WT), they were not recruited to LAMP- and Arl8b-marked lysosomes and remained predominantly cytosolic in comparison to the wild-type form of RUFY4 (**Figures 23j-l**). Moreover, interestingly, we also observed a substantial increase in the size of

LAMP1 puncta upon co-expression of RUFY4 (WT) and Arl8b, which was not seen when Arl8b-binding-defective mutants of RUFY4 were co-expressed with Arl8b **(Figure 23m)**. These results indicate RUN-domain of RUFY4 is essential and sufficient for its interaction with Arl8b and therefore its recruitment to the lysosomes**.**

E) RUFY4 regulates peripheral lysosome distribution in osteoclasts but is not required for osteoclast differentiation *in vitro*

Because RUFY4 is a RANKL-inducible gene, we first looked at its role in RANKL-mediated osteoclastogenesis. To this end, we employed an RNA interference approach to silence RUFY4 in osteoclasts. The efficiency of RUFY4 silencing was found to be >90%, as confirmed by Western blotting and qRT-PCR (**Figures 24a** and **24b**). We evaluated the mRNA levels of several osteoclast differentiation markers; *Nfatc1, Dcstamp, CathepsinK,* and *Ocstamp* (Fujiwara et al., 2016; Ohmae et al., 2017) in osteoclasts upon RUFY4 silencing and found no significant difference when compared to control siRNA treated cells (**Figures 24c-24f**). These results were also corroborated by the TRAP staining and quantification of the TRAP positive multi-nucleated cells in control and RUFY4 siRNA treated cells (**Figures 24g** and **24h**). However, when compared to control siRNA-treated cells, the culture supernatant from RUFY4-silenced cells showed a 25% reduction in TRAP activity (**Figure 24i**). Based on our results using RUFY4 expression in HeLa cells, we know that Arl8b recruits RUFY4 to lysosomes. However, to further establish its subcellular localization, RUFY4 was endogenously labeled using our in-house antibody produced in rabbit. As shown in the representative confocal micrograph, we report for the first time that RUFY4 localizes to peripheral LAMP2-marked lysosomes in osteoclasts (**Figures 24j**).

To learn more about role of RUFY4 in osteoclast biology, we next investigated the effect of RUFY4 depletion on lysosome distribution in osteoclasts. To accomplish this, both control and RUFY4 siRNA treated cells were immunostained for lysosomes (using anti-LAMP2 antibody) and the actin ring was labeled with phalloidin (**Figures 24k** and **24l**). As indicated in representative micrographs in the **Figures 24k** and **24l**, we noticed a distinct pattern in the lysosome positioning of RUFY4-deficient osteoclasts as compared to control cells. The lysosomes were not present in the vicinity of actin ring (see insets in **Figures 24k and 24l**) and it is likely that the absence of RUFY4 prevents lysosomes from docking to the plasma membrane (ruffle border).

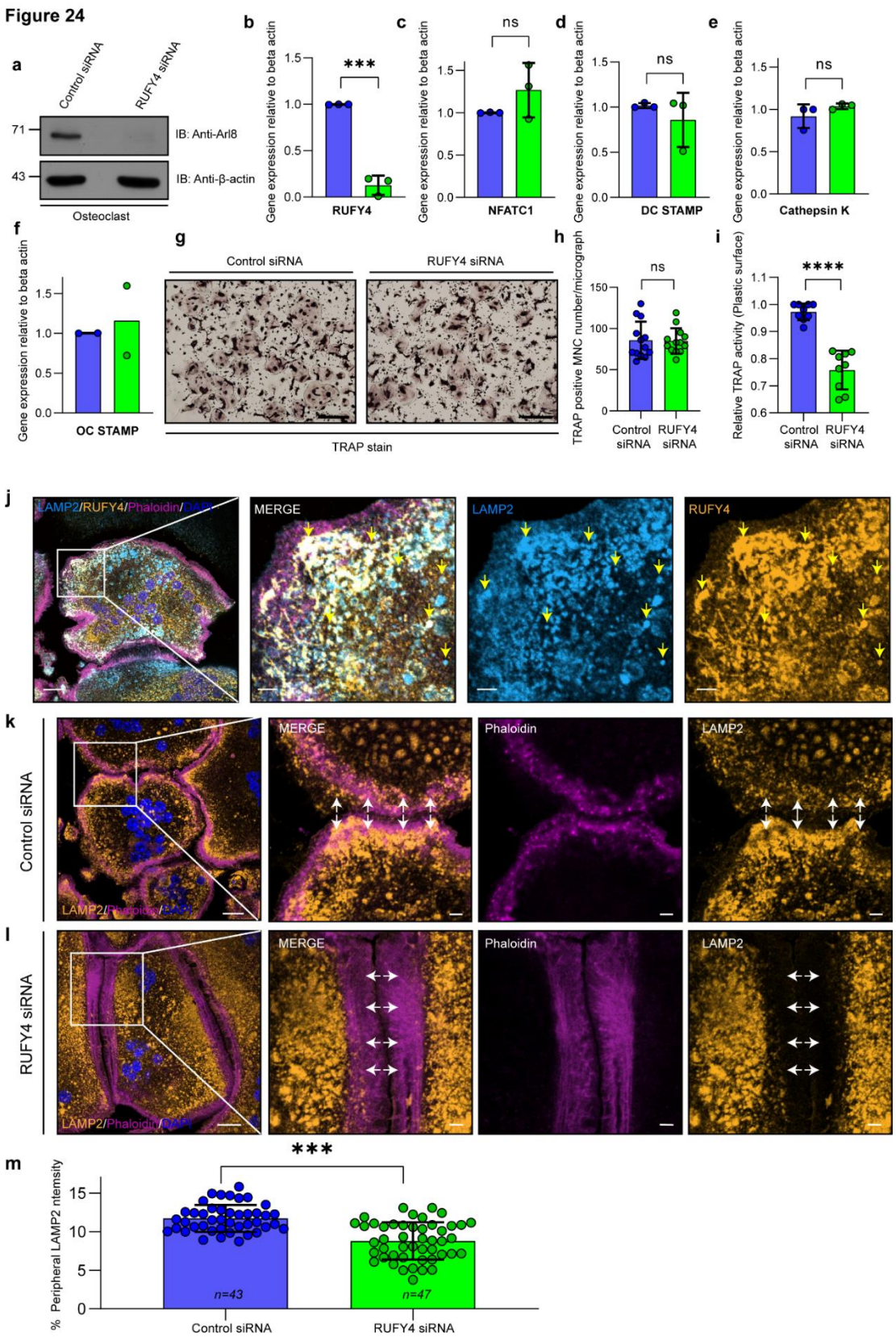

Figure 24: RUFY4 regulates peripheral lysosome distribution in osteoclasts but is dispensable for osteoclastogenesis. **(a)** Lysates from control and RUFY4 siRNA treated osteoclasts were immunoblotted (IB) with anti-RUFY4 antibody to determine the knockdown efficiency, β-actin used as a loading control. **(b)** qRT-PCR analysis to determine the efficiency

of *Rufy4* siRNA. **(c-f)** qRT-PCR analysis of the mRNA levels of several osteoclast differentiation markers; *Nfatc1, Dcstamp, CathepsinK, and Ocstamp*. Values plotted are the mean ± S.D. from three independent experiments except in (f) (***p<0.001; ns, not significant; two-tailed Student's t-test). **(g-h**) TRAP staining of control and RUFY4 siRNA treated osteoclasts cultured on a plastic surface. The number of TRAP positive multinucleated cells (> 3 nuclei) was quantified and plotted. Values plotted are the mean ± S.D. from two independent experiments (ns, not significant; two-tailed Student's t-test). The total number of micrographs analyzed is indicated on the graph. **(i)** M easurement of TRAP activity in the culture supernatants of control and RUFY4 silenced osteoclasts cultured on plastic surfaces.Values plotted are the mean ± S.D. from three independent experiments (***p<0.001; two-tailed Student's t-test). **(j)** Representative confocal micrograph showing immunostaining of RUFY4 and LAMP2 in osteoclasts. In the inset, selected region of the cell are magnified to show co-localized pixels of RUFY4 with LAMP2 (denoted by yellow arrowheads). **(k-m)** Confocal micrographs showing immunofluorescent staining of LAMP-2 in control and RUFY4 silenced osteoclasts cultured on glass coverslips. In the insets, white arrows point out the distribution of LAMP-2–positive lysosomes at the periphery of osteoclasts. The percentage of peripheral lysosome intensity quantified from these experiments is shown in (m). The values plotted are the mean ± S.D. from two independent experiments. The total number of cells analyzed is indicated on the graph (***p<0.001; two-tailed Student's t-test). Scale bars: 20 µm (main); 4 µm (inset).

Moreover, quantification of fluorescence signals showed that in RUFY4-depleted cells, the percentage of LAMP2-positive lysosomes inside a 4 µm wide shell taken from the cell periphery was significantly lower than in control siRNA-treated cells (**Figure 24m**). These findings suggest a potential role of the Arl8b-RUFY4 complex in the bone resorption activity of osteoclasts.

F) RUFY4 act as a linker between the small GTPase Arl8b and LC3 to mediate fusion of lysosome and ruffle border

To elucidate the mechanism of action of RUFY4, we used a GST-pulldown coupled mass spectrometry approach. GST-RUFY4 was used as a bait protein to find putative interaction partners in cell lysates of osteoclasts. Interestingly, we identified peptides corresponding to the LC3 protein in the GST-RUFY4 eluate. Notably, it has been shown that LC3B-II (a lipidated form of the LC3B protein) is present on the ruffle border and that recruitment of this protein is essential for ruffle border formation, lysosome secretion, and bone resorption. Moreover, mice lacking LC3 lipidated machinery (autophagy proteins such as ATG5, ATG4b, and ATG7) exhibited non-resorbing osteoclasts owing to faulty lysosome fusion and cathepsin-K secretion (Deselm et al., 2011, Gelman and Elazar, 2011; Tran et al., 2016; Ohmae et al., 2017).

In addition to this, a previous study has reported that RUFY4 is a positive regulator of autophagy and is involved in both autophagosome formation and autophagosome fusion with lysosomes (Terawaki et al., 2015a). Consequently, we confirmed RUFY4 and LC3B interaction by incubating recombinant GST-LC3B protein with cell lysates of RUFY4-FLAG expressing HEK293T cells, and we found that RUFY4-FLAG was interacting with purified GST-LC3B **(Figure 25a)**.

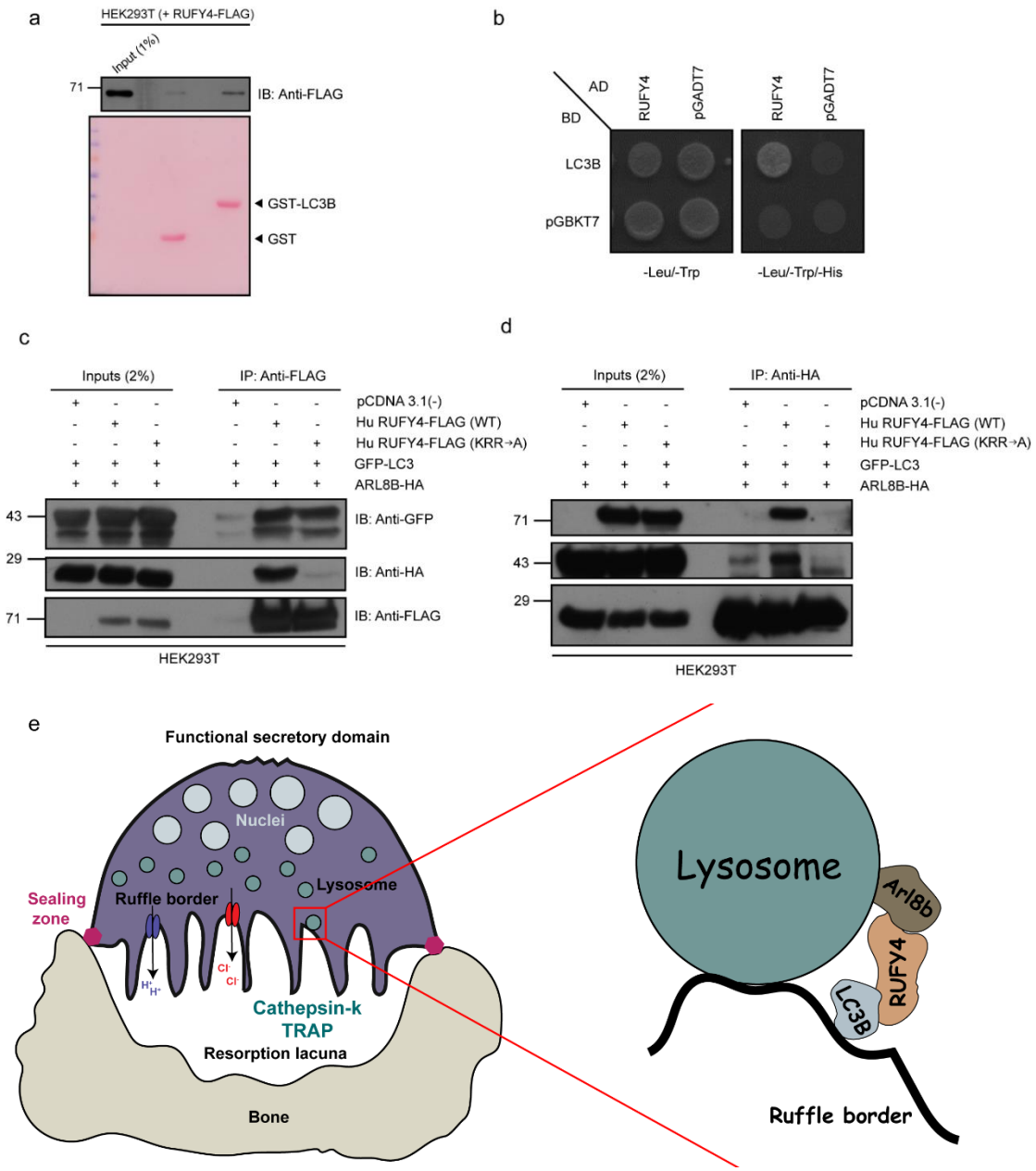

Figure 25: RUFY4 promotes the interaction of Arl8b and LC3B. (a) Recombinant GST or GST-LC3B fusion proteins bound to glutathione resin were incubated with lysates from HEK293T cells expressing RUFY4-FLAG. The precipitates were immunoblotted with anti-HA antibodies and GST-tagged proteins were visualized using Ponceau S staining. **(b)** Yeast two-hybrid assay. Cotransformants were spotted on -Leu/-Trp and -Leu/-Trp/-His media to confirm

viability and interactions, respectively. **(c)** The lysates of HEK293T cells expressing indicated plasmids were IP with anti-FLAG antibodies-conjugated-agarose beads and the precipitates were IB with the indicated antibodies. **(d)** The lysates of HEK293T cells expressing indicated plasmids were IP with anti-HA antibodies-conjugated-agarose beads and the precipitates were IB with the indicated antibodies. **(e)** Proposed model of lysosome function regulation by small GTPase Arl8b and its effector RUFY4. Here we report that RUFY4 function as a linker that can simultaneously binds to Arl8b and LC3B, present on lysosome and ruffle border respectively. Arl8b-RUFY4-LC3B complex mediates the fusion of lysosome to the ruffle border and subsequent secretion of their luminal content required for bone resorption.

Supporting this result, we observed interaction of RUFY4 with LC3B in a yeast two hybrid assay (**Figure 25b**). Following that, we performed immunoprecipitation of RUFY4-FLAG (WT) and RUFY4-FLAG (KRR→A) after co-expressing Arl8b-HA and GFP-LC3B in HEK293T cells to confirm if Arl8b, RUFY4 and LC3B are part of the same complex. As expected, Arl8b-HA was only co-immunoprecipitated with RUFY4-FLAG. However, GFP-LC3B is bound to both the WT and KRR→A forms of RUFY4 (**Figure 25c**). This implies that RUFY4 interacts with both Arl8b and LC3B but through distinct binding regions. Next, in order to determine if RUFY4 works as a linker between Arl8b and LC3B, we performed a co-IP experiment using epitope-tagged Arl8b and LC3B in the presence of RUFY4-FLAG (WT) or RUFY4-FLAG (KRR→A). As shown in the **Figure 25d**, ectopic expression of WT, but not the (KRR→A) mutant of RUFY4, enhanced the interaction between Arl8b-HA and GFP-LC3B. Altogether, these findings suggest that RUFY4 facilitates the interaction of lysosomal small G-protein Arl8b, and LC3B located on the ruffle border, thereby mediating lysosome fusion to the ruffle border and subsequent secretion of their luminal content (**Figure 25e)**.

Discussion

Bone remodeling is a process that occurs throughout our lives in order to regenerate bone in our bodies. The coordinated activity of osteoclasts and osteoblasts is critical for maintaining the balance between bone resorption and bone formation (Kim et al., 2020). In order to resorb bone, osteoclasts require an acidic environment in the sealing zone and release of acid hydrolases capable of degrading collagen. Interestingly both of these requirements are met by lysosomes. Various independent studies have shown that proteins involved in vesicular trafficking and fusion are required for osteoclast ruffle

border formation and bone resorption activity (Coxon & Taylor, 2008; Zhao, 2012). Moreover, the relevance of lysosomes for osteoclasts has been well established for a long period of time, as evident by the fact that mutations in genes involved in lysosome biogenesis and trafficking impair bone resorption activity and result in conditions such as osteopetrosis (Lacombe et al., 2013). One such gene is *PLEKHM*1, a mutation in the *PLEKHM1* gene known to cause osteopetrosis in rats and humans (Van Wesenbeeck et al., 2007). PLEKHM1 is a well-characterized effector of Rab7, a small G protein that has also been shown to be indispensable for the bone resorption activity of osteoclasts (Zhao et al., 2001). Furthermore, PLEKHM1 also linked Rab7-positive lysosomes to microtubules for trafficking to the ruffle border via its interaction with FAM98A and NDEL1 (Fujiwara et al., 2016).

Interestingly, in a previous study, we showed that the Rab7 effector-PLEKHM1 also interacts with Arl8b and functions as a linker to facilitate lysosome clustering and fusion with late endosomes and autophagosomes (Marwaha et al., 2017). The small G protein Arl8b is a well-known regulator of spatial distribution of lysosomes in mammalian cells (Bagshaw et al., 2006). Lysosome positioning mediated by Arl8b regulates a variety of cellular processes in different cell types, including plasma membrane repair, nutrient sensing and response, natural killer cell–mediated cytotoxicity, antigen presentation, cell migration, tubular lysosome formation in macrophages., lysosome exocytosis, lysosome-mediated ER remodeling, focal adhesion disassembly, and cancer cell metastasis (Dykes et al., 2016; Korolchuk et al., 2011; Lu et al., 2020; Michelet et al., 2018; Rabanal-Ruiz et al., 2021; Rui Jia & Bonifacino, 2019; Saric et al., 2015). However, all above-mentioned lysosome functions mediated by Arl8b are attributed to its binding with effector protein SKIP/PLEKHM2, which in turn binds and recruits kinesin-1 motor to promote anterograde motility of lysosomes (Rosa-Ferreira & Munro, 2011). Recently, our group has shown that Arl8b also mediates the long-range retrograde movement of lysosomes via its effector protein RUFY3, which couples the JIP4-dynein-dynactin complex to lysosomes (Kumar et al., 2022). Surprisingly, despite having several roles in lysosome positioning and function, the role of alr8b in osteoclasts remains unknown.

Herein we have established the role of Arl8b in osteoclast biology. In line with function of Arl8b in other cell types, Arl8b localizes to the lysosomes in osteoclasts and regulate their peripheral distribution near the actin ring. We used CRISPR/Cas9 tool to create an Arl8b knockout (KO) in the RAW264.7 cells. Our findings on osteoclasts derived from Arl8b knockout cells revealed that Arl8b plays a critical role in osteoclast bone resorption activity, however, Arl8b depletion has no impact on osteoclastogenesis.

In addition to this we have found RUFY4 as a novel osteoclast-specific effector protein of Arl8b. Our study has shown that the RUFY4 expression is RANKL inducible and it localizes to peripheral lysosomes in the osteoclasts. Moreover, using various biochemical and confocal experiments with domain deletion mutants of RUFY4, we demonstrated that N- terminal RUN domain of RUFY4 is essential and sufficient for its binding to Arl8b and recruitment to lysosomes. RUFY4 has previously been shown to play a role as positive regulator of autophagy in primary dendritic cells (Terawaki et al., 2015b). Notably, the expression of RUFY4 in dendritic cells is Interleukin 4-inducible (Terawaki et al., 2015b). The same study has demonstrated that RUFY4 via its RUN domain binds to Rab7 and further increases the co-localization of RAB7 with LAMP1-marked lysosomes. However, we did not find direct interaction of RUFY4 with RAB7 in our *in-vitro* GST-pull down assay. One possibility is that Arl8b, RUFY4, and Rab7 are all part of the same complex that regulates osteoclast bone resorption activity, although the likelihood of RUFY4 working as a dual adaptor for both Arl8b and Rab7, similarly to PLEKHM1, is less and requires further investigation.

Interestingly, it has been shown that LC3B-II (a lipidated form of the LC3B protein) is present on the ruffle border and that recruitment of this protein is required for the development of the ruffle border, lysosome secretion, and bone resorption. Furthermore, mice lacking the LC3 lipidated machinery had non-resorbing osteoclasts due to defective lysosome fusion and cathepsin-K secretion (Deselm et al., 2011; Ohmae et al., 2017). In addition to this, as mentioned earlier a previous study has reported that RUFY4 is a positive regulator of autophagy and is involved in both autophagosome formation and autophagosome fusion with lysosomes (Terawaki et al., 2015a). In line with this, we found that RUFY4 interacts with LC3 and acts as a linker between the Arl8b-positive lysosome and the LCB-marked ruffle border. This helps

lysosomes to fuse with the ruffle border, which is a key mechanism for lysosome secretion and bone resorption. However, there is a strong possibility that the other proteins, such as fusion machinery (HOPS and SNAREs), which are known for their function in membrane fusion events (Khatter et al., 2015; Spang, 2016), are involved in lysosome fusion with ruffle border. Hence, it will be interesting to know what other proteins are associated with the Arl8b-RUFY4-LC3B complex and how their interactions influence osteoclast biology.

The fascinating question that remains unanswered is whether or not RUFY4, like its family member RUFY3, also links dynein-dynactin machinery to Arl8b for lysosome trafficking or if they compete for binding to Arl8b. In addition to this, another interesting question is to find out the functional relationship between different effector proteins of Arl8b. Surprisingly, several proteins and molecular machinery that govern endosomal trafficking in other cell types are either dispensable for osteoclast biology or have some unrelated or independent functions in osteoclast. One example is PLEKHM1, which is known for its role in autophagy and as a regulator for endocytic trafficking, but osteoclasts lacking PLEKHM1 did not show any of these defects (Fujiwara et al., 2016; Marwaha et al., 2017). Thus, it will be interesting to find out whether or not SKIP-Arl8b, PLEKHM1-Arl8b, and RUFY3-Arl8b complexes have the same function in osteoclasts as in the other mammalian cells or if they have some osteoclast specific interactions and functions.

In conclusion, our study established the role of Arl8b in osteoclasts. Arl8b regulates both the distribution of lysosomes and the bone resorption activity of osteoclasts. Furthermore, the findings of this study revealed RUFY4 as a RANKL-inducible gene and an osteoclast-specific effector of Arl8b that regulates peripheral distribution of lysosomes.

Materials and Methods

Cell Culture and RNAi

RAW264.7, HeLa and HEK293T cells (from ATCC) were maintained in DMEM media (Gibco) supplemented with 10% FBS (Gibco) at 37°C with 5% CO_2 in a humidified cell culture chamber. Each cell type was regularly screened for the absence of

mycoplasma contamination by using the MycoAlert Mycoplasma Detection Kit (Lonza) and was cultured for no more than 15 passages. For gene silencing, siRNA oligos or SMARTpool were purchased from Dharmacon and prepared according to the manufacturer's instructions. Following siRNA oligos were used in this study: Control pool siRNA, 5'-; ON-TARGETplus RUFY4 SMARTpool).Transient transfection of siRNAs was performed with DharmaFECT 1 (Dharmacon) according to the manufacturer's instructions.

Generation of Arl8b KO cells using CRISPR/Cas9

Arl8b KO RAW264.7 cells were generated using the Arl8b sg/RNA (5′-target sequence: GATGGAGCTGACGCTCG-3′) and CRISPR/Cas9 All-in-One Lentivector Set, respectively (human; Applied Biological Materials). In brief, using X-tremeGENE HP DNA Transfection Reagent (Roche), the All-in-One plasmid was transfected into HEK293T cells along with lentiviral packaging plasmids to produce viral particles. Culture supernatants from transfected HEK293T cells were collected after 24 and 48 hours, which then pooled, centrifuged, and concentrated using a Lenti-X concentrator (Takara Bio Inc.). RAW264.7 cells were then incubated with supernatants containing lentiviral particles in the presence of 8 µg/ml polybrene (Sigma-Aldrich). Lentiviral-infected cells were grown in puromycin containing (5 µg/ ml; Sigma-Aldrich) medium for 72 hours to select KO cell population. Consequently, selected KO cells were reseeded in 96-well plates for single-colony formation. The identification of the KO cell clones was confirmed by immunoblot analysis.

Mammalian expression constructs

All the DNA constructs used in this study are listed in appendix Table 3.

Antibodies and chemicals

The following antibodies were used in this study: Rabbit anti-HA (sc-805; Santa Cruz Biotechnology, Inc.), mouse anti-HA (901503: BioLegend), mouse anti-His (SAB1305538; Sigma-Aldrich), Mouse anti-LAMP1 (555798; BD Bioscience), rat anti- Lamp2 (ab13524; abcam), rabbit anti-FLAG (2368, Cell Signaling Technology). Rabbit anti–RUFY4 antibody used in this study was generated against the N-terminal His tag RUFY4 protein. Rabbit anti–Arl8 antibody used in this study has been described

previously (Marwaha et al., 2017). All the Alexa fluorophore–conjugated secondary antibodies were purchased from Thermo Fisher Scientific. HRP-conjugated goat anti-mouse and goat anti-rabbit were purchased from Jackson ImmunoResearch Laboratories. Alexa Fluor 647 phalloidin (A12380), and DAPI (D1306) were purchased from Thermo Fisher Scientific. Polybrene (H9268), and puromycin (P8833) were purchased from Sigma-Aldrich. RANKL was purchased from R&D Biosystem (390-TN-010).

Osteoclast culture and TRAP staining

RAW264.7 cells were seeded at 0.05 million cells/well in 24-well plate and cultured in α -minimum essential medium (MEM) (Gibco) with 10% fetal bovine serum (FBS) containing either recombinant mouse RANKL (R&D, 30 ng/ml) or recombinant GST-RANKL (200 ng/ml). The fresh medium and RANKL were changed every other day. After osteoclast differentiation, cells were washed with PBS, fixed and stained for TRAP (tartrate-resistant acid phosphatase) activity using a leukocyte acid phosphatase kit (Sigma). TRAP-positive multinucleated giant (>3 nuclei) cells were counted as osteoclasts. To differentiate osteoclast from Bone marrow derive macrophages (BMDM), Bone marrow was harvested from the tibiae and femurs of 6-week-old C57BL/6 as described in our previous work (Arya et al., 2018). Isolated BMDM was cultured in α-MEM (Gibco) with 10% fetal bovine serum (FBS), in presence of 30ng/ml M-CSF. Next day, non-adherent cells containing osteoclasts precursors were collected and further seeded in a 24 well plate at cell density of 100,000 cells per well in alpha MEM media supplemented with M-CSF (30ng/ml) and RANKL (100 ng/ml) for 5-6 days .The fresh media containing MCSF and RANKL was supplemented on day 3.

Resorption area measurement

RAW264.7 macrophages were cultured and differentiated into osteoclasts for 4 days on Osteo assay surface plates (Corning). At day-5, cells were washed twice with 1X PBS followed by the removal of osteoclasts from the surface using bleach treatment for 5 min. Post-bleach treatment wells were washed twice with 1X PBS and kept in the biosafety cabinet for drying. Images were taken using a Nikon microscope. The percentage of area resorbed over the total area was calculated using the Fiji software.

Dentine pit volume and measurement of CTx-1 in culture media

RAW264.7 macrophages were cultured and differentiated into osteoclasts on dentine discs (immunodiagnostic system) for 5–6 days. After washing the dentine discs with deionized water, the cells were gently removed from the dentine surface using a brush. The slices were then incubated with 20 mg/ml Alexa 488-conjugated wheat germ agglutinin (Invitrogen) for 30 min at room temperature. Dentine discs were washed thrice with deionized water and mounted using Fluoromount G (SouthernBiotech).The total pit volume was quantified using IMARIS software. The CTx-1 concentration in the culture medium was determined using the CrossLaps for Culture ELISA kit (Immunodiagnostic Systems) following the manufacturer's instructions.

Transfection and Immunofluorescence

Cells grown on glass coverslips (VWR) were transfected with desired plasmid constructs for 16-18 hours using X-treme GENE-HP DNA transfection reagent (Roche). Cells were then fixed in 4% PFA in PHEM buffer (60 mM Pipes, 10 mM EGTA, 25 mM Hepes, and 2 mM MgCl2, final pH 6.8) for 10 min at room temperature. After fixation, cells were incubated with blocking solution (0.2% saponin + 5% FBS in PHEM buffer) washed once in 1X PBS, and incubated for 1 h with the indicated primary antibodies in staining solution (PHEM buffer + 0.2% saponin). Subsequently, Cells were washed three times with 1X PBS and incubated for 30 min with the appropriate secondary antibodies made in staining solution, nuclei were stained with DAPI and Phalloidin (Invitrogen) was used to stain actin. Cells were mounted in Fluoromount G and images were captured using Carl Zeiss 710 Confocal Laser Scanning Microscope with a Plan Apochromat 63×/1.4 NA oil immersion objective and high-resolution microscopy monochrome cooled camera AxioCamMRm Rev. 3 FireWire (D) (1.4 megapixels, pixel size 6.45 µm × 6.45 µm). ZEN Pro 2011 (ZEISS) software was used for image acquisition. Some confocal images were also captured using Nikon A1R confocal microscope equipped with a Plan Apo VC 60/1.4 numeric aperture oil immersion objective and in this case for image acquisition, NIS-Elements AR 4.1 (Nikon) software was used.

Image analysis and quantification

Analysis of lysosome distribution: To quantify the distribution of lysosomes based on LAMP2 signal intensity, Fiji software was used. A boundary was drawn along the periphery of each selected cell using the “freehand” selection tool and LAMP2 signal intensity was measured. Next, the same ROI was then decrement by 4 µm and again LAMP2 signal intensity was measured. Finally, peripheral LAMP2 intensity in a 4 µm shell was calculated by subtracting the intensity of 1st ROI from 2nd. Percentage of LAMP1 distribution was plotted by dividing the peripheral intensity with whole-cell LAMP2 intensity.

Particle size quantification: Fiji's "Analyze Particle" tool and "Otsu" threshold were used to determine the size of lysosomes based on Lamp1 signal intensity.

Cell lysates, Co-immunoprecipitation and Immunoblotting

To prepare cell lysate, cells were lysed on ice in RIPA lysis buffer (10 mM Tris-Cl pH 8.0, 1 mM EDTA, 0.5 mM EGTA, 1% Triton X-100, 0.1% sodium dodecyl sulfate, 0.1% sodium deoxycholate and 140 mM NaCl) supplemented with protease inhibitor cocktail (Sigma),. After incubation on ice for 10 minutes with intermittent vortexing, the lysed cells were centrifuged at 13, 200 rpm for 10 minutes at 4°C and the supernatants were collected and quantitated (BCA; Sigma). The equal amount of all samples were subjected to SDS-PAGE and then transferred onto polyvinylidene fluoride membranes (Bio-Rad Laboratories). Membranes were kept overnight at 4°C in blocking solution (10% skim milk in 0.05% PBS-Tween 20). After blocking the membrane washed once in 0.05% PBS-Tween 20 and then incubated with Indicated primary and secondary antibodies (prepared in 0.05% PBS-Tween 20). The membranes were washed for 10 min thrice with 0.05% PBS-Tween 20 or 0.3% PBS- Tween 20 after 2-h incubation with primary antibody and 1-h incubation with secondary antibody, respectively. The blots were developed using a chemiluminescence-based method. To identify secreted cathepsin-K, Culture supernatant was collected and subjected to western blot analysis as mentioned above.

To conduct co-immunoprecipitation experiments, indicated cells were resuspended in ice-cold TAP lysis buffer (20 mM Tris pH 8.0, 150 mM NaCl, 0.5% NP-40, 1 mM

$MgCl_2$, 1 mM Na_3VO_4, 1 mM NaF, 1 mM PMSF and protease inhibitor cocktail) and kept on rotation at 4°C for 30 min. The lysates were then incubated with indicated antibody conjugated-agarose beads at 4°C rotation for 3 hr, followed by four washes with TAP wash buffer (20 mM Tris pH 8.0, 150 mM NaCl, 0.1% NP-40, 1 mM $MgCl_2$, 1 mM Na_3VO_4, 1 mM NaF and 1 mM PMSF). The samples were then subjected to SDS-PAGE for further analysis.

Recombinant protein purification, GST-pulldown assay, and mass spectrometry analysis

The *E. coli* BL21 strain was used to express and purify all of the recombinant proteins used in this study (Invitrogen). To setup primary cultures, a single transformed colony was inoculated in Luria–Bertani (LB) broth containing appropriate antibiotics and incubated at 37° C in a shaking incubator. Following 8–12 hours of culturing, 1% of the primary inoculum was used to setup secondary cultures, which were then incubated at 37°C with shaking until an absorbance of 0.6 at 600 nm was achieved. To induce protein expression, 0.3 mM IPTG (Sigma-Aldrich) was added to the cells, which were then incubated at 16°C with shaking for 16 hours. After induction, the bacterial cultures were centrifuged at 6,000 rpm for 10 minutes, washed with 1XPBS, and resuspended in lysis buffer (20 mM Tris and 150 mM NaCl, pH 7.4) containing a protease inhibitor tablet (Roche) and 1 mM PMSF (Sigma-Aldrich). Next, sonication was used to lyse the bacterial cells, which were then centrifuged at 11,000 rpm for 30 minutes at 4°C. The clear supernatants were incubated on rotation for 1-2 hrs at 4°C with glutathione resin (Gbiosciences) to allow binding of GST-tagged proteins or with His60 Ni Superflow resin (Takara) for binding of His-tagged proteins. To eliminate contaminants, the beads were washed at least six times with wash buffer (20 mM Tris, 300 mM NaCl, pH 7.4).

For performing GST-pulldown assay mammalian cells were lysed in ice-cold TAP lysis buffer (20 mM Tris (pH 8.0), 150 mM NaCl, 0.5% NP-40, 1 mM $MgCl_2$, 1 mM Na_3VO_4, 1 mM NaF, 1 mM PMSF, and protease inhibitor cocktail). The equal amount of lysates were incubated with GST or GST-tagged proteins bound to glutathione resin at 4°C for 3-4 hr with rotation. Following incubation, the beads were washed six times with TAP lysis buffer to remove non-specific bindings. Next, elution was done by boiling the samples in Laemmli buffer and subjected them to SDS-PAGE for further analysis.

For GST-pulldown experiments using purified proteins, recombinant His-Arl8b, His-Rab7, GST and GST-tagged proteins were quantified using BCA protein assay kit (Sigma-Aldrich). 5 µg of GST (as a control) and GST-RUFY4 (RUN) protein were bound to glutathione beads for 3 hr at 4˚C on rotation. The beads were blocked with 5% BSA for 2 hr at 4˚C on rotation to prevent non-specific binding. The beads were washed with TAP lysis buffer (20 mM Tris (pH 8.0), 150 mM NaCl, 0.5% NP-40, 1 mM $MgCl_2$, 1 mM Na_3VO_4, 1 mM NaF, 1 mM PMSF, and protease inhibitor cocktail) minimum three times and incubated with 5 µg of His-Arl8b and His-Rab7 at 4°C for 1hr with rotation. After binding, the beads were washed five times with TAP lysis buffer followed by elution in 4x Laemmli buffer and SDS-PAGE for further analysis.

In order to identify the novel interacting partners for Arl8b, a GST-pulldown coupled mass spectrometry approach was used as described (Garg et al., 2011; Marwaha et al., 2017). In brief, recombinant GST-Arl8b and GST-only (as a control) proteins were incubated with osteoclast cell lysate (differentiated from RAW264.7 cells). After performing the pull down, the samples were subjected to SDS-PAGE and the gel was run only for 20 min. The coomassie stained single bands from GST-Arl8b and GST-only lanes were then cut out and submitted to the Taplin Mass Spectrometry Facility (Harvard Medical School, Boston, USA) for protein identification.

Quantitative RT-PCR analysis

Total RNA isolation from mammalian cells was done according to the manufacturer's instructions using the RNeasy kit (74104; Qiagen). The RNA was quantified and cDNA was synthesized using the SuperScript III First-Strand Synthesis System for qRT-PCR (18080051; Invitrogen). Quantitative PCR was performed on the obtained cDNA using SYBR Green Universal Mix (11762100; Invitrogen) according to the manufacturer's instructions. The following primer sequences were used for quantitative RT-PCR: *Rufy4* (Bio-Rad), *Cathepsin k* (Bio-Rad), *Dcstamp* (Forward primer: CTA GCTGGCTGGACTTCATCC; Reverse Primer: TCATGCTGTCTAGGAGACCTC), *Ocstamp* (Forward primer: TGGGCCTCCATATGACCTCGAGTAG; Reverse Primer: TCAAAGGCTTGTAATTGGAGGAGT), *Nfatc1* (Forward primer: CCGTTG CTTCCAGAAAATAACA; Reverse Primer: TGTGGGATGTGAACTCG GAA

Summary

Summary

Lysosomes are engaged in a wide range of cellular processes, including autophagy, nutrition sensing and metabolic signaling, plasma membrane repair, immunological response, cell migration, cancer metastasis, bone resorption, and gene regulation (Ballabio & Bonifacino, 2020; Lawrence & Zoncu, 2019; Oyarzún et al., 2019; Tsukuba et al., 2017). There are distinct pools of lysosomes in the cells that serve distinct roles depending on their positioning in the cells (Cabukusta & Neefjes, 2018). Moreover, various internal and external cues (such as nutrient availability, pathogens, intracellular pH, oxidative stress, membrane contact sites) are known to play role in maintaining the spatial distribution of lysosomes. Lysosomes sense these cues and alter their positioning and motility to meet different cellular requirements (Bonifacino & Neefjes, 2017; Dykes et al., 2016; Johnson et al., 2016; Korolchuk et al., 2011; Laopanupong et al., 2021; Saric et al., 2015; Takemasu et al., 2019; Tuli et al., 2013; Willett et al., 2017).

Lysosomes, like other organelles, move throughout cells along microtubule tracks. These tracks are radially spread throughout a non-polarized cell, with minus-ends pointing towards the MTOC (Microtubule-organizing center) in the perinuclear/juxta-nuclear region and plus-ends dispersed around the cell's periphery. Retrograde (minus end-directed) and anterograde (plus end-directed) lysosome movement is controlled by dynein and kinesin motor proteins (Granger et al., 2014; Hunt & Stephens, 2011). However, small GTPases together with their effectors and other adaptor proteins generally facilitate couplings between motor proteins and lysosomes (Donaldson & Jackson, 2011; Homma et al., 2021; Kjos et al., 2018).

Arl8b, a small G protein, is an important player in maintaining lysosomal positioning and functions in the subcellular space (Khatter et al., 2015b). Overexpression of Arl8b has been demonstrated to enhance the proportion of lysosomes that migrate bi-directionally along microtubule pathways (Hofmann and Munro, 2006). Subsequent studies demonstrated that Arl8b interacts with the effector protein SKIP/PLEKHM2, which then binds and engages the kinesin-1 motor to induce anterograde lysosome movement (Keren-Kaplan and Bonifacino, 2021; Pu et al., 2015; Rosa-Ferreira and

Munro, 2011; Tuli et al., 2013). However, it remained unknown if Arl8b could facilitate long-distance retrograde lysosome migration.

In our study presented in the chapter 2, we identified RUFY3 as an Arl8b effector that enables lysosome retrograde motion. We found that RUFY3 interacts with the JIP4-dynein-dynactin complex, allowing Arl8b to associate with the retrograde motor complex. As a consequence of RUFY3 silencing, the positioning of Arl8b-positive endosomes is disrupted, and Arl8b colocalization with Rab7-marked late endosomal compartments is decreased. Additionally, we showed that RUFY3 regulates nutrient-dependent lysosome distribution, despite the fact that RUFY3 deficiency has no effect on autophagosome-lysosome fusion or autophagic cargo degradation. Interestingly, in RUFY3-depleted cells, lysosome size is dramatically reduced, which could be rescued by inhibiting the lysosome reformation regulating component PIKFYVE. These results point to a paradigm in which the "perinuclear cloud" arrangement of lysosomes governs the positioning and size of these proteolytic compartments.

Chapter 3 provides insights into the role of the small G protein Arl8b in the regulation of bone remodelling activity of the osteoclasts. We found that Arl8b had a distinct localization underneath the actin rings and ruffled borders in osteoclasts, and that Arl8b-deficient osteoclasts had severely reduced lysosome secretion. Furthermore, we identified a novel Arl8b effector, RUN and FYVE domain-containing protein family member 4 (RUFY4), which is specifically expressed in osteoclasts upon RANKL stimulation and localizes to the osteoclasts' peripheral lysosomes. Interestingly, RUFY4 interacts with LC3 and functions as a linker between the LC3-marked ruffle border and Arl8b-positive lysosomes, enabling lysosome fusion to the ruffle border, a crucial mechanism required for lysosome secretion and bone resorption. When RUFY4 was silenced in osteoclasts, the peripheral positioning of lysosomes in the region of actin rings was decreased, resulting in a significant reduction in TRAP activity and osteoclast resorption capacity. Our study identifies the Arl8b-RUFY4 complex as a critical component of osteoclast-mediated bone remodeling.

Overall, the research findings presented here show that the small G protein Arl8b and its effector proteins (RUFY3 and RUFY4) play a wide range of roles in regulating lysosome positioning, motility, size, and organelle membrane fusion events in different cell types.

References

Abu-Remaileh, M., Wyant, G. A., Kim, C., Laqtom, N. N., Abbasi, M., Chan, S. H., Freinkman, E., & Sabatini, D. M. (2017). Lysosomal metabolomics reveals V-ATPase- and mTOR-dependent regulation of amino acid efflux from lysosomes. *Science*, *358*(6364), 807–813. https://doi.org/10.1126/science.aan6298

Aeschlimann, D., & Evans, B. (2004). The vital osteoclast: how is it regulated? *Cell Death and Differentiation*, *11*, 5–7. https://doi.org/10.1038/sj.cdd.4401470

Appelqvist, H., Wäster, P., Kågedal, K., & Öllinger, K. (2013). The lysosome: From waste bag to potential therapeutic target. In *Journal of Molecular Cell Biology* (Vol. 5, Issue 4, pp. 214–226). https://doi.org/10.1093/jmcb/mjt022

Araujo, M. E. G., Liebscher, G., Hess, M. W., & Huber, L. A. (2020). Lysosomal size matters. *Traffic*, *21*(1), 60–75. https://doi.org/10.1111/tra.12714

Arya, S. B., Kumar, G., Kaur, H., Kaur, A., & Tuli, A. (2018). ARL11 regulates lipopolysaccharide-stimulated macrophage activation by promoting mitogen-activated protein kinase (MAPK) signaling. *Journal of Biological Chemistry*, *293*(25). https://doi.org/10.1074/jbc.RA117.000727

Bagshaw, R. D., Callahan, J. W., & Mahuran, D. J. (2006). The Arf-family protein, Arl8b, is involved in the spatial distribution of lysosomes. *Biochemical and Biophysical Research Communications*, *344*(4), 1186–1191. https://doi.org/10.1016/j.bbrc.2006.03.221

Ballabio, A., & Bonifacino, J. S. (2020). Lysosomes as dynamic regulators of cell and organismal homeostasis. In *Nature Reviews Molecular Cell Biology* (Vol. 21, Issue 2, pp. 101–118). Nature Research. https://doi.org/10.1038/s41580-019-0185-4

Bissig, C., Hurbain, I., Raposo, G., & van Niel, G. (2017). PIKfyve activity regulates reformation of terminal storage lysosomes from endolysosomes. *Traffic*, *18*(11), 747–757. https://doi.org/10.1111/tra.12525

Biswas, R. S., Anna Baker, D., Hruska, K. A., & Chellaiah, M. A. (2004). *Polyphosphoinositides-dependent regulation of the osteoclast actin cytoskeleton and bone resorption*. http://www.biomedcentral.com/1471-2121/5/19

Bonifacino, J. S., & Neefjes, J. (2017). Moving and positioning the endolysosomal system. In *Current Opinion in Cell Biology* (Vol. 47, pp. 1–8). Elsevier Ltd. https://doi.org/10.1016/j.ceb.2017.01.008

Borchers, A.-C., Langemeyer, L., & Ungermann, C. (2021). *Who's in control? Principles of Rab GTPase activation in endolysosomal membrane trafficking and beyond*. https://doi.org/10.1083/jcb.202105120

Bowman, S. L., Bi-Karchin, J., Le, L., & Marks, M. S. (2019). *The road to lysosome-related organelles: Insights from Hermansky-Pudlak syndrome and other rare diseases*. https://doi.org/10.1111/tra.12646

Boyce, B. F., & Xing, L. (2008). Functions of RANKL/RANK/OPG in bone modeling and remodeling. In *Archives of Biochemistry and Biophysics* (Vol. 473, Issue 2, pp. 139–146). https://doi.org/10.1016/j.abb.2008.03.018

Braulke, T., & Bonifacino, J. S. (2009). Sorting of lysosomal proteins. *Biochimica et Biophysica Acta - Molecular Cell Research*, *1793*(4), 605–614. https://doi.org/10.1016/j.bbamcr.2008.10.016

Bright, N. A., Davis, L. J., & Luzio, J. P. (2016). Endolysosomes Are the Principal Intracellular Sites of Acid Hydrolase Activity. *Current Biology*, *26*(17), 2233–2245. https://doi.org/10.1016/j.cub.2016.06.046

Cabukusta, B., & Neefjes, J. (2018). Mechanisms of lysosomal positioning and movement. *Traffic*. https://doi.org/10.1111/tra.12587

Cason, S. E., Carman, P. J., Van Duyne, C., Goldsmith, J., Dominguez, R., & Holzbaur, E. L. F. (2021). Sequential dynein effectors regulate axonal autophagosome motility in a maturation-dependent pathway. *Journal of Cell Biology*, *220*(7). https://doi.org/10.1083/jcb.202010179

Char, R., & Pierre, P. (2020). The RUFYs, a Family of Effector Proteins Involved in Intracellular Trafficking and Cytoskeleton Dynamics. *Frontiers in Cell and Developmental Biology*, *8*(August). https://doi.org/10.3389/fcell.2020.00779

Cheng, X. T., Xie, Y. X., Zhou, B., Huang, N., Farfel-Becker, T., & Sheng, Z. H. (2018). Characterization of LAMP1-labeled nondegradative lysosomal and endocytic compartments in neurons. *The Journal of Cell Biology*, *217*(9), 3127–3139. https://doi.org/10.1083/JCB.201711083

Choy, C. H., Saffi, G., Gray, M. A., Wallace, C., Dayam, R. M., Ou, Z. Y. A., Lenk, G., Puertollano, R., Watkins, S. C., & Botelho, R. J. (2018). Lysosome enlargement during inhibition of the lipid kinase PIKfyve proceeds through lysosome coalescence. *Journal of Cell Science*, *131*(10). https://doi.org/10.1242/JCS.213587

Chu, B. B., Liao, Y. C., Qi, W., Xie, C., Du, X., Wang, J., Yang, H., Miao, H. H., Li, B. L., & Song, B. L. (2015). Cholesterol transport through lysosome-peroxisome membrane contacts. *Cell*, *161*(2), 291–306. https://doi.org/10.1016/J.CELL.2015.02.019

Cinti, A., Le Sage, V., Milev, M. P., Valiente-Echeverría, F., Crossie, C., Miron, M.-J., Panté, N., Olivier, M., & Mouland, A. J. (2017a). HIV-1 enhances mTORC1 activity and repositions lysosomes to the periphery by co-opting Rag GTPases. *Scientific Reports*, *7*(1), 5515. https://doi.org/10.1038/s41598-017-05410-0

Cinti, A., Le Sage, V., Milev, M. P., Valiente-Echeverría, F., Crossie, C., Miron, M. J., Panté, N., Olivier, M., & Mouland, A. J. (2017b). HIV-1 enhances mTORC1 activity and repositions lysosomes to the periphery by co-opting Rag GTPases. *Scientific Reports*, *7*(1). https://doi.org/10.1038/s41598-017-05410-0

Coxon, F. P., & Taylor, A. (2008). Vesicular trafficking in osteoclasts. In *Seminars in Cell and Developmental Biology* (Vol. 19, Issue 5, pp. 424–433). https://doi.org/10.1016/j.semcdb.2008.08.004

Crockett, J. C., Rogers, M. J., Coxon, F. P., Hocking, L. J., & Helfrich, M. H. (2011). Bone remodelling at a glance. *Journal of Cell Science*, *124*(7), 991–998. https://doi.org/10.1242/jcs.063032

Dai, R., Wu, Z., Chu, H. Y., Lu, J., Lyu, A., Liu, J., & Zhang, G. (2020). Cathepsin K: The Action in and Beyond Bone. *Frontiers in Cell and Developmental Biology*, *8*, 433. https://doi.org/10.3389/FCELL.2020.00433/BIBTEX

Deselm, C. J., Miller, B. C., Zou, W., Beatty, W. L., Van Meel, E., Takahata, Y., Klumperman, J., Tooze, S. A., Teitelbaum, S. L., & Virgin, H. W. (2011). Autophagy Proteins Regulate the Secretory Component of Osteoclastic Bone Resorption. *Developmental Cell*, *21*, 966–974. https://doi.org/10.1016/j.devcel.2011.08.016

Diwu, Z., Chen, C. S., Zhang, C., Klaubert, D. H., & Haugland, R. P. (1999). A novel acidotropic pH indicator and its potential application in labeling acidic organelles of live cells. *Chemistry & Biology*, *6*(7), 411–418. https://doi.org/10.1016/S1074-5521(99)80059-3

Donaldson, J. G., & Jackson, C. L. (2011). ARF family G proteins and their regulators: roles in membrane transport, development and disease. *Nature Reviews Molecular Cell Biology 2011 12:6*, *12*(6), 362–375. https://doi.org/10.1038/nrm3117

Du, W., Su, Q. P., Chen, Y., Zhu, Y., Jiang, D., Rong, Y., Zhang, S., Zhang, Y., Ren, H., Zhang, C., Wang, X., Gao, N., Wang, Y., Sun, L., Sun, Y., & Yu, L. (2016). Kinesin 1 Drives Autolysosome Tubulation. *Developmental Cell*, *37*(4), 326–336. https://doi.org/10.1016/j.devcel.2016.04.014

Dykes, S. S., Gray, A. L., Coleman, D. T., Saxena, M., Stephens, C. A., Carroll, J. L., Pruitt, K., & Cardelli, J. A. (2016). The Arf-like GTPase Arl8b is essential for three-dimensional invasive growth of prostate cancer <i>in vitro</i> and xenograft formation and growth <i>in vivo</i> *Oncotarget*, *7*(21), 31037–31052. https://doi.org/10.18632/oncotarget.8832

Ebner, M., & Koch, P. A. (2019). *Phosphoinositides in the control of lysosome function and homeostasis*. *August*. https://doi.org/10.1042/BST20190158

Feng, X. (2005). RANKing Intracellular Signaling in Osteoclasts. *IUBMB Life (International Union of Biochemistry and Molecular Biology: Life)*, *57*(6), 389–395. https://doi.org/10.1080/15216540500137669

Fennelly, C., & Amaravadi, R. K. (2017). Lysosomal Biology in Cancer. *Methods in Molecular Biology (Clifton, N.J.)*, *1594*, 293–308. https://doi.org/10.1007/978-1-4939-6934-0_19

Filipek, P. A., de Araujo, M. E. G., Vogel, G. F., De Smet, C. H., Eberharter, D., Rebsamen, M., Rudashevskaya, E. L., Kremser, L., Yordanov, T., Tschaikner, P., Fürnrohr, B. G., Lechner, S., Dunzendorfer-Matt, T., Scheffzek, K., Bennett, K. L., Superti-Furga, G., Lindner, H. H., Stasyk, T., & Huber, L. A. (2017). LAMTOR/Ragulator is a negative regulator of Arl8b- and BORC-dependent late endosomal positioning. *The Journal of Cell Biology*, *216*(12), 4199–4215. https://doi.org/10.1083/jcb.201703061

Fink Eriksen, E. (2010). *Cellular mechanisms of bone remodeling*. https://doi.org/10.1007/s11154-010-9153-1

Fujiwara, T., Ye, S., Castro-Gomes, T., Winchell, C. G., Andrews, N. W., Voth, D. E., Varughese, K. I., Mackintosh, S. G., Feng, Y., Pavlos, N., Nakamura, T., Manolagas, S. C., & Zhao, H. (2016). PLEKHM1/DEF8/RAB7 complex regulates lysosome positioning and bone homeostasis. *JCI Insight*, *1*(17). https://doi.org/10.1172/jci.insight.86330

Fukuda, M. (2016). Lysosome-Related Organelles. *Encyclopedia of Cell Biology*, *2*, 235–242. https://doi.org/10.1016/B978-0-12-394447-4.20020-5

Gan, Q., Wang, X., Zhang, Q., Yin, Q., Jian, Y., Liu, Y., Xuan, N., Li, J., Zhou, J., Liu, K., Jing, Y., Wang, X., & Yang, C. (2019). *The amino acid transporter SLC-36.1 cooperates with PtdIns3P 5-kinase to control phagocytic lysosome reformation Phagocytic removal of apoptotic cells involves formation, maturation, and digestion of cell corpse-containing phagosomes*. https://doi.org/10.1083/jcb.201901074

Garg, S., Sharma, M., Ung, C., Tuli, A., Barral, D. C., Hava, D. L., Veerapen, N., Besra, G. S., Hacohen, N., & Brenner, M. B. (2011). Lysosomal Trafficking, Antigen Presentation, and Microbial Killing Are Controlled by the Arf-like GTPase Arl8b. *Immunity*, *35*(2), 182–193. https://doi.org/10.1016/j.immuni.2011.06.009

Gelman, A., & Elazar, Z. (2011). Autophagic factors cut to the bone. In *Developmental Cell*. https://doi.org/10.1016/j.devcel.2011.10.021

Ghosh, S., Dellibovi-Ragheb, T. A., Kerviel, A., Pak, E., Qiu, Q., Fisher, M., Takvorian, P. M., Bleck, C., Hsu, V. W., Fehr, A. R., Perlman, S., Achar, S. R., Straus, M. R., Whittaker, G. R., de Haan, C. A. M., Kehrl, J., Altan-Bonnet, G., & Altan-Bonnet, N. (2020). β-Coronaviruses Use Lysosomes for Egress Instead of the Biosynthetic Secretory Pathway. *Cell*, *183*(6), 1520. https://doi.org/10.1016/J.CELL.2020.10.039

Granger, E., McNee, G., Allan, V., & Woodman, P. (2014). The role of the cytoskeleton and molecular motors in endosomal dynamics. In *Seminars in Cell and Developmental Biology* (Vol. 31, pp. 20–29). Elsevier Ltd. https://doi.org/10.1016/j.semcdb.2014.04.011

Gruenberg, J., Griffiths, G., & Howell, K. E. (1989). Characterization of the early endosome and putative endocytic carrier vesicles in vivo and with an assay of vesicle fusion in vitro. *Journal of Cell Biology*, *108*(4), 1301–1316. https://doi.org/10.1083/jcb.108.4.1301

Guardia, C. M., Farías, G. G., Jia, R., Pu, J., Bonifacino Correspondence, J. S., & Bonifacino, J. S. (2016). BORC Functions Upstream of Kinesins 1 and 3 to Coordinate Regional Movement of Lysosomes along Different Microtubule Tracks. *CellReports*, *17*, 1950–1961. https://doi.org/10.1016/j.celrep.2016.10.062

Guha, S., Coffey, E. E., Lu, W., Lim, J. C., Beckel, J. M., Laties, A. M., Boesze-Battaglia, K., & Mitchell, C. H. (2014). Approaches for detecting lysosomal alkalinization and impaired degradation in fresh and cultured RPE cells: Evidence for a role in retinal degenerations. *Experimental Eye Research*, *126*, 68–76. https://doi.org/10.1016/j.exer.2014.05.013

Heckmann, B. L., & Green, D. R. (2019). LC3-associated phagocytosis at a glance. In *Journal of cell science* (Vol. 132, Issue 5). NLM (Medline). https://doi.org/10.1242/jcs.222984

Heuser, J. (1989). Changes in Lysosome Shape and Distribution Correlated with Changes in Cytoplasmic pH. In *The Journal of Cell Biology* (Vol. 108). https://rupress.org/jcb/article-pdf/108/3/855/377552/855.pdf

Hirokawa, N., Noda, Y., Tanaka, Y., & Niwa, S. (2009a). Kinesin superfamily motor proteins and intracellular transport. In *Nature Reviews Molecular Cell Biology* (Vol. 10, Issue 10, pp. 682–696). https://doi.org/10.1038/nrm2774

Hofmann, I., & Munro, S. (2006). An N-terminally acetylated Arf-like GTPase is localised to lysosomes and affects their motility. *Journal of Cell Science*, *119*(8), 1494–1503. https://doi.org/10.1242/jcs.02958

Homma, Y., Hiragi, S., & Fukuda, M. (2021). Rab family of small GTPases: an updated view on their regulation and functions. *The FEBS Journal*, *288*(1), 36–55. https://doi.org/10.1111/FEBS.15453

Hong, Z., Pedersen, N. M., Wang, L., Torgersen, M. L., Stenmark, H., & Raiborg, C. (2017). PtdIns3P controls mTORC1 signaling through lysosomal positioning. *The Journal of Cell Biology*, *216*(12), 4217–4233. https://doi.org/10.1083/jcb.201611073

Hunt, S. D., & Stephens, D. J. (2011). The role of motor proteins in endosomal sorting. *Biochemical Society Transactions*, *39*(5), 1179–1184. https://doi.org/10.1042/BST0391179

Huotari, J., & Helenius, A. (2011). Endosome maturation. In *EMBO Journal* (Vol. 30, Issue 17, pp. 3481–3500). https://doi.org/10.1038/emboj.2011.286

Inpanathan, S., & Botelho, R. J. (2019). The Lysosome Signaling Platform: Adapting With the Times. *Frontiers in Cell and Developmental Biology*, *7*, 113. https://doi.org/10.3389/fcell.2019.00113

Jean Gruenberg and herald stenmark. (2004). The biogenesis ofmultivesicular endosomes. *Nature PublishingGroup*, *2004*, 352. www.nature.com/reviews/molcellbio

Jia, R., Guardia, C. M., Pu, J., Chen, Y., & Bonifacino, J. S. (2017). BORC coordinates encounter and fusion of lysosomes with autophagosomes. *Autophagy*, *13*(10), 1648–1663. https://doi.org/10.1080/15548627.2017.1343768

Johansson, M., Rocha, N., Zwart, W., Jordens, I., Janssen, L., Kuijl, C., Olkkonen, V. M., & Neefjes, J. (2007). Activation of endosomal dynein motors by stepwise assembly of Rab7-RILP-p150Glued, ORP1L, and the receptor betalll spectrin. *The Journal of Cell Biology*, *176*(4), 459–471. https://doi.org/10.1083/JCB.200606077

Johnson, D. E., Ostrowski, P., Jaumouillé, V., & Grinstein, S. (2016). The position of lysosomes within the cell determines their luminal pH. *The Journal of Cell Biology*, *212*(6), 677–692. https://doi.org/10.1083/jcb.201507112

Jongsma, M. L., Bakker, J., Cabukusta, B., Liv, N., Elsland, D. van, Fermie, J., Akkermans, J. L., Kuijl, C., Zanden, S. Y. van der, Janssen, L., Hoogzaad, D., Kant, R. van der, Wijdeven, R. H., Klumperman, J., Berlin, I., & Neefjes, J. (2020). SKIP-HOPS recruits TBC1D15 for a Rab7-to-Arl8b identity switch to control late endosome transport. *The EMBO Journal*. https://doi.org/10.15252/embj.2019102301

Jongsma, M. L. M., Berlin, I., Wijdeven, R. H. M., Van Veelen, P. A., Spaapen, R. M., Neefjes, J., Janssen, L., Janssen, G. M. C., Garstka, M. A., Janssen, H., & Mensink, M. (2016). An ER-Associated Pathway Defines Endosomal Architecture for Controlled Cargo Transport Article An ER-Associated

Pathway Defines Endosomal Architecture for Controlled Cargo Transport. *Cell*, *166*, 152–166. https://doi.org/10.1016/j.cell.2016.05.078

Jordens, I., Fernandez-Borja, M., Marsman, M., Dusseljee, S., Janssen, L., Calafat, J., Janssen, H., Wubbolts, R., & Neefjes, J. (2001). The Rab7 effector protein RILP controls lysosomal transport by inducing the recruitment of dynein-dynactin motors. *Current Biology*, *11*(21), 1680–1685. https://doi.org/10.1016/S0960-9822(01)00531-0

Joseph, J., Tan, S. H., Karpova, T. S., McNally, J. G., & Dasso, M. (2002). SUMO-1 targets RanGAP1 to kinetochores and mitotic spindles. *The Journal of Cell Biology*, *156*(4), 595–602. https://doi.org/10.1083/JCB.200110109

Kane, P. M. (2006). The where, when, and how of organelle acidification by the yeast vacuolar H+-ATPase. *Microbiology and Molecular Biology Reviews : MMBR*, *70*(1), 177–191. https://doi.org/10.1128/MMBR.70.1.177-191.2006

Kenkre, J. S., & Bassett, J. H. D. (2018). The bone remodelling cycle. In *Annals of Clinical Biochemistry* (Vol. 55, Issue 3, pp. 308–327). https://doi.org/10.1177/0004563218759371

Keren-Kaplan, T., & Bonifacino, J. S. (2021). ARL8 Relieves SKIP Autoinhibition to Enable Coupling of Lysosomes to Kinesin-1. *Current Biology*, *31*(3), 540-554.e5. https://doi.org/10.1016/j.cub.2020.10.071

Kesisova, I. A., Robinson, B. P., & Spiliotis, E. T. (2021). A septin GTPase scaffold of dynein–dynactin motors triggers retrograde lysosome transport. *Journal of Cell Biology*, *220*(2). https://doi.org/10.1083/JCB.202005219

Khatter, D., Raina, V. B., Dwivedi, D., Sindhwani, A., Bahl, S., & Sharma, M. (2015). The small GTPase Arl8b regulates assembly of the mammalian HOPS complex on lysosomes. *Journal of Cell Science*, *128*(9), 1746–1761. https://doi.org/10.1242/jcs.162651

Khatter, D., Sindhwani, A., & Sharma, M. (2015). Arf-like GTPase Arl8: Moving from the periphery to the center of lysosomal biology. *Cellular Logistics*, *5*(3). https://doi.org/10.1080/21592799.2015.1086501

Kim, J. H., & Kim, N. (2016). *Signaling Pathways in Osteoclast Differentiation*. 12–17.

Kim, J. M., Lin, C., Stavre, Z., Greenblatt, M. B., & Shim, J. H. (2020). Osteoblast-Osteoclast Communication and Bone Homeostasis. *Cells*, *9*(9), 1–14. https://doi.org/10.3390/cells9092073

Kimura, S., Noda, T., & Yoshimori, T. (2008). Dynein-dependent Movement of Autophagosomes Mediates Efficient Encounters with Lysosomes. In *CELL STRUCTURE AND FUNCTION* (Vol. 33). http://rsb.info.nih.gov/ij/

Kitagishi, Y., & Matsuda, S. (2013). RUFY, rab and rap family proteins involved in a regulation of cell polarity and membrane trafficking. *International Journal of Molecular Sciences*, *14*(3), 6487–6498. https://doi.org/10.3390/ijms14036487

Kjos, I., Vestre, K., Guadagno, N. A., Borg Distefano, M., & Progida, C. (2018). Rab and Arf proteins at the crossroad between membrane transport and cytoskeleton dynamics. In *Biochimica et Biophysica Acta - Molecular Cell Research* (Vol. 1865, Issue 10, pp. 1397–1409). Elsevier B.V. https://doi.org/10.1016/j.bbamcr.2018.07.009

Klionsky, D. J., Abdel-Aziz, A. K., Abdelfatah, S., Abdellatif, M., Abdoli, A., Abel, S., Abeliovich, H., Abildgaard, M. H., Abudu, Y. P., Acevedo-Arozena, A., Adamopoulos, I. E., Adeli, K., Adolph, T. E., Adornetto, A., Aflaki, E., Agam, G., Agarwal, A., Aggarwal, B. B., Agnello, M., … Tong, C. K. (2021). Guidelines for the use and interpretation of assays for monitoring autophagy (4th edition) 1. *Autophagy*, *17*(1), 1–382. https://doi.org/10.1080/15548627.2020.1797280

Komori, T. (2020). Functions of Osteocalcin in Bone, Pancreas, Testis, and Muscle. *International Journal of Molecular Sciences*, *21*(20), 1–15. https://doi.org/10.3390/IJMS21207513

Korolchuk, V. I., Saiki, S., Lichtenberg, M., Siddiqi, F. H., Roberts, E. A., Imarisio, S., Jahreiss, L., Sarkar, S., Futter, M., Menzies, F. M., O'Kane, C. J., Deretic, V., & Rubinsztein, D. C. (2011a). Lysosomal positioning coordinates cellular nutrient responses. *Nature Cell Biology*, *13*(4), 453–462. https://doi.org/10.1038/ncb2204

Korolchuk, V. I., Saiki, S., Lichtenberg, M., Siddiqi, F. H., Roberts, E. A., Imarisio, S., Jahreiss, L., Sarkar, S., Futter, M., Menzies, F. M., O'Kane, C. J., Deretic, V.,

& Rubinsztein, D. C. (2011b). Lysosomal positioning coordinates cellular nutrient responses. *Nature Cell Biology*, *13*(4), 453–462. https://doi.org/10.1038/ncb2204

Kumar, G., Arya, S., & Tuli, A. (2018). Method for Studying the Effect of Gene Silencing on Bacterial Infection-induced ERK1/2 Signaling in Bone-marrow Derived Macrophages. *Bio-Protocol*, *8*(24), 1–16. https://doi.org/10.21769/bioprotoc.3123

Kumar, G., Chawla, P., Dhiman, N., Chadha, S., Sharma, S., Sethi, K., Sharma, M., & Tuli, A. (2022). RUFY3 links Arl8b and JIP4-Dynein complex to regulate lysosome size and positioning. *Nature Communications*, *13*(1), 1–21. https://doi.org/10.1038/s41467-022-29077-y

Lacombe, J., Karsenty, G., & Ferron, M. (2013). Regulation of lysosome biogenesis and functions in osteoclasts. *Cell Cycle*, *12*(17), 2744–2752. https://doi.org/10.4161/cc.25825

Lafourcade, C., Sobo, K., Kieffer-Jaquinod, S., Garin, J., & van der Goot, F. G. (2008). Regulation of the V-ATPase along the endocytic pathway occurs through reversible subunit association and membrane localization. *PloS One*, *3*(7). https://doi.org/10.1371/JOURNAL.PONE.0002758

Laopanupong, T., Prombutara, P., Kanjanasirirat, P., Benjaskulluecha, S., Boonmee, A., Palaga, T., Méresse, S., Paha, J., Siregar, T. A. P., Khumpanied, T., Borwornpinyo, S., Chaiprasert, A., Utaisincharoen, P., & Ponpuak, M. (2021). Lysosome repositioning as an autophagy escape mechanism by Mycobacterium tuberculosis Beijing strain. *Scientific Reports 2021 11:1*, *11*(1), 1–17. https://doi.org/10.1038/s41598-021-83835-4

Lawrence, R. E., & Zoncu, R. (2019). The lysosome as a cellular centre for signalling, metabolism and quality control. *NaTuRE CELL BioLogy* |, *21*, 133–142. https://doi.org/10.1038/s41556-018-0244-7

Lee, H. K., Mattei, L. M., Steinberg, B. E., Alberts, P., Lee, Y. H., Chervonsky, A., Mizushima, N., Grinstein, S., & Iwasaki, A. (2010). In Vivo Requirement for Atg5 in Antigen Presentation by Dendritic Cells. *Immunity*, *32*(2), 227–239. https://doi.org/10.1016/j.immuni.2009.12.006

Lee, N. K. (2010). Molecular Understanding of Osteoclast Differentiation and

Physiology. *Endocrinol Metab*, *25*(4), 264–269. https://doi.org/10.3803/EnM.2010.25.4.264

Lee, N. K. (2017). RANK Signaling Pathways and Key Molecules Inducing Osteoclast Differentiation. *Biomedical Science Letters*, *23*(4), 295–302. https://doi.org/10.15616/BSL.2017.23.4.295

Levine, B., & Kroemer, G. (2019). Leading Edge Review Biological Functions of Autophagy Genes: A Disease Perspective. *Cell*, *176*, 11–42. https://doi.org/10.1016/j.cell.2018.09.048

Li, X., Rydzewski, N., Hider, A., Zhang, X., Yang, J., Wang, W., Gao, Q., Cheng, X., & Xu, H. (2016). A molecular mechanism to regulate lysosome motility for lysosome positioning and tubulation. *Nature Cell Biology*, *18*(4), 404–417. https://doi.org/10.1038/ncb3324

Lim, C. Y., & Zoncu, R. (2016). The lysosome as a command-and-control center for cellular metabolism. In *Journal of Cell Biology*. https://doi.org/10.1083/jcb.201607005

Liu, K., Jian, Y., Sun, X., Yang, C., Gao, Z., Zhang, Z., Liu, X., Li, Y., Xu, J., Jing, Y., Mitani, S., He, S., & Yang, C. (2016). Negative regulation of phosphatidylinositol 3-phosphate levels in early-to-late endosome conversion. *Journal of Cell Biology*, *212*(2), 181–198. https://doi.org/10.1083/jcb.201506081

Lomaga, M. A., Yeh, W.-C., Sarosi, I., Duncan, G. S., Furlonger, C., Ho, A., Morony, S., Capparelli, C., Van, G., Kaufman, S., Van Der Heiden, A., Itie, A., Wakeham, A., Khoo, W., Sasaki, T., Cao, Z., Penninger, J. M., Paige, C. J., Lacey, D. L., … Mak, T. W. (1999). *TRAF6 deficiency results in osteopetrosis and defective interleukin-1, CD40, and LPS signaling*. www.genesdev.org

Lu, M., van Tartwijk, F. W., Lin, J. Q., Nijenhuis, W., Parutto, P., Fantham, M., Christensen, C. N., Avezov, E., Holt, C. E., Tunnacliffe, A., Holcman, D., Kapitein, L., Schierle, G. S. K., & Kaminski, C. F. (2020). The structure and global distribution of the endoplasmic reticulum network are actively regulated by lysosomes. *Science Advances*, *6*(51), eabc7209. https://doi.org/10.1126/sciadv.abc7209

Luxenburg, C., Geblinger, D., Klein, E., Anderson, K., Hanein, D., Geiger, B., &

Addadi, L. (2007). The Architecture of the Adhesive Apparatus of Cultured Osteoclasts: From Podosome Formation to Sealing Zone Assembly. *PLoS ONE*, *2*(1), e179. https://doi.org/10.1371/journal.pone.0000179

Luzio, J. P., Hackmann, Y., Dieckmann, N. M. G., & Griffiths, G. M. (2014). The Biogenesis of Lysosomes and Lysosome-Related Organelles. *Cold Spring Harbor Perspectives in Biology*, *6*(9), a016840–a016840. https://doi.org/10.1101/cshperspect.a016840

Ma, L., Ouyang, Q., Werthmann, G. C., Thompson, H. M., & Morrow, E. M. (2017). Live-cell microscopy and fluorescence-based measurement of luminal pH in intracellular organelles. *Frontiers in Cell and Developmental Biology*, *5*(AUG). https://doi.org/10.3389/fcell.2017.00071

Marchesin, V., Castro-Castro, A., Lodillinsky, C., Castagnino, A., Cyrta, J., Bonsang-Kitzis, H., Fuhrmann, L., Irondelle, M., Infante, E., Montagnac, G., Reyal, F., Vincent-Salomon, A., & Chavrier, P. (2015). ARF6-JIP3/4 regulate endosomal tubules for MT1-MMP exocytosis in cancer invasion. *The Journal of Cell Biology*, *211*(2), 339–358. https://doi.org/10.1083/JCB.201506002

Marino, S., Logan, J. G., Mellis, D., & Capulli, M. (2014). Generation and culture of osteoclasts. *BoneKEy Reports*, *3*. https://doi.org/10.1038/bonekey.2014.65

Marwaha, R., Arya, S. B., Jagga, D., Kaur, H., Tuli, A., & Sharma, M. (2017a). The Rab7 effector PLEKHM1 binds Arl8b to promote cargo traffic to lysosomes. *The Journal of Cell Biology*, *216*(4), 1051–1070. https://doi.org/10.1083/jcb.201607085

Marwaha, R., Arya, S. B., Jagga, D., Kaur, H., Tuli, A., & Sharma, M. (2017b). The Rab7 effector PLE KHM1 binds Arl8b to promote cargo traffic to lysosomes. *Journal of Cell Biology*, *216*(4), 1051–1070. https://doi.org/10.1083/jcb.201607085

Matsumoto, N., Sekiya, M., Tohyama, K., Ishiyama-Matsuura, E., Sun-Wada, G.-H., Wada, Y., Futai, M., & Nakanishi-Matsui, M. (2018). Essential Role of the a3 Isoform of V-ATPase in Secretory Lysosome Trafficking via Rab7 Recruitment OPEN. *ScienTific REPORtS* |, *8*, 6701. https://doi.org/10.1038/s41598-018-24918-7

Matte, U., & Pasqualim, G. (2016). Lysosome: The story beyond the storage. In *Journal*

of Inborn Errors of Metabolism and Screening (Vol. 4). SAGE Publications Inc. https://doi.org/10.1177/2326409816679431

McGrath, M. J., Eramo, M. J., Gurung, R., Sriratana, A., Gehrig, S. M., Lynch, G. S., Lourdes, S. R., Koentgen, F., Feeney, S. J., Lazarou, M., McLean, C. A., & Mitchell, C. A. (2021). Defective lysosome reformation during autophagy causes skeletal muscle disease. *Journal of Clinical Investigation*, *131*(1). https://doi.org/10.1172/JCI135124

Meneses-Salas, E., García-Melero, A., Kanerva, K., Blanco-Muñoz, P., Morales-Paytuvi, F., Bonjoch, J., Casas, J., Egert, A., Beevi, S. S., Jose, J., Llorente-Cortés, V., Rye, K. A., Heeren, J., Lu, A., Pol, A., Tebar, F., Ikonen, E., Grewal, T., Enrich, C., & Rentero, C. (2020). Annexin A6 modulates TBC1D15/Rab7/StARD3 axis to control endosomal cholesterol export in NPC1 cells. *Cellular and Molecular Life Sciences*, *77*(14), 2839–2857. https://doi.org/10.1007/S00018-019-03330-Y

Michelet, X., Tuli, A., Gan, H., Geadas, C., Sharma, M., Remold, H. G., & Brenner, M. B. (2018). Lysosome-Mediated Plasma Membrane Repair Is Dependent on the Small GTPase Arl8b and Determines Cell Death Type in Mycobacterium tuberculosis Infection. *The Journal of Immunology*, ji1700829. https://doi.org/10.4049/jimmunol.1700829

Miyamoto, T. (2011). Regulators of Osteoclast Differentiation and Cell-Cell Fusion. In *Keio J Med* (Vol. 60, Issue 4). https://www.jstage.jst.go.jp/article/kjm/60/4/60_4_101/_pdf/-char/en

Mohamed, A. M. F. S. (2008). An Overview of Bone Cells and their Regulating Factors of Differentiation. *The Malaysian Journal of Medical Sciences : MJMS*, *15*(1), 4. /pmc/articles/PMC3341892/

Mrakovic, A., Kay, J. G., Furuya, W., Brumell, J. H., & Botelho, R. J. (2012). Rab7 and Arl8 GTPases are Necessary for Lysosome Tubulation in Macrophages. *Traffic*, *13*(12), 1667–1679. https://doi.org/10.1111/tra.12003

Mulari, M. T. K., Zhao, H., Lakkakorpi, P. T., & Väänänen, H. K. (2003). Osteoclast Ruffled Border Has Distinct Subdomains for Secretion and Degraded Matrix Uptake. *Traffic*, *4*(2), 113–125. https://doi.org/10.1034/j.1600-0854.2003.40206.x

Nakamura, S., & Yoshimori, T. (2017). New insights into autophagosome–lysosome fusion. *Journal of Cell Science*, *130*(7), 1209–1216. https://doi.org/10.1242/jcs.196352

Naslavsky, N., & Caplan, S. (2018). The enigmatic endosome - Sorting the ins and outs of endocytic trafficking. In *Journal of Cell Science* (Vol. 131, Issue 13). Company of Biologists Ltd. https://doi.org/10.1242/jcs.216499

Neefjes, J., Jongsma, M. M. L., & Berlin, I. (2017). Stop or Go? Endosome Positioning in the Establishment of Compartment Architecture, Dynamics, and Function. *Trends in Cell Biology*, *27*, 580–594. https://doi.org/10.1016/j.tcb.2017.03.002

Ohmae, S., Noma, N., Toyomoto, M., Shinohara, M., Takeiri, M., Fuji, H., Takemoto, K., Iwaisako, K., Fujita, T., Takeda, N., Kawatani, M., Aoyama, M., Hagiwara, M., Ishihama, Y., & Asagiri, M. (2017). Actin-binding protein coronin 1A controls osteoclastic bone resorption by regulating lysosomal secretion of cathepsin K. *Scientific Reports*, *7*, 41710. https://doi.org/10.1038/srep41710

Olenick, M. A., & Holzbaur, E. L. F. (2019). Cell science at a glance dynein activators and adaptors at a glance. *Journal of Cell Science*, *132*(6). https://doi.org/10.1242/jcs.227132

Oyarzún, J. E., Lagos, J., Vázquez, M. C., Valls, C., De la Fuente, C., Yuseff, M. I., Alvarez, A. R., & Zanlungo, S. (2019). Lysosome motility and distribution: Relevance in health and disease. *Biochimica et Biophysica Acta - Molecular Basis of Disease*, *1865*(6), 1076–1087. https://doi.org/10.1016/J.BBADIS.2019.03.009

Pankiv, S., Alemu, E. A., Brech, A., Bruun, J. A., Lamark, T., Øvervatn, A., Bjørkøy, G., & Johansen, T. (2010). FYCO1 is a Rab7 effector that binds to LC3 and PI3P to mediate microtubule plus end - Directed vesicle transport. *Journal of Cell Biology*. https://doi.org/10.1083/jcb.200907015

Pavlos, N. J., Cheng, T. S., Qin, A., Ng, P. Y., Feng, H.-T., Ang, E. S. M., Carrello, A., Sung, C.-H., Jahn, R., Zheng, M.-H., & Xu, J. (2011). Tctex-1, a Novel Interaction Partner of Rab3D, Is Required for Osteoclastic Bone Resorption. *Molecular and Cellular Biology*, *31*(7), 1551. https://doi.org/10.1128/MCB.00834-10

Pedersen, N. M., Wenzel, E. M., Wang, L., Antoine, S., Chavrier, P., Stenmark, H., & Raiborg, C. (2020). Protrudin-mediated ER–endosome contact sites promote MT1-MMP exocytosis and cell invasion. *Journal of Cell Biology*, *219*(8). https://doi.org/10.1083/JCB.202003063/VIDEO-1

Perera, R. M., & Zoncu, R. (2016). The Lysosome as a Regulatory Hub. *Annual Review of Cell and Developmental Biology*, *32*(1), 223–253. https://doi.org/10.1146/annurev-cellbio-111315-125125

Podinovskaia, M., Prescianotto-Baschong, C., Buser, D. P., & Spang, A. (2021). A novel live-cell imaging assay reveals regulation of endosome maturation. *ELife*, *10*, 1–32. https://doi.org/10.7554/eLife.70982

Pols, M. S., van Meel, E., Oorschot, V., ten Brink, C., Fukuda, M., Swetha, M., Mayor, S., & Klumperman, J. (2013). ARTICLE hVps41 and VAMP7 function in direct TGN to late endosome transport of lysosomal membrane proteins. *Nature Communications*. https://doi.org/10.1038/ncomms2360

Ponsford, A. H., Ryan, T. A., Raimondi, A., Cocucci, E., Wycislo, S. A., Fröhlich, F., Swan, L. E., & Stagi, M. (2020). Live imaging of intra-lysosome pH in cell lines and primary neuronal culture using a novel genetically encoded biosensor. *Autophagy*, *00*(00), 1–19. https://doi.org/10.1080/15548627.2020.1771858

Poüs, C., & Codogno, P. (2011). Lysosome positioning coordinates mTORC1 activity and autophagy. *Nature Publishing Group*, *13*. https://doi.org/10.1038/ncb2229

Pryor, P. R., Mullock, B. M., Bright, N. A., Gray, S. R., & Luzio, J. P. (2000). The role of intraorganellar Ca2+ in late endosome-lysosome heterotypic fusion and in the reformation of lysosomes from hybrid organelles. *Journal of Cell Biology*, *149*(5), 1053–1062. https://doi.org/10.1083/jcb.149.5.1053

Pu, J., Guardia, C. M., Keren-Kaplan, T., & Bonifacino, J. S. (2016). Mechanisms and functions of lysosome positioning. *Journal of Cell Science*. https://doi.org/10.1242/jcs.196287

Pu, J., Keren-Kaplan, T., & Bonifacino, J. S. (2017). A Ragulator-BORC interaction controls lysosome positioning in response to amino acid availability. *Journal of Cell Biology*, *216*(12), 4183–4197. https://doi.org/10.1083/jcb.201703094

Pu, J., Schindler, C., Jia, R., Jarnik, M., Backlund, P., & Bonifacino, J. S. (2015). BORC, a Multisubunit Complex that Regulates Lysosome Positioning. *Developmental Cell*, *33*(2), 176–188. https://doi.org/10.1016/j.devcel.2015.02.011

Rabanal-Ruiz, Y., Byron, A., Wirth, A., Madsen, R., Sedlackova, L., Hewitt, G., Nelson, G., Stingele, J., Wills, J. C., Zhang, T., Zeug, A., Fässler, R., Vanhaesebroeck, B., Maddocks, O. D. K., Ponimaskin, E., Carroll, B., & Korolchuk, V. I. (2021). mTORC1 activity is supported by spatial association with focal adhesions. *Journal of Cell Biology*, *220*(5). https://doi.org/10.1083/JCB.202004010/VIDEO-1

Raiborg, C. (2018). How Nutrients Orchestrate Lysosome Positioning. *Contact*, *1*, 251525641875611. https://doi.org/10.1177/2515256418756111

Raiborg, C., Wenzel, E. M., Pedersen, N. M., Olsvik, H., Schink, K. O., Schultz, S. W., Vietri, M., Nisi, V., Bucci, C., Brech, A., Johansen, T., & Stenmark, H. (2015). Repeated ER-endosome contacts promote endosome translocation and neurite outgrowth. *Nature*, *520*(7546), 234–238. https://doi.org/10.1038/nature14359

Reggiori, F., & Ungermann, C. (2017). Autophagosome Maturation and Fusion. *Journal of Molecular Biology*, *429*(4), 486–496. https://doi.org/10.1016/j.jmb.2017.01.002

Reiner, D. J., & Lundquist, E. A. (2016). Small GTPases. *WormBook : The Online Review of C. Elegans Biology*, *108*. https://doi.org/10.1002/ejoc.201200111

Rink, J., Ghigo, E., Kalaidzidis, Y., & Zerial, M. (2005). Rab conversion as a mechanism of progression from early to late endosomes. *Cell*, *122*(5), 735–749. https://doi.org/10.1016/J.CELL.2005.06.043

Rishal, I., Kam, N., Perry, R. B. T., Shinder, V., Fisher, E. M. C., Schiavo, G., & Fainzilber, M. (2012). A Motor-Driven Mechanism for Cell-Length Sensing. *Cell Reports*, *1*(6), 608. https://doi.org/10.1016/J.CELREP.2012.05.013

Rojas, R., Van Vlijmen, T., Mardones, G. A., Prabhu, Y., Rojas, A. L., Mohammed, S., Heck, A. J. R., Raposo, G., Van Der Sluijs, P., & Bonifacino, J. S. (2008). Regulation of retromer recruitment to endosomes by sequential action of Rab5 and Rab7. *The Journal of Cell Biology*, *183*(3), 513–526. https://doi.org/10.1083/JCB.200804048

Rosa-Ferreira, C., & Munro, S. (2011). Arl8 and SKIP Act Together to Link Lysosomes to Kinesin-1. *Developmental Cell*. https://doi.org/10.1016/j.devcel.2011.10.007

Ross, F. P. (2009). Osteoclast Biology and Bone Resorption. *Primer on the Metabolic Bone Diseases and Disorders of Mineral Metabolism: Seventh Edition*, 16–22. https://doi.org/10.1002/9780470623992.ch3

Roy, M., & Roux, S. (2020). Rab GTPases in Osteoclastic Bone Resorption and Autophagy. *International Journal of Molecular Sciences*, *21*(20), 7655. https://doi.org/10.3390/ijms21207655

Rucci, N., & Teti, A. (2016). The "love–hate" relationship between osteoclasts and bone matrix. *Matrix Biology*, *52–54*, 176–190. https://doi.org/10.1016/J.MATBIO.2016.02.009

Rui Jia, A., & Bonifacino, J. S. (2019). Lysosome Positioning Influences mTORC2 and AKT Signaling. *Molecular Cell*, *75*, 1–13. https://doi.org/10.1016/j.molcel.2019.05.009

Sabatini, D. D., & Adesnik, M. (2013). Christian de Duve: Explorer of the cell who discovered new organelles by using a centrifuge. *Proceedings of the National Academy of Sciences*. https://doi.org/10.1073/pnas.1312084110

Saftig, P., & Klumperman, J. (2009). *Lysosome biogenesis and lysosomal membrane proteins: trafficking meets function*. https://doi.org/10.1038/nrm2745

Saitoh, S. I., Abe, F., Kanno, A., Tanimura, N., Mori Saitoh, Y., Fukui, R., Shibata, T., Sato, K., Ichinohe, T., Hayashi, M., Kubota, K., Kozuka-Hata, H., Oyama, M., Kikko, Y., Katada, T., Kontani, K., & Miyake, K. (2017). TLR7 mediated viral recognition results in focal type i interferon secretion by dendritic cells. *Nature Communications*, *8*(1). https://doi.org/10.1038/s41467-017-01687-x

Sapmaz, A., Berlin, I., Bos, E., Wijdeven, R. H., Janssen, H., Konietzny, R., Akkermans, J. J., Erson-Bensan, A. E., Koning, R. I., Kessler, B. M., Neefjes, J., & Ovaa, H. (2019). USP32 regulates late endosomal transport and recycling through deubiquitylation of Rab7. *Nature Communications*, *10*(1). https://doi.org/10.1038/S41467-019-09437-X

Saric, A., Hipolito, V. E. B., Kay, J. G., Canton, J., Antonescu, C. N., & Botelho, R. J. (2015). mTOR controls lysosome tubulation and antigen presentation in macrophages and dendritic cells. *Molecular Biology of the Cell*, *27*, 321–333. https://doi.org/10.1091/mbc.E15-05-0272

Schiefermeier, N., Scheffler, J. M., de Araujo, M. E. G., Stasyk, T., Yordanov, T., Ebner, H. L., Offterdinger, M., Munck, S., Hess, M. W., Wickström, S. A., Lange, A., Wunderlich, W., Fässler, R., Teis, D., & Huber, L. A. (2014). The late endosomal p14-MP1 (LAMTOR2/3) complex regulates focal adhesion dynamics during cell migration. *The Journal of Cell Biology*, *205*(4), 525–540. https://doi.org/10.1083/JCB.201310043

Schindelin, J., Arganda-Carreras, I., Frise, E., Kaynig, V., Longair, M., Pietzsch, T., Preibisch, S., Rueden, C., Saalfeld, S., Schmid, B., Tinevez, J. Y., White, D. J., Hartenstein, V., Eliceiri, K., Tomancak, P., & Cardona, A. (2012). Fiji: an open-source platform for biological-image analysis. *Nature Methods*, *9*(7), 676–682. https://doi.org/10.1038/NMETH.2019

Schink, K. O., Tan, K.-W., & Stenmark, H. (2016). Phosphoinositides in Control of Membrane Dynamics. *Norway Annu. Rev. Cell Dev. Biol*, *32*, 143–171. https://doi.org/10.1146/annurev-cellbio-111315-125349

Scorrano, L., De Matteis, M. A., Emr, S., Giordano, F., Hajnóczky, G., Kornmann, B., Lackner, L. L., Levine, T. P., Pellegrini, L., Reinisch, K., Rizzuto, R., Simmen, T., Stenmark, H., Ungermann, C., & Schuldiner, M. (2019). Coming together to define membrane contact sites. *Nature Communications*, *10*(1). https://doi.org/10.1038/s41467-019-09253-3

Sharma, A., Kumar, G., Sharma, S., Walia, K., Chouhan, P., Mandal, B., & Tuli, A. (2021). Methods for binding analysis of small GTP-binding proteins with their effectors. *Methods in Cell Biology*, *166*, 235–250. https://doi.org/10.1016/BS.MCB.2021.06.003

Shrestha, R., Kaplan, J., & Ward, D. M. (2016a). Conventional and Secretory Lysosomes. In *Encyclopedia of Cell Biology* (pp. 225–234). Elsevier. https://doi.org/10.1016/B978-0-12-394447-4.20019-9

Shrestha, R., Kaplan, J., & Ward, D. M. (2016b). Conventional and Secretory Lysosomes. *Encyclopedia of Cell Biology*, *2*, 225–234. https://doi.org/10.1016/B978-0-12-394447-4.20019-9

Sindhwani, A., Arya, S. B., Kaur, H., Jagga, D., Tuli, A., & Sharma, M. (2017a). *Salmonella exploits the host endolysosomal tethering factor HOPS complex to promote its intravacuolar replication*. https://doi.org/10.1371/journal.ppat.1006700

Sindhwani, A., Arya, S. B., Kaur, H., Jagga, D., Tuli, A., & Sharma, M. (2017b). *Salmonella exploits the host endolysosomal tethering factor HOPS complex to promote its intravacuolar replication*. https://doi.org/10.1371/journal.ppat. 1006700

Soppina, V., Rai, A. K., Ramaiya, A. J., Barak, P., & Mallik, R. (2009). Tug-of-war between dissimilar teams of microtubule motors regulates transport and fission of endosomes. In *PNAS November* (Vol. 17).

Sørensen, M. G., Henriksen, K., Neutzsky-Wulff, A. V., Dziegiel, M. H., & Karsdal, M. A. (2007). Diphyllin, a novel and naturally potent V-ATPase inhibitor, abrogates acidification of the osteoclastic resorption lacunae and bone resorption. *Journal of Bone and Mineral Research*, *22*(10), 1640–1648. https://doi.org/10.1359/jbmr.070613

Spang, A. (2016). Membrane Tethering Complexes in the Endosomal System. *Frontiers in Cell and Developmental Biology*, *4*(May), 35. https://doi.org/ 10.3389/fcell.2016.00035

Spits, M., Heesterbeek, I. T., Voortman, L. M., Akkermans, J. J., Wijdeven, R. H., Cabukusta, B., & Neefjes, J. (2021). Mobile late endosomes modulate peripheral endoplasmic reticulum network architecture. *EMBO Reports*. https://doi.org/10.15252/embr.202050815

Staudt, C., Puissant, E., & Boonen, M. (2017). Subcellular Trafficking of Mammalian Lysosomal Proteins: An Extended View. *International Journal of Molecular Sciences*, *18*(1). https://doi.org/10.3390/IJMS18010047

Stenbeck, G. (2004). Endocytic trafficking in actively resorbing osteoclasts. *Journal of Cell Science*. https://doi.org/10.1242/jcs.00935

Stenbeck, Gudrun, & Coxon, F. P. (2014). Role of vesicular trafficking in skeletal dynamics. *Current Opinion in Pharmacology*, *16*(1), 7–14. https://doi.org/10. 1016/j.coph.2014.01.003

Takayanagi, H., Kim, S., Koga, T., Nishina, H., Isshiki, M., Yoshida, H., Saiura, A., Isobe, M., Yokochi, T., Inoue, J.-I., Wagner, E. F., & Mak, T. W. (2002). Induction and Activation of the Transcription Factor NFATc1 (NFAT2) Integrate RANKL Signaling in Terminal Differentiation of Osteoclasts. *Developmental Cell*, *3*, 889–901. https://ac.els-cdn.com/S1534580702003696/1-s2.0-S1534580702003696-main.pdf?_tid=f19dfce6-4a7a-4e16-93bd-bf22b42056c9&acdnat=1528339484_da9981a402b599bd41be2c38baa10dea

Takemasu, S., Nigorikawa, K., Yamada, M., Tsurumi, G., Kofuji, S., Takasuga, S., & Hazeki, K. (2019). Phosphorylation of TMEM55B by Erk/MAPK regulates lysosomal positioning. *Journal of Biochemistry*, *166*(2), 175–185. https://doi.org/10.1093/jb/mvz026

Takito, J., Inoue, S., & Nakamura, M. (2018). The sealing zone in osteoclasts: A self-organized structure on the bone. In *International Journal of Molecular Sciences* (Vol. 19, Issue 4, p. 984). MDPI AG. https://doi.org/10.3390/ijms19040984

Tan, J. K., Mohamad Hazir, N. S., & Alias, E. (2021). Impacts of hypoxia on osteoclast formation and activity: Systematic review. *International Journal of Molecular Sciences*, *22*(18). https://doi.org/10.3390/ijms221810146

Teitelbaum, S. L. (2000). Bone Resorption by Osteoclasts. *Science*, *289*(5484). http://science.sciencemag.org/content/289/5484/1504/tab-pdf

Teitelbaum, S. L. (2007). Rous-Whipple Award Lecture Osteoclasts: What Do They Do and How Do They Do It? *Am J Pathol*, *170*, 427–435. https://www.ncbi.nlm.nih.gov/pmc/articles/PMC1851862/pdf/7126.pdf

Terawaki, S., Camosseto, V., Prete, F., Wenger, T., Papadopoulos, A., Rondeau, C., Combes, A., Rodrigues, C. R., Manh, T. P. V., Fallet, M., English, L., Santamaria, R., Soares, A. R., Weil, T., Hammad, H., Desjardins, M., Gorvel, J. P., Santos, M. A. S., Gatti, E., & Pierre, P. (2015a). RUN and FYVE domain-containing protein 4 enhances autophagy and lysosome tethering in response to Interleukin-4. *Journal of Cell Biology*. https://doi.org/10.1083/jcb.201501059

Terawaki, S., Camosseto, V., Prete, F., Wenger, T., Papadopoulos, A., Rondeau, C., Combes, A., Rodrigues, C. R., Manh, T. P. V., Fallet, M., English, L., Santamaria, R., Soares, A. R., Weil, T., Hammad, H., Desjardins, M., Gorvel, J. P., Santos, M. A. S., Gatti, E., & Pierre, P. (2015b). RUN and FYVE domain-containing protein 4 enhances autophagy and lysosome tethering in response to Interleukin-4. *Journal of Cell Biology*, *210*(7), 1133–1152. https://doi.org/10.1083/jcb.201501059

Tinevez, J.-Y., Perry, N., Schindelin, J., Hoopes, G. M., Reynolds, G. D., Laplantine, E., Bednarek, S. Y., Shorte, S. L., & Eliceiri, K. W. (2017). TrackMate: An open and extensible platform for single-particle tracking. *Methods*, *115*, 80–90. https://doi.org/10.1016/j.ymeth.2016.09.016

Tran, A., Coxon, F., McDermott, E., Ganley, I., Odgren, P., Martinez, J., Green, D., & Helfrich, M. (2016). The role of LC3 and autophagy in bone resorption by osteoclasts. *Bone Abstracts*, 2–3. https://doi.org/10.1530/boneabs.5.P195

Tsukuba, T., Sakai, E., Nishishita, K., Kadowaki, T., & Okamoto, K. (2017). *New functions of lysosomes in bone cells*. https://doi.org/10.1016/j.job.2017.01.004

Tuli, A., & Sharma, M. (2019). How to do business with lysosomes: Salmonella leads the way. In *Current Opinion in Microbiology* (Vol. 47, pp. 1–7). Elsevier Ltd. https://doi.org/10.1016/j.mib.2018.10.003

Tuli, A., Thiery, J., James, A. M., Michelet, X., Sharma, M., Garg, S., Sanborn, K. B., Orange, J. S., Lieberman, J., & Brenner, M. B. (2013). Arf-like GTPase Arl8b regulates lytic granule polarization and natural killer cell-mediated cytotoxicity. *Molecular Biology of the Cell*, *24*(23), 3721–3735. https://doi.org/10.1091/mbc.E13-05-0259

Udia, C., Ferreira, R.-, & Munro, S. (2011). *Developmental Cell Arl8 and SKIP Act Together to Link Lysosomes to Kinesin-1*. https://doi.org/10.1016/j.devcel.2011.10.007

Väänänen, H. K., Zhao, H., Mulari, M., & Halleen, J. M. (2000). The cell biology of osteoclast function. *J Cell Sci*, *113 (Pt 3*, 377–381. http://www.ncbi.nlm.nih.gov/pubmed/10639325

Van Der Beek, J., Jonker, C., Van Der Welle, R., Liv, N., & Klumperman, J. (2019). *REVIEW SUBJECT COLLECTION: CELL BIOLOGY AND DISEASE CORVET, CHEVI and HOPS-multisubunit tethers of the endo-lysosomal system in health and disease*. https://doi.org/10.1242/jcs.189134

Van Wesenbeeck, L., Villa, A., Van Hul, W., Odgren, P. R., Coxon, F. P., Frattini, A., Moens, P., Perdu, B., MacKay, C. A., Van Hul, E., Timmermans, J.-P., Vanhoenacker, F., Jacobs, R., Peruzzi, B., Teti, A., Helfrich, M. H., & Rogers, M. J. (2007). Involvement of PLEKHM1 in osteoclastic vesicular transport and osteopetrosis in incisors absent rats and humans. *The Journal of Clinical Investigation*, *117*(4). https://doi.org/10.1172/JCI30328

Visentin, L., Dodds, R. A., Valente, M., Misiano, P., Bradbeer, J. N., Oneta, S., Liang, X., Gowen, M., & Farina, C. (2000). A selective inhibitor of the osteoclastic V-H+-ATPase prevents bone loss in both thyroparathyroidectomized and ovariectomized rats. *Journal of Clinical Investigation*. https://doi.org/10.1172/JCI6145

Walsh, J. S. (2015). Normal bone physiology, remodelling and its hormonal regulation. *Surgery*, *33*, 1–6. https://doi.org/10.1016/j.mpsur.2014.10.010

Wang, G., Zhang, Q., Song, Y., Wang, X., Guo, Q., Zhang, J., Li, J., Han, Y., Miao, Z., & Li, F. (2015). PAK1 regulates RUFY3-mediated gastric cancer cell migration and invasion. *Cell Death & Disease*, *6*(77), e1682. https://doi.org/10.1038/cddis.2015.50

Wang, W., Gao, Q., Yang, M., Zhang, X., Yu, L., Lawas, M., Li, X., Bryant-Genevier, M., Southall, N. T., Marugan, J., Ferrer, M., & Xu, H. (2015). Up-regulation of lysosomal TRPML1 channels is essential for lysosomal adaptation to nutrient starvation. *Proceedings of the National Academy of Sciences of the United States of America*, *112*(11), E1373–E1381. https://doi.org/10.1073/pnas.1419669112

Wartosch, L., Bright, N. A., & Luzio, J. P. (2015). Lysosomes. In *Current Biology* (Vol. 25, Issue 8, pp. R315–R316). Cell Press. https://doi.org/10.1016/j.cub.2015.02.027

Watts, N. B. (1999). *Clinical Utility of Biochemical Markers of Bone Remodeling*. http://clinchem.aaccjnls.org/content/clinchem/45/8/1359.full.pdf

Wei, Z., Sun, M., Liu, X., Zhang, J., & Jin, Y. (2014). Rufy3, a protein specifically expressed in neurons, interacts with actin-bundling protein Fascin to control the growth of axons. *Journal of Neurochemistry*, *130*(5), 678–692. https://doi.org/10.1111/jnc.12740

Wijdeven, R. H., Janssen, H., Nahidiazar, L., Janssen, L., Jalink, K., Berlin, I., & Neefjes, J. (2016). Cholesterol and ORP1L-mediated ER contact sites control autophagosome transport and fusion with the endocytic pathway. *Nature Communications*, *7*. https://doi.org/10.1038/ncomms11808

Willett, R., Martina, J. A., Zewe, J. P., Wills, R., Hammond, G. R. V., & Puertollano, R. (2017). TFEB regulates lysosomal positioning by modulating TMEM55B expression and JIP4 recruitment to lysosomes. *Nature Communications*, *8*(1), 1580. https://doi.org/10.1038/s41467-017-01871-z

Wong, Y. C., Ysselstein, D., & Krainc, D. (2018). Mitochondria–lysosome contacts regulate mitochondrial fission via RAB7 GTP hydrolysis. *Nature 2018 554:7692*, *554*(7692), 382–386. https://doi.org/10.1038/nature25486

Xie, R., Wang, J., Liu, X., Wu, L., Zhang, H., Tang, W., Li, Y., Xiang, L., Peng, Y., Huang, X., Bai, Y., Liu, G., Li, A., Wang, Y., Chen, Y., Ren, Y., Li, G., Gong, W., Liu, S., & Wang, J. (2017). RUFY3 interaction with FOXK1 promotes invasion and metastasis in colorectal cancer. *Scientific Reports*, *7*(1), 1–11. https://doi.org/10.1038/s41598-017-04011-1

Xiu, Y., Xu, H., Zhao, C., Li, J., Morita, Y., Yao, Z., Xing, L., & Boyce, B. F. (2014). Chloroquine reduces osteoclastogenesis in murine osteoporosis by preventing TRAF3 degradation. *Journal of Clinical Investigation*, *124*(1), 297–310. https://doi.org/10.1172/JCI66947

Yang, C., & Wang, X. (2021). *Lysosome biogenesis: Regulation and functions*. https://doi.org/10.1083/jcb.202102001

Ye, S., Fowler, T. W., Pavlos, N. J., Ng, P. Y., Liang, K., Feng, Y., Zheng, M., Kurten, R., Manolagas, S. C., & Zhao, H. (2011). LIS1 regulates osteoclast formation and function through its interactions with dynein/dynactin and Plekhm1. *PLoS ONE*, *6*(11). https://doi.org/10.1371/journal.pone.0027285

Yip, Y. Y., Sanger, A., Morton, P. E., Eden, E. R., & Dodding, Mark PStarling, G. P. (2016). Folliculin directs the formation of a Rab34– RILP complex to control the nutrient-dependent dynamic distribution of lysosomes. *EMBO Reports*, *17*(6), 823–841. https://doi.org/10.15252/embr.201541382

Yordanov, T. E., Hipolito, V. E. B., Liebscher, G., Vogel, G. F., Stasyk, T., Herrmann, C., Geley, S., David Teis, |, Botelho, R. J., Hess, M. W., Lukas, |, & Huber, A. (2019). *Biogenesis of lysosome-related organelles complex-1 (BORC) regulates late endosomal/lysosomal size through PIKfyve-dependent phosphatidylinositol-3,5-bisphosphate*. https://doi.org/10.1111/tra.12679/ Abstract

Zhao, H. (2012). Membrane Trafficking in Osteoblasts and Osteoclasts: New Avenues for Understanding and Treating Skeletal Diseases. *Traffic*, *13*, 1307–1314. https://doi.org/10.1111/j.1600-0854.2012.01395.x

Zhao, H., Laitala-Leinonen, T., Parikka, V., & Väänänen, H. K. (2001). Downregulation of small GTPase Rab7 impairs osteoclast polarization and bone resorption. *The Journal of Biological Chemistry*, *276*(42), 39295–39302. https://doi.org/10.1074/JBC.M010999200

Zhao, Q., Gao, S. M., & Wang, M. C. (2020). Molecular Mechanisms of Lysosome and Nucleus Communication. In *Trends in Biochemical Sciences* (Vol. 45, Issue 11, pp. 978–991). Elsevier Ltd. https://doi.org/10.1016/j.tibs.2020.06.004

Zhao, Y., Chen, G., Zhang, W., Xu, N., Zhu, J. Y., Jia, J., Sun, Z. J., Wang, Y. N., & Zhao, Y. F. (2012). Autophagy regulates hypoxia-induced osteoclastogenesis through the HIF-1α/BNIP3 signaling pathway. *Journal of Cellular Physiology*, *227*(2), 639–648. https://doi.org/10.1002/JCP.22768

Zhu, S., Rea, S. L., Cheng, T., Feng, H. T., Walsh, J. P., Ratajczak, T., Tickner, J., Pavlos, N., Xu, H.-Z., & Xu, J. (2016). Bafilomycin A1 Attenuates Osteoclast Acidification and Formation, Accompanied by Increased Levels of SQSTM1/p62 Protein; Bafilomycin A1 Attenuates Osteoclast Acidification and Formation, Accompanied by Increased Levels of SQSTM1/p62 Protein. *J. Cell. Biochem*, *117*, 1464–1470. https://doi.org/10.1002/jcb.25442

Appendix

A) pList of DNA constructs used in this study (Chapter 2).

Plasmid Name	**Description**	**Source**
***Yeast two-hybrid constructs*:**		
pGADT7	GAL4-activation domain yeast two-hybrid vector	Clontech
pGADT7-RUFY3 (WT)	Full-length human RUFY3 (1-620 aa) cloned into the pGADT7 vector	This study
pGADT7-RUFY3 (Δ446-561)	Human RUFY3 lacking amino acids 446-561 cloned into the pGADT7 vector	This study
pGADT7-RUFY3 (441-561)	Human RUFY3 amino acids 441-561 cloned into the pGADT7 vector	This study
pGADT7-RUFY3 (RK→A)	Human RUFY3 with point mutations at amino acid positions R462 and K465 to A; cloned into the pGADT7 vector	This study
pGAD-C1-RILP	RILP cloned into the pGAD-C1 vector	Gift from Prof. Mitsunori Fukuda
pGBKT7	GAL4-DNA binding domain yeast two-hybrid vector	Clontech
pGBKT7-Arl8b (WT)	Human Arl8b (lacking first 17 aa) cloned into the pGBKT7 vector	Described previously (Marwaha et al., 2017)
pGBKT7-Arl8b (Q75L)	Human Arl8b (lacking first 17 aa) with Q75L point mutation cloned into the pGBKT7 vector	Described previously (Marwaha et al., 2017)
pGBKT7-Arl8b (T34N)	Human Arl8b (lacking first 17 aa) with T34N point mutation cloned into the pGBKT7 vector	Described previously (Marwaha et al., 2017)
pGBD-C1-Rab7	Human Rab7a cloned into the pGBD-C1 vector	Described previously (Marwaha et al., 2017)

Mammalian expression constructs:		
pcDNA3.1(-)	Mammalian expression vector	Invitrogen
pcDNA3.1(-)-RUFY3 (UT)	Full-length human RUFY3 (1-620 aa) without any tag cloned into the pcDNA3.1(-) vector	This study
pcDNA3.1(-)- RUFY3-FLAG	C-terminal FLAG-tagged full-length human RUFY3 (1-620 aa) cloned into the pcDNA3.1(-) vector	This study
pcDNA3.1(-)-RUFY3 (RK→A)-FLAG	C-terminal FLAG-tagged human RUFY3 with point mutations at amino acid positions R462 and K465 to A; cloned into the pcDNA3.1(-) vector	This study
pcDNA3.1(-)- RUFY3-FLAG (RESCUE)	C-terminal FLAG-tagged full-length human RUFY3 (1-620 aa) rescue construct against RUFY3 siRNA cloned into the pcDNA3.1(-) vector	This study
pcDNA3.1(-)- RUFY3-HA	C-terminal HA-tagged full-length human RUFY3 (1-620 aa) cloned into the pcDNA3.1(-) vector	This study
pcDNA3.1(-)-RUFY3 (Δ446-561)-HA	C-terminal HA-tagged human RUFY3 lacking amino acids 446-561; cloned into the pcDNA3.1(-) vector	This study
pcDNA3.1(-)-RUFY3 (RK→A)-HA	C-terminal HA-tagged human RUFY3 with point mutations at amino acid positions R462 and K465 to A; cloned into the pcDNA3.1(-) vector	This study
pcDNA3.1(-)- RUFY3 (v2)-HA	C-terminal HA-tagged human RUFY3 (1-469 aa; variant 2) cloned into the pcDNA3.1(-) vector	This study
pEGFP-C1	EGFP expressing mammalian expression vector	Clontech
pEGFP-C1-RUFY3 (WT)	Full-length human RUFY3 (1-620 aa) cloned into the pEGFP-C1 vector	This study
pEGFP-C1-RUFY3 (RESCUE)	Full-length human RUFY3 (1-620 aa) rescue construct against RUFY3 siRNA cloned into the pEGFP-C1 vector	This study

pcDNA3.1(+)-Arl8b (UT)	Full-length human Arl8b (untagged; UT) cloned into the pcDNA3.1(+) vector	Described previously (Marwaha et al., 2017)
pcDNA3.1(-)-Arl8b (WT)-FLAG	Full-length human Arl8b with C-terminal FLAG tagged cloned into the pcDNA3.1(-) vector	This study
pcDNA3.1(-)-Arl8b (WT)-HA	Full-length human Arl8b with C-terminal HA tagged cloned into the pcDNA3.1(-) vector	Described previously (Marwaha et al., 2017)
pcDNA3.1(-)-Arl8b (Q75L)-HA	Full-length human Arl8b Q75L with C-terminal HA tagged cloned into the pcDNA3.1(-) vector	Described previously (Marwaha et al., 2017)
pcDNA3.1(-)-Arl8b (T34N)-HA	Full-length human Arl8b T34N with C-terminal HA tagged cloned into the pcDNA3.1(-) vector	Described previously (Marwaha et al., 2017)
pEGFP-C1-RILP	N-terminal GFP-tagged RILP cloned into the pEGFP-C1 vector	Described previously (Marwaha et al., 2017)
pEGFP-C1-TMEM55B	N-terminal GFP-tagged TMEM55B cloned into the pEGFP-C1 vector	This study
pEGFP-C1-Rab11	N-terminal GFP-tagged Rab11 cloned into the pEGFP-C1 vector	Gift from Prof. Steve Caplan
pCMV-Tag2B-JIP4	N-terminal FLAG-tagged human JIP4 (isoform 2) cloned into the pCMV-Tag2B vector	Gift from Dr. Clement Lee
pLJC5-TMEM192-3xHA	C-terminal HA-tagged TMEM192 cloned into the pLJC5 vector	Addgene plasmid # 102930
pLJC5-TMEM192-2xFLAG	C-terminal FLAG-tagged TMEM192 cloned into the pLJC5 vector	Addgene plasmid # 102929
Mito-Rab7-HA	Rab7A (QL)-BirA-HA-MAO	Addgene plasmid # 128904

Mito-Arl8b-HA	Human Arl8b (lacking first 17 aa) cloned into the Rab7A (QL)-BirA-HA-MAO vector by replacing Rab7 (QL) cassette	This study
Mito-FRB	Mito (Tom70p) fused to FRB	Gift from Prof. Martin Lowe
2x-FKBP-GFP	FKBP fused to GFP cloned into the pcDNA3.1(-) vector	This study
2x-FKBP-GFP-RUFY3	FKBP fused to GFP-RUFY3 cloned into the pcDNA3.1(-) vector	This study
Bacterial expression constructs:		
pGEX6P2-RUFY3	Human RUFY3 (1-620 aa) cloned into the pGEX6P2 vector	This study
pGEX6P2-RUFY3 (Δ446-561)	Human RUFY3 lacking amino acids 446-561 cloned into the pGEX6P2 vector	This study
pGEX6P2-RUFY3 (441-561)	Human RUFY3 amino acids 441-561 cloned into the pGEX6P2 vector	This study
pGEX6P2-RUFY3 RK→A (441-561)	Human RUFY3 (441-561 aa) with point mutations at amino acid positions R462 and K465 to A; cloned into the pGEX6P2 vector	This study
pETDuet-1-Arl8b	Full-length human Arl8b with N-terminal His tag cloned into the pETDuet-1 vector	This study
pGEX4T3-Arl8b	Full-length human Arl8b with N-terminal GST tag cloned into the pGEX4T3 vector	Described previously (Marwaha et al., 2017)

B) List of antibodies used in this study (Chapter 2).

(WB: Western Blot; IF: Immunofluorescence; IP: Immunoprecipitation)		
Antibody	**Source**	**Identifier**
Rabbit anti-RUFY3 (WB-1:1500)	Novus Biologicals	NBP1-89614
Rabbit anti-JIP4 (WB-1:1000; IF-1:100; IP-1 µg)	Cell Signaling Technology	5519
Rabbit anti-Rab5 (WB-1:1000)	Cell Signaling Technology	2143
Rabbit anti-Calreticulin (WB-1:1000)	Cell Signaling Technology	12238
Rabbit anti-Catalase (WB-1:1000)	Cell Signaling Technology	12980
Rabbit anti-Rab7 (WB-1:1000)	Cell Signaling Technology	9367
Rabbit anti-Arl8b (WB-1:1000; IF-1:30)	Cell Signaling Technology	56085
Rabbit anti-FLAG tag (IF-1:500)	Cell Signaling Technology	2368
Rabbit anti-LC3B (WB-1:1000)	Cell Signaling Technology	3868
Rabbit anti-LAMP1 (WB-1:5000; IF-1:1000)	Abcam	ab24170
Rabbit anti-Cathepsin D (WB-1:1500; IF-1:200)	Abcam	ab75852
Rabbit anti-TfR (IF-1:500)	Abcam	ab84036
Rabbit anti-RUFY3 (IP-1 µg)	Abcam	ab237511
Rabbit anti-VDAC (WB-1:1000)	Thermo Fisher Scientific	PA1-954A
Rabbit anti-FLAG tag (WB-1:4000)	Thermo Fisher Scientific	PA1-984B
Rabbit anti-LC3 (IF-1:1000)	MBL International Corporation	PM036

Rabbit anti-HA tag (WB-1:4000; IF-1:500)	Sigma-Aldrich	H6908
Mouse anti-HA-conjugated agarose beads (IP-12 µL slurry)	Sigma-Aldrich	A2095
Mouse IgG-conjugated agarose beads (IP-12 µL slurry)	Sigma-Aldrich	A0919
Rabbit IgG-conjugated agarose beads (IP-12 µL slurry)	Sigma-Aldrich	A2909
Rabbit anti-Arl8 (WB-1:1000)	Custom-made	Previously described (Garg S et al., Immunity 2011)
Mouse anti-Rab5 (IF-1:200)	BD Bioscience	610281
Mouse anti-LAMP1 (IF-1:500)	BD Bioscience	555798
Mouse anti-p150 (WB-1:1500; IF-1:100)	BD Bioscience	610474
Mouse anti-CD63 (IF-1:200)	BD Bioscience	556019
Mouse anti-DIC (WB-1:5000)	BioLegend	904901
Mouse anti-HA tag (WB-1:4000; IF-1:500)	BioLegend	901503
Anti-FLAG affinity gel (IP-12 µL slurry)	BioLegend	651503
Mouse anti-Tom-20 (IF-1:500)	Santa Cruz Biotechnology	sc-17764
Mouse anti-Arl8-conjugated-agarose beads (IP-30 µL slurry)	Santa Cruz Biotechnology	sc-398635 AC
Mouse anti-Rab7 (IF-1:30)	Santa Cruz Biotechnology	sc-376362
Mouse anti-GAPDH (WB-1:2000)	Santa Cruz Biotechnology	sc-166574
Mouse anti-β-tubulin (WB-1:4000)	Sigma-Aldrich	T4026

Mouse anti-FLAG tag (WB-1:4000; IF-1:500)	Sigma-Aldrich	F1804
Mouse anti-His tag (WB-1:5000)	Sigma-Aldrich	SAB1305538
Mouse anti-GST tag (WB-1:5000)	Thermo Fisher Scientific	MA4-004
Alexa-Fluor 488-conjugated goat anti-rabbit IgG (IF-1:500)	Thermo Fisher Scientific	A-11034
Alexa-Fluor 568-conjugated goat anti-rabbit IgG (IF-1:500)	Thermo Fisher Scientific	A-11036
Alexa-Fluor 488-conjugated goat anti-mouse IgG (IF-1:500)	Thermo Fisher Scientific	A-11029
Alexa-Fluor 568-conjugated goat anti-mouse IgG (IF-1:500)	Thermo Fisher Scientific	A-11031
Alexa-Fluor 633-conjugated goat anti-mouse IgG (IF-1:500)	Thermo Fisher Scientific	A-21050
HRP-conjugated goat anti-rabbit IgG (WB-1:5000)	Jackson ImmunoResearch	111-035-144
HRP-conjugated goat anti-mouse IgG (WB-1:5000)	Jackson ImmunoResearch	115-035-166

C) List of DNA constructs used in this study (chapter 3).

Plasmid Name	Description	Source
***Yeast two-hybrid constructs*:**		
pGADT7	GAL4-activation domain yeast two-hybrid vector	Clontech
pGADT7-RUFY1 (WT)	Full-length human RUFY1 (1-708 aa) cloned into the pGADT7 vector	This study
pGADT7-RUFY2 (WT)	Full-length human RUFY2 (1-641 aa) cloned into the pGADT7 vector	This study
pGADT7-RUFY3 (WT)	Full-length human RUFY3 (1-620 aa) cloned into the pGADT7 vector	This study
pGADT7-RUFY4 (WT)	Full-length human RUFY4 (1-571 aa) cloned into the pGADT7 vector	This study
pGADT7-RUFY4 (ΔRUN)	Human RUFY4 lacking amino acids 1-166 cloned into the pGADT7 vector	This study
pGADT7-RUFY4 (RUN)	Human RUFY4 amino acids 1-166 created by inserting stop codon at amino acid position 167 in the Full-length human RUFY4 (1-571 aa) cloned into the pGADT7 vector	This study
pGADT7-RUFY4 (KRR→A)	Human RUFY4 with point mutations at amino acid positions K100, R102 and K106 to A; cloned into the pGADT7 vector	This study
pGBKT7	GAL4-DNA binding domain yeast two-hybrid vector	Clontech
pGBKT7-Arl8b (WT)	Human Arl8b (lacking first 17 aa) cloned into the pGBKT7 vector	Described previously (Marwaha et al., 2017)
pGBKT7-Arl8b (Q75L)	Human Arl8b (lacking first 17 aa) with Q75L point mutation cloned into the pGBKT7 vector	Described previously (Marwaha et al., 2017)

pGBKT7-Arl8b (T34N)	Human Arl8b (lacking first 17 aa) with T34N point mutation cloned into the pGBKT7 vector	Described previously (Marwaha et al., 2017)
pGBKT7-Human LC3b	Human LC3B cloned in pGBKT7 vector	Gift from Prof. Eiji Morita
Mammalian expression constructs:		
pcDNA3.1(-)	Mammalian expression vector	Invitrogen
pcDNA3.1(-)-FLAG-RUFY4	N-terminal FLAG-tagged full-length human RUFY4 cloned into the pcDNA3.1(-) vector	This study
pcDNA3.1(-)- RUFY4-FLAG	C-terminal FLAG-tagged full-length human RUFY4 (1-571 aa) cloned into the pcDNA3.1(-) vector	This study
pcDNA3.1(-)-FLAG-RUFY4 (RUN)	N-terminal FLAG-tagged human RUFY4 amino acids 1-166, created by inserting stop codon at amino acid position 167 in the Full-length human RUFY4 (1-571 aa) cloned into the pcDNA3.1(-) vector	This study
pcDNA3.1(-)-FLAG-RUFY4 (ΔRUN)	N-terminal FLAG-tagged human RUFY4 lacking amino acids 1-166 cloned into the pcDNA3.1(-) vector	This study
pcDNA3.1(-)-FLAG-RUFY4 (KRR→A)	N-terminal FLAG-tagged human RUFY4 with point mutations at amino acid positions K100, R102 and K106 to A; cloned into the pcDNA3.1(-) vector	This study
pcDNA3.1(-)- RUFY4-FLAG	C-terminal FLAG-tagged full-length human RUFY4 (1-571 aa) cloned into the pcDNA3.1(-) vector	This study
pEGFP-C1	EGFP expressing mammalian expression vector	Clontech
Mouse-Arl8b (WT)-GFP	Mouse Arl8b with C-terminal GFP expressing plasmid	origene

pcDNA3.1(-)-Arl8b (WT)-HA	Full-length human Arl8b with C-terminal HA tagged cloned into the pcDNA3.1(-) vector	Described previously (Marwaha et al., 2017)
pcDNA3.1(-)-Arl8b (Q75L)-HA	Full-length human Arl8b Q75L with C-terminal HA tagged cloned into the pcDNA3.1(-) vector	Described previously (Marwaha et al., 2017)
pcDNA3.1(-)-Arl8b (T34N)-HA	Full-length human Arl8b T34N with C-terminal HA tagged cloned into the pcDNA3.1(-) vector	Described previously (Marwaha et al., 2017)
pcDNA3.1(-)-Arl11 (WT)-HA	Full-length human Arl11with C-terminal HA tagged cloned into the pcDNA3.1(-) vector	Described previously (Arya et al., 2017)
EGFP-LC3	LC3 with N-terminal EGFP expressing plasmid	Gift from Dr Ashwani Kumar
Bacterial expression constructs:		
pGEX6P2-RUFY4 (RUN)	Human RUFY4 (1-166 aa) cloned into the pGEX6P2 vector	This study
pGEX4T3-Arl8b	Full-length human Arl8b with N-terminal GST tag cloned into the pGEX4T3 vector	Described previously (Marwaha et al., 2017)
pETDuet-1-Arl8b	Full-length human Arl8b with N-terminal His tag cloned into the pETDuet-1 vector	This study
pRSF-His-Rab7	Rab7 with N-terminal His tag cloned into the pRSF vector	Gift from A. Spang
pGEX6P2-Human LC3b (1-120)	Human LC3b (1-120) cloned in pGEX6P2	This study

JBC EDITORS' PICK

⌘ *Author's Choice*

ARL11 regulates lipopolysaccharide-stimulated macrophage activation by promoting mitogen-activated protein kinase (MAPK) signaling

Received for publication, October 31, 2017, and in revised form, March 20, 2018 Published, Papers in Press, April 4, 2018, DOI 10.1074/jbc.RA117.000727

Subhash B. Arya[1], **Gaurav Kumar**[2], **Harmeet Kaur**[3], **Amandeep Kaur**[4], **and Amit Tuli**[5]

From the Division of Cell Biology and Immunology, CSIR-Institute of Microbial Technology (IMTECH), Chandigarh 160036, India

Edited by Ursula Jakob

ADP-ribosylation factor-like GTPase 11 (*ARL11*) is a cancer-predisposing gene that has remained functionally uncharacterized to date. In this study, we report that ARL11 is endogenously expressed in mouse and human macrophages and regulates their activation in response to lipopolysaccharide (LPS) stimulation. Accordingly, depletion of ARL11 impaired both LPS-stimulated pro-inflammatory cytokine production by macrophages and their ability to control intracellular replication of *Salmonella*. LPS-stimulated activation of extracellular signal–regulated kinase (ERK) and p38 mitogen-activated protein kinase (MAPK) was substantially compromised in *Arl11*-silenced macrophages. In contrast, increased expression of ARL11 led to constitutive ERK1/2 phosphorylation, resulting in macrophage exhaustion. Finally, we found that ARL11 forms a complex with phospho-ERK in macrophages within minutes of LPS stimulation. Taken together, our findings establish ARL11 as a novel regulator of ERK signaling in macrophages, required for macrophage activation and immune function.

ARL11, also known as ADP-ribosylation factor-like tumor suppressor gene 1 (*ARLTS1*), is a member of the Arf-like (ARL) family of small GTP-binding proteins that regulate diverse cellular processes, including vesicular trafficking, cytoskeletal organization, signaling, and ciliogenesis (1, 2). Similarly to the other members of the RAS superfamily of small GTPases, ARL proteins also function as molecular switches that cycle between inactive (GDP-bound) and active (GTP-bound) conformations. *ARL11* was first identified in a screening for putative tumor suppressor genes at chromosome location 13q14.3, a region frequently deleted in a variety of sporadic and hereditary hematopoietic and solid tumors (3–6). Subsequent studies reported down-regulation of *ARL11* expression in several sporadic lung cancer and ovarian tumors attributed to promoter methylation and loss of heterozygosity at the *ARL11* gene locus (7, 8). Further support for its tumor suppressor function has come from the finding that SNPs G446A (W149X) and T442C (C148R) in the *ARL11* gene are associated with familial risk for chronic lymphocytic leukemia (CLL)[6] and for breast, prostate, and colorectal cancers (9–15). On the other hand, ectopic expression of ARL11 in lung carcinoma was reported to induce apoptosis, suggesting that ARL11 down-regulation promotes tumor cell survival (8).

A high degree of conservation of *ARL11* homologs in metazoans such as zebrafish, *Drosophila*, *Arabidopsis*, and mammals suggests an important cellular function of this gene. However, thus far, the physiological role of ARL11 is not known. Expression studies have revealed that mammalian *ARL11* transcripts are mostly abundant in lymphoid tissues (spleen, bone marrow, and lymph nodes), which is also supported by co-expression analysis from data mining approaches (8, 14).

We also searched for *Arl11* transcript expression in different immune cell types compiled in the Immunological Genome Project (ImmGen) database (https://www.immgen.org/)[7] (37) and found that transcripts of *Arl11* predominated in macrophages, followed by monocytes and neutrophils. This led us to investigate the function of this uncharacterized protein in macrophages.

Here, we demonstrate that ARL11 expression is up-regulated upon lipopolysaccharide (LPS) stimulation in macrophages and regulates the pro-inflammatory macrophage effector functions. ARL11 was required for LPS- or pathogen-mediated activation of ERK1/2 and p38 mitogen-activated protein kinases (MAPKs). Notably, ERK1/2 colocalized with ARL11 at the cor-

This work was supported by Wellcome Trust/Department of Biotechnology (DBT) India Alliance Intermediate Fellowship IA/I/14/2/501543 (to A. T.). This work received infrastructure and financial support from CSIR-IMTECH (OLP-144, communication 046/2017). The authors declare that they have no conflicts of interest with the contents of this article.

⌘ *Author's Choice*—Final version free via Creative Commons CC-BY license.

This article was selected as one of our Editors' Picks.

This article contains Figs. S1–S7 and Videos S1 and S2.

[1] Supported by the CSIR-JRF. To whom correspondence may be addressed. E-mail: subhasharya8@gmail.com.

[2] Supported by the CSIR-UGC.

[3] Supported by the Wellcome Trust/DBT India Alliance and CSIR-IMTECH. Present address: Dept. of Biological Sciences, Indian Institute of Science Education and Research (IISER) Mohali 140306, India.

[4] Supported by a DST-INSPIRE Fellowship.

[5] To whom correspondence may be addressed. E-mail: atuli@imtech.res.in.

[6] The abbreviations used are: CLL, chronic lymphocytic leukemia; LPS, lipopolysaccharide; MAPK, mitogen-activated protein kinase; ERK, extracellular signal–regulated kinase; BMDM, bone marrow–derived mouse macrophage; TLR, Toll-like receptor; TNFα, tumor necrosis factor α; JNK, c-Jun N-terminal kinase; MAPKK, mitogen-activated protein kinase kinase; IL, interleukin; MEK, mitogen-activated protein kinase/extracellular signal-regulated kinase kinase; cfu, colony-forming units; p.i., post-infection; HA, hemagglutinin; FRAP, fluorescence recovery after photobleaching; cyto D, cytochalasin D; EGF, epidermal growth factor; FBS, fetal bovine serum; DMEM, Dulbecco's modified Eagle's medium; PE, phycoerythrin; PFA, paraformaldehyde; DAPI, 4′,6-diamidino-2-phenylindole; ROI, region of interest; GAPDH, glyceraldehyde-3-phosphate dehydrogenase.

[7] Please note that the JBC is not responsible for the long-term archiving and maintenance of this site or any other third party hosted site.

© 2018 by The American Society for Biochemistry and Molecular Biology, Inc. Published in the U.S.A.

Vol 8, Iss 24, Dec 20, 2018
DOI:10.21769/BioProtoc.3123

Method for Studying the Effect of Gene Silencing on Bacterial Infection-induced ERK1/2 Signaling in Bone-marrow Derived Macrophages

Gaurav Kumar[#], Subhash B. Arya[$, #] and Amit Tuli*

Division of Cell Biology and Immunology, CSIR-Institute of Microbial Technology (IMTECH), Chandigarh, India; [$]Present address: Department of Pharmacology, Life Sciences Institute, University of Michigan, Ann Arbor, Michigan, USA
*For correspondence: atuli@imtech.res.in
[#]Contributed equally to this work

[Abstract] Macrophages are highly phagocytic cells that utilize various pathogen recognition receptors (PRRs) to recognize pathogen-associated molecular patterns (PAMPs). These PAMPs can be present within the microbe, such as bacterial CpG DNA, and are recognized by Toll-like receptor 9 (TLR9), a PRR present on the endosomal membrane of macrophages. PAMPs can also be present on the surface of microbes, such as Lipopolysaccharide (LPS), which decorates the outer membrane of gram-negative bacteria like *Salmonella typhimurium* and *Escherichia coli*. LPS is recognized by TLR4 present on the plasma membrane of macrophages, and LPS-TLR4 association leads to activation of signaling cascades including MAPK phosphorylation, which in turn promotes macrophage activation and microbial killing. This protocol describes the method for studying the role of a gene of interest in Extracellular signal-regulated protein kinases 1 and 2 (ERK1/2) signaling, induced by bacterial infection in primary bone-marrow derived macrophages (BMDMs).
Keywords: Bone-marrow derived macrophages, *Salmonella*, Infection, ERK signaling, Western blotting

[Background] Macrophages are phagocytic cells which can either be resident to specific tissues as Kupffer cells (in the liver) and peritoneal macrophages (in peritoneal cavity) or, can enter tissues in response to an infection. The primary function of macrophages involves phagocytosis and clearance of old damaged cells, and recycling of nutrients in the serum (recently reviewed in Shapouri-Moghaddam *et al.,* 2018). However, for macrophages to clear microbes, there exists a need for their activation. Macrophages obtained from many tissues such as alveoli and peritoneal cavity includes high numbers of pre-activated macrophage population. However, macrophages derived from myeloid progenitor cells present in the bone marrow are comparatively naive and more responsive to activating stimulus (Epelman *et al.,* 2014). Upon encounter of gram-negative bacteria by macrophages, LPS present on either the surface of a bacterium or shed by bacteria in the blood flow is captured by LBP (LPS-binding protein) and presented as a ligand to TLR4, a type I transmembrane protein present on the plasma membrane of macrophage that mediate the recognition of PAMPS such as LPS (Shimazu *et al.,* 1999). The engagement of LPS with TLR4 (along with other co-stimulatory molecules) leads to recruitment of several adaptor proteins at the cytoplasmic tail of TLR4 followed by a cascade of intracellular events leading to activation of the nuclear factor-κB (NF-κB) and mitogen-activated protein kinase (MAPK)

Copyright © 2018 The Authors; exclusive licensee Bio-protocol LLC.

nature COMMUNICATIONS

ARTICLE

https://doi.org/10.1038/s41467-022-29077-y OPEN

RUFY3 links Arl8b and JIP4-Dynein complex to regulate lysosome size and positioning

Gaurav Kumar[1], Prateek Chawla[2], Neha Dhiman[2], Sanya Chadha[1], Sheetal Sharma[1], Kanupriya Sethi[1], Mahak Sharma[2] & Amit Tuli[1]✉

The bidirectional movement of lysosomes on microtubule tracks regulates their whole-cell spatial arrangement. Arl8b, a small GTP-binding (G) protein, promotes lysosome anterograde trafficking mediated by kinesin-1. Herein, we report an Arl8b effector, RUFY3, which regulates the retrograde transport of lysosomes. We show that RUFY3 interacts with the JIP4-dynein-dynactin complex and facilitates Arl8b association with the retrograde motor complex. Accordingly, RUFY3 knockdown disrupts the positioning of Arl8b-positive endosomes and reduces Arl8b colocalization with Rab7-marked late endosomal compartments. Moreover, we find that RUFY3 regulates nutrient-dependent lysosome distribution, although autophagosome-lysosome fusion and autophagic cargo degradation are not impaired upon RUFY3 depletion. Interestingly, lysosome size is significantly reduced in RUFY3 depleted cells, which could be rescued by inhibition of the lysosome reformation regulatory factor PIKFYVE. These findings suggest a model in which the perinuclear cloud arrangement of lysosomes regulates both the positioning and size of these proteolytic compartments.

[1] Divison of Cell Biology and Immunology, CSIR-Institute of Microbial Technology (IMTECH), Chandigarh, India. [2] Department of Biological Sciences, Indian Institute of Science Education and Research (IISER), Mohali, Punjab, India. ✉email: atuli@imtech.res.in

CHAPTER

Methods for binding analysis of small GTP-binding proteins with their effectors

11

Abhishek Sharma, Gaurav Kumar, Sheetal Sharma, Kshitiz Walia, Priya Chouhan, Bidisha Mandal, and Amit Tuli*

Division of Cell Biology and Immunology, CSIR-Institute of Microbial Technology (IMTECH), Chandigarh, India

**Corresponding author: e-mail address: atuli@imtech.res.in*

Chapter outline

1 Introduction....236
2 Yeast two-hybrid (Y2H) assay....238
2.1 Materials....239
2.1.1 Yeast transformation....239
2.1.2 Yeast spotting....239
2.1.3 Preparation of stock reagents and media....240
2.2 Protocol....240
2.2.1 Setting up yeast culture....240
2.2.2 Yeast transformation....240
2.2.3 Yeast spotting for detecting interactions....241
3 Co-immunoprecipitation (co-IP)....243
3.1 Materials....244
3.1.1 Transfection....244
3.1.2 Preparation of cell lysates for Co-IP....244
3.1.3 Immunoblotting....245
3.2 Protocol....245
3.2.1 Transfection of HEK293T cells with expression plasmids....245
3.2.2 Preparation of cell lysates for Co-IP....246
3.2.3 Immunoblotting....246
4 Notes....247
Acknowledgments....249
Funding....249
Contributions....249
References....249

Methods in Cell Biology, Volume 166, ISSN 0091-679X, https://doi.org/10.1016/bs.mcb.2021.06.003
Copyright © 2021 Elsevier Inc. All rights reserved.